

# The Roles of Osteoblast-mTORC1 in the Regulation of Glucose Metabolism

**Pawanrat Tangseefa**

BSc (Biomedical Science)

Myeloma Research Laboratory  
Discipline of Physiology  
Adelaide Medical School  
Faculty of Health and Medical Sciences  
The University of Adelaide  
&  
Cancer Program, Precision Medicine Theme  
South Australian Health & Medical Research Institute  
(SAHMRI)



Supervisors

Prof. Andrew C. W. Zannettino, Dr. Stephen Fitter, Dr. Sally K. Martin  
and Prof. Christopher G. Proud

A thesis submitted for the degree of Doctor of Philosophy

February 2020

## TABLE OF CONTENTS

<b>TABLE OF CONTENTS</b> .....	<b>i</b>
<b>DECLARATION</b> .....	<b>iv</b>
<b>ACKNOWLEDGEMENT</b> .....	<b>v</b>
<b>LIST OF ABBREVIATIONS</b> .....	<b>vii</b>
<b>LIST OF PUBLICATIONS</b> .....	<b>viii</b>
<b>CHAPTER 1: INTRODUCTION</b> .....	<b>2</b>
1.1 Abstract .....	3
1.2 Introduction .....	4
1.3 The discovery of OCN as an endocrine regulator of energy metabolism .....	6
1.3.1 Sensitizing effects of OCN: direct and indirect mechanisms .....	6
1.3.2 The undercarboxylated form of OCN is responsible for the metabolic functions of OCN.....	8
1.4 Insulin signalling, bone remodelling and regulation of OCN .....	8
1.4.1 Insulin signalling in OBs favours bone remodelling to increase OCN bioactivity .....	8
1.4.2 Insulin signalling in OBs is required for proper glycaemic control .....	10
1.5 Skeletal insulin resistance disrupts whole-body glucose homeostasis.....	11
1.5.1 mTORC1 negatively regulates insulin signalling – implications for insulin resistance.....	12
1.5.2 mTORC1 in bone – integrating bone development and skeletal regulation of glucose metabolism?.....	14
1.6 The discovery of the OCN receptor, GPRC6A, and its role in male fertility .....	16
1.7 Endocrine roles of OCN in humans .....	21
1.7.1 Differences in the regulation of OCN between mice and humans .....	21
1.7.2 Clinical observations of OCN in humans .....	22
1.8 OCN and evidence for other osteokines.....	24
1.9 Summary and Objectives.....	25
1.10 References .....	27
<b>CHAPTER 2: LOSS OF MTORC1 FUNCTION IN PRE-OSTEOBLASTS IS ASSOCIATED WITH SYSTEMIC IMPROVEMENT IN GLUCOSE HOMEOSTASIS WHICH OCCURS INDEPENDENTLY OF OSTEOCALCIN.</b>	<b>34</b>
2.1 Abstract .....	36
2.3.1 Transgenic mice.....	39
2.3.2 Metabolic phenotyping. ....	39
2.3.3 Indirect calorimetry and body composition analyses. ....	40
2.3.4 Faecal lipid assessment. ....	40
2.3.5 ELISA. ....	40
2.3.6 Male reproductive organ assessment. ....	40
2.3.7 Histology and Immunohistochemistry.....	41

2.3.8 Protein isolation and Western blotting.....	41
2.3.9 RNA isolation and quantitative RT-PCR.....	42
2.3.10 Statistical analysis.....	42
2.4 Results .....	43
2.4.1 Loss of mTORC1 function in pre-osteoblasts is associated with altered body composition in male but not female mice .....	43
2.4.2 Improved glucose metabolism and increased insulin sensitivity in <i>Rptor<sub>ob</sub><sup>-/-</sup></i> mice.....	46
2.4.3 Male <i>Rptor<sub>ob</sub><sup>-/-</sup></i> mice have increased total energy expenditure and increase fat oxidation .....	49
2.4.4 Metabolic improvements in <i>Rptor<sub>ob</sub><sup>-/-</sup></i> mice occur independently of osteocalcin .....	52
2.4.5 Loss of mTORC1 function in pre-OBs is associated with reproductive defects in males .....	52
2.4.6 The improved metabolic profile of <i>Rptor<sub>ob</sub><sup>-/-</sup></i> mice is associated with elevated serum adiponectin levels.....	55
2.5.1 Skeletal mTORC1, insulin signalling and glucose uptake .....	59
2.5.2 Metabolic phenotypes independent of OCN <i>Rptor<sub>ob</sub><sup>-/-</sup></i> .....	60
2.5.3 Sex-dimorphism and energy imbalance in <i>Rptor<sub>ob</sub><sup>-/-</sup></i> mice .....	61
2.5.4 OCN-independent mechanisms and a possible link between local nutrient-sensing in bone and whole-body energy homeostasis .....	62
2.6 Acknowledgements .....	64
2.7 Supplementary data .....	64
2.7.1 Supplementary Figures .....	64
2.7.2 Supplementary Tables.....	70
2.8 References .....	72
<b>CHAPTER 3: LOSS OF BONE-SPECIFIC MTORC1 PROTECTS AGAINST DIET-INDUCED OBESITY AND ASSOCIATED METABOLIC DYSFUNCTION .....</b>	<b>75</b>
3.1 Abstract .....	77
3.2 Introduction .....	79
3.3 Materials and Methods .....	82
3.3.1 High-fat diet studies.....	82
3.3.2 Calculation of Food Quotient. ....	82
3.3.3 Histology and Immunohistochemistry.....	82
3.3.4 Protein isolation and Western blotting.....	82
3.3.5 RNA isolation and quantitative RT-PCR.....	82
3.3.6 RNA high-throughput sequencing and gene expression analysis.....	82
3.4 Results .....	84

3.4.1 <i>Rptor<sub>ob</sub><sup>-/-</sup></i> mice are protected against high-fat diet-induced obesity.....	84
3.4.2 <i>Rptor<sub>ob</sub><sup>-/-</sup></i> mice are resistant to liver steatosis and adipocyte hypertrophy and exhibit increased browning of white adipose tissue .....	87
3.4.3 <i>Rptor<sub>ob</sub><sup>-/-</sup></i> mice are resistant to diet-induced insulin resistance .....	92
3.4.6 Transcriptional changes associated with OB-specific <i>Rptor</i> deletion in male HFD-fed mice. ....	98
3.4.5 Increased insulin signalling and glycolysis in bone of <i>Rptor<sub>ob</sub><sup>-/-</sup></i> mice .....	101
3.5 Discussion .....	105
3.5.1 Increased OB insulin signalling.....	105
3.5.2 Osteoblast glucose uptake and utilisation.....	106
3.5.3 Whole-body metabolic flexibility.....	107
3.6 Acknowledgements .....	109
3.7 Supplementary data .....	110
3.7.1 Supplementary Figures .....	110
3.7.2 Supplementary Table .....	115
3.8 References .....	119
<b>CHAPTER 4: DISCUSSION AND CONCLUSION.....</b>	<b>124</b>
4.1 General Discussion.....	125
4.2 Future directions.....	139
4.3 Conclusion.....	144
4.4 References .....	145
<b>APPENDIX I: GSEA REPORT FOR POSITIVELY ENRICHED GENE SETS</b>	<b>152</b>
<b>APPENDIX II: GSEA REPORT FOR NEGATIVELY ENRICHED GENE SETS</b>	<b>156</b>
<b>APPENDIX III: DETAILS OF AMENDMENTS MADE TO THE THESIS.....</b>	<b>161</b>

## ABSTRACT

Recent studies have shown that osteoblasts (OBs), the bone-forming cells of the skeleton, play a central role in regulating systemic glucose metabolism, with dysregulation of insulin signalling in OBs eliciting profound effects on glucose homeostasis. mTORC1 is the primary nutrient sensor in eukaryotic cells that coordinates anabolic and catabolic processes to control cell growth. mTORC1 is a crucial mediator and prolonged mTORC1 activation leads to insulin resistance suggesting modulation of mTORC1 function in OBs may affect glucose homeostasis. Furthermore, as aberrant activation of mTORC1 signalling leads to the development of insulin resistance, a chronic pathology associated with the development of type 2 diabetes mellitus (T2DM), aberrant mTORC1 signalling in OBs may contribute to the development of T2DM and associated diseases.

This project investigated the role of OB-specific mTORC1 in the regulation of systemic glucose and energy metabolism. To achieve this, mice with conditional deletion of *Rptor*, an essential component of mTORC1, in pre-OBs were utilised (*Rptor<sub>ob</sub><sup>-/-</sup>*). The metabolic phenotype of these mice was evaluated using a complementary suite of metabolic tests, coupled with detailed assessment of the effect of OB-specific mTORC1 disruption on insulin-responsive tissues. The role of skeletal mTORC1 signalling in the development of insulin resistance in response to an obesogenic high fat diet (HFD; 40% calories from fat) was also explored.

*Rptor<sub>ob</sub><sup>-/-</sup>* mice exhibited enhanced insulin secretion and sensitivity when fed with a normal diet. While both sexes were markedly lean and showed a preference for fat utilisation and elevated ketone body levels, sex-dependent differences in body composition and energy metabolism were observed. Specifically, a significant decrease in fat mass, white adipocyte size and an increase in glucose tolerance was observed in male, but not female, *Rptor<sub>ob</sub><sup>-/-</sup>* mice compared to controls. Mechanistically, these improved metabolic indices were found to occur independently of osteocalcin, the major bone secretagogue, and instead were likely attributable to elevated adiponectin levels arising from increased bone marrow adiposity.

When placed on HFD for 12 weeks, *Rptor<sub>ob</sub><sup>-/-</sup>* mice were resistant to diet-induced weight gain and displayed a significant reduction in fat mass, adipocyte hypertrophy and hepatic steatosis. *Rptor<sub>ob</sub><sup>-/-</sup>* mice had significantly lower fasting glucose and insulin

levels and exhibited increased tolerance to glucose and improved insulin sensitivity. The obesity-resistant phenotype of *Rptor<sub>ob</sub><sup>-/-</sup>* mice was independent of food intake, physical activity or lipid absorption. Instead, *Rptor<sub>ob</sub><sup>-/-</sup>* mice maintained greater substrate flexibility and exhibited browning of white adipose.

RNA-sequencing and gene set enrichment analysis revealed positively enriched gene sets for glycolysis and insulin signalling pathways in the bones of *Rptor<sub>ob</sub><sup>-/-</sup>* mice. Consistent with this, potentiated insulin signalling was observed in *Rptor<sub>ob</sub><sup>-/-</sup>* bone and *Rptor* knockout OBs *in vitro* where a profound increase in basal and insulin-dependent glucose uptake was observed.

The studies detailed in this thesis demonstrate that suppression of skeletal mTORC1 signalling in mice leads to a dramatic improvement in glucose metabolism and protection from diet-induced obesity and insulin resistance. Collectively, these results point to a critical role for the mTORC1 complex in osteoblasts in integrating whole-body nutrient status and local insulin signalling to maintain systemic glucose homeostasis.

## DECLARATION

I certify that this work contains no material which has been accepted for the award of any other degree or diploma in my name, in any university or other tertiary institution and, to the best of my knowledge and belief, contains no material previously published or written by another person, except where due reference has been made in the text. In addition, I certify that no part of this work will, in the future, be used in a submission in my name, for any other degree or diploma in any university or other tertiary institution without the prior approval of the University of Adelaide and where applicable, any partner institution responsible for the joint-award of this degree.

I acknowledge that copyright of published works contained within this thesis resides with the copyright holder(s) of those works.

I also give permission for the digital version of my thesis to be made available on the web, via the University's digital research repository, the Library Search and also through web search engines, unless permission has been granted by the University to restrict access for a period of time.

I acknowledge the support I have received for my research through the provision of an Australian Government Research Training Program Scholarship.

Signed:

Pawanrat Tangseefa

## ACKNOWLEDGEMENT

I would like to express my deep sense of gratitude and profound respect to my incredibly amazing supervisors Prof. Andrew Zannettino, Dr. Stephen Fitter and Dr. Sally Martin. Your continued motivation and support over the years has truly made the completion of this thesis a reality. Thank you Andrew for letting me to be part of your lab and allowing me to experience the closeness of “family” again while being away from home. Thank you Sally for all the helps with animal experiments, insightful suggestions and always encouraging feedbacks. Thank you Steve, without your undeniably supportive attitude in times of emotional and academic breakdowns, I would not have gotten this far. The ‘Fitter’ analogy of a thesis completion graph will be forever embedded as part of the very many fond memories during my time as a PhD student. Thank you all for your faith in me even at times when I doubted myself and always lighting up the hope when the path ahead seemed a little too dark. I could not have hoped to have better supervisors, mentors and “family” for this chapter of my life.

My sincere thanks are to Prof. Christopher Proud, Prof. Amanda Page, Prof. Gary Witter and A/Prof Paul Baldock for critical review in perfecting the manuscripts and providing insightful comments, information and suggestions on different aspects of my project. I would especially thank Prof. Amanda Page for assisting me with an early-morning metabolic cages set-up and data analysis.

I would also like to acknowledge Adelaide Graduate Research Scholarship and Adelaide Medical School short-term Scholarship for financial assistant during my PhD study.

Thank you to all the students, both past and present, of the Myeloma Research Laboratory and Mesenchymal Stem Cell Laboratory who have, physically and emotionally, helped and encouraged me over years: Dr. Chee Man Cheong, Dr. Ankit Dutta, Dr. Natasha Friend, Kimberley Evans, Mara Zeissig, Khatora Opperman, Natalya Plakhova, Justine Clark, Chee Ho H'ng and Clara Pribadi.

Thank you also to all the post doctorate researchers and laboratory officers who have provided their support and expertise during my time: Rosa Harmer, Sharon Paton, Alanah Bradey, Dr. Kate Vandyke, Dr. Melissa Cantley, Dr. Jacqueline Noll, Dr. Bill Panagopoulos, Dr. Duncan Hewett, Dr. Krzysztof Mroziak, Dr. Agnes Arthur, Dr. Esther Camp-Dotlic, Dr. Jim Cakouros and Prof. Stan Gronthos. Special thanks to Vicki



Wilczek for assisting with mouse genotyping and running several qRT-PCR. Also thank you to Proud's lab research assistants, Lauren Sandeman and Wan Xian Kang, for sharing and introducing several 'shortcut' molecular techniques that have made my life a lot easier.

Many other people in SAHMRI have also assisted in this project. Thank you Dr. Mark Van Der Hoek for preparing cDNA library and running RNA-sequencing, Dr. Jimmy Breen for sharing his expertise in bioinformatics and analysing the RNA-sequencing data, Chui Yan Mah (Shanice) for helping with gene set enrichment analysis. I would also like to acknowledge the staffs at SAHMRI Bioresources, especially Rianna Fitzgerald, Dylan Harnas and Amanda Wilson for providing training and taking care of my mice throughout these years. To members of Reproductive Immunology Lab, Dr. Peck Yin Chin (Loretta) and Camilla Dorian, thanks for assisting me with mouse DXA scanning and analysis.

Thank you to the previous students at the Adelaide Oversea Student Accommodation: Haruka Ishimoto, Leong Weng Heng, Vannica Pich, John Bosco Yu, Douglas Sia, Yuan Qi Yeoh and Vione Chin. Our late night ice-cream and chit-chat sessions, dinner, Saturday brunch and grocery shopping that have helped to relax and re-energise me. A very special thank you to Dr. Michael Herrera for all the delicious meals, grammatical correction, valuable advices and words of encouragement.

Finally, the biggest thank you goes to my parents and my lovely two younger sisters for their love and endless support throughout the year. Without for you all in my life, I would not be who I am, nor would I have achieved this their accomplishment. To my loving and encouraging partner, Soh Zhi Qin. Thank you for your never-ending patience, companion, care and love throughout the hard time and always motivating me to do my best.

Thank you all for being with me in this 'Journey'... I could not have done it without any of you.

## LIST OF ABBREVIATIONS

ATGL	Adipose triglyceride lipase	INSR	Insulin receptor
AN	Anorexic nervosa	IRS1	Insulin receptor substrate 1
AMPK	AMP-dependent kinase	ITTs	Insulin tolerance tests
AUC	Area under the curve	KO	Knock out
BCAAs	Branched chain amino acids	MC4R	Melancortin 4 receptor
BMAT	Bone marrow adipose tissue	LCN2	Lipocalin 2
BMP7	Bone morphogenetic protein 7	LDHA	Lactate dehydrogenase A
CREB	cAMP response element binding protein	LH	Luteinizing hormone
CTSK	Cathepsin K	LMW	Low molecular weight
DEGs	Differentially-expressed genes	LPL	Lipoprotein lipase
DNL	<i>De novo</i> lipogenesis	NPY	Neuropeptide Y
DR	Dietary restriction	OB	Osteoblasts
DXA	Dual X-ray absorbitometer	OC	Osteoclasts
ECM	Extracellular matrix	OCN	Osteocalcin
Fasn	Fatty acid synthase	OGN	Osteoglycin
FFA	Free fatty acids	OPG	Osteoprotegerin
FGF21	Fibroblast growth factor 21	OST-PTP	Osteotesticular protein tyrosine phosphatase
FQ	Food quotient	PDK1	Phosphoinositide-dependent kinase-1
GAP	GTPase-activating protein	PFKM1	6-Phosphofructokinase
Gla	$\gamma$ -carboxyglutamyl	PGK1	Phosphoglycerate kinase 1
Glu	Glutamic acid	PI3K	Phosphatidylinositol 3-kinase
GLUT1	Glucose transporter 1	PTP1B	Protein-tyrosine phosphatase 1B
GLUT4	Glucose transporter 4	RQ	Respiratory quotient
GnRH	Gonadotropin-releasing hormone	PPAR $\gamma$	peroxisome proliferator-activated receptor $\gamma$
Grb10	Growth factor receptor-bound protein 10	RTK	Receptor tyrosine kinase
GSEA	Gene Set Enrichment Analysis	RANKL	Receptor activator of nuclear factor kappa B ligand
GSIS	Glucose-stimulated insulin secretion tests	SERCA	Sarco/Endo-plasmic reticulum (SR/ER) Ca <sup>2+</sup> -ATPase
GSK3 $\beta$	Glycogen synthases 3 $\beta$	SHBG	Sex hormone-binding globulin
GTTs	Glucose tolerance tests	SOST	Sclerostin
gWAT	Gonadal white adipose tissue	T2DM	Type 2 diabetes mellitus
HFD	High fat diet	TCA	Tricarboxylic acid
HIFs	Hypoxia-inducible factors	TEE	Total energy expenditure
HKII	Hexokinase 2	TG	Triglycerides
HMW	High molecular weight	UCP1	Uncoupling protein 1
HOMA-IR	resistance	unOCN	undercarboxylated Ocn
iAUC	Incremental area under the curve	VHL	Von Hippel–Lindau
IL-6	Interleukin-6	WAT	White adipose tissue
iBAT	Interscapular brown adipose tissue	WT	Wild type
iWAT	Inguinal white adipose tissue	$\beta$ OHB	$\beta$ -hydroxybutyrate

## LIST OF PUBLICATIONS

### Scientific Manuscripts

1. Tangseefa P, Martin SK, Fitter S, Baldock PA, Proud CG, Zannettino ACW. Osteocalcin-dependent regulation of glucose metabolism and fertility: Skeletal implications for the development of insulin resistance. *Journal of Cellular Physiology*. 2018 May;233(5):3769-3783. doi: 10.1002/jcp.26163.

2. Tangseefa P, Martin SK, Chin PY, Baldock PA, Wittert GA, Page AJ, Proud CG, Fitter S, Zannettino ACW. The mTORC1 complex in pre-osteoblasts regulates whole-body energy metabolism independently of osteocalcin. *Nature Communication*. (Submitted).

### Conference Proceedings

1. South Australian Health and Medical Research Institute (SAHMRI) Annual Scientific Meeting. Adelaide, South Australia. October 2019. *Poster Presentation*: Loss of bone-specific mTORC1 protects against diet-induced obesity and induces browning of white fat

2. 13<sup>th</sup> Annual Florey Postgraduate Research Conference, Faculty of Health Science, Adelaide, South Australia, Adelaide. September 2019. *Poster Presentation*: Loss of bone-specific mTORC1 protects against diet-induced obesity and induces browning of white fat

3. 5<sup>th</sup> International Meeting on Bone Marrow Adiposity, Odense, Denmark. August 2019. *Oral Presentation*: Inactivation of osteoblast-specific nutrient sensing mTORC1 mimic metabolic improvement properties of caloric restriction

4. South Australian Health and Medical Research Institute (SAHMRI) Annual Scientific Meeting. Adelaide, South Australia. October 2018. *Poster presentation*: Metabolic and reproductive abnormalities in mice with impaired skeletal-mTORC1 function mirror a dietary restriction phenotype

5. 12<sup>th</sup> Annual Florey Postgraduate Research Conference, Faculty of Health Science, Adelaide, South Australia, Adelaide. September 2018. *Poster presentation*: Metabolic and reproductive abnormalities in mice with impaired skeletal-mTORC1 function mirror a dietary restriction phenotype

6. Adelaide Protein Group (APG) Student Awards, Adelaide, South Australia, Adelaide. May 2018. *Oral Presentation (finalist)*: Metabolic and reproductive abnormalities in mice with impaired skeletal-mTORC1 function mirror a dietary restriction phenotype

7. South Australian Health and Medical Research Institute (SAHMRI) Annual Scientific Meeting. Adelaide, South Australia. October 2017. *Poster Presentation:* Metabolic and reproductive abnormalities in mice with impaired skeletal-mTORC1 function mirror a dietary restriction phenotype
8. ANZOS-OSSANZ-AOCO Joint Annual Scientific Meeting 2017, Adelaide, South Australia. October 2017. *Oral Presentation:* Metabolic and reproductive abnormalities in mice with impaired skeletal-mTORC1 function mirror a dietary restriction phenotype
9. 11<sup>th</sup> Annual Florey Postgraduate Research Conference, Faculty of Health Science, Adelaide, South Australia, Adelaide. September 2017. *Poster Presentation:* Metabolic and reproductive abnormalities in mice with impaired skeletal-mTORC1 function mirror a dietary restriction phenotype
10. Joint Annual Scientific Meeting of the Endocrine Society of Australia and the Society for Reproductive Biology, Perth, Western Australia, Australia. August 2017. *Oral Presentation:* Metabolic and reproductive abnormalities in mice with impaired skeletal-mTORC1 function mirror a dietary restriction phenotype
11. EMBL PhD training course, Monash University, Melbourne, Victoria, Australia. July 2017. *Poster Presentation:* Metabolic and reproductive abnormalities in mice with impaired skeletal-mTORC1 function mirror a dietary restriction phenotype
12. Australian Society for Medical Research (ASMR) SA Scientific Meeting. Adelaide, South Australia, Australia. June 2017. *Oral Presentation:* The role of osteoblast-mTORC1 in the regulation of glucose metabolism.
13. South Australian Health and Medical Research Institute (SAHMRI) Annual Scientific Meeting. Adelaide, South Australia. October 2016. *Poster Presentation:* The role of osteoblast-mTORC1 in the regulation of glucose metabolism.
14. 6<sup>th</sup> Australia and New Zealand Society for Cell and Developmental Biology Adelaide Meeting, Adelaide, South Australia, Australia. November 2016. *Poster Presentation:* The role of osteoblast-mTORC1 in the regulation of glucose metabolism.
15. 11<sup>th</sup> Annual Florey Postgraduate Research Conference, Faculty of Health Science, Adelaide, South Australia, Adelaide. September 2017. *Poster Presentation:* The role of osteoblast-mTORC1 in the regulation of glucose metabolism.

*“It always seems impossible until it’s done” – Nelson Mandela*

**CHAPTER 1:**  
**INTRODUCTION**

**Osteocalcin-dependent regulation of glucose metabolism and fertility: skeletal implications for the development of insulin resistance.**

Pawanrat Tangseefa<sup>1,2</sup>, Sally K Martin<sup>1,2</sup>, Stephen Fitter<sup>1,2</sup>, Paul A Baldock<sup>3</sup>,  
Christopher G Proud<sup>4,5,6</sup>, Andrew CW Zannettino<sup>1,2</sup>

<sup>1</sup> Myeloma Research Laboratory, Adelaide Medical School, Faculty of Health and Medical Science, University of Adelaide, Adelaide, SA 5005, Australia

<sup>2</sup> Cancer Theme, South Australian Health and Medical Research Institute, Adelaide, SA 5001 Australia

<sup>3</sup> Skeletal Metabolism Group, Garvan Institute of Medical Research, Sydney, NSW 2010, Australia

<sup>4</sup> Nutrition & Metabolism Group, South Australian Health and Medical Research Institute, Adelaide, SA 5001, Australia

<sup>5</sup> School of Biological Sciences, University of Adelaide, Adelaide, SA 5005, Australia

<sup>6</sup> Department of Biochemistry and Genetics, School of Medicine, Zhejiang University, Hangzhou 310058, People's Republic of China

**Keywords:** glucose metabolism, insulin resistance, male fertility, mTORC1, osteocalcin

Chapter 1 incorporates the following published review article:

Tangseefa P, Martin SK, Fitter S, Baldock PA, Proud CG, Zannettino ACW. Osteocalcin-dependent regulation of glucose metabolism and fertility: Skeletal implications for the development of insulin resistance. *Journal of Cellular Physiology*. 2018 May;233(5):3769-3783. doi: 10.1002/jcp.26163.

## 1.1 Abstract

The skeleton has recently emerged as a critical insulin target tissue that regulates whole body glucose metabolism and male reproductive function. While our understanding of these new regulatory axes remains in its infancy, the bone-specific protein, osteocalcin, has been shown to be centrally involved. Undercarboxylated osteocalcin acts as a secretagogue in a feed-forward loop to stimulate pancreatic  $\beta$ -cell proliferation and insulin secretion, improve insulin sensitivity and promote testosterone production. Importantly, dysregulation of insulin signalling in bone causes a reduction in serum osteocalcin levels that is associated with elevated blood glucose and reduced serum insulin levels, suggesting the significant role of the skeleton in the development of diet-induced insulin resistance. Insulin signalling is negatively regulated by the mammalian target of rapamycin complex 1 (mTORC1) which becomes hyper-activated in response to nutrient overload. Loss- and gain-of function models suggest that mTORC1 function in bone is essential for normal skeletal development; however, the role of this complex in the regulation of glucose metabolism remains to be determined. This review highlights our current understanding of the role played by osteocalcin in the skeletal regulation of glucose metabolism and fertility. In particular, it examines data emerging from transgenic mouse models which have revealed a pancreas-bone-testis regulatory axis and discusses recent human studies which seek to corroborate findings from mouse models with clinical observations. Moreover, we review recent studies which suggest dysregulation of insulin signalling in bone leads to the development of insulin resistance and discuss the potential role of mTORC1 signalling in this process.



## 1.2 Introduction

Bone is a specialized connective tissue that provides mechanical support for organs, acts as an anchor site for muscles to facilitate locomotion, protects vital organs, houses the hematopoietic bone marrow and serves as a metabolic reservoir for calcium and phosphate to maintain mineral homeostasis. In healthy adults, old bone is constantly being resorbed by osteoclasts (OCs) and new bone is formed by osteoblasts (OBs) in a coordinated process known as bone remodeling<sup>1</sup>. Under normal physiological conditions, the two phases of bone remodelling (i.e. bone resorption and bone formation) occur in a sequential and balanced manner to maintain a net balance in bone volume.

Maintenance of skeletal integrity comes at a high cost in terms of energy demand. This is best illustrated in anorexia nervosa, where reduced food intake leads to impaired bone growth in children and low bone mass in adults<sup>2,3</sup>. Conversely, obesity is associated with an increase in bone density and protection against osteoporosis in males<sup>4</sup>. Moreover, osteoporosis is positively associated with sarcopenia, whereas increased muscle mass is associated with increased bone mass and reduced fracture risk in post-menopausal women<sup>5</sup>. Skeletal integrity and bone growth are also influenced by sex steroid hormones; gonadal failure in both genders triggers bone loss, and the absence of sex hormones in post-menopausal women leads to osteoporosis<sup>6,7</sup>. Taken together, these clinical observations highlight the existence of an interconnected regulatory network coordinating bone growth, energy metabolism and reproductive function.

The OB-specific protein, osteocalcin (OCN), has recently been identified as a hormone that regulates glucose homeostasis, energy expenditure, male fertility, brain development and cognition. OCN is regulated by insulin signalling in OBs (Figure 1.1) and, in a feed-forward loop, OCN stimulates pancreatic  $\beta$ -cell proliferation and insulin secretion and improves insulin sensitivity in peripheral tissues. This newly assigned metabolic role for the skeleton raises important questions as to the normal physiological and pathophysiological regulation of glucose metabolism by the skeleton. This review focuses on the role played by OCN in the skeletal regulation of glucose metabolism and male fertility and highlights the importance of the skeleton in the regulation of whole-body metabolism. Furthermore, this review describes recent studies which suggest that dysregulation of insulin signalling in bone leads to the development of insulin resistance and discusses the potential role of mTORC1 signalling in this process.

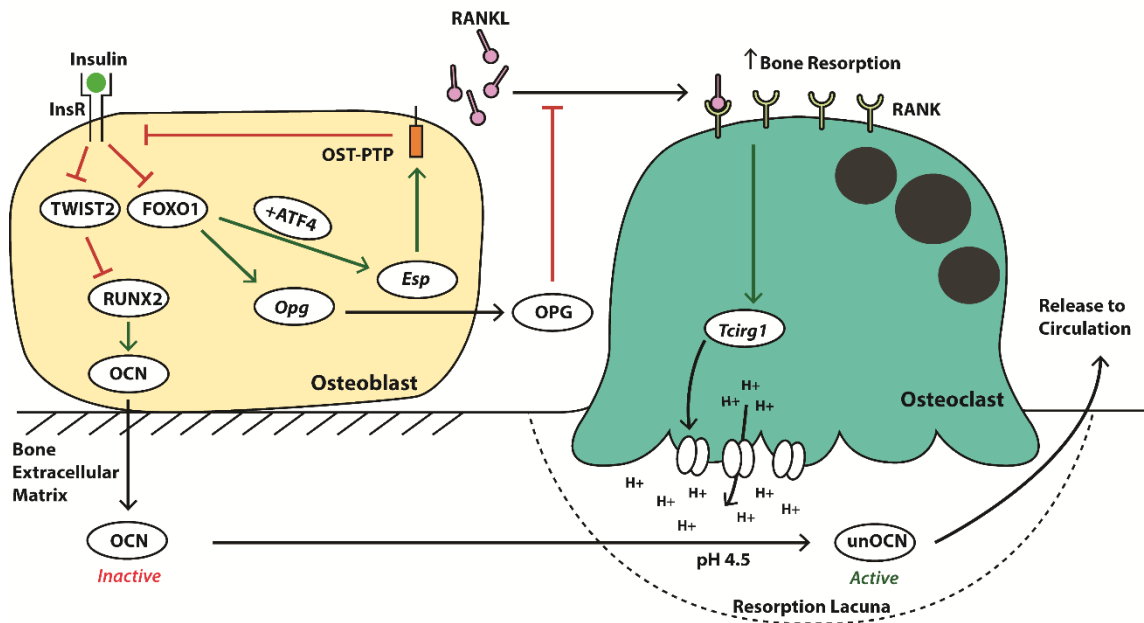


**Figure 1.1 Insulin signalling in osteoblasts promotes osteocalcin bio-activation.** In the absence of insulin, FOXO1, in cooperation with ATF4, activates *Esp* gene expression and the production of OST-PTP, which in turn negatively regulates InsR signalling. FoxO1 also increases expression of *Opg*, a decoy receptor for RANKL, which inhibits osteoclast differentiation and bone resorption by interrupting the interaction between RANKL and RANK, a receptor for RANKL. Simultaneously, FOXO1 and TWIST2 act on RUNX2 to prevent *Bglap*, gene encoding OCN expression, and OCN production. Activation of insulin signalling inhibits FOXO1 and TWIST2 which promotes OCN production and activation (via decarboxylation). Insulin suppresses OPG production, which stimulates osteoclast activity and the formation of an acidic resorption lacunae, facilitating the decarboxylation of OCN into its bio-active, undercarboxylated form (unOCN) and its release into the circulation. (Modified from <sup>35</sup> with permission from the publisher, Elsevier.)

### 1.3 The discovery of OCN as an endocrine regulator of energy metabolism

OCN is a highly conserved 11kDa protein that is initially synthesized as pre-pro-OCN, which undergoes proteolytic cleavage to form the mature OCN peptide<sup>8</sup>. OCN undergoes further posttranslational modification in the lumen of the endoplasmic reticulum, whereby a second carboxyl group is added to glutamic acid (Glu) residues 13, 17 and 20 (mouse) or 17, 21 and 24 (human) to form  $\gamma$ -carboxyglutamyl (Gla) residues. This vitamin K (VK)-dependent  $\gamma$ -carboxylation leads to a conformational change in OCN that confers a high affinity for calcium and hydroxyapatite, the mineral component of the bone extracellular matrix (ECM)<sup>9</sup>. During bone remodelling, the low pH present within OC resorption lacunae promotes the decarboxylation of Gla-OCN into Glu-OCN (herein referred to as undercarboxylated OCN (unOCN)), which reduces its affinity for bone and facilitates its release into the circulation<sup>10</sup>.

OCN is the most abundant non-collagen bone matrix protein and has been widely used as a biochemical serum marker of bone formation<sup>11</sup>. While the precise molecular mechanisms remain unclear, OCN has been shown to control bone mineralization and to limit bone formation in mice<sup>12</sup>. Intriguingly, in addition to having an increased bone mass phenotype, *Ocn* knockout mice (*Ocn*<sup>-/-</sup>) have increased levels of visceral fat<sup>12,13</sup>, which suggests that OCN may also regulate energy metabolism. In line with this, *Ocn*<sup>-/-</sup> mice exhibit hyperglycaemia, hypoinsulinemia, impaired insulin secretion and sensitivity and are glucose intolerant<sup>13</sup>. These defects in glucose homeostasis are accompanied by a reduction in pancreatic islet size and number and reduced  $\beta$ -cell mass and insulin content<sup>13</sup>. *In vitro*, OCN increases glucose-stimulated insulin secretion in  $\beta$ -cells, maintained in either low or high glucose<sup>14</sup> and dose-dependently induces the expression of  $\beta$ -cell *Ins1*, *Ins2*, *Ccnd2* and *Cdk4*<sup>15</sup>. *In vivo*, long-term administration of OCN to wild-type (WT) mice improves glucose-stimulated insulin secretion and glucose tolerance<sup>15</sup>. Taken together, these findings demonstrate that OCN directly acts on pancreatic  $\beta$ -cells to promote insulin expression and secretion and  $\beta$ -cell proliferation.

#### 1.3.1 Sensitizing effects of OCN: direct and indirect mechanisms

Despite increased levels of visceral fat, the insulin-resistant phenotype observed in *Ocn*<sup>-/-</sup> mice is associated with significantly lower serum levels of adiponectin, an adipocyte-specific insulin-sensitizing hormone<sup>13</sup>. This observation suggests that OCN may also regulate insulin sensitivity via adiponectin. Indeed, compound mice harbouring a

heterozygous deletion of *Ocn* and *Adipoq* exhibit lower adiponectin levels and are insulin resistant, despite no detectable changes in insulin secretion, fasting glucose levels and serum insulin levels<sup>13</sup>. Furthermore, mice deficient in *Esp* (encoding osteotesticular protein tyrosine phosphatase (OST-PTP)), which regulates OCN carboxylation: *Esp*<sup>-/-</sup> mice) display improved glucose tolerance and increased insulin sensitivity, a metabolic phenotype which is opposite to that observed in *Ocn*<sup>-/-</sup> mice<sup>13</sup>. Importantly, *Esp*<sup>-/-</sup> mice also have significantly elevated serum unOCN levels and increased adiponectin levels<sup>13</sup>. Furthermore, *in vitro* studies have shown that supplementation of adipocyte cultures with unOCN, but not Gla-OCN, results in a dose-dependent increase in adiponectin expression<sup>13,15</sup>. Uncarboxylated OCN has subsequently been shown to induce an accumulation of cAMP in adipocytes that activates CREB (cAMP response element binding protein) leading to the upregulation of peroxisome proliferator-activated receptor  $\gamma$  (*PPAR* $\gamma$ ) and induction of adiponectin gene expression<sup>16</sup>. It should also be noted that addition of adiponectin to OB cultures stimulates OCN secretion<sup>17</sup>, and siRNA-mediated knockdown of *AdipoR1* in MC3T3-E1 cells, leads to a decrease in OCN expression<sup>18</sup>. These data suggest that an endocrine loop between bone and adipose tissue may exist, where OCN regulates adipose-derived adiponectin levels and insulin sensitivity and, in turn, adiponectin acts on bone to regulate OCN levels.

Independent to the insulin-sensitizing effects of adiponectin, OCN can also directly regulate glucose metabolism in skeletal muscle. *In vitro*, unOCN enhances insulin-stimulated glucose uptake and up-regulates Akt signalling by activation of ERK kinase (MEK) in differentiated C2C12 myotubes<sup>19</sup>. *In vivo*, transient or chronic administration of unOCN to 12-week-old mice was found to improve the exercise capacity of WT mice without affecting insulin levels<sup>20</sup>. Furthermore, chronic administration of unOCN to aged mice (15 months of age) restored their exercise capacity to the same level as 3-month-old mice and led to increased muscle mass<sup>20,21</sup>. This improvement in exercise capacity can be attributed to the OCN-dependent increase in glycogen and fatty acid catabolism in muscle fibers<sup>21</sup>. Furthermore, OCN signalling in muscle fibres directly stimulates glucose uptake by inducing the translocation of the glucose transporter, GLUT4, to the plasma membrane<sup>21</sup>. OCN was identified as a major regulator of interleukin-6 (IL-6) expression in muscle, a myokine whose plasma levels increase during exercise and enhances exercise capacity. IL-6 promotes glucose uptake and fatty acid oxidation in muscle and stimulates hepatic gluconeogenesis and glucose release<sup>22</sup>.

Moreover, *in vitro*, IL-6 stimulates the expression of *Rankl* and suppresses *Opg* in OBs, factors that favour bone resorption<sup>21</sup>. Thus, in a feedforward loop, OCN stimulates IL-6 production in muscle which in turn binds to OBs to favour the decarboxylation (activation) of OCN by stimulating bone resorption.

### ***1.3.2 The undercarboxylated form of OCN is responsible for the metabolic functions of OCN***

While both Gla-OCN and unOCN are detectable in the peripheral circulation<sup>23,24</sup>, several *in vivo* mouse models have suggested that the endocrine functions of OCN are mediated by unOCN, and not Gla-OCN. unOCN administration to WT mice significantly improves glucose tolerance and insulin sensitivity<sup>25,26</sup>, and intermittent injection of unOCN can protect mice from diet-induced insulin resistance and obesity<sup>25</sup>. Moreover, unOCN administration to *Ocn*<sup>-/-</sup> mice improves their glucose tolerance and insulin secretion<sup>13</sup>. In addition, partial or complete OB-specific inactivation of  $\gamma$ -glutamyl carboxylase (*Ggcx*), results in a 3-fold or >15-fold increase in unOCN levels, respectively<sup>27</sup>. This increase in unOCN levels is associated with either unchanged or decrease in circulating levels of Gla-OCN in the partial or complete OB-specific inactivation of *Ggcx*, respectively, (with total OCN levels remaining unchanged), and improved glucose tolerance in mice fed with normal chow<sup>27</sup>. Importantly, inactivation of OB-specific *Ggcx* is sufficient to prevent diet-induced glucose intolerance in mice fed with a high fat diet (HFD)<sup>27</sup>. Conversely, while *in vivo* administration of Gla-OCN has not been performed so far, *in vitro* studies have revealed that Gla-OCN fails to induce *Adipoq* expression in cultured adipocytes and *Ins* and *Ccnd1* expression in islet cultures<sup>13</sup>. Taken together, these data demonstrate that the endocrine function of OCN is mediated by unOCN, but not Gla-OCN.

## **1.4 Insulin signalling, bone remodelling and regulation of OCN**

### ***1.4.1 Insulin signalling in OBs favours bone remodelling to increase OCN bioactivity***

OBs express abundant levels of the insulin receptor (INSR) and respond to insulin by upregulating the expression of anabolic bone markers and increasing collagen synthesis, alkaline phosphatase production and glucose uptake<sup>28,29</sup>. In addition, localized insulin delivery accelerates fracture healing by enhancing bone formation *in vivo*<sup>30</sup>, whereas insulin deficiency, as observed in patients with type 1 diabetes, is associated with low bone mass, early onset of osteopenia or osteoporosis and an elevated risk of bone fracture<sup>31</sup>.

Insulin signalling in OBs controls OB development and differentiation. Mice with OB-specific deletion of INSR ( $INSR^{OB-/-}$ ) display impaired postnatal trabecular bone formation and decreased serum levels of bone resorption markers<sup>32</sup>, and the addition of insulin to OB cultures increases OB proliferation and differentiation<sup>33</sup>. While OC numbers in  $INSR^{OB-/-}$  mice are unchanged compared to controls, OC activity is significantly reduced<sup>32</sup>. This reduction in OC activity is secondary to increased expression of osteoprotegerin (OPG), a soluble decoy receptor for the potent osteoclastic factor, receptor activator of nuclear factor kappa B ligand (RANKL). Binding of OPG to RANKL prevents the binding of RANKL to the RANK receptor on OCs, thereby inhibiting osteoclastogenesis (Figure 1.1).

Importantly,  $INSR^{OB-/-}$  mice have significantly decreased serum levels of total OCN and unOCN compared to WT controls. The impaired OC activity and low circulating unOCN levels in  $INSR^{OB-/-}$  mice suggests that OCs might be responsible for the decreased decarboxylation of OCN in these mice. Indeed,  $Opg^{-/-}$  mice, which exhibit increased OC numbers, have significantly higher serum unOCN levels while OC ablation in adult mice results in significantly lower serum unOCN levels<sup>34</sup>.

As outlined in Figure 1.1, insulin signalling favours bone resorption by increasing the expression of *CTSK* (Cathepsin K), a lysosomal protease, and *Tcirg1*, a proton pump component, in OCs<sup>32</sup>. The increased expression of *Tcirg1* enhances proton transport into OC resorption lacunae and increases bone matrix acidification (i.e. lowering pH), facilitating the decarboxylation of OCN and its release into the circulation. These data suggest that insulin signalling in OBs indirectly controls the bio-activation of OCN by modulating osteoclast activity<sup>35</sup>.

OB-insulin signalling also directly induces OCN expression by attenuating the negative actions of the Twist2 transcription factor on RUNX2, an OB-specific transcription factor and key activator of *Bglap*<sup>13,36</sup>. Moreover, OB-insulin signalling indirectly regulates OCN expression and activity through its downstream targets, FoxO1 and ATF4. In the absence of insulin signalling, FOXO1 induces *Esp* and *Opg* expression<sup>37</sup> and physically interacts with RUNX2 preventing it from binding to its cognate binding site within the *Bglap* promoter<sup>38</sup>. ATF4, a negative regulator of insulin signalling and a transcription factor required for OB function, has been shown to co-localize with FOXO1 to induce the expression of *Esp*<sup>39</sup>. As a result, OB-specific *FoxO1* knockout mice (*FoxO1*<sup>OB-/-</sup>) exhibit increased *Ocn* expression, decreased *Esp* expression and increased serum unOCN levels<sup>37</sup>, whereas over-expression of ATF4, either in all tissues or selectively in OBs, leads to decreased serum unOCN levels and elevated *Esp* expression<sup>40</sup>. Importantly, *FoxO1*<sup>OB-/-</sup>, *Atf4*<sup>OB-/-</sup> and *FoxO1*<sup>OB-/-</sup>*Atf4*<sup>-/-</sup> mice display improved glucose disposal and insulin sensitivity due to increased  $\beta$ -cell mass and increased serum adiponectin levels, which highlights the synergistic effect of these two OB transcription factors in regulating glucose homeostasis<sup>37,39,40</sup>. In addition, phosphorylation-mediated destabilization of FOXO1 by insulin signalling in OBs leads to nuclear exclusion of FOXO1, thereby reducing its ability to activate the *Esp* and *Opg* promoters and inhibit Runx2 activity. Thus, in a feed-forward loop, insulin signalling in OBs promotes the production of unOCN by OBs, which in turn enhances insulin production and release by pancreatic  $\beta$ -cells<sup>13,35</sup>.

#### ***1.4.2 Insulin signalling in OBs is required for proper glycaemic control***

Deletion of the INSR in OBs not only affects bone development but also results in metabolic abnormalities including hyperglycaemia, hypoinsulinemia, insulin resistance and increased peripheral adipose deposits<sup>32,35</sup>. Importantly, OBs express significant levels of GLUT4, an insulin-dependent glucose transporter<sup>41</sup>. *In vitro* ablation of GLUT4 in OBs impairs insulin-stimulated glucose uptake while OB-specific GLUT4 knockout ( $\Delta$ Glut4) mice exhibit increased peripheral fat deposition, hyperinsulinemia and insulin resistance<sup>41</sup>. Analysis of the transcript levels of insulin-sensitive genes in white adipose tissue and skeletal muscle of  $\Delta$ Glut4 mice revealed unchanged or increased expression levels, indicating that the development of insulin resistance in these mice is attributable to a defect in glucose utilization by bone cells<sup>41</sup>.

Further evidence for the importance of bone as a significant site of glucose disposal has been revealed in studies utilizing radiolabelled glucose and whole-body bio-distribution studies. Using euglycaemic hyperinsulinemic clamping, administration of 2-[U-<sup>14</sup>C] deoxyglucose to 12-week-old WT mice revealed that, in the insulin-independent manner, bone takes up 20% of the quantity of glucose taken up by skeletal muscle and 50% of what is taken up by white adipose tissue<sup>42</sup>. In a more-recent study, using anaesthetized mice to reduce variance in uptake due to locomotion, the magnitude of <sup>18</sup>F-fluorodeoxyglucose ([<sup>18</sup>F]-FDG) uptake in bone (tibia) was shown to be significantly higher than classical insulin target and glucose-storing tissues including liver, muscle (quadriceps) and adipose tissues (gonadal WAT) (50%, 80% and 90% higher in bone respectively)<sup>43</sup>. Furthermore, insulin administration significantly increased skeletal accumulation of [<sup>18</sup>F]-FDG while decreased skeletal accumulation of [<sup>18</sup>F]-FDG is observed in INSR<sup>OB-/-</sup> mice<sup>43</sup>. Importantly, in WT mice fed a HFD to induce an insulin-resistant state, the skeletal uptake of [<sup>18</sup>F]-FDG is significantly reduced<sup>43</sup>. While the mode of glucose administration, age of the mice and experimental design are likely to account for the observed difference in uptake rates observed in these studies; taken together, these results highlight the importance of the skeleton as an insulin-target tissue and raises important questions as to the role of the skeleton in the development and treatment of diet-induced induced insulin resistance.

### **1.5 Skeletal insulin resistance disrupts whole-body glucose homeostasis**

While OBs have been shown to contribute to the maintenance of whole-body glucose homeostasis, their role in the development of insulin resistance, a major cause of type 2 diabetes mellitus (T2DM), has only recently been investigated. As previously discussed, insulin signalling in OBs is essential for whole-body glucose homeostasis in mice fed with normal chow. When challenged with a HFD, mice over-expressing the INSR in OBs have smaller fat deposits and lower fasting glucose and insulin levels, metabolic responses associated with improved glucose disposal and insulin sensitivity<sup>44</sup>. Conversely, INSR<sup>OB-/-</sup> mice fed a HFD have significantly lower serum levels of unOCN and develop more severe metabolic abnormalities compared to WT littermates<sup>25</sup>. These findings suggest that insulin signalling in bone plays an important role in the development of diet-induced insulin resistance. Indeed, WT mice fed a HFD develop insulin resistance in OBs, as evidenced by a decrease in insulin-stimulated activation of AKT, an important insulin effector protein<sup>44</sup>. This decrease in responsiveness to insulin can be partially rescued by over-expressing INSR in OBs. Conversely, reducing the



level of INSR in OBs by deleting one allele of INSR (*Coll1a1-INSR<sup>+/-</sup>*) exacerbates HFD-induced skeletal insulin resistance<sup>44</sup>. Of note, the metabolic abnormalities observed in *INSR<sup>OB-/-</sup>* and *Coll1a1-INSR<sup>+/-</sup>* mice fed a HFD can be rescued by daily administration of unOCN<sup>25,44</sup>. These data demonstrate that insulin resistance in OBs leads to a reduction in serum unOCN levels which, at least in part, leads to impaired glucose tolerance and insulin resistance in mice.

### ***1.5.1 mTORC1 negatively regulates insulin signalling – implications for insulin resistance***

mTORC1 is a central regulator of growth and metabolism in all eukaryotes and is controlled by nutrients, growth factors and cellular energy status (reviewed in <sup>45</sup>). In response to insulin, mTORC1 signalling promotes mRNA translation, ribosome biogenesis, protein synthesis and the activation of anabolic cellular processes<sup>46</sup> (Fig. 1.2). mTORC1 also negatively regulates insulin signalling by disrupting the interaction between INSR and its adaptor protein, IRS1. Several pathways involved in this mTORC1-mediated negatively regulation of insulin signalling include (1) activation of S6K1 which mediates IRS1 phosphorylation at Ser 270/307/636/1101 and thus induces ubiquitin mediated-proteosomal degradation of IRS1<sup>47</sup>, (2) activation and stabilization of the receptor tyrosine kinase (RTK) inhibitor growth factor receptor-bound protein 10 (Grb10), which inhibits IRS1 from binding to activated INSR<sup>48,49</sup>, or (3) direct phosphorylation of IRS1 at Ser 636/639, sites that lie in close proximity to the PI3-kinase activation motif, the phosphorylation of which suppresses IRS1-mediated PI3-kinase activation<sup>50</sup>. Importantly, dysregulation of mTORC1 signalling has been implicated in the development of insulin resistance (reviewed in <sup>51</sup>). Under conditions of nutrient excess, hyperactivation of mTORC1 leads to sustained stimulation of S6K1 and S6K1-mediated serine phosphorylation and degradation of IRS1, which eventually results in desensitization of insulin signalling<sup>52</sup>. In this insulin-resistant state, glucose uptake in muscle and glycogen synthesis in both liver and muscle are impaired, while gluconeogenesis in liver increases. Collectively, these conditions exacerbate the hyperglycemic condition. Therefore, as a consequence of chronically high nutrient levels in the circulation, mTORC1 remains active and maintains the negative feedback loop to the INSR, ultimately leading to insulin insensitivity<sup>53</sup>.

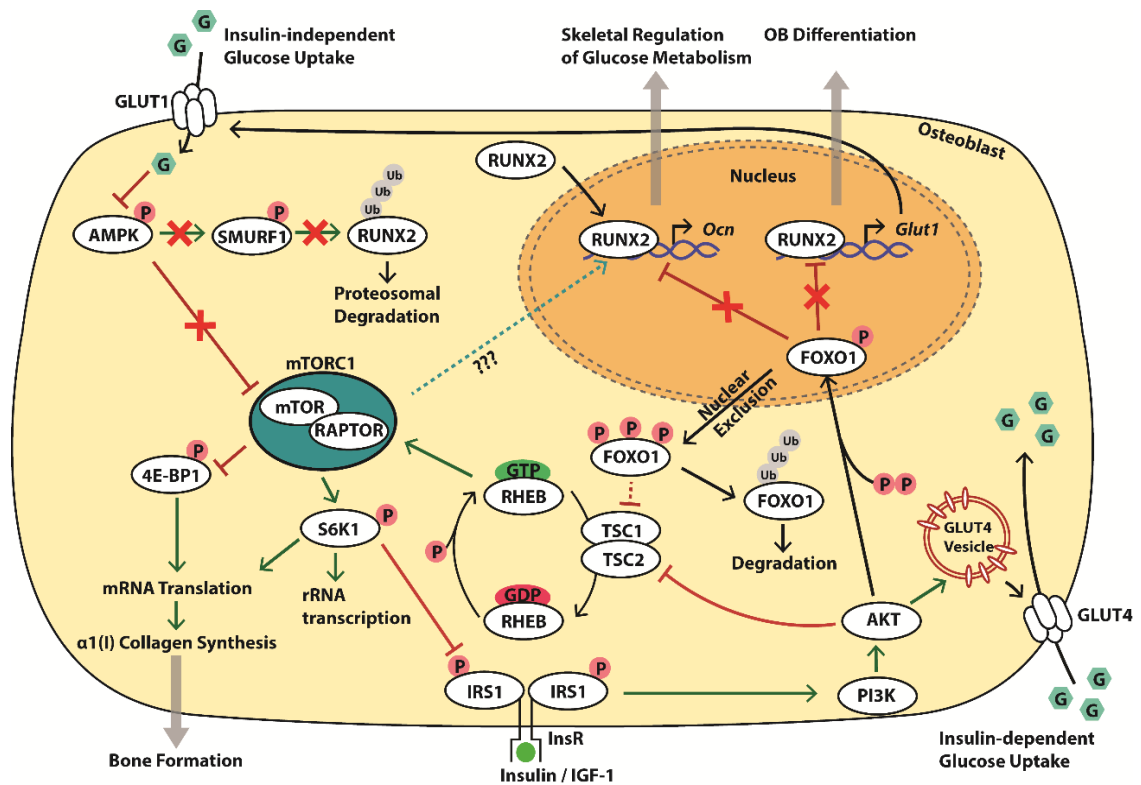


**Figure 1.2 Glucose uptake by osteoblasts integrates bone formation and the skeletal regulation of glucose metabolism.** In an insulin-independent manner, glucose uptake via GLUT1 inhibits the activity of AMPK and promotes the activity of mTORC1, resulting in increased protein synthesis. Furthermore, glucose uptake inhibits the ability of AMPK to favour RUNX2 proteosomal degradation by phosphorylating SMURF1, an E3 ubiquitin protein ligase. The accumulation of RUNX2 leads to transcriptional activation of *Glut1* and *Ocn*. OB insulin signalling activates AKT, which promotes glucose uptake into the cell by increasing translocation of GLUT4 to the plasma membrane. Activation of AKT results in the nuclear exclusion of FOXO1, thereby removing its inhibitory effects on RUNX2 transcriptional activity. Akt also attenuates the inhibitory effects of the TSC1/TSC2 complex on RHEB leading to activation of mTORC1. While not yet confirmed in OBs, the physical association of cytoplasmic FOXO1 and TSC2 could result in the degradation of the TSC1/TSC2 complex, further enhancing activation of mTORC1. In a feed-back loop, mTORC1 negatively regulates insulin signalling by disrupting the interaction between InsR and IRS1 via activation of S6K1. The molecular link between TSC-mTOR and FOXO1 suggests a role for OB mTORC1 in the regulation of bone formation, OCN production and skeletal glucose metabolism.

Deletion of the major mTORC1 effector proteins, S6K1, 4E-BP1 or 4E-BP2, in mice also causes significant perturbations in glucose metabolism. Whole-body inactivation of S6K1 leads to hypoinsulinemia, impaired glucose tolerance and reduced  $\beta$ -cell mass associated with reduced insulin secretion in mice fed with a normal diet<sup>54</sup>. These mice also maintain normal fasting glucose levels, which is suggestive of insulin hypersensitivity<sup>54</sup>, and are also protected against obesity and HFD-induced insulin resistance<sup>47</sup>. Conversely, global deletion of 4E-BP1 and 4E-BP2, which are negatively regulated by mTORC1, has the opposite metabolic phenotype to that of S6K1<sup>-/-</sup> mice, with increased adiposity and sensitivity to diet-induced obesity which eventually leads to insulin resistance<sup>55</sup>. Consistent with these results, overexpression of 4E-BP1 protects against HFD-induced obesity and insulin resistance in male mice, whereas the overexpression of 4E-BP1 does not provide any beneficial protection to HFD-fed female mice<sup>56</sup>. Moreover, mice with ablation of Grb10 (Grb10<sup>-/-</sup>) in peripheral tissues (except brain)<sup>57</sup> or disrupted Grb10 genes (Grb10 $\Delta$ 2-4<sup>m/+</sup>)<sup>58</sup> have increased body weight but reduced adiposity, increased insulin sensitivity and glucose tolerance and enhanced insulin signalling in insulin-target tissues such as skeletal muscle and fat. Furthermore, conditional deletion of raptor, an essential component of mTORC1, in adipose tissue results in lean mice that are protected against diet-induced obesity<sup>59</sup>. In contrast, raptor deletion in skeletal muscle leads to glucose intolerance<sup>60</sup>, suggesting that mTORC1 in skeletal muscle exerts a positive effect on whole body glucose handling. Collectively, these findings suggest that dysregulation of mTORC1 in the skeleton may have a significant impact on whole-body energy metabolism.

### ***1.5.2 mTORC1 in bone – integrating bone development and skeletal regulation of glucose metabolism?***

Recent studies have demonstrated that mTORC1 signalling is a crucial regulator of bone formation and OB differentiation. Mice in which *Raptor*, an essential component of mTORC1, is deleted in OBs (*Raptor*<sub>ob</sub><sup>-/-</sup>) are severely osteopenic and *Raptor*-null OBs fail to undergo mineralization<sup>61,62</sup>; bone phenotypes that are similar to *INSR*<sup>OB-/-</sup> and *Gprc6a*<sup>-/-</sup> mice<sup>32,63</sup>. Transcriptomic analyses revealed that raptor-null OBs have an immature bone phenotype, suggesting that mTORC1 signalling is crucial for the differentiation of pre-OBs into mature OBs<sup>61,62</sup>. Importantly, total OCN levels are significantly decreased in *Raptor*<sub>ob</sub><sup>-/-</sup> mice<sup>61</sup>. While this may be secondary to the stall in osteogenesis, these data provide evidence that mTORC1 in OBs is important for OCN expression.

While the function of mTORC1 in OBs requires further investigation, mTORC1-dependent regulation of protein synthesis is thought to play a key role. Conditional deletion of *Raptor* in the developing mesenchyme (*Prx-1-Cre*)<sup>64</sup> and pre-osteoblasts (*Osx-Cre*)<sup>61</sup> causes a significant reduction in protein synthesis, which may account for the defects in limb length and bone mineralisation observed in these mice. In support of this, a significant reduction in mTORC1 activity and protein synthesis was observed in mice in which Glut1, a glucose transporter, was deleted in pre-osteoblasts (*Glut1<sub>osx</sub><sup>-/-</sup>*)<sup>42</sup>. These mice displayed a significant delay in OB differentiation which was due, in part, to AMPK-dependent inhibition of mTORC1 function. Further characterisation of *Glut1<sub>osx</sub><sup>-/-</sup>* mice revealed that Glut1-dependent uptake of glucose is an early determinant of osteogenesis where glucose acts to block AMPK activity, thereby promoting protein synthesis by mTORC1 and suppressing SMURF1-dependent degradation of Runx2, a master regulator of osteogenesis<sup>42,65</sup> (Fig. 1.2).

Conversely, mice with constitutively active mTORC1 signalling in OBs, via OB-specific deletion of *Tsc1* ( $\Delta$ Tsc1) or *Tsc2* ( $\Delta$ Tsc2), negative regulators of mTORC1, exhibit increased bone mass and OB number, however OB function is impaired<sup>66,67</sup>. Moreover,  $\Delta$ Tsc2 mice display a 4.5-fold increase in total OCN levels and a 10-fold increase in unOCN levels that is associated with hypoglycaemia and hyperinsulinemia at one week of age<sup>67</sup>. Interestingly, with age,  $\Delta$ Tsc2 mice develop metabolic abnormalities similar to those of *INSR<sup>OB-/-</sup>* mice, including increased peripheral adiposity, hyperglycaemia and decreased pancreatic  $\beta$ -cell mass<sup>67</sup>. The metabolic abnormalities in these mice appear to arise from chronic exposure to high levels of OCN which leads to the down-regulation of its receptor in pancreatic islet cells<sup>67</sup>. The dramatic increase in OCN production in these mice appears to be attributable to the inhibition of FOXO1 activity, as demonstrated by increased levels of FOXO1 phosphorylation (inhibitory) in the *Tsc2*-deficient OBs<sup>67</sup>. In support of this, FOXO1 can associate with TSC2, which leads to the degradation of the TSC1-TSC2 complex and the activation of mTORC1<sup>68</sup> (Fig. 1.2). This direct interaction between TSC2 and FOXO1 provides a potential molecular link between TSC-mTOR and FOXO1 activities and OCN production. Of note, conditional deletion of a single mTOR allele in  $\Delta$ Tsc2 mice rescues these metabolic abnormalities and normalizes the perturbations in bone formation<sup>67</sup>. Collectively, these findings suggest that bone-specific mTORC1 plays a key role in the skeletal regulation of glucose metabolism. Moreover, dysregulation of

mTORC1 function in bone may play an important role in the development of diet-induced insulin resistance.

### **1.6 The discovery of the OCN receptor, GPRC6A, and its role in male fertility**

The identification of OCN as a bone-derived regulator of glucose metabolism raised the possibility that the skeleton may also be involved in other inter-organ endocrine loops. Given that steroid sex hormones are also well-known regulators of bone remodelling, it was postulated that the skeleton may also regulate reproductive function<sup>69</sup>. The first evidence to support this was the observation that *Ocn*<sup>-/-</sup> mice are poor breeders and have smaller litter sizes compared to WT mice<sup>70</sup>. This reduced fecundity is associated with lower testosterone levels, oligospermia and a reduction in reproductive organ weight, all of which can be subsequently reversed by OCN administration<sup>70</sup>. In contrast, *Esp*<sup>-/-</sup> mice display the opposite reproductive phenotype to that of *Ocn*<sup>-/-</sup> mice<sup>70</sup>. Moreover, *in vitro* co-culture of Leydig cells with OB-conditioned media significantly increases Leydig cell testosterone production, with no change in sex hormone production observed in ovarian cell co-cultures<sup>70</sup>. Notably, estrogen levels in both *Ocn*<sup>-/-</sup> and *Esp*<sup>-/-</sup> mice are comparable to control mice and no reproductive abnormalities are observed in female *Ocn*<sup>-/-</sup> mice<sup>70</sup>.

Given that the role of OCN in sex hormone production is restricted to males, Oury *et al.* concluded that OCN must act through a testis-specific receptor, and sought to identify this receptor by comparing the expression of putative G-protein coupled receptors in the testis and ovary. From these studies, GPRC6A was identified as a putative OCN receptor<sup>70</sup>. GPRC6A is broadly expressed in many organs including the bone, pancreas, muscle, fat, testis, liver and prostate and is activated by a number of unrelated ligands such as extracellular cations and amino acids<sup>71,72</sup>. Of note, *Gprc6a*<sup>-/-</sup> and *Ocn*<sup>-/-</sup> mice have nearly identical metabolic and reproductive phenotypes, including hyperglycaemia, glucose intolerance, insulin resistance and reduced testosterone levels (Table 1.1)<sup>63,73</sup>.

**Table 1.1 A Summary of the Skeletal and Metabolic Phenotypes of Transgenic Knockout Mouse Strains.**

<b>Knockout strain:</b>	<i>Esp</i> <sup>-/-</sup>	<i>Ocn</i> <sup>-/-</sup>	<i>InsR</i> <sup>0B-/-</sup>	<i>Gprc6a</i> <sup>-/-</sup>	$\Delta Tsc2$
<b>Bone Phenotype</b>					
Bone phenotype	Increased expression of genes involved in bone resorption	Increased bone mass and rates of bone formation without impairing bone resorption or mineralization	Low bone mass, decreased expression of genes involved in bone resorption and OC activity	Impaired bone mineralization and decreased bone density	Disorganized bone with accumulation of immature OBs and slightly reduced OCs number
<b>Metabolic Phenotype</b>					
Steady-state Glucose	Neonatal death from severe hypoglycaemia associated with hyperinsulinemia	Hyperglycaemia	Hyperglycaemia during fed state	Hyperglycaemia	Hypoglycaemia at early age. Increased fasting glucose levels with age
<b>Glucose tolerance</b>	↑	↓	↓	↓	↓
<b>Serum insulin levels</b>	↑	↓	↓	↓	↓
<b>Insulin secretion</b>	↑	↓	↓	↓	↓
<b>Insulin sensitivity</b>	↑	↓	↓	↓	↑ at 6 weeks old ↓ at 12 weeks old
<b>Pancreatic <math>\beta</math>-cell mass and area</b>	↑	↓	↓	-	↓
<b>Serum adiponectin levels</b>	↑	↓	-	-	-
<b>Energy expenditure</b>	↑	↓	↓	-	-
<b>Serum triglyceride levels</b>	↓	↑	-	-	-
<b>Serum total OCN and unOCN levels</b>	↑	-	↓	-	↑
<b>Adipocyte number and fat pad mass</b>	↓	↑	-	↑ fat mass	-
<b>Male Reproductive Phenotype</b>					
<b>Circulating testosterone</b>	High	Low	Low	Low	-
<b>Sperm count</b>	↑ 30%	↓ 50%	↓ 30%	-	-
<b>Volume of male reproductive organs (testis, epididymis, seminal vesicle)</b>	↑	↓	↓	↓	-
<b>Fertility</b>	Normal	↓ 2-fold smaller litter size and lower litter frequency	-	Normal but reduced litter sizes from homozygous null mice	-
<b>References</b>	13	13,70	32,35,73	63,70	67

- = Not determined

↑ = Increased

↓ = Decreased

The biochemical mechanisms by which OCN-GPRC6A modulates  $\beta$ -cell function have since been studied both *in vitro* and *in vivo*<sup>74,75</sup>. In two independent *in vivo* studies,  $\beta$ -cell-specific deletion of *Gprc6a* (*Gprc6a<sub>Pdx</sub>*<sup>-/-</sup> and *Gprc6a* <sup>$\beta$ -cell-cko</sup>) was found to reduce pancreatic weight, islet number and insulin protein content, and lead to abnormal glucose tolerance but normal insulin sensitivity<sup>74,76</sup>. Collectively, these studies demonstrate that pancreatic GPRC6A directly controls  $\beta$ -cell proliferation and insulin production. Furthermore, compound heterozygous knockout mice lacking one copy of both *Bglap* and *Gprc6a* in pancreatic  $\beta$ -cells display an identical metabolic phenotype to that of *Ocn*<sup>-/-</sup> and *Gprc6a*<sup>-/-</sup> mice, demonstrating that OCN and GPRC6A lie in the same genetic cascade<sup>76</sup>. Importantly, insulin resistance and hyperglycaemia are only observed in mice with global knockout of GPRC6A (*Gprc6a*<sup>-/-</sup> mice) but not a  $\beta$ -cell specific knockout of GPRC6A (*Gprc6a<sub>Pdx</sub>*<sup>-/-</sup> or *Gprc6a* <sup>$\beta$ -cell-cko</sup> mice), suggesting that GPRC6A may also control insulin sensitivity in peripheral tissues.

Additionally, Leydig cell-specific deletion of GPRC6A (*Gprc6a*<sup>Leydig+/-</sup>) in mice leads to reproductive defects similar to that of *Gprc6a*<sup>-/-</sup> mice<sup>73</sup>. While further studies are required to identify the biochemical pathways by which OCN mediates its effects in Leydig cells, it has been reported that OCN signalling regulates the expression of genes associated with testosterone production in a cAMP response element-binding protein (CREB)-dependent manner<sup>70</sup>, and that GPRC6A transduces the non-genomic responses of free testosterone *in vitro*<sup>77</sup>. *In vivo* studies in *Gprc6a*<sup>-/-</sup> mice have also shown that GPRC6A is a crucial mediator of testosterone biosynthesis in Leydig cells and is necessary for testosterone-mediated stimulation of insulin secretion in the pancreatic islets<sup>78</sup>. Taken together, these observations confirm a role for OCN-GPRC6A-testosterone in regulating energy homeostasis and male fertility.

Intriguingly, using a computational approach, unOCN has been predicted to have a similar structure to that of sex hormone-binding globulin (SHBG), a glycoprotein that is bound by testosterone under physiological conditions, and both unOCN and SHBG activate GPRC6A via a common binding site<sup>79</sup>. It is therefore possible that testosterone, via SHBG-mediated activation of GPRC6A in Leydig cells, may act in an autocrine manner to enhance its own production and thereby affect peripheral tissues to regulate glucose and fat metabolism. In addition, SHBG may be a negative regulator of the OCN-testosterone endocrine loop by competing for the same binding site.

As discussed earlier, the ability of OCN to affect glucose metabolism is influenced by OC bone resorption, and OB insulin signalling enhances bone resorption<sup>35</sup>. This raises the possibility that OB insulin signalling may regulate testosterone biosynthesis in the testis in an OCN-dependent manner. In support of this, *INSR*<sup>OB-/-</sup> mice have a similar reproductive phenotype to that of *Ocn*<sup>-/-</sup> mice<sup>73</sup> and compound mutant mice lacking one allele of *INSR* and *Bglap* display abnormalities similar to that of *INSR*<sup>OB-/-</sup> and *Ocn*<sup>-/-</sup> mice (Table 1.1)<sup>70</sup>. As summarized in Fig. 1.3, these observations point to the existence of a pancreas-bone-testis axis where communication between organs is facilitated by three hormones: OCN, insulin and testosterone.



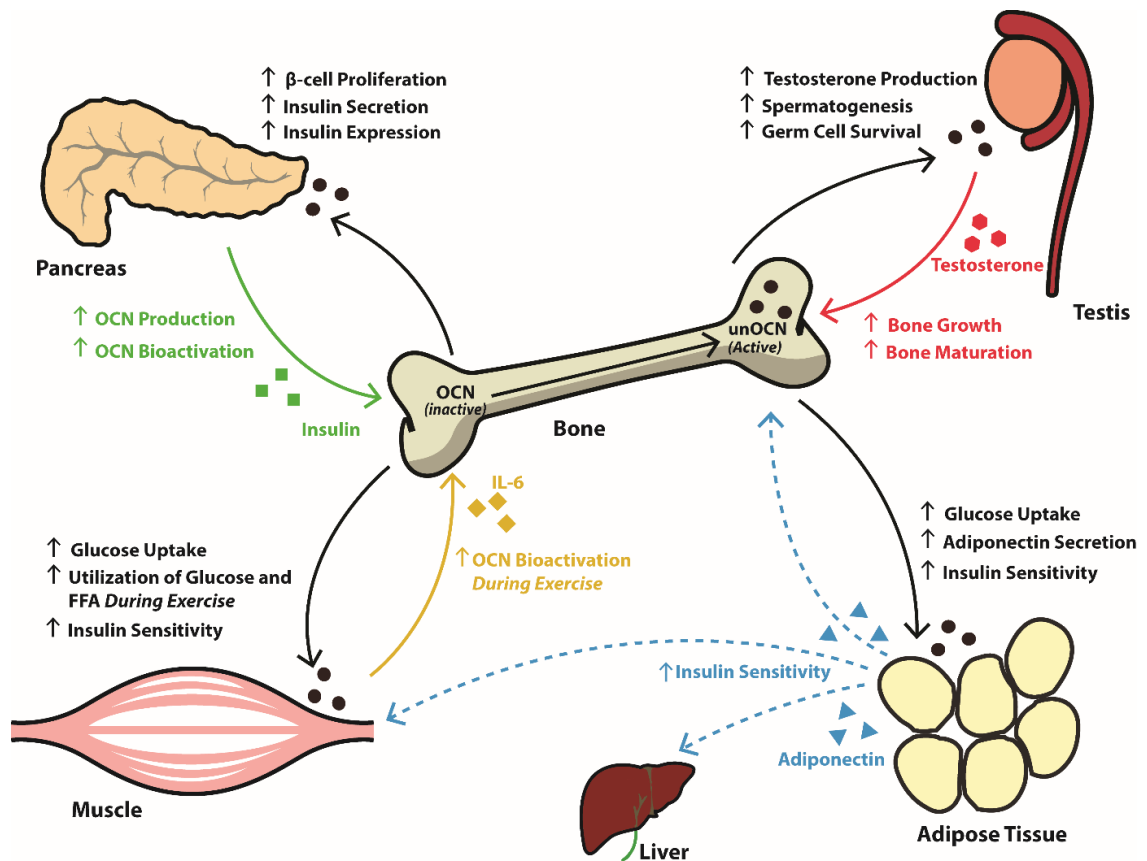


**Figure 1.3 Osteocalcin-dependent endocrine functions of bone.** Insulin signalling in bone stimulates the production and decarboxylation of OCN into its bio-active, undercarboxylated form (unOCN). unOCN is then released into the circulation where it binds to its putative receptor, GPRC6A, expressed by  $\beta$ -cells (pancreas), Leydig cells (testis), myofibers (muscle) and adipocytes (adipose tissue). Bone-derived unOCN stimulates  $\beta$ -cell insulin secretion, promotes glucose uptake in muscle and adipose tissues and promotes testosterone biosynthesis by Leydig cells. Testosterone, in turn, favours bone growth, maintenance and maturation. Furthermore, OCN promotes uptake and catabolism of glucose and FFA in muscle and the release of interleukin-6, a myokine that favours adaptation to exercise and enhances exercise capacity. In a feedforward manner, IL-6 then acts on the bone to increase OCN decarboxylation. A growing body of evidence suggests that the insulin sensitizing effects of unOCN are due, in part, to an increase in adiponectin secretion from adipocytes, which acts on peripheral tissues. (Modified from<sup>80</sup> with permission from the publisher, Elsevier.)

## 1.7 Endocrine roles of OCN in humans

### 1.7.1 Differences in the regulation of OCN between mice and humans

In the pioneering studies by Ferron *et al*, which identified OCN as a bone-derived regulator of glucose metabolism, the authors showed that unOCN administration to wild-type mice improves insulin sensitivity<sup>25</sup>, and that unOCN administration to HFD-fed mice leads to reduced weight gain and improved glucose tolerance and insulin sensitivity compared to controls<sup>15,25</sup>. However, in more recent studies, unOCN administration to male mice fed a HFD or high-sucrose diet was found to induce glucose intolerance, insulin resistance and adipocyte hypertrophy while increasing circulating testosterone and adiponectin levels<sup>81</sup>. In contrast, unOCN administration to female mice was found to improve glucose metabolism under normal, HFD or high-sucrose diet conditions<sup>82</sup>.

While these sex-dependent effects in mice need to be investigated further, the potentially positive metabolic effects associated with unOCN administration raises the possibility of utilizing unOCN to treat metabolic disorders in humans. However, for a number of reasons, the translation of these findings to the human setting has proved problematic. Firstly, in humans, *Esp* is a pseudogene with no functional product. Whilst a functional human homologue for murine *Esp* has not been identified, a protein closely related to OST-PTP, protein-tyrosine phosphatase 1B (PTP1B), is expressed in human OBs and has been shown to dephosphorylate INSR, suggesting that it may play a similar role to *Esp*<sup>35,83</sup>. Thus, the mechanisms by which OCN is decarboxylated and modulates insulin signalling in humans are different to those of mice. Secondly, the circadian rhythm of OCN differs between humans and mice. In mice, OCN levels peak during the light period and are at their lowest during the dark period whereas in humans, OCN levels fall in the early morning, rise in the afternoon and peak at night<sup>84</sup>. While the differences in OCN circadian regulation between these two species could, at least in part, be explained by the fact that humans are active in the light period whereas mice are active in the dark period, it may also be attributed to modulation in glucocorticoid levels. In humans, high serum levels of cortisol in the morning are thought to be responsible for the daytime nadir in serum OCN levels and the night time peak is due to the decline of cortisol levels in the evening<sup>85</sup>. Similarly, in rodents, the levels of corticosterone remain constant from early morning to afternoon followed by a significant elevation at 20:00 in the evening<sup>86</sup>. Therefore, the time point at which

samples are collected should be taken into account when extrapolating findings from mouse studies into the human setting. Lastly, while all three Gla residues (i.e. 13, 17, and 20) in murine OCN are fully carboxylated, the corresponding residues in human OCN are differentially carboxylated with lower frequencies of carboxylation at residue 17 and 21 and near complete carboxylation of residue 24<sup>87</sup>. As a result, humans have various forms of circulating carboxylated OCN and variations in carboxylation status are associated with vitamin K intake<sup>88</sup>.

### ***1.7.2 Clinical observations of OCN in humans***

Since the discovery of metabolic functions of OCN in rodents, a number of cross-sectional studies have been performed to examine the clinical significance of OCN in humans. Whilst the current evidence for using OCN levels as a predictor of metabolic disorders or male infertility in humans remains inconclusive, as outlined below, many clinical studies have provided supportive associations between OCN levels, glucose metabolism and testosterone levels.

#### ***1.7.2.1 OCN levels and metabolism***

Circulating OCN levels have been shown to inversely correlate with body mass index, fat mass and plasma glucose levels in adults and elderly men and women<sup>89,90</sup>. Elevated levels of total OCN are also associated with lower fasting glucose and acetylated haemoglobin (HbA1c) levels, higher insulin secretion and increased serum adiponectin levels in both diabetic and non-diabetic patients<sup>91</sup>, and lower levels of unOCN are associated with impaired glucose tolerance in children<sup>92</sup>. Interestingly, untreated T2DM and pre-diabetic patients exhibit decreased levels of unOCN and total OCN, and increased OCN levels are associated with improved  $\beta$ -cell function<sup>93</sup>. A recent Japanese study of T2DM patients also found that levels of unOCN positively correlate with the C-peptide response in glucagon loading and meal tolerance tests, suggesting that unOCN could be used for the assessment of insulin secretion in patients with T2DM<sup>94</sup>. Correlations between total OCN levels and glucose metabolism also appear to be age- and sex-dependent, as elevated levels of total OCN are associated with lower HbA1c levels in young men and women (<50 years of age) and only older men (>50 years of age)<sup>91</sup>. Furthermore, serum OCN levels are strongly associated with adiponectin levels in women and testosterone levels in men<sup>95</sup> suggesting sex-dependent mechanisms may play a role in mediated in the metabolic effects of OCN.

### 1.7.2.2 OCN and testosterone

In pubescent males, a significant association between serum OCN and testosterone levels has been observed<sup>96</sup>. Moreover, in patients with Klinefelter syndrome (a male-specific genetic disorder in which males are born with an extra copy of the X chromosome; KS), reduced testosterone levels are one of the major causes of impaired bone density, marked by a significant reduction in bone formation markers including OCN levels<sup>97</sup>. Interestingly, a high incidence of metabolic disorders was reported in 70 KS patients compared to aged-matched controls (50% and 10% respectively)<sup>98</sup>. In healthy men aged 25-65 years, low testosterone levels are associated with insulin resistance and glucose intolerance and an increased risk of developing T2DM<sup>99,100</sup>. Furthermore, circulating total OCN levels are positively correlated to testosterone levels in T2DM patients<sup>101</sup>.

The effect of testosterone administration on OCN levels and metabolism remains unclear. While increased bone mineral density is normally observed following testosterone treatment, OCN levels initially increase during the first 3 months of treatment, then plateau before trending towards a reduction after 6 months of treatment<sup>102,103</sup>. Systematic analysis of the *OCN* and *GPRC6A* loci in a cohort of patients with primary testicular failure identified a heterozygous missense variant in the transmembrane domain of GPRC6A (F464Y), which prevents localization of the receptor to the cell membrane and transduction of the GPRC6A signalling pathway<sup>73</sup>. Interestingly, patients harbouring this mutation shared a similar history of glucose intolerance and displayed similar reproductive hormone defects to those observed in *Ocn*<sup>-/-</sup> and *Gprc6a*<sup>-/-</sup> mice, suggesting that the OCN/GPRC6A pathway is conserved between mice and humans<sup>13,63,70,73</sup>.

Taken together, these results suggest an important role for OCN in human biology and a possible role for OCN in the control of testosterone levels in patients with T2DM. While these data raise the possibility of (1) utilizing unOCN as a therapeutic treatment and/or marker for the development of metabolic disease and (2) using the *GPRC6A* loci as a primary genetic screen for testicular failure in humans, prospective studies using larger and more diverse cohorts of patients are necessary to confirm these observations. In addition, further insights into the biochemical pathways that control OCN production and its tissue-specific functions are required.

## 1.8 OCN and evidence for other osteokines

Recent evidence suggests that, in addition to OCN, OBs secrete other factors or “osteokines” that regulate insulin sensitivity. This was first demonstrated in mice with conditional ablation of OBs<sup>26</sup>. Mice with a 50% reduction in OB numbers are glucose intolerant and insulin insensitive; metabolic phenotypes which are consistent with the significant reduction in total OCN levels observed in these animals. However, while restoration of OCN levels rescued the glucose intolerance and normalized insulin levels, OCN only partially restored insulin sensitivity<sup>26</sup>. Furthermore, the ablation of OBs was associated with changes in metabolism, including a decrease in gonadal fat mass and increased energy expenditure, phenotypes not observed in OCN knockout animals<sup>13</sup> suggesting that OCN-independent mechanisms may play a role in the skeletal control of glucose metabolism. Further evidence for this is seen in mice with conditional deletion of Y1, the receptor for neuropeptide Y (NPY)<sup>104</sup>. Deletion of Y1 in OBs was found to enhance bone mass, which was associated with a modest increase in total OCN levels<sup>104</sup>. However, these mice are glucose intolerant and hypoinsulinemic as a result of reduced islet number and  $\beta$ -cell area. Co-culture of Y1-null OBs with Min6 cells, an OCN-responsive islet cell line, failed to stimulate Ins1 and Ins2 gene expression relative to WT OBs, suggesting that Y1 may regulate the expression and/or secretion of factor(s) independent to OCN<sup>104</sup>. More recently, Lipocalin 2 (LCN2) has been identified as an additional OB-secreted factor that regulates glucose metabolism<sup>105</sup>. Mice with global or bone-specific deletion of Lcn2 are glucose intolerant, insensitive to insulin and hypoinsulinemic due to reduced islet number and reduced  $\beta$ -cell mass and proliferation<sup>105</sup>. Bone mass and OCN expression were not affected in these mice, suggesting that the metabolic phenotype was not secondary to the bone defect or a reduction in OCN levels<sup>105</sup>. Furthermore, LCN2 was shown to directly stimulate insulin secretion from primary islet cells, suggesting that OB-secreted LCN2 regulates glucose metabolism by modulating insulin production<sup>105</sup>. Intriguingly, OB-secreted LCN2 was shown to regulate appetite by binding to the melanocortin 4 receptor (MC4R) in the hypothalamus, which activates the MC4R-dependent appetite suppressing pathway<sup>105</sup>. It is also important to note that LCN2 was identified based on the transcriptional profile of OBs isolated from Foxo1<sub>OB</sub><sup>-/-</sup> mice, where Lcn2 expression was upregulated 5-fold<sup>105</sup>. As noted in Section 1.3.1, FOXO1 is a negative regulator of OCN expression and bio-activation (carboxylation)<sup>37</sup> suggesting the expression levels of LCN2 and OCN are regulated, at least in part, through a common signalling pathway. While OCN has not

been shown to control appetite, the findings that LCN2 can suppress appetite and regulate insulin secretion, insulin sensitivity and glucose tolerance, further highlight the endocrine functions of bone and the complexity of inter-tissue communications in the regulation of whole-body metabolism.

### **1.9 Summary and Objectives**

The identification of the skeleton as an important endocrine organ has considerably expanded our understanding of skeletal physiology and whole-body energy metabolism. The classical view of skeleton as a hormone-responsive tissue should now be replaced by one in which the skeleton actively communicates with other organ systems to coordinate the balance between its own remodelling process and overall energy status. OCN is now recognized as a bone-derived hormone that regulates glucose metabolism and male reproductive function by stimulating pancreatic  $\beta$ -cell insulin secretion, improving insulin sensitivity in peripheral tissues and enhancing Leydig cell testosterone production. Remarkably, insulin signalling in OBs is a positive regulator of OCN production and bio-activation, and accumulating evidence from transgenic mouse models has confirmed the existence of a pancreas-bone-testis axis mediated by OCN.

To date, the involvement of the skeleton in the development of insulin resistance and the mechanism(s) underlying pathological effects of insulin resistance on the skeleton is not fully understood. Modulation of insulin receptor levels in OBs, to emulate a loss of responsiveness to insulin, suggests that skeletal insulin resistance has global effects on glucose metabolism and insulin sensitivity. At the molecular level, insulin signalling in OBs activates mTORC1, a central signalling hub that senses fluctuations in intracellular nutrients and extracellular growth factors and integrates these multiple signals to control cellular growth and metabolism. At present, the role played by OB-specific mTORC1 in the control of systemic glucose metabolism and the regulation of insulin-stimulated OCN bio-activation and testosterone production remains to be determined. As aberrant activation of mTORC1 signalling leads to the development of insulin resistance, the major cause of T2DM, gaining a greater understanding of the function of the mTORC1 pathway in bone is likely to aid the future development of targeted therapies for the treatment of T2DM and associated diseases.

The Aim of this project was to investigate the role of OB-specific mTORC1 in the regulation of skeletal glucose metabolism and systemic energy metabolism. To achieve this, mice with conditional deletion of *Rptor*, an essential component of mTORC1, in pre-osteoblast were utilised (*Rptor<sub>ob</sub><sup>-/-</sup>* mice). The metabolic phenotype of *Rptor<sub>ob</sub><sup>-/-</sup>* mice was measured using a complementary suite of metabolic tests (e.g. glucose tolerance tests, insulin tolerance tests, indirect calorimetry assessment, serum analyses) coupled with detailed assessment of the effect of disrupting mTORC1 function in OBs on insulin sensitivity in the major insulin-responsive tissues. Furthermore, given that hyper-activation of mTORC1 signalling has been implicated in the development of insulin resistance (reviewed in <sup>51</sup>), the role of OB-specific mTORC1 signalling in the development of diet-induced insulin resistance was also explored.

The central hypothesis of this project was that OB-mTORC1 plays a central role in the skeletal regulation of systemic glucose homeostasis, and that inhibition of mTORC1 signalling in bone will protect against diet-induced insulin resistance. In order to test this hypothesis, the studies outlined herein were designed to address the following Research Questions:

1. Does suppression of OB-mTORC1 function influence whole-body energy metabolism?
2. What is the effect of OB-mTORC1 disruption on distal insulin-responsive tissues?
3. What are the mechanisms by which suppression of OB-mTORC1 function improve gluco-regulatory function?
4. Does suppression of OB-mTORC1 function protect mice from diet-induced insulin resistance?

## 1.10 References

1. Harada S, Rodan GA. Control of osteoblast function and regulation of bone mass. *Nature* **423**, 349-355 (2003).
2. Legroux-Gerot I, Vignau J, Collier F, Cortet B. Bone loss associated with anorexia nervosa. *Joint Bone Spine* **72**, 489-495 (2005).
3. Misra M, Klibanski A. Bone metabolism in adolescents with anorexia nervosa. *J Endocrinol Invest* **34**, 324-332 (2011).
4. Premaor MO, *et al.* The association between fracture site and obesity in men: a population-based cohort study. *J Bone Miner Res* **28**, 1771-1777 (2013).
5. Sjöblom S, Suuronen J, Rikkonen T, Honkanen R, Kröger H, Sirola J. Relationship between postmenopausal osteoporosis and the components of clinical sarcopenia. *Maturitas* **75**, 175-180 (2013).
6. Riggs BaM, L. . Involutional Osteoporosis. *New England Journal of Medicine* **314**, 1676-1686 (1986).
7. Riggs B, Khosla, S. and Melton, L. . A Unitary Model for Involutional Osteoporosis Estrogen Deficiency Causes Both Type I and Type II Osteoporosis in Postmenopausal Women and Contributes to Bone Loss in Aging Men. *J Bone Miner Res* **13**, 763-773 (1998).
8. Lee A, Hodges, S. and Eastell, R. . Measurement of osteocalcin. *ann clin biochem* **37**, 432-446 (2000).
9. Sunnerhagen M, Drakenberg T, Forsen S, Stenflo J. Effect of Ca<sup>2+</sup> on the structure of vitamin K-dependent coagulation factors. *Haemostasis* **26 Suppl 1**, 45-53 (1996).
10. Malashkevich VN, Almo SC, Dowd TL. X-ray crystal structure of bovine 3 Glu-osteocalcin. *Biochemistry* **52**, 8387-8392 (2013).
11. Kanbur NO, Derman O, Sen TA, Kinik E. Osteocalcin. A biochemical marker of bone turnover during puberty. *Int J Adolesc Med Health* **14**, 235-244 (2002).
12. Ducy P, *et al.* Increased bone formation in osteocalcin-deficient mice. *Nature* **382**, 448-452 (1996).
13. Lee NK, *et al.* Endocrine regulation of energy metabolism by the skeleton. *Cell* **130**, 456-469 (2007).
14. Hinoi E, *et al.* The sympathetic tone mediates leptin's inhibition of insulin secretion by modulating osteocalcin bioactivity. *J Cell Biol* **183**, 1235-1242 (2008).
15. Ferron M, Hinoi E, Karsenty G, Ducy P. Osteocalcin differentially regulates beta cell and adipocyte gene expression and affects the development of metabolic diseases in wild-type mice. *Proc Natl Acad Sci U S A* **105**, 5266-5270 (2008).
16. Otani T, *et al.* Signaling pathway for adiponectin expression in adipocytes by osteocalcin. *Cell Signal* **27**, 532-544 (2015).
17. Luo XH, *et al.* Adiponectin stimulates human osteoblasts proliferation and differentiation via the MAPK signaling pathway. *Exp Cell Res* **309**, 99-109 (2005).



18. Kanazawa I, Yamaguchi T, Yano S, Yamauchi M, Yamamoto M, Sugimoto T. Adiponectin and AMP kinase activator stimulate proliferation, differentiation, and mineralization of osteoblastic MC3T3-E1 cells. *BMC Cell Biol* **8**, 51 (2007).
19. Tsuka S, *et al.* Promotion of insulin-induced glucose uptake in C2C12 myotubes by osteocalcin. *Biochem Biophys Res Commun* **459**, 437-442 (2015).
20. Mera P, Laue K, Wei J, Berger JM, Karsenty G. Osteocalcin is necessary and sufficient to maintain muscle mass in older mice. *Mol Metab* **5**, 1042-1047 (2016).
21. Mera P, *et al.* Osteocalcin Signaling in Myofibers Is Necessary and Sufficient for Optimum Adaptation to Exercise. *Cell Metab* **25**, 218 (2017).
22. Guo B, *et al.* Molecular Communication from Skeletal Muscle to Bone: A Review for Muscle-Derived Myokines Regulating Bone Metabolism. *Calcif Tissue Int* **100**, 184-192 (2017).
23. Ferron M, Wei J, Yoshizawa T, Ducy P, Karsenty G. An ELISA-based method to quantify osteocalcin carboxylation in mice. *Biochem Biophys Res Commun* **397**, 691-696 (2010).
24. Price PA, Williamson MK, Lothringer JW. Origin of the vitamin K-dependent bone protein found in plasma and its clearance by kidney and bone. *J Biol Chem* **256**, 12760-12766 (1981).
25. Ferron M, McKee MD, Levine RL, Ducy P, Karsenty G. Intermittent injections of osteocalcin improve glucose metabolism and prevent type 2 diabetes in mice. *Bone* **50**, 568-575 (2012).
26. Yoshikawa Y, *et al.* Genetic evidence points to an osteocalcin-independent influence of osteoblasts on energy metabolism. *J Bone Miner Res* **26**, 2012-2025 (2011).
27. Ferron M, Lacombe J, Germain A, Oury F, Karsenty G. GGCX and VKORC1 inhibit osteocalcin endocrine functions. *J Cell Biol* **208**, 761-776 (2015).
28. Ituarte EA, Halstead LR, Iida-Klein A, Ituarte HG, Hahn TJ. Glucose transport system in UMR-106-01 osteoblastic osteosarcoma cells: regulation by insulin. *Calcif Tissue Int* **45**, 27-33 (1989).
29. Pun K, Lau, P. and Ho, P. . The characterization, regulation, and function of insulin receptors on osteoblast-like clonal osteosarcoma cell line. *J Bone Miner Res* **4**, 853-862 (1989).
30. Paglia DN, *et al.* Effects of local insulin delivery on subperiosteal angiogenesis and mineralized tissue formation during fracture healing. *J Orthop Res* **31**, 783-791 (2013).
31. Vestergaard P. Discrepancies in bone mineral density and fracture risk in patients with type 1 and type 2 diabetes--a meta-analysis. *Osteoporosis international : a journal established as result of cooperation between the European Foundation for Osteoporosis and the National Osteoporosis Foundation of the USA* **18**, 427-444 (2007).
32. Fulzele K, *et al.* Insulin receptor signaling in osteoblasts regulates postnatal bone acquisition and body composition. *Cell* **142**, 309-319 (2010).

33. Fulzele K, DiGirolamo DJ, Liu Z, Xu J, Messina JL, Clemens TL. Disruption of the insulin-like growth factor type 1 receptor in osteoblasts enhances insulin signaling and action. *J Biol Chem* **282**, 25649-25658 (2007).
34. Lacombe J, Karsenty G, Ferron M. In vivo analysis of the contribution of bone resorption to the control of glucose metabolism in mice. *Mol Metab* **2**, 498-504 (2013).
35. Ferron M, *et al.* Insulin signaling in osteoblasts integrates bone remodeling and energy metabolism. *Cell* **142**, 296-308 (2010).
36. Bialek P, Kern, B., Yang, X., Schrock, M., Sobic, D., Hong, N., Wu, H., Yu, K., Ornitz, D., Olson, E., Justice, M. and Karsenty, G. . A Twist Code Determines the Onset of Osteoblast Differentiation. *Developmental Cell* **6**, 423-435 (2004).
37. Rached MT, *et al.* FoxO1 is a positive regulator of bone formation by favoring protein synthesis and resistance to oxidative stress in osteoblasts. *Cell Metab* **11**, 147-160 (2010).
38. Yang S, *et al.* Foxo1 mediates insulin-like growth factor 1 (IGF1)/insulin regulation of osteocalcin expression by antagonizing Runx2 in osteoblasts. *J Biol Chem* **286**, 19149-19158 (2011).
39. Kode A, *et al.* FoxO1 protein cooperates with ATF4 protein in osteoblasts to control glucose homeostasis. *J Biol Chem* **287**, 8757-8768 (2012).
40. Yoshizawa T, *et al.* The transcription factor ATF4 regulates glucose metabolism in mice through its expression in osteoblasts. *J Clin Invest* **119**, 2807-2817 (2009).
41. Li Z, *et al.* Glucose Transporter-4 Facilitates Insulin-Stimulated Glucose Uptake in Osteoblasts. *Endocrinology* **157**, 4094-4103 (2016).
42. Wei J, *et al.* Glucose Uptake and Runx2 Synergize to Orchestrate Osteoblast Differentiation and Bone Formation. *Cell* **161**, 1576-1591 (2015).
43. Zoch ML, Abou DS, Clemens TL, Thorek DLJ, Riddle RC. In vivo radiometric analysis of glucose uptake and distribution in mouse bone. *Bone Research* **4**, 16004 (2016).
44. Wei J, *et al.* Bone-specific insulin resistance disrupts whole-body glucose homeostasis via decreased osteocalcin activation. *The Journal of Clinical Investigation* **124**, 1781-1793 (2014).
45. Dibble CC, Manning BD. Signal integration by mTORC1 coordinates nutrient input with biosynthetic output. *Nat Cell Biol* **15**, 555-564 (2013).
46. Ma X. M. BJ. Molecular mechanisms of mTOR-mediated translational control. *Cell Mol Biol* **10**, 307-318 (2009).
47. Um SH, *et al.* Absence of S6K1 protects against age- and diet-induced obesity while enhancing insulin sensitivity. *Nature* **431**, 200-205 (2004).
48. Hsu PP, *et al.* The mTOR-regulated phosphoproteome reveals a mechanism of mTORC1-mediated inhibition of growth factor signaling. *Science* **332**, 1317-1322 (2011).
49. Yu Y, *et al.* Phosphoproteomic Analysis Identifies Grb10 as an mTORC1 Substrate That Negatively Regulates Insulin Signaling. *Science* **332**, 1322-1326 (2011).

50. Tzatsos A, Kandror KV. Nutrients suppress phosphatidylinositol 3-kinase/Akt signaling via raptor-dependent mTOR-mediated insulin receptor substrate 1 phosphorylation. *Mol Cell Biol* **26**, 63-76 (2006).
51. Blagosklonny MV. TOR-centric view on insulin resistance and diabetic complications: perspective for endocrinologists and gerontologists. *Cell Death Dis* **4**, e964 (2013).
52. Gual P, Le Marchand-Brustel Y, Tanti JF. Positive and negative regulation of insulin signaling through IRS-1 phosphorylation. *Biochimie* **87**, 99-109 (2005).
53. Newgard CB, *et al.* A branched-chain amino acid-related metabolic signature that differentiates obese and lean humans and contributes to insulin resistance. *Cell Metab* **9**, 311-326 (2009).
54. Pende M, Kozma, S., Jacquet, M., Oorschot, V., Le Marchand-Brustel, Y., Klumperman, J., Thorens, B. and Thomas, G. . Hypoinsulinaemia, glucose intolerance and diminished  $\beta$ -cell size in S6K1-deficient mice. *Nature* **408**, 994-997 (2000).
55. Le Bacquer O, *et al.* Elevated sensitivity to diet-induced obesity and insulin resistance in mice lacking 4E-BP1 and 4E-BP2. *J Clin Invest* **117**, 387-396 (2007).
56. Tsai SY, *et al.* Increased 4E-BP1 Expression Protects against Diet-Induced Obesity and Insulin Resistance in Male Mice. *Cell Rep*, (2016).
57. Wang L, *et al.* Peripheral disruption of the Grb10 gene enhances insulin signaling and sensitivity in vivo. *Mol Cell Biol* **27**, 6497-6505 (2007).
58. Smith FM, *et al.* Mice with a disruption of the imprinted Grb10 gene exhibit altered body composition, glucose homeostasis, and insulin signaling during postnatal life. *Mol Cell Biol* **27**, 5871-5886 (2007).
59. Polak P, Cybulski N, Feige JN, Auwerx J, Ruegg MA, Hall MN. Adipose-specific knockout of raptor results in lean mice with enhanced mitochondrial respiration. *Cell Metab* **8**, 399-410 (2008).
60. Bentzinger CF, *et al.* Skeletal muscle-specific ablation of raptor, but not of rictor, causes metabolic changes and results in muscle dystrophy. *Cell Metab* **8**, 411-424 (2008).
61. Fitter S, *et al.* mTORC1 Plays an Important Role in Skeletal Development by Controlling Preosteoblast Differentiation. *Molecular and Cellular Biology* **37**, e00668-00616 (2017).
62. Chen J, Long F. mTORC1 signaling promotes osteoblast differentiation from preosteoblasts. *PLoS One* **10**, e0130627 (2015).
63. Pi M, *et al.* GPRC6A null mice exhibit osteopenia, feminization and metabolic syndrome. *PLoS One* **3**, e3858 (2008).
64. Chen J, Long F. mTORC1 signaling controls mammalian skeletal growth through stimulation of protein synthesis. *Development (Cambridge, England)* **141**, 2848-2854 (2014).
65. Shimazu J, Wei J, Karsenty G. Smurf1 Inhibits Osteoblast Differentiation, Bone Formation, and Glucose Homeostasis through Serine 148. *Cell Rep* **15**, 27-35 (2016).

66. Huang B, *et al.* mTORC1 prevents preosteoblast differentiation through the notch signaling pathway. *PLoS genetics* **11**, e1005426 (2015).
67. Riddle R, *et al.* Tsc2 Is a Molecular Checkpoint Controlling Osteoblast Development and Glucose Homeostasis. *Molecular and Cellular Biology* **34**, 1850-1862 (2014).
68. Cao Y, *et al.* Interaction of FoxO1 and TSC2 induces insulin resistance through activation of the mammalian target of rapamycin/p70 S6K pathway. *J Biol Chem* **281**, 40242-40251 (2006).
69. Riggs B, Khosla, S. and Melton, L. . Sex Steroids and the Construction and Conservation of the Adult Skeleton. *Endocrine Reviews* **23**, 840-846 (2002).
70. Oury F, *et al.* Endocrine regulation of male fertility by the skeleton. *Cell* **144**, 796-809 (2011).
71. Kuang D, Yao Y, Lam J, Tsushima RG, Hampson DR. Cloning and characterization of a family C orphan G-protein coupled receptor. *J Neurochem* **93**, 383-391 (2005).
72. Pi M, *et al.* Identification of a novel extracellular cation-sensing G-protein-coupled receptor. *J Biol Chem* **280**, 40201-40209 (2005).
73. Oury F, *et al.* Osteocalcin regulates murine and human fertility through a pancreas-bone-testis axis. *J Clin Invest* **123**, 2421-2433 (2013).
74. Pi M, *et al.* Evidence for Osteocalcin Binding and Activation of GPRC6A in  $\beta$ -Cells. *Endocrinology* **157**, 1866-1880 (2016).
75. Pi M, Wu Y, Quarles LD. GPRC6A mediates responses to osteocalcin in beta-cells in vitro and pancreas in vivo. *J Bone Miner Res* **26**, 1680-1683 (2011).
76. Wei J, Hanna T, Suda N, Karsenty G, Ducy P. Osteocalcin promotes beta-cell proliferation during development and adulthood through Gprc6a. *Diabetes* **63**, 1021-1031 (2014).
77. Pi M, Parrill AL, Quarles LD. GPRC6A mediates the non-genomic effects of steroids. *Journal of Biological Chemistry* **285**, 39953-39964 (2010).
78. Pi M, *et al.* Structural and Functional Evidence for Testosterone Activation of GPRC6A in Peripheral Tissues. *Molecular Endocrinology* **29**, 1759-1773 (2015).
79. De Toni L, *et al.* Osteocalcin and Sex Hormone Binding Globulin Compete on a Specific Binding Site of GPRC6A. *Endocrinology* **157**, 4473-4486 (2016).
80. Karsenty G, Oury F. Regulation of male fertility by the bone-derived hormone osteocalcin. *Mol Cell Endocrinol* **382**, 521-526 (2014).
81. Yasutake Y, *et al.* Long-term oral administration of osteocalcin induces insulin resistance in male mice fed a high-fat, high-sucrose diet. *American journal of physiology Endocrinology and metabolism* **310**, E662-E675 (2016).
82. Mizokami A, *et al.* Oral administration of osteocalcin improves glucose utilization by stimulating glucagon-like peptide-1 secretion. *Bone* **69**, 68-79 (2014).
83. Cousin W, Courseaux A, Ladoux A, Dani C, Peraldi P. Cloning of hOST-PTP: the only example of a protein-tyrosine-phosphatase the function of which has been lost between rodent and human. *Biochem Biophys Res Commun* **321**, 259-265 (2004).

84. Gundberg CM, Markowitz ME, Mizruchi M, Rosen JF. Osteocalcin in human serum: a circadian rhythm. *J Clin Endocrinol Metab* **60**, 736-739 (1985).
85. Heshmati HM, Riggs BL, Burritt MF, McAlister CA, Wollan PC, Khosla S. Effects of the Circadian Variation in Serum Cortisol on Markers of Bone Turnover and Calcium Homeostasis in Normal Postmenopausal Women<sup>1</sup>. *The Journal of Clinical Endocrinology & Metabolism* **83**, 751-756 (1998).
86. Gong S, *et al.* Dynamics and correlation of serum cortisol and corticosterone under different physiological or stressful conditions in mice. *PLoS One* **10**, e0117503 (2015).
87. Cairns JR, Price PA. Direct demonstration that the vitamin K-dependent bone Gla protein is incompletely gamma-carboxylated in humans. *J Bone Miner Res* **9**, 1989-1997 (1994).
88. Booth SL, Centi A, Smith SR, Gundberg C. The role of osteocalcin in human glucose metabolism: marker or mediator? *Nature Reviews Endocrinology* **9**, 43-55 (2013).
89. Hu W, *et al.* Serum osteocalcin levels are inversely associated with plasma glucose and body mass index in healthy Chinese women. *Acta Pharmacol Sin* **35**, 1521-1526 (2014).
90. Pittas AG, Harris SS, Eliades M, Stark P, Dawson-Hughes B. Association between serum osteocalcin and markers of metabolic phenotype. *J Clin Endocrinol Metab* **94**, 827-832 (2009).
91. Jung KY, *et al.* Age- and sex-specific association of circulating osteocalcin with dynamic measures of glucose homeostasis. *Osteoporosis international : a journal established as result of cooperation between the European Foundation for Osteoporosis and the National Osteoporosis Foundation of the USA* **27**, 1021-1029 (2016).
92. Pollock NK, *et al.* Lower bone mass in prepubertal overweight children with prediabetes. *J Bone Miner Res* **25**, 2760-2769 (2010).
93. Liu D-M, *et al.* Association between osteocalcin and glucose metabolism: a meta-analysis. *Osteoporosis International* **26**, 2823-2833 (2015).
94. Takashi Y, Koga M, Matsuzawa Y, Saito J, Omura M, Nishikawa T. Undercarboxylated osteocalcin can predict insulin secretion ability in type 2 diabetes. *J Diabetes Investig*, (2016).
95. Buday B, Pach FP, Literati-Nagy B, Vitai M, Vecsei Z, Koranyi L. Serum osteocalcin is associated with improved metabolic state via adiponectin in females versus testosterone in males. Gender specific nature of the bone–energy homeostasis axis. *Bone* **57**, 98-104 (2013).
96. Kirmani S, Atkinson EJ, Melton LJ, 3rd, Riggs BL, Amin S, Khosla S. Relationship of testosterone and osteocalcin levels during growth. *J Bone Miner Res* **26**, 2212-2216 (2011).
97. Stagi S, *et al.* Bone Mineral Status in Children and Adolescents with Klinefelter Syndrome. *Int J Endocrinol* **2016**, 3032759 (2016).
98. Gravholt CH, Jensen AS, Host C, Bojesen A. Body composition, metabolic syndrome and type 2 diabetes in Klinefelter syndrome. *Acta Paediatr* **100**, 871-877 (2011).

99. Li C, Ford ES, Li B, Giles WH, Liu S. Association of testosterone and sex hormone-binding globulin with metabolic syndrome and insulin resistance in men. *Diabetes Care* **33**, 1618-1624 (2010).
100. Pitteloud N, Mootha, V., Dwyer, A., Hardin, M., Lee, H., Eriksson, K., Tripathy, D., Yialamas, M., Groop, L., Elahi, D. and Hayes, F. Relationship Between Testosterone Levels, Insulin Sensitivity, and Mitochondrial Function in Men. *Diabetes Care* **28**, 1636-1642 (2005).
101. Cui R, Su, B., Sheng, C., Cheng, X., Yang, P., Bu, L., Qu, S. Total osteocalcin in serum predicts testosterone level in male type 2 diabetes mellitus. *International Journal of Clinical and Experimental Medicine* **7**, 1145-1149 (2014).
102. Deb P, Gupta SK, Godbole MM. Effects of short-term testosterone replacement on areal bone mineral density and bone turnover in young hypogonadal males. *Indian Journal of Endocrinology and Metabolism* **16**, 947-951 (2012).
103. Wang C, *et al.* Effects of transdermal testosterone gel on bone turnover markers and bone mineral density in hypogonadal men. *Clin Endocrinol (Oxf)* **54**, 739-750 (2001).
104. Lee NJ, *et al.* NPY signalling in early osteoblasts controls glucose homeostasis. *Mol Metab* **4**, 164-174 (2015).
105. Mosialou I, *et al.* MC4R-dependent suppression of appetite by bone-derived lipocalin 2. *Nature* **543**, 385-390 (2017).

**CHAPTER 2:  
LOSS OF MTORC1 FUNCTION IN PRE-OSTEOBLASTS  
IS ASSOCIATED WITH SYSTEMIC IMPROVEMENT IN  
GLUCOSE HOMEOSTASIS WHICH OCCURS  
INDEPENDENTLY OF OSTEOCALCIN**

## **Loss of mTORC1 function in pre-osteoblasts is associated with systemic improvement in glucose homeostasis which occurs independently of osteocalcin**

Pawanrat Tangseefa<sup>1,2</sup>, Sally K. Martin<sup>1,2</sup>, Peck Yin Chin<sup>3</sup>, Paul A. Baldock<sup>4</sup>, Gary A. Wittert<sup>1,5,6</sup>, Amanda J. Page<sup>1,6</sup>, Christopher G. Proud<sup>6,7</sup>, Stephen Fitter<sup>1,2,9\*</sup>, Andrew C.W. Zannettino<sup>1,2,8,9\*</sup>

<sup>1</sup>Adelaide Medical School, Faculty of Health and Medical Science, University of Adelaide, Adelaide, Australia.

<sup>2</sup>Cancer Program, Precision Medicine Theme, South Australian Health and Medical Research Institute, Adelaide, Australia.

<sup>3</sup>Research Centre for Reproductive Health, School of Paediatrics and Reproductive Health, University of Adelaide, Adelaide, SA, Australia.

<sup>4</sup>Skeletal Metabolism Group, Garvan Institute of Medical Research, Sydney, Australia.

<sup>5</sup>Freemasons Foundation Centre for Men's Health, University of Adelaide, Adelaide, Australia.

<sup>6</sup>Nutrition, Diabetes & Metabolism Program, Lifelong Health Theme, South Australian Health and Medical Research Institute, Adelaide, Australia.

<sup>7</sup>School of Biological Sciences, University of Adelaide, Adelaide, Australia.

<sup>8</sup>Central Adelaide Local Health Network, Adelaide, Australia

<sup>9</sup>contributed equally to this work

**Keywords:** mTORC1, osteoblast, insulin resistance, glucose tolerance, metabolism, osteocalcin, adiponectin, BMAT, calorie restriction

**Running title:** Osteoblast-mTORC1 regulates energy metabolism

Chapter 2 incorporates the following submitted article currently under review at Nature Communications:

Tangseefa P, Martin SK, Chin PY, Baldock PA, Wittert GA, Page AJ, Proud CG, Fitter S, Zannettino ACW. The mTORC1 complex in pre-osteoblasts regulates whole-body energy metabolism independently of osteocalcin.



## 2.1 Abstract

Recent studies have shown that the skeleton plays a central role in regulating systemic glucose metabolism, although the mechanisms by which this occurs remain to be fully elucidated. mTORC1 is a crucial mediator of insulin signalling and a primary nutrient sensor that coordinates anabolic and catabolic processes and, as such, is likely to be critically involved in the skeletal regulation of whole-body energy homeostasis. To investigate this, mice in which *Rptor*, an essential component of mTORC1, was specifically deleted in osteoblasts (*Rptor<sub>ob</sub><sup>-/-</sup>*) were generated and a comprehensive *in vivo* assessment of the metabolic phenotype was performed.

Under normal chow conditions, *Rptor<sub>ob</sub><sup>-/-</sup>* mice exhibited enhanced glucose tolerance and increased insulin sensitivity. A net negative energy balance in *Rptor<sub>ob</sub><sup>-/-</sup>* mice resulted in lean mice and a shift in whole-body fuel utilisation toward fat oxidation, which was associated with elevated ketone body levels. Mechanistically, these improved metabolic indices occur independently of osteocalcin and instead may be attributable to elevated serum adiponectin levels arising from increased bone marrow adiposity. These studies also revealed sex-dependent differences in body composition and energy metabolism, with a significant decrease in fat mass, white adipocyte size and an increase in glucose tolerance observed in male, but not female, *Rptor<sub>ob</sub><sup>-/-</sup>* mice. Furthermore, while both sexes show a preference for fat utilisation and elevated serum ketone body levels, increased energy expenditure (with unaltered food intake) and lower serum triglyceride levels were observed only in male *Rptor<sub>ob</sub><sup>-/-</sup>* mice.

These results point to an integral role for osteoblasts in the regulation of nutritional status and glucose metabolism and extend the current knowledge of how osteoblasts contribute to the whole-body homeostatic balances.

## 2.2 Introduction

The skeleton is a highly metabolic tissue that plays an important role in coordinating global energy utilisation via hormonal interactions with other tissues. More recently, the skeleton has been identified as an insulin target tissue that plays a central role in regulating glucose metabolism. Deletion of the insulin receptor (INSR) in the bone-forming osteoblast (OB)<sup>1,2</sup> (INSR<sub>OB</sub><sup>-/-</sup> mice) resulted in elevated blood glucose levels, reduced serum insulin levels and insulin resistance. Consistent with this, mice with OB-specific deletion of either FoxO1<sup>3</sup> or ATF4<sup>4</sup>, negative regulators of insulin signalling, display the opposite phenotype of INSR<sub>OB</sub><sup>-/-</sup> mice with improved glucose disposal and insulin sensitivity due to increased  $\beta$ -cell mass, and increased serum adiponectin levels. To date, OBs and hepatocytes are the only cell types in which disruption of insulin signalling hampers glucose metabolism in mice fed a normal diet<sup>1</sup>, which highlights the importance of these tissues in regulating glucose homeostasis.

Mechanistically, studies to date have shown that insulin signalling in OBs regulates whole-body glucose metabolism via a feed-forward loop involving the bone-specific protein, OCN. Undercarboxylated OCN (unOCN) acts as a hormone to directly improve glucose handling by stimulating pancreatic  $\beta$ -cell proliferation<sup>5</sup> and insulin secretion<sup>6</sup> and indirectly through its stimulation of glucagon-like peptide-1 secretion by the gut<sup>7</sup>. unOCN also increases insulin sensitivity in liver, muscle and adipose tissue by regulating levels of adiponectin<sup>6,8</sup>, an adipokine that modulates glucose homeostasis independently of insulin. Consistent with these observations, daily administration of OCN to mice fed a high-fat diet was shown to partially restore their insulin sensitivity and glucose tolerance<sup>8,9</sup>.

mTORC1 is the primary nutrient-sensing pathway in cells that, in response to nutrients, hormones, growth factors and the cellular energy status, controls cellular growth and metabolism<sup>10</sup>. Activation of mTORC1 by insulin regulates genes that control metabolism, protein synthesis and cell growth. In a negative feedback loop, mTORC1 regulates insulin signalling by disrupting the interaction between the INSR and insulin receptor substrate 1 (IRS1), thus allowing tight regulation of insulin signalling. Accumulating evidence from gene deletion studies in which *Rptor*, (encoding RAPTOR, an essential component of mTORC1) is selectively deleted in specific insulin-responsive tissues has revealed an important role for mTORC1 in the control of whole-body glucose metabolism. For example, conditional deletion of *Rptor* in adipose

tissue results in lean mice that are protected against diet-induced obesity<sup>11,12</sup> while deletion of *Rptor* in skeletal muscle leads to glucose intolerance<sup>13</sup>. These data suggest that mTORC1 has tissue-specific effects in regulating whole-body energy metabolism.

The mTORC1 pathway has been shown to play a crucial role in skeletal development. Mice in which *Rptor* is deleted in OBs have low bone mass (osteopenia) and skeletal fragility<sup>14,15</sup>. Moreover, a reduction in mTORC1 activity and protein synthesis is observed in mice with OB-specific deletion of *Glut1*, a glucose transporter<sup>16</sup>. Glucose uptake by GLUT1 has been shown to promote bone formation and OB differentiation by suppressing AMPK-dependent inhibition of mTORC1 function. Conversely, conditional deletion of *Tsc2*, a negative regulator of mTORC1, in OBs ( $\Delta Tsc2$  mice) results in the accumulation of poorly differentiated OBs<sup>17</sup>. With age,  $\Delta Tsc2$  mice develop a metabolic phenotype similar to mice lacking the INSR in OBs<sup>17</sup>, which suggests a potential role for mTORC1 signalling in integrating bone development and glucose metabolism in response to insulin.

To investigate the role of OB-specific mTORC1 signalling in the regulation of whole-body glucose metabolism, mice with conditionally deleted *Rptor* in osteoprogenitor cells using Osterix-Cre (*Rptor<sub>ob</sub><sup>-/-</sup>*) were generated. These results show that *Rptor<sub>ob</sub><sup>-/-</sup>* mice display a significant sex-specific improvement in glucose metabolism and a lean phenotype which results from increased energy expenditure and a shift in whole-body fuel utilisation toward increased fat oxidation.

## 2.3 Materials and Methods

**2.3.1 Transgenic mice.** All mice were bred and housed in pathogen-free conditions at the SAHMRI Bioresources Facility (SAHMRI, Adelaide, Australia) under a 12 hour light–dark cycle (lights on at 06:00) and constant temperature (20–23°C), with *ad libitum* access to food (Teklad global 18% protein diet #2918, Harlan, IN, USA; detailed in Supplementary Table 2.1) and water. All studies were performed with Institutional Ethics approval (SAHMRI Animal Ethics Committee, #SAM164). Conditional knockout mice in which *Rptor*, a unique and essential component of mTORC1, was disrupted in early osteoprogenitor cells were generated using *Osx1-GFP:Cre* mice<sup>1</sup>, R26eYFP mice<sup>2</sup> and *Rptor<sup>fl/fl</sup>* mice<sup>3</sup> as previously described<sup>4</sup>. The *Osx1-GFP:Cre* and *Rptor<sup>fl/fl</sup>* mice lines were bred separately. The *Osx1-GFP:Cre* and *Rptor<sup>fl/fl</sup>* mice lines were bred separately. The *Osx1-GFP:Cre* line was maintained by mating F1 males harboring a single copy of the *tTA:Osx1-GFP:cre* transgene with wildtype C57BL/6J females. For the *Rptor<sup>fl/fl</sup>* line, all F2 mice were produced from the offspring of F1 breeders. For the *Osx1-GFP:Cre* x *Rptor<sup>fl/fl</sup>* crosses, all F2 mice were produced by new crosses between separate F1 male *Osx1-GFP:Cre* and female *Rptor<sup>fl/fl</sup>* mice. As preliminary studies revealed that serum OCN levels (both total and undercarboxylated), fasting glucose levels and glucose metabolism (glucose tolerance and insulin sensitivity) were unaltered in *Osx1-GFP:Cre* mice relative to age/sex matched wildtype mice, wildtype *Osx1-GFP:Cre-negative; Rptor<sup>fl/fl</sup>* littermates were used as the control group (Supplementary Figure 2.1, A-I). It is also important to note that no detectable off-target Cre recombinase activity in metabolic tissues including spleen, liver, brain and intestine has been observed in *Osx1-GFP:Cre* mice<sup>5</sup>. Furthermore, as *Osx1-GFP:Cre* line has been reported to develop malocclusion when maintain without doxycycline<sup>6</sup> all *Osx1-GFP:Cre*-positive animals were closely monitored and their teeth were trimmed fortnightly. Animals were weighed twice-weekly for the duration of the study and at the end of the study, body length and whole-body lean and fat mass were measured post-mortem using a dedicated mouse dual X-ray absorbitometer (DXA) (Lunar Piximus II, GE Medical Systems, Madison WI, USA).

**2.3.2 Metabolic phenotyping.** Insulin and glucose tolerance tests (ITTs and GTTs) were performed following intraperitoneal injection of 0.75U/kg insulin (Novo Nordisk Pharmaceuticals, Australia) or 2g/kg glucose, respectively after a 6-hour (07:00–13:00) fast. Blood glucose levels were measured at indicated time points using a handheld glucometer (Accu-check, Roche, Australia). At 0- and 30-minute time points of the

GTT, ~50  $\mu\text{L}$  of whole blood was collected and serum was immediately frozen at  $-80^{\circ}\text{C}$  for later assessment of glucose-stimulated insulin levels using a commercial insulin ELISA kit (EZRFI-13K, Millipore, MA, USA) as per manufacturer's instructions. Blood ketone levels ( $\beta$ -hydroxybutyrate) were measured after a 6-hour fast using a handheld ketone meter (FreeStyle, Abbott, Australia).

**2.3.3 Indirect calorimetry and body composition analyses.** Indirect calorimetry assessments were performed using the Promethion metabolic cage system (Sable Systems, NV, USA). Mice were single-housed in Promethion cages for 72-96 hours with *ad libitum* access to food and water. Monitoring was performed for 24–48 hours following an initial 24 hour acclimatisation period. RQ was calculated as the ratio of  $\text{VCO}_2/\text{VO}_2$  with an RQ=0.7 indicative of pure fat oxidation and an RQ=1.0 indicative of pure carbohydrate oxidation.

**2.3.4 Faecal lipid assessment.** Dried faeces (1 g) were collected from individually-housed mice. Faeces were pulverised using a mortar and pestle and rehydrated in 5 mL of normal saline. A 2:1 chloroform: methanol solution was used to extract the lipids from suspension as previously described<sup>22</sup>.

**2.3.5 ELISA.** Non-fasted blood samples were collected at the end of the study via cardiac puncture into Minicollect tubes (Greiner bio one, Kremsmünster, Austria). Sera was isolated by centrifugation at  $845 \times g$  for 10 minutes at room temperature and stored at  $-80^{\circ}\text{C}$ . Commercial ELISA kits were used for the measurement of: triglycerides and free fatty acids (ab65336 and ab65341 respectively, Abcam, Cambridge, MA, USA), leptin and adiponectin (EZML-82K and EZMADP respectively, Millipore, Burlington, MA, USA), OCN (MK129, Takara, Kusatsu, Japan), unOCN (BT-470, Alfa Aesar, Lancashire, United Kingdom), lipocalin-2 (RDSMLCN20, R&D Systems, Minneapolis, MN, USA) and testosterone (55TESMS-E01, R-Biopharm, Darmstadt, Germany), as per manufacturer's instructions.

**2.3.6 Male reproductive organ assessment.** Male reproductive organs (testes, seminal vesicles and epididymides) were dissected and weighed. Caudal epididymides were incised to allow sperm extravasation for 60 minutes at  $37^{\circ}\text{C}$  into 1 mL of PBS. Sperm counts were performed on a 1:10 dilution of the suspension, and an average of two sperm counts was recorded for each mouse.

**2.3.7 Histology and Immunohistochemistry.** Pancreas and adipose tissues (inguinal and gonadal) were carefully dissected from surrounding tissues, fixed in 10% formalin, and embedded in paraffin. Haematoxylin and eosin (H&E) staining was performed on 5  $\mu$ m adipose tissue sections. For assessment of adipocyte cell size, Image J<sup>23</sup> was used to measure cell size and distribution as percentage of total cells in n=5 images per mouse. For pancreatic tissues, immunohistochemistry was performed using rabbit anti-insulin antibody (ab209483, Abcam, Cambridge, MA, USA, 1:1000). The number and size of insulin-positive islet cells was quantified from at least five sections per pancreas (each 50  $\mu$ m apart) using a camera attached to a microscope (Leica Microsystems, Wetzlar, Germany) and Osteomeasure software (Osteometrics, Decatur, GA, USA). Total pancreatic surface was also measured using Image J and used to determine islet cell number per mm<sup>2</sup> and  $\beta$ -cell area (area positive for insulin immunostaining divided by the total pancreatic surface).

**2.3.8 Protein isolation and Western blotting.** For insulin signalling studies, mice were fasted for 6 hours (07:00-13:00) prior to administration of insulin (150mU/g BW, i.p) or PBS control. After 20 minutes, mice were euthanized and tissues (liver, and skeletal muscle) were harvested, snap-frozen in liquid nitrogen and stored at -80 °C prior to further analysis. Tissue samples were lysed in modified RIPA buffer (1% NP40, 20 mM Tris pH 7.4, 2 mM EDTA, 150 mM NaCl, 2 mM Na<sub>3</sub>VO<sub>4</sub>, 2 mM NaF, 0.1% SDS, 2.5 mM Na<sub>4</sub>P<sub>2</sub>O<sub>7</sub>.H<sub>2</sub>O, 10% glycerol, 1 mM  $\beta$ -glycerol phosphate and protease inhibitors (cOmplete™, Roche, Basel, Switzerland) and homogenised using a TissueRuptor (QIAGEN, Victoria, Australia). Equal amounts of protein (50  $\mu$ g, unless otherwise stated) were resolved by SDS-PAGE and transferred to Immobilon-FL PVDF Membrane (MerckMillipore, Darmstadt, Germany). Immunoblotting was performed with the following antibodies: phospho-AKT (Ser473), phospho-INSR (Tyr1150/1151), total AKT, total INSR (Cell Signaling Technology, Danvers, MA, USA), and  $\beta$ -Actin (Sigma, St. Louis, MO, USA). After incubation with fluorescently-tagged secondary antibody, membranes were scanned using a Li-Cor Odyssey imaging system (LI-COR Biosciences, Lincoln, NE, USA). Quantitative analysis was performed using Image Studio software (LI-COR Biosciences).

For analysis of adiponectin multimers, serum samples were electrophoresed on 3-8% Criterion™ XT Tris-Acetate Protein gradient gels (Bio-rad, Hercules, CA, USA) and protein complexes transferred to Immobilon-FL PVDF Membrane (Merck, Darmstadt, Germany), blocked for 1 hour in 5% (w/v) milk/TBST and probed for 16 hours at 4°C

using an adiponectin-specific antibody (Sigma). Bound antibody was detected using a fluorescently-tagged secondary antibody and visualised as described above.

**2.3.9 RNA isolation and quantitative RT-PCR.** Unless otherwise stated, all RNA extractions were carried out using TRIzol reagent (Sigma) according to manufacturer's instructions. Total RNA (1.5 µg) was reverse transcribed into cDNA using Superscript IV Reverse Transcriptase (Invitrogen, Carlsbad, CA, USA). Real-time PCR reactions were performed using RT<sup>2</sup> SYBR Green ROX reagent (QIAGEN, Hilden, Germany) in a CFX Connect™ Real-Time PCR machine (Bio-Rad). Forward and reverse primer pairs, designed to amplify across intron-exon boundaries, are listed in Supplementary Table 2.2. The efficiencies of PCR were assessed with visual assessment of geometric amplification slopes and relative mRNA expression was determined using the  $2^{-\Delta\Delta C_t}$  method<sup>7</sup>.

**2.3.10 Statistical analysis.** All data are presented as mean ± standard error of the mean (SEM). Statistical analyses were performed using a one-way or two-way ANOVA with a Tukey test or an unpaired Students t-test using GraphPad Prism (GraphPad Software Inc, CA, USA). Significance was accepted at  $p < 0.05$ , with asterisks denoting p-value levels: \* $p < 0.05$ ; \*\* $p < 0.01$ ; \*\*\* $p < 0.001$ .

## 2.4 Results

### 2.4.1 Loss of mTORC1 function in pre-osteoblasts is associated with altered body composition in male but not female mice

To investigate the role of OB-mTORC1 in the skeletal regulation of metabolism, mice with conditional deletion of *Rptor* in osteoprogenitor cells using the *Osx1-GFP::Cre* mice<sup>18</sup> were generated as previously described<sup>15</sup>. Owing to previously observed gene dosage effects in these mice<sup>15,25</sup>, both heterozygous (*Rptor<sub>ob</sub><sup>-/+</sup>*) and homozygous (*Rptor<sub>ob</sub><sup>-/-</sup>*) knockout animals were analysed in this study.

During the first 2 months of life, both male and female *Rptor<sub>ob</sub><sup>-/-</sup>* mice weighed significantly less than the control mice (Fig. 2.1A and B), and were approximately 10% shorter in length than the controls (Fig. 2.1C). Whilst the lower body weight of male *Rptor<sub>ob</sub><sup>-/-</sup>* mice could be attributed, in part, to their shorter length, male *Rptor<sub>ob</sub><sup>-/-</sup>* mice were found to have a significantly lower BMI (Fig. 2.1D) suggesting the lower body weight may also be due to changes in their body composition. In contrast, while both female *Rptor<sub>ob</sub><sup>-/+</sup>* and *Rptor<sub>ob</sub><sup>-/-</sup>* mice were shorter than the controls, female *Rptor<sub>ob</sub><sup>-/+</sup>* mice had significantly higher BMI than both control and *Rptor<sub>ob</sub><sup>-/-</sup>* mice, however no difference was observed between the control and *Rptor<sub>ob</sub><sup>-/-</sup>* mice (Fig. 2.1D). To examine this further, whole-body DXA scans were performed. In the males, both *Rptor<sub>ob</sub><sup>-/+</sup>* and *Rptor<sub>ob</sub><sup>-/-</sup>* mice had significantly lower total fat mass compared to controls (Fig. 2.1E). Similar to the males, female *Rptor<sub>ob</sub><sup>-/-</sup>* mice also displayed lower body weight and fat mass relative to controls (Fig. 2.1E). Correcting fat mass to account for the differences in total body weight (as a percentage of total body weight: Fig. 2.1F) or body length (fat mass index, FMI: fat mass/height<sup>2</sup>, Fig. 2.1G) showed that the males show a preferential loss of fat mass that is disproportionate to the decreased body mass, whereas decreased fat mass in the females is proportionate to their decreased body mass.

Consistent with the differences in adiposity observed in *Rptor<sub>ob</sub><sup>-/+</sup>* and *Rptor<sub>ob</sub><sup>-/-</sup>* mice, quantitative assessment of discrete white adipose tissue (WAT) depots at necropsy revealed a reduction in both gonadal and inguinal WAT in male *Rptor<sub>ob</sub><sup>-/+</sup>* and *Rptor<sub>ob</sub><sup>-/-</sup>* mice compared to controls, but not females (Fig. 2.1H and Supplementary Fig. 2.2A). In contrast, no difference in interscapular brown adipose tissue (iBAT) depots was observed in *Rptor<sub>ob</sub><sup>-/+</sup>* and *Rptor<sub>ob</sub><sup>-/-</sup>* mice of either sex, relative to control mice (Fig. 2.1H and Supplementary Fig. 2.2A). Further histological examination of gWAT and



iWAT depots revealed a marked reduction in adipocyte size in male *Rptor<sub>ob</sub><sup>-/-</sup>* mice, as evidenced by an increase in the frequency of smaller adipocytes (Fig. 2.1I-K), but this was not observed in female mice (Supplementary Fig. 2.2B).

The higher proportion of small adipocytes observed in *Rptor<sub>ob</sub><sup>-/-</sup>* iWAT and gWAT could either be attributable to (i) enhanced adipogenesis (resulting in an increase in small, newly-generated adipocytes), (ii) decreased lipogenesis and/or enhanced lipolysis in existing adipocytes, or (iii) a combination of both. To address this question, the expression levels of genes involved in adipogenesis, lipogenesis and lipolysis were analysed by qRT-PCR. As shown in Fig. 2.1L and M, the expression levels of *Cebpa* and *Pparg*, master regulators of adipogenesis, and their downstream target gene, lipoprotein lipase (*Lpl*), were significantly increased in iWAT and gWAT collected from male *Rptor<sub>ob</sub><sup>-/-</sup>* mice, suggesting that adipogenesis is enhanced in both of these fat depots. In contrast, while expression levels of *Srebp1c* were unaltered in both fat depots, levels of fatty acid synthase (*Fasn*), an important *Srebp1c* target gene, were significantly reduced in *Rptor<sub>ob</sub><sup>-/-</sup>* gWAT and increased in *Rptor<sub>ob</sub><sup>-/-</sup>* iWAT compared to the controls, and no significant changes in adipose triglyceride lipase (*Atgl*), an important lipolysis enzyme, were observed (Fig. 2.1L and M). Consistent with the lack of differences in adipocyte size in female *Rptor<sub>ob</sub><sup>-/+</sup>* and *Rptor<sub>ob</sub><sup>-/-</sup>* mice, no significant change in the expression levels of genes involved in adipogenesis, lipogenesis and lipolysis were observed (Supplementary Figure 2.2B-D).

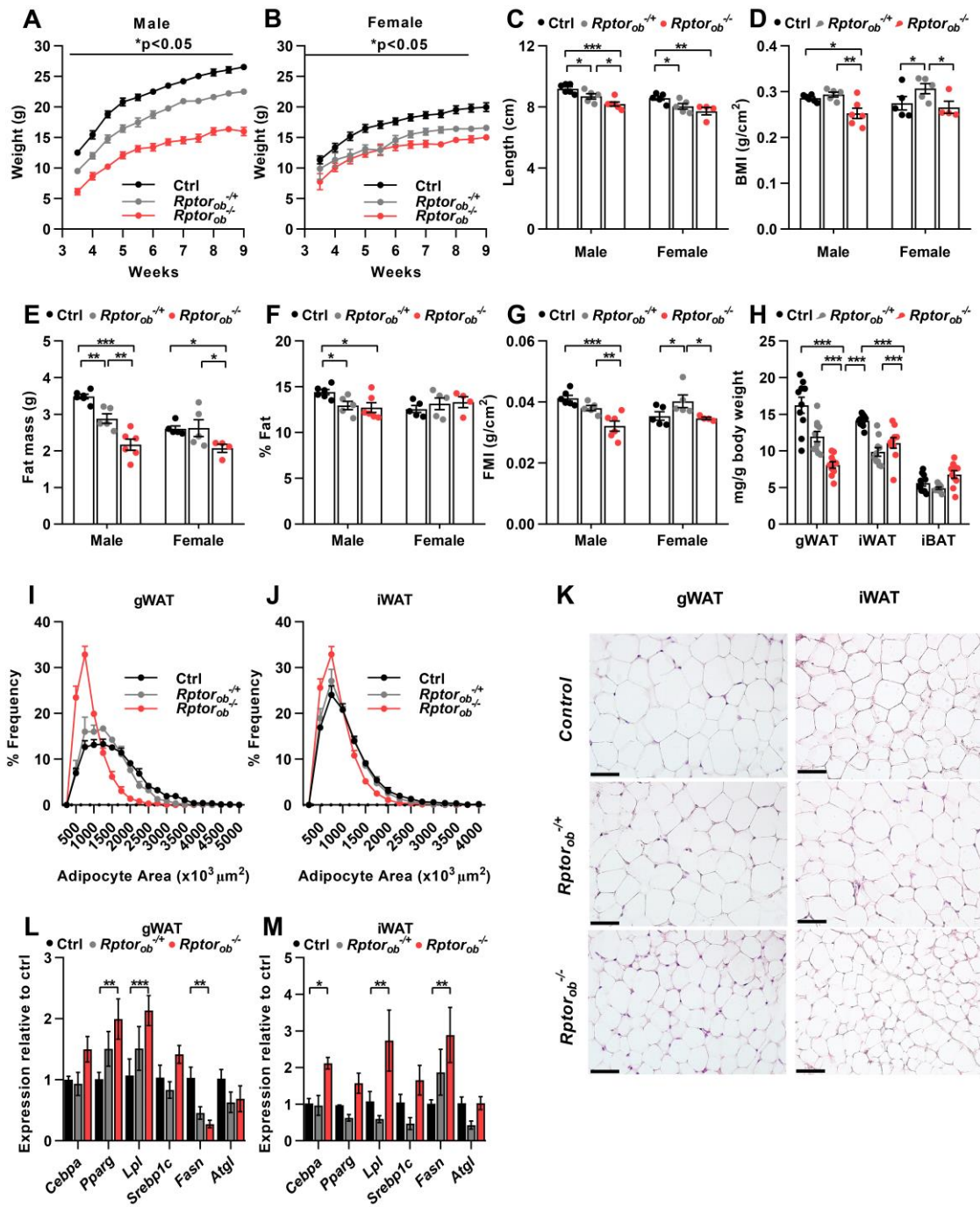


**Fig. 2.1 Loss of OB-mTORC1 function results in altered body composition. (A-B)** Temporal body weight changes in male and female mice ( $n \geq 15$ /genotype). **(C)** Body length of 9-week old mice, as measured from nose to anus ( $n=5-6$ /genotype). **(D)** Body mass index (BMI) ( $n=5-6$ /genotype). **(E)** DXA analysis of fat mass and **(F)** % fat mass normalised to total body weight ( $n=5-6$ /genotype). **(G)** Fat mass index (FMI) ( $n=5-6$ /genotype). **(H)** Body weight-adjusted gonadal and inguinal white adipose tissue (gWAT and iWAT) and interscapular brown adipose tissue (iBAT) mass in male mice at 9-weeks of age ( $n=10$ /genotype). **(I-J)** Size distribution of gWAT and iWAT adipocytes of male mice calculated from H&E stained sections using Image J ( $n=5$  sections/mouse,  $n=3-6$ /genotype). **(K)** Representative H&E section of gWAT and iWAT from male mice, scale bar = 50 $\mu$ m. **(L-M)** Relative expression of adipogenesis - , lipogenesis - and lipolysis - related genes, normalised to  $\beta$ -actin, in gWAT and iWAT from male mice ( $n=3-5$ /genotype). All panels except K: data are expressed as mean  $\pm$  SEM. \* $p < 0.05$ , \*\* $p < 0.01$ , \*\*\* $p < 0.001$ , two-way ANOVA with Tukey's post-hoc test.

#### 2.4.2 Improved glucose metabolism and increased insulin sensitivity in *Rptor<sub>ob</sub><sup>-/-</sup>* mice

The striking effects of OB-mTORC1 inhibition on body composition suggested that metabolism was likely to be significantly altered in *Rptor<sub>ob</sub><sup>-/-</sup>* mice. Indeed, upon further examination, *Rptor<sub>ob</sub><sup>-/-</sup>* mice were found to have significantly lower fasting glucose levels (Fig. 2.2A: 22.8% and 22.0% lower compared to controls in males and females, respectively). Fasting glucose levels were also significantly lower in male, but not the female, *Rptor<sub>ob</sub><sup>-/+</sup>* mice compared to controls (Fig. 2.2A). When fasted animals were challenged with a bolus of glucose, male mice exhibited enhanced glucose clearance compared to controls, whereas no change in glucose tolerance was observed in male *Rptor<sub>ob</sub><sup>-/+</sup>* mice or in the female cohort (Fig. 2.2B-D). Strikingly, the hypoglycaemia and increased glucose tolerance observed in male *Rptor<sub>ob</sub><sup>-/-</sup>* mice was not attributable to hyperinsulinemia, as the fasting insulin levels of both male and female *Rptor<sub>ob</sub><sup>-/-</sup>* mice were 50% lower than control levels (Fig. 2.2E). Fasting insulin levels were also significantly lower in heterozygous mice of both genders relative to controls (Fig. 2.2E).

Enumeration of insulin-positive pancreatic islets in male *Rptor<sub>ob</sub><sup>-/-</sup>* mice revealed that the hypoinsulinemia was not due to a reduction in the number of islets, although trends toward a reduction in  $\beta$ -cell area ( $p=0.065$ ) and islet size ( $p=0.077$ ) were observed (Supplementary Fig. 2.3A and B). No significant changes in islet morphology were observed in female mice (Supplementary Fig. 2.3B). Despite lower circulating insulin levels (Fig. 2.2E), the ability of both male and female *Rptor<sub>ob</sub><sup>-/+</sup>* and *Rptor<sub>ob</sub><sup>-/-</sup>* mice to secrete insulin in response to a glucose bolus (glucose-stimulated insulin secretion tests [GSIS]) remained functional as demonstrated by a significant increase in insulin levels at 30 minutes post glucose bolus compared to the basal levels (Fig. 2.2F and G). Moreover, the relative insulin levels at 30 minutes (i.e. insulin fold induction relative to basal levels to account for lower basal insulin levels) in response to glucose bolus were significantly higher in *Rptor<sub>ob</sub><sup>-/+</sup>* and *Rptor<sub>ob</sub><sup>-/-</sup>* mice relative to controls in both sexes (Fig. 2.2H).

The reduced fasting insulin and glucose levels observed in *Rptor<sub>ob</sub><sup>-/-</sup>* mice, coupled with their improved glucose disposal and ability to maintain lower levels of circulating insulin after glucose bolus, suggested that these mice were more sensitive to insulin compared to their *Rptor<sub>ob</sub><sup>-/+</sup>* and control littermates. To address this question, insulin tolerance tests (ITTs) were performed to assess their peripheral sensitivity to insulin. As shown in Fig. 2.2I-K, both male and female *Rptor<sub>ob</sub><sup>-/-</sup>* mice were more insulin sensitive

compared to controls, whereas no difference was observed in *Rptor<sup>ob</sup><sup>-/+</sup>* mice of both genders.

To further investigate insulin sensitivity in *Rptor<sup>ob</sup><sup>-/-</sup>* mice, gene expression levels of known markers of insulin sensitivity (muscle: *Pcg1 $\alpha$*  and its target genes, *Mcad* and *Nrf1*; liver: *Foxa2*) and insulin-targeted genes involved in carbohydrate metabolism in primary insulin target tissues were analysed. Somewhat unexpectedly, no significant changes in the expression levels of these genes were observed in either tissue (Supplementary Fig. 2.4A and B). Furthermore, the levels of insulin-stimulated phosphorylation of the INSR at Tyr<sup>1150/1151</sup> and its downstream effector protein AKT at Ser<sup>473</sup> *in vivo* were unchanged in both tissues by Western blot (Supplementary Fig. 2.4C-F).

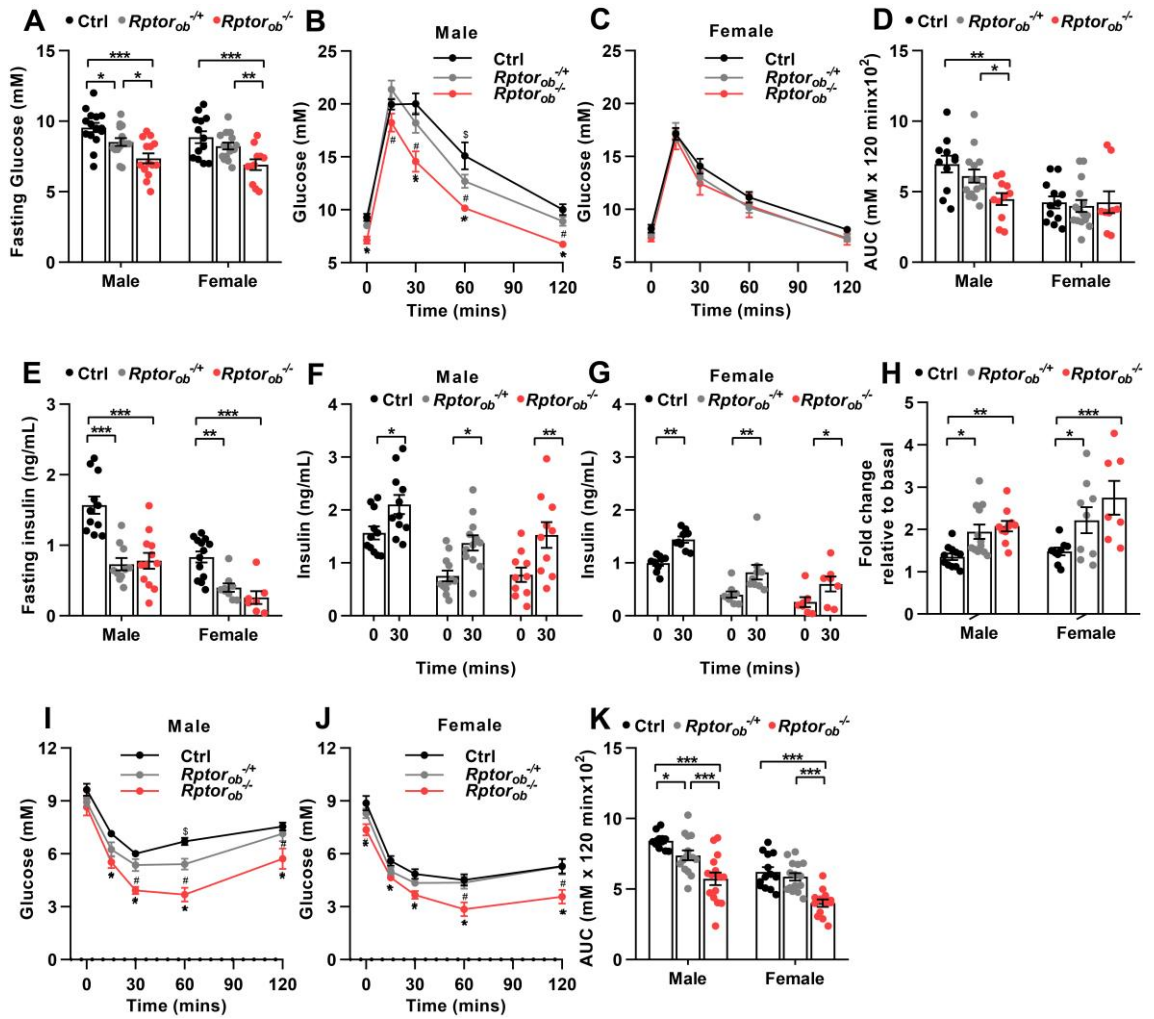


**Fig. 2.2 Loss of OB-mTORC1 function leads to improved whole-body glucose metabolism.** (A) Fasting blood glucose levels in 9-week old male and female mice (n=11-15/genotype). (B-C) GTT blood glucose levels in mice at 9-week of age, and (D) Incremental area under the curve analysis (n=10-15/genotype). (E) Fasting serum insulin levels at 9-week of age (n=7-13/genotype). (F-G) Glucose-stimulated insulin levels in male and female mice, and (H) fold change in insulin levels at 30 minutes relative to basal levels (n=7-12/genotype). (I-J) ITT blood glucose levels in male and female mice at 8-week of age, and (K) Area under the curve analysis (n=8-15/group). All panels except B, C, I and J: data are expressed as mean  $\pm$  SEM. \*p<0.05, \*\*p<0.01, \*\*\*p<0.001, two-way ANOVA with Tukey's post-hoc test. For panel B, C, I and J: \*p<0.05 between *Rptor<sub>ob</sub><sup>-/-</sup>* and Ctrl, #p<0.05 between *Rptor<sub>ob</sub><sup>-/-</sup>* and *Rptor<sub>ob</sub><sup>-/+</sup>* and §p<0.05 between *Rptor<sub>ob</sub><sup>-/+</sup>* and Ctrl, two-way ANOVA with Tukey's post-hoc test.

### **2.4.3 Male *Rptor<sub>ob</sub><sup>-/-</sup>* mice have increased total energy expenditure and increase fat oxidation**

To further examine the underlying mechanisms associated with the altered body composition of *Rptor<sub>ob</sub><sup>-/-</sup>* mice, serum metabolite markers, food intake, energy expenditure and physical activity were examined. To account for the differences in their body size, each of these metabolic parameters were normalised to their lean mass. In line with their reduced adiposity (Fig. 2.1E), circulating leptin levels were found to be significantly lower in both male and female *Rptor<sub>ob</sub><sup>-/-</sup>* mice (Fig. 2.3A). Importantly, whilst absolute food intake was lower in male *Rptor<sub>ob</sub><sup>-/-</sup>* mice (Fig. 2.3B) compared to controls, when normalised to lean mass there were no significant differences in food intake across the three genotypes (Fig. 2.3C), which indicates that their food consumption was proportional to body size. Faecal lipid content was examined to determine if food malabsorption may account for the lean phenotype of male *Rptor<sub>ob</sub><sup>-/-</sup>* mice. However, no difference in faecal lipid content was observed (Fig. 2.3D). In contrast, in female *Rptor<sub>ob</sub><sup>-/-</sup>* mice, food intake (both absolute and normalised) was significantly lower (Fig. 2.3B and C) and faecal lipid content showed a trend toward a reduction (Fig. 2.3D;  $p=0.066$ ).

As whole-body adiposity is determined by the balance between food intake and caloric utilisation, increased energy expenditure could account for reduced adiposity of both male *Rptor<sub>ob</sub><sup>-/+</sup>* and *Rptor<sub>ob</sub><sup>-/-</sup>* mice in the presence of unaltered proportional caloric intake. Total energy expenditure (TEE) normalised to lean mass (kcal/g of lean mass), was significantly higher in male *Rptor<sub>ob</sub><sup>-/-</sup>* mice during both the light and dark period despite no significant changes in physical activity, both ambulatory (X+Y movements: walking) and Z-axis (rearing) (Fig. 2.3E-H). Respiratory quotient (RQ) was also significantly lower in male *Rptor<sub>ob</sub><sup>-/-</sup>* mice during both the light and dark periods (Fig. 2.3I and J), indicating a preference for fat oxidation. Of note, there were no differences between male *Rptor<sub>ob</sub><sup>-/+</sup>* and control mice in any of the parameters measured. Conversely, physical activity (both ambulatory (X+Y movements: walking) and Z-axis (rearing): Fig. 2.3E and F) was lower in both female *Rptor<sub>ob</sub><sup>-/+</sup>* and *Rptor<sub>ob</sub><sup>-/-</sup>* mice while TEE was equivalent to that of controls (Fig. 2.3K and L). The lower RQ of female *Rptor<sub>ob</sub><sup>-/-</sup>* mice, while only observed during the light period, suggested a preference for fat oxidation (Fig. 2.3M and N).

To further examine this potential shift in energy utilisation towards fat oxidation in *Rptor<sup>ob</sup><sup>-/-</sup>* mice, circulating levels of ketone bodies, free fatty acids (FFA) and triglycerides (TG) were measured. Serum levels of  $\beta$ -hydroxybutyrate ( $\beta$ OHB), the primary ketone body, were significantly higher in both male and female *Rptor<sup>ob</sup><sup>-/-</sup>* mice compared to controls (Fig. 2.3O), whilst circulating TG levels were lower (Fig. 2.3P) and FFA levels unchanged (Fig. 2.3Q) in male *Rptor<sup>ob</sup><sup>-/-</sup>* mice compared to the controls. No changes in TG or FFA levels were observed in female mice.



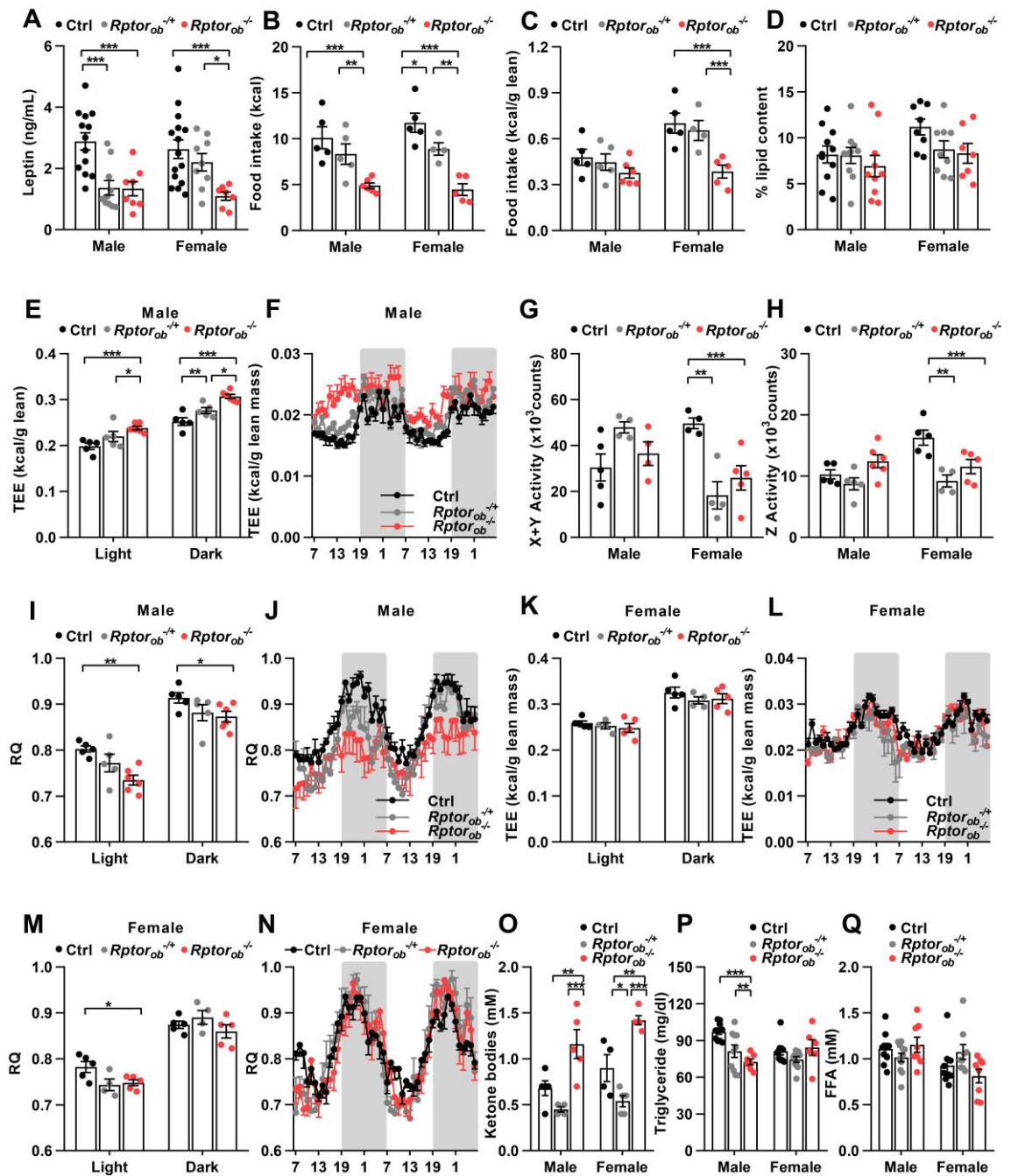


**Fig. 2.3 Loss of OB-mTORC1 function shifts whole-body fuel utilisation toward fat oxidation.** (A) Serum leptin levels in 9-week old male and female mice (n=7-15/genotype). (B) Food intake per day, measured over 48-h, presented as absolute food intake (kcal/day), or (C) normalised to lean mass (kcal/g lean mass/day). (D) Faecal lipid content (% lipid/g faeces) (n=7-10/genotype). (E) Ambulatory X+Y axis activity per day. (F) Z-axis (rearing) locomotor activity per day. (G) Total energy expenditure, normalised to lean mass, per light and dark cycle, and (H) over a 48-h time course in male mice. (I) Average respiratory quotient (RQ) per light and dark cycle, or (J) over a 48-h time course in male mice. (K) Total energy expenditure, normalised to lean mass, per light and dark cycle, and (L) over a 48-h time course in female mice. (M) Average respiratory quotient (RQ) per light and dark cycle, or (N) over a 48-h time course in female mice. (O) Fasting serum ketone body levels (n=4-5/genotype). (P) Serum triglyceride levels measured at non-fasted condition (n=6-10/genotype). (Q) Serum free fatty acid levels measured at non-fasted condition (n=8-11/genotype). All panels: data are expressed as mean  $\pm$  SEM from n=5-6/group, unless indicated otherwise. \*p<0.05, \*\*p<0.01, \*\*\*p<0.001, two-way ANOVA with Tukey's post-hoc test. Panels H, J, L, N: shaded regions represent dark cycle.

#### **2.4.4 Metabolic improvements in *Rptor<sub>ob</sub><sup>-/-</sup>* mice occur independently of osteocalcin**

Previous pioneering studies by the Karsenty laboratory have attributed the skeletal regulation of whole-body glucose metabolism to the actions of OCN<sup>1,6</sup>. OCN binds avidly to bone hydroxyapatite and, following decarboxylation to its active form (undercarboxylated OCN: unOCN), is released into the circulation<sup>26</sup>. unOCN binds to its receptor on pancreatic  $\beta$ -cells to increase insulin secretion and  $\beta$ -cell proliferation<sup>27</sup> and on muscle, adipose tissues, and liver to increase insulin sensitivity and glucose uptake into these tissues. To investigate whether the metabolic improvements in *Rptor<sub>ob</sub><sup>-/-</sup>* mice are attributable to OCN, expression levels of the OCN gene, *Bglap*, in the long bones and circulating serum OCN levels were investigated. Consistent with previously-published studies<sup>15</sup>, mRNA and serum levels of both total OCN and unOCN were both significantly lower in male and female *Rptor<sub>ob</sub><sup>-/-</sup>* mice (Fig. 2.4A-C).

In addition to OCN, more-recent studies have shown that the skeleton can regulate appetite and glucose homeostasis via lipocalin-2 (LCN2)<sup>28</sup>, an OB-enriched, secreted protein. To determine if increased LCN2 levels may be compensating for the decreased unOCN levels observed in *Rptor<sub>ob</sub><sup>-/+</sup>* and *Rptor<sub>ob</sub><sup>-/-</sup>* mice, serum LCN2 levels were measured; however no differences were found across the three genotypes (Fig. 2.4D). More recently, osteoglycin (OGN) has been identified as a novel downstream mediator of NPY/Y1 signaling in OBs that plays a role in coordinating bone accrual and global energy balance<sup>29,30</sup>. Under the conditions of a negative energy balance, an increase in NPY signaling in bone leads to an increase in OGN secretion, which then suppresses bone formation and increases systemic glucose uptake by enhancing insulin action<sup>30</sup>. In line with the improved glucose metabolism (Fig. 2.2) and low bone mass phenotype of male *Rptor<sub>ob</sub><sup>-/-</sup>* mice<sup>15</sup>, the circulating OGN levels were elevated ~2.6 and 1.7-fold in male and female *Rptor<sub>ob</sub><sup>-/-</sup>* mice relative to controls respectively (Fig. 2.4E). Taken together, these findings suggest that the improvements in glucose and energy metabolism observed in *Rptor<sub>ob</sub><sup>-/-</sup>* mice may result from an increase in OGN secretion and OGN-dependent regulation of insulin sensitivity.

#### **2.4.5 Loss of *mTORC1* function in pre-OBs is associated with reproductive defects in males**

While the reduced levels of serum OCN and unOCN observed in the *Rptor<sub>ob</sub><sup>-/-</sup>* mice suggested that OCN was not responsible for the improvement in glucose metabolism, it prompted a question as to whether the low levels of OCN were associated with any

other physiological outcomes. Previous studies have shown that OCN is important for male fertility by acting on Leydig cells in the testes to promote testosterone production and spermatogenesis<sup>31</sup>. Consistent with this, male *Rptor<sub>ob</sub><sup>-/-</sup>* and *Rptor<sub>ob</sub><sup>-/+</sup>* mice have significantly smaller testes and seminal vesicles compared to controls, while epididymal weights were unchanged across all genotypes (Fig. 2.4F). Circulating testosterone levels were also significantly lower in both *Rptor<sub>ob</sub><sup>-/+</sup>* and *Rptor<sub>ob</sub><sup>-/-</sup>* mice compared to the controls (Fig. 2.4G). Interestingly, despite both *Rptor<sub>ob</sub><sup>-/+</sup>* and *Rptor<sub>ob</sub><sup>-/-</sup>* mice having lower testosterone levels, only *Rptor<sub>ob</sub><sup>-/-</sup>* mice have a lower sperm count compared to controls (Fig. 2.4H). Gene expression analyses also confirmed a significantly lower expression of genes involved in testosterone biosynthesis, such as *StAR*, *Cyp17* and *Cyp11a*, whilst genes involved in estradiol production (i.e. *Cyp19a* and *Hsd17b3*) were unchanged in *Rptor<sub>ob</sub><sup>-/-</sup>* mice (Fig. 2.4H). Consistent with the lower circulating testosterone levels in *Rptor<sub>ob</sub><sup>-/+</sup>* mice, *StAR* expression was found to be significantly lower in these mice relative to controls (Fig. 2.4H).

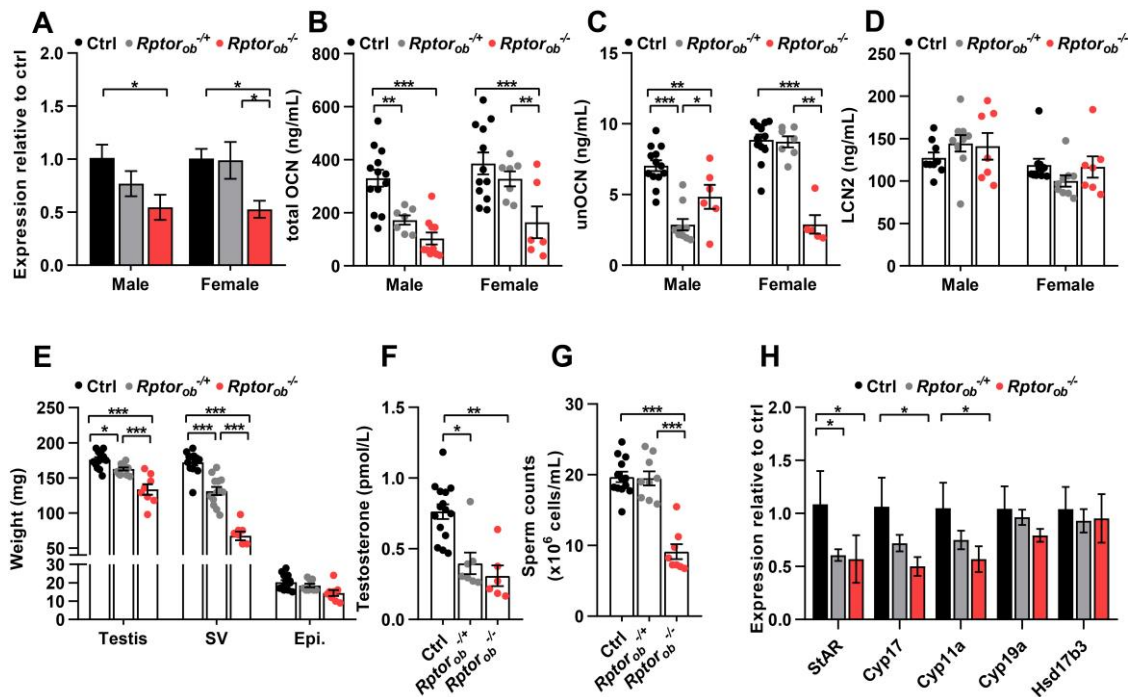


**Fig. 2.4 Improvements in glucose metabolism observed in *Rptor<sub>ob</sub><sup>-/-</sup>* mice occur independently of osteocalcin.** (A) *Bglap* gene expression in flushed long bones (femur/tibia, n=3-4/genotype) from 9-week old male and female mice. (B) Serum OCN (total) levels (n=6-13/genotype). (C) Serum unOCN levels (n=5-13/genotype). (D) Serum lipocalin-2 levels (n=7-10/genotype). (E) Serum osteoglycin levels (n=7-10/genotype). (F) Male reproductive organ weights (testis, seminal vesicles (SV), Epididymides (Epi.), n=8-13/genotype). (G) Serum testosterone levels (n=6-15/genotype). (H) Sperm counts (n=8-13/genotype). (I) Relative expression of genes involved in testosterone biosynthesis (*StAR*, *Cyp17*, *Cyp11a*) and estradiol production (*Cyp19a*, *Hsd17b3*), normalised to  $\beta$ -actin, in testicle samples from male mice (n=3/genotype). All panels: data are expressed as mean  $\pm$  SEM. \*p<0.05, \*\*p<0.01, \*\*\*p<0.001, two-way ANOVA with Tukey's post-hoc test.

#### **2.4.6 The improved metabolic profile of *Rptor<sub>ob</sub><sup>-/-</sup>* mice is associated with elevated serum adiponectin levels**

The low total body fat in *Rptor<sub>ob</sub><sup>-/-</sup>* mice raised a question as to whether changes in serum adipokine levels could be playing a role in their metabolic phenotype. Adiponectin has been shown to play an important role in sensitising tissues to insulin and elevated adiponectin levels are associated with improved insulin sensitivity<sup>32</sup>. In particular, levels of the high molecular weight (HMW) form of adiponectin, the most bio-active form, correlate negatively with insulin resistance<sup>33</sup>. Indeed, adiponectin mRNA expression and circulating adiponectin protein levels are significantly lower under conditions of excess adiposity (i.e. obesity) and diabetes in both mice and humans<sup>34</sup>, while its levels are markedly higher under conditions of extreme leanness such as dietary restriction (DR) and anorexia nervosa (AN)<sup>35</sup>. Consistent with the improvement in insulin sensitivity observed in male and female *Rptor<sub>ob</sub><sup>-/-</sup>* mice (Fig. 2.2G), serum adiponectin levels were significantly higher (~1.5-fold in both sexes) relative to controls (Fig. 2.5A). For the heterozygous knockout mice, adiponectin levels remained unchanged in both males and females (Fig. 2.5A) which is consistent with the lack of improvement in their insulin sensitivity (Fig. 2.2I-J). Western blot analysis of the adiponectin complexes revealed a 2-fold increase in the HMW complex in both male and female *Rptor<sub>ob</sub><sup>-/-</sup>* mice (Fig. 2.5B-E).

While WAT has long been considered as the major source of adiponectin, recent studies have shown that bone marrow adipose tissue (BMAT) is also a significant source of adiponectin under the condition of restricted dietary<sup>36</sup>. Consequently, expression levels of adiponectin transcripts and protein in both WAT and whole bone were examined. As shown in Fig. 5F and G, levels of *Adipoq* mRNA expression were unchanged in both iWAT and gWAT in both *Rptor<sub>ob</sub><sup>-/+</sup>* and *Rptor<sub>ob</sub><sup>-/-</sup>* male mice relative to controls, whereas a trend toward lower *AdipoQ* expression was detected in gWAT from female *Rptor<sub>ob</sub><sup>-/+</sup>* and *Rptor<sub>ob</sub><sup>-/-</sup>* mice. Strikingly, however, levels of *Adipoq* mRNA expression were ~2.3-fold higher in the BMAT-containing long bones (combined Tibia/femur: Tib/fem) of *Rptor<sub>ob</sub><sup>-/-</sup>* mice (Fig. 2.5F-G). At the protein level, adiponectin levels were ~4-fold and ~1.5-fold higher in lysates from male and female *Rptor<sub>ob</sub><sup>-/-</sup>* long bones (tibia/femur), respectively, compared to controls (Fig. 2.5H-K). No genotypic differences in adiponectin levels were observed in both iWAT and gWAT depots. Although the physiological role of BMAT remains largely unknown, its expansion has been reported in response to changes in nutrient availability including dietary restriction

(DR) in mice<sup>37</sup> and AN in humans<sup>35</sup>, high-fat diet feeding<sup>38</sup> and leptin deficiency<sup>39</sup>. Of note, previously-published reported a significant increase in BMAT in *Rptor<sup>ob</sup><sup>-/-</sup>* mice<sup>15</sup> and herein we have shown that BMAT expansion in *Rptor<sup>ob</sup><sup>-/-</sup>* mice is associated with hypoleptinemia (Fig. 2.3A). More recently, BMAT expansion, in response to DR, has been associated with increased serum levels of glucocorticoids<sup>40</sup>. Consistent with this finding, the circulating levels of corticosterone were significantly increased in *Rptor<sup>ob</sup><sup>-/-</sup>* mice (Fig. 2.5L).

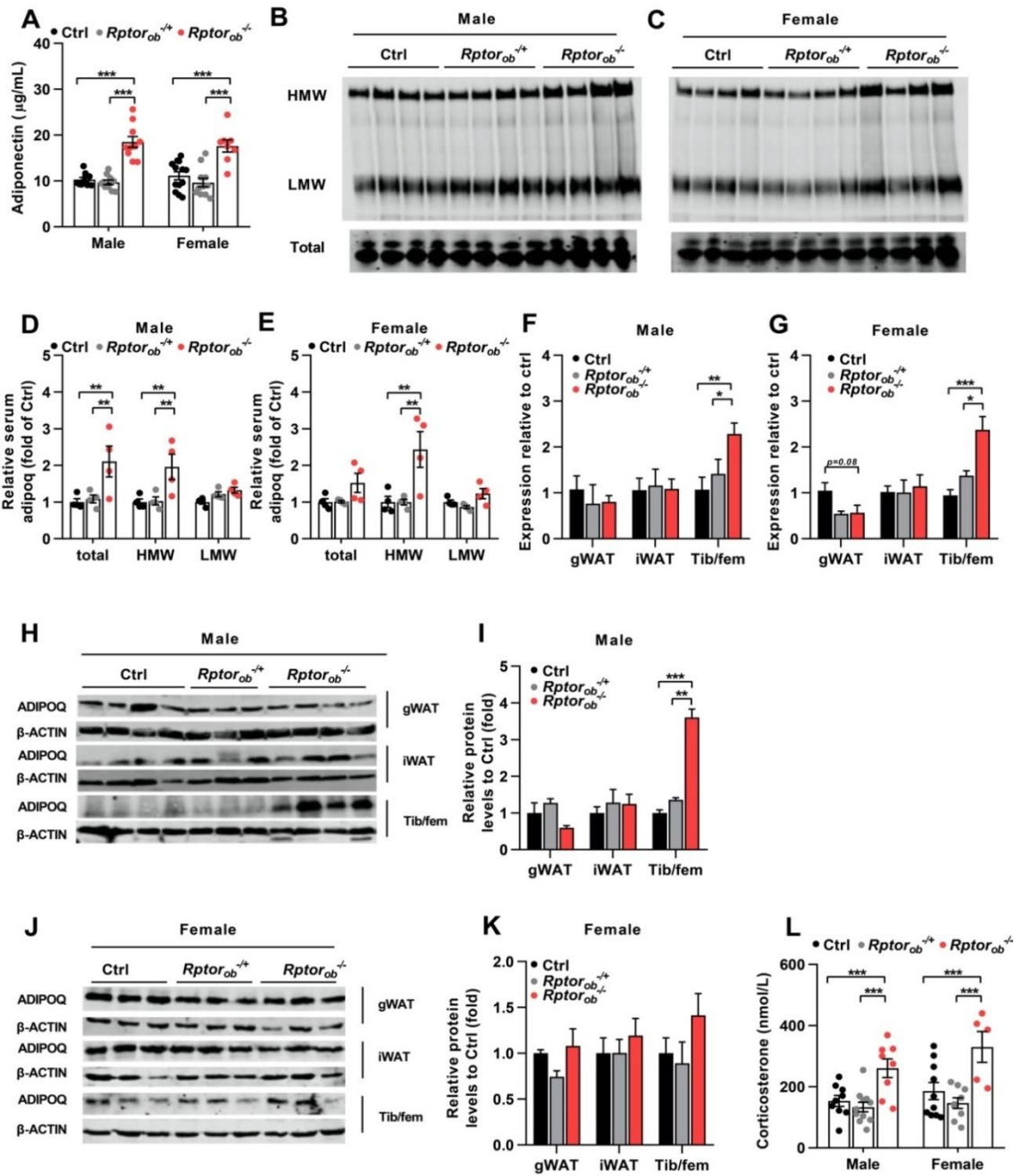




**Fig. 2.5 Bone marrow adipose-derived adiponectin levels are increased in *Rptor<sup>ob</sup><sup>-/-</sup>* mice.** (A) Serum adiponectin levels in 9-week old male and female mice (n=8-13/genotype). (B-E) Western blot analysis of high molecular weight (HMW), low molecular weight (LMW) and total adiponectin levels in sera from male and female mice (n=4/genotype). (F-G) *Adipoq* gene expression, normalised to  $\beta$ -actin, in gWAT, iWAT and whole long bone (tibia/femur) samples (n=3-5/genotype). (H) Levels of total adiponectin protein expression in gWAT, iWAT and whole long bone (tibia/femur) samples in male mice (n=3-4/genotype) and (I) Quantitative analysis of adiponectin protein levels, relative to  $\beta$ -actin, from (H). (J) Levels of total adiponectin protein expression in gWAT, iWAT and whole long bone (tibia/femur) samples in females mice (n=3/genotype) and (K) Quantitative analysis of adiponectin protein levels, relative to  $\beta$ -actin, from (J). (L) Serum corticosterone levels in 9-week old male and female mice (n=5-11/genotype). All panels except B, C, H, I: data are expressed as mean  $\pm$  SEM. \*p<0.05, \*\*p<0.01, \*\*\*p<0.001, two-way ANOVA with Tukey's post-hoc test.

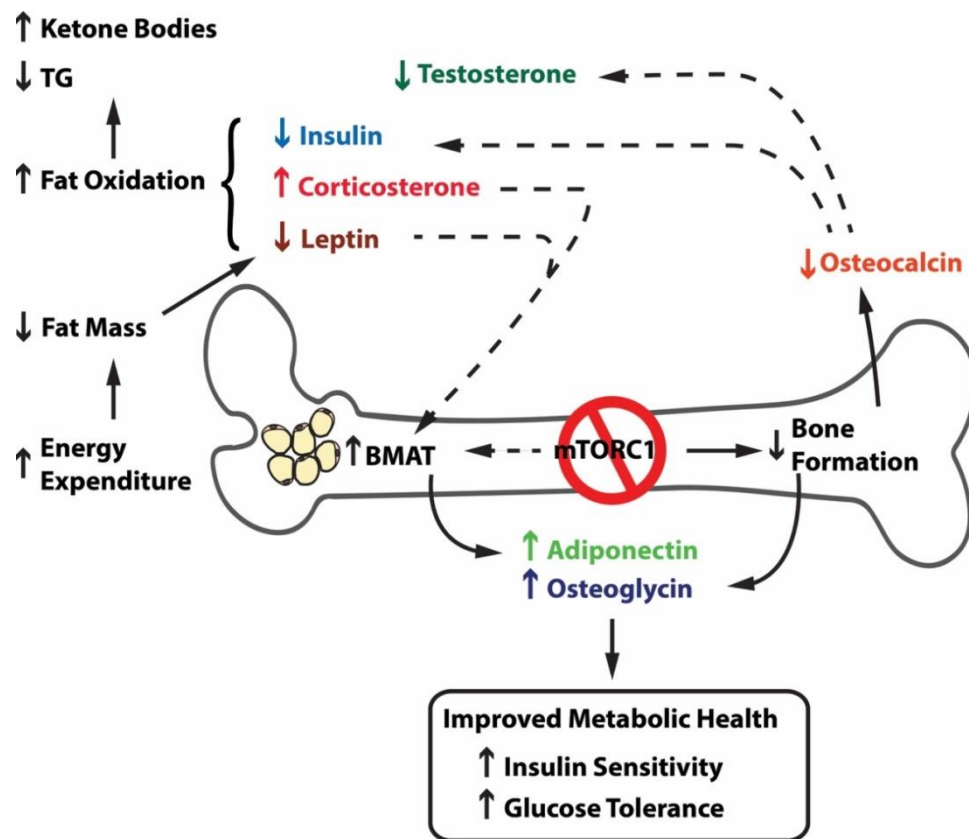


**Fig. 2.6 Schematic summary.** Inactivation of mTORC1 via deletion of *Rptor* in early osteoprogenitor cells leads to a decrease in bone formation and subsequent lower circulating osteocalcin levels. While these reduced osteocalcin levels lead to the reduced testosterone levels in the male mice and may contribute to lower circulating insulin levels in both sexes, the increase in serum osteoglycin and the elevated levels of bone marrow adipose tissue (BMAT)-derived adiponectin results in an overall improvement in metabolic health, including an increase in insulin sensitivity and glucose tolerance. The expansion of BMAT is associated with low leptin and increased corticosterone levels in the *Rptor<sup>ob</sup><sup>-/-</sup>* mice. Furthermore, at least in the male mice, the increase in energy expenditure with unaltered food intake results in a lean phenotype and a shift in whole-body fuel utilisation toward fat oxidation, causing elevated ketone body levels.

## 2.5 Discussion

Recent advances in skeletal research have revealed previously unimagined functions for the skeleton, with OBs, the bone-forming cells of the skeleton, now known to play an important role in the regulation of systemic glucose metabolism. The results presented herein further support the concept that OBs play a critical role in gluco-regulation and energy homeostasis. Importantly, these results suggest an integral role for OBs in the regulation of nutritional status and glucose metabolism and extend the knowledge of how OBs contribute to the whole-body homeostatic balances (Fig. 2.6).

### 2.5.1 Skeletal mTORC1, insulin signalling and glucose uptake

Previous studies have demonstrated that mTORC1 plays an important role in bone formation and OB differentiation as mice with inactivated mTORC1 in OBs are severely osteopenic<sup>14,15,41</sup>. In this current study, it was revealed that *Rptor<sub>ob</sub><sup>-/-</sup>* mice also display a marked whole-body metabolic phenotype characterised by low glycaemic levels, enhanced glucose tolerance, increased insulin sensitivity and increased insulin secretion. mTORC1 is a crucial mediator of insulin signalling and the bone phenotypes of *Rptor<sub>ob</sub><sup>-/-</sup>* and *INSR<sub>OB</sub><sup>-/-</sup>* mice are very similar<sup>2</sup>. However, unexpectedly, the metabolic phenotype of *Rptor<sub>ob</sub><sup>-/-</sup>* mice is the complete opposite to *INSR<sub>OB</sub><sup>-/-</sup>* mice, which exhibit hyperglycaemia, decreased insulin sensitivity and increased peripheral adiposity<sup>1</sup>.

The disparity in the metabolic phenotypes might be a consequence of removing the mTORC1-dependent negative feedback control of insulin signalling in *Rptor<sub>ob</sub><sup>-/-</sup>* mice. mTORC1, both directly<sup>42</sup> and indirectly via S6K1<sup>43</sup>, phosphorylates IRS-1, promoting its ubiquitination and degradation. mTORC1 also phosphorylates and stabilises receptor tyrosine kinase (RTK) inhibitor growth factor receptor-bound protein 10 (Grb10)<sup>44</sup>, leading to feedback inhibition of the phosphatidylinositol 3-kinase (PI3K) pathways. The removal of these mTORC1-regulated negative controls could potentiate insulin signalling, leading to insulin hypersensitivity in the OBs of the *Rptor<sub>ob</sub><sup>-/-</sup>* mice. Consistent with this view, the metabolic phenotypes of the *Rptor<sub>ob</sub><sup>-/-</sup>* mice are similar to those of mice with OB-specific deletion of either *FoxO1* or *Atf4*, negative regulators of insulin signalling<sup>4,45</sup>. Furthermore, it is possible that this potentiated insulin signalling could also explain the hypoglycaemia in the *Rptor<sub>ob</sub><sup>-/-</sup>* mice, whereby hyper-activation of insulin signalling in OBs activates AKT, which promotes translocation of glucose transport 4 (GLUT4) to the plasma membrane and thus increases GLUT4-mediated glucose uptake into the OBs<sup>46</sup>. In support of this, significantly higher levels of *Glut4*

mRNA (Supplementary Fig. S2.5A) and genes involving in glycolysis (Supplementary Fig. 2.5B) were observed in the bones of male *Rptor<sub>ob</sub><sup>-/-</sup>* mice. However, further investigations are required to verify if there is an increase in translocation of GLUT4 to the plasma membrane and glucose uptake in OBs in the *Rptor<sub>ob</sub><sup>-/-</sup>* mice.

Given that bone constitutes approximately 15% of body mass, increased glucose uptake into the bone could lower overall glucose levels. While this mechanism has not yet been confirmed in the bones of *Rptor<sub>ob</sub><sup>-/-</sup>* mice, hyper-activation of PKB/AKT as a result of mTOR deficiency in muscle (mTOR<sup>-/-</sup>) has been reported to increase basal glucose uptake<sup>47</sup>. Moreover, the hyper-activation of PKB/AKT was also reported in mice with muscle-specific *Rptor* deletion (RAmKO)<sup>13</sup>, indicating that mTORC1 disruption is likely to be responsible for the changes observed in mTOR<sup>-/-</sup> mice<sup>47</sup>. Furthermore, RAmKO are glucose intolerant, suggesting that mTORC1 in skeletal muscle exerts a positive effect on whole-body glucose handling<sup>13</sup>. In contrast, conditional deletion of *Rptor* in adipose tissue (*raptor<sup>ad</sup><sup>-/-</sup>*), results in lean mice that are resistant to diet-induced obesity<sup>11</sup>. These contradicting findings suggest that mTORC1 has tissue-specific functions that affect different aspects of whole-body energy metabolism. Collectively, the data described herein indicate that dysregulation of mTORC1 in the skeleton has a significant impact on whole-body glucose metabolism and thus highlights the importance of skeletal contribution to the regulation of glucose homeostasis.

### 2.5.2 Metabolic phenotypes independent of OCN

Previous studies have demonstrated that unOCN, a bone-derived secretagogue, acts in a feed-forward loop to enhance pancreatic  $\beta$ -cell insulin secretion and improve insulin sensitivity in peripheral tissues<sup>6</sup>. Moreover, in both animal and human studies<sup>6,48</sup>, circulating OCN levels are generally inversely correlated with plasma glucose levels, fat mass and the degree of impaired glucose metabolism. Based on these data, it was initially hypothesised that the improved metabolic characteristics of *Rptor<sub>ob</sub><sup>-/-</sup>* mice were attributable to the actions of OCN. However, the unexpectedly lower levels of both total and unOCN in the *Rptor<sub>ob</sub><sup>-/-</sup>* mice were incongruent with a role of OCN in mediating systemic metabolic phenotypes in *Rptor<sub>ob</sub><sup>-/-</sup>* mice. Moreover, *Ocn*-deficient mice (*Ocn<sup>-/-</sup>*) are phenotypically opposite to *Rptor<sub>ob</sub><sup>-/-</sup>* mice, in that *Ocn<sup>-/-</sup>* mice exhibit higher adiposity, hyperglycaemia, hypoinsulinemia, impaired insulin secretion and sensitivity and are glucose intolerant<sup>6</sup>. These defects in glucose homeostasis are accompanied by impairment in pancreatic  $\beta$ -cell proliferation and insulin secretion and development of

insulin resistance in other insulin-targeted tissues<sup>6</sup>. While low serum levels of unOCN could possibly lead to the hypoinsulinemia in *Rptor<sub>ob</sub><sup>-/-</sup>* mice, no impairment in other OCN-mediated effects on the bone-pancreas axis were observed (i.e. both pancreatic histology and insulin secretion were normal in *Rptor<sub>ob</sub><sup>-/-</sup>* mice). Furthermore, there was no reduction in markers of insulin sensitivity nor altered activation of the insulin signalling pathway observed in peripheral tissues of *Rptor<sub>ob</sub><sup>-/-</sup>* mice.

The low serum levels of OCN observed in the *Rptor<sub>ob</sub><sup>-/-</sup>* mice are likely secondary to the stall in osteogenesis in response to reduced mTORC1 activity in pre-OBs. In support of this, reduction of mTORC1 activity in pre-OBs either pharmacologically (via rapamycin)<sup>49</sup> or genetically<sup>15</sup> has previously been reported to dramatically reduced OCN expression and serum levels of total OCN in mice. Conversely, hyper-activation of mTORC1 in OBs, by deleting *Tsc2* ( $\Delta$ Tsc2 mice), leads to an increase in bone mass and markedly elevated circulating OCN levels<sup>17</sup>. The chronic exposure to high levels of OCN, however, has been shown to lead to the desensitisation of OCN targeted tissues, including pancreatic  $\beta$ -cells, thus resulting in development of metabolic abnormalities similar to those of *INSR<sub>OB</sub><sup>-/-</sup>* mice<sup>1,17</sup>. While there is the possibility that metabolic improvement observed in *Rptor<sub>ob</sub><sup>-/-</sup>* mice is due to low levels of OCN priming its targeted tissue to be highly sensitive to OCN, this is unlikely, as serum unOCN levels were reduced in both *Rptor<sub>ob</sub><sup>-/+</sup>* and *Rptor<sub>ob</sub><sup>-/-</sup>* mice, but only *Rptor<sub>ob</sub><sup>-/-</sup>* mice showed improvement in the metabolic phenotypes.

### **2.5.3 Sex-dimorphism and energy imbalance in *Rptor<sub>ob</sub><sup>-/-</sup>* mice**

Given that an improvement in glucose tolerance was restricted to the male *Rptor<sub>ob</sub><sup>-/-</sup>* mice, this could arise from the sex-dependent action of OCN and the effects of sex steroid hormones. In support of this concept, long-term intermittent or daily oral administration of unOCN has been shown to improve glucose tolerance and increase fasting insulin and pancreatic  $\beta$ -cells area (without affecting insulin sensitivity) in female wildtype mice fed either chow or high-fat, high-sucrose diet<sup>7</sup>. Conversely, in male mice, administration of unOCN leads to an increase in circulating testosterone levels, glucose intolerance and resistance to insulin under high-fat, high-sucrose diet<sup>50</sup>. Importantly, orchietomy of male mice fed such a diet resulted in similar beneficial phenotypes of unOCN administration to female mice, while these effects were reversed in orchietomised male mice or intact female mice supplemented with testosterone. Furthermore, ovariectomy in females or orchietomised males supplemented with

estradiol did not negate the beneficial effects of unOCN, indicating that the advantageous effects of unOCN was independent of female sex hormones while the deleterious effects of unOCN is mediated by the increase in testosterone. Low unOCN in the male *Rptor<sub>ob</sub><sup>-/-</sup>* mice could contribute to the lower testosterone levels (GPRC6A, a putative OCN receptor, is expressed only in testicular Leydig cells) protecting them from high testosterone-induced glucose intolerance and resistance to insulin. Moreover, there is a possibility that the reduction in circulating testosterone could result in higher estrogen levels in male *Rptor<sub>ob</sub><sup>-/-</sup>* mice. While serum estrogen levels were not measured in this study, low testosterone with high estrogen levels have been reported in the GPRC6A knockout mice<sup>51</sup>. Notwithstanding, gene expression levels of *Cyp19a*, an aromatase responsible for conversion of testosterone to estrogen, was normal in male *Rptor<sub>ob</sub><sup>-/-</sup>* mice (Fig. 2.4H).

The altered body composition (i.e. reduced %fat) observed in the male *Rptor<sub>ob</sub><sup>-/-</sup>* mice did not occur in the female *Rptor<sub>ob</sub><sup>-/-</sup>* mice, which could be attributable to sex asymmetry (and thus sex hormones) in metabolism (reviewed in<sup>52</sup>). Females resist the loss of energy stores better than males, which may also have contributed to this sex-specific phenotype. Indeed, sex-specific differences in the ability to resist loss of fat storage are known to occur in other stains of mice<sup>53,54</sup>. In the female *Rptor<sub>ob</sub><sup>-/-</sup>* mice, unaltered energy expenditure with lower food intake (either absolute or adjusted to their body size) suggest that they are in caloric deficiency. Recent evidence suggests skeletally derived LCN2 can suppress food intake<sup>28</sup>, however no changes in circulating LCN2 levels were observed in female *Rptor<sub>ob</sub><sup>-/-</sup>* mice. In contrast, significantly lower circulating leptin levels were observed in the female *Rptor<sub>ob</sub><sup>-/-</sup>* mice despite lower food intake. It is suspected that the hypoleptinemia in *Rptor<sub>ob</sub><sup>-/-</sup>* mice is a consequence of low adiposity and negative energy balance as a result of restricted dietary intake in these mice and that this hypoleptinemia may account for the hypercorticosteronaemia in these mice. Further investigation is required to determine if other appetite-regulating hormones (i.e. ghrelin, neuropeptide Y, etc.) could play a role.

#### **2.5.4 OCN-independent mechanisms and a possible link between local nutrient-sensing in bone and whole-body energy homeostasis**

Apart from OCN, OGN, also known as mimecan, is a proteoglycan that has recently been shown to coordinate the control of bone production and whole-body energy status. Levels of circulating OGN inversely correlate with energy balance and bone formation.

In wild-type mice fed a HFD (i.e. a positive energy balance), OGN levels are decreased whereas in human gastric bypass patients (i.e. a negative energy balance), serum OGN levels correlate with body weight lost and lower glycemic levels<sup>30</sup>. In line with the imbalance of increased energy expenditure with unaltered food intake and low bone mass phenotype of male *Rptor<sub>ob</sub><sup>-/-</sup>* mice, circulating levels of OGN were significantly increased in these mice. Collectively, this study supports the notion that the skeleton actively communicates with other organ systems to coordinate the balance between its own remodeling process and overall energy status.

In male *Rptor<sub>ob</sub><sup>-/-</sup>* mice, the failure to build up the energy store (as evident by a marked reduction in body fat and accumulation of small adipocytes in the fat depots) is likely due to the increased energy expenditure with unaltered caloric intake state. This lipotrophy could represent an adaptive response to the concurrent low insulin and glucose levels, which together increase the production of ketone bodies by increased mobilisation of fatty acid from the fat storage to the liver, as alternative energy sources, in order to prevent hypoglycaemic death. In support of this, recent studies have shown that during short-term starvation in lean rats, both hypoleptinemia and insulinopenia are necessary to maintain euglycaemia and thus promote survival<sup>55</sup>. Hypoleptinemia stimulates secretion of corticosterone which, in the presence of hypoinsulinemia, leads to WAT lipolysis and the shift from whole-body carbohydrate to fat/ketone oxidation<sup>55</sup>. Furthermore, the changes in body composition with significant reduction in total body weight and fat mass while paradoxically increased bone-marrow adipose tissues (BMAT) are observed under starvation both in dietary restricted mouse models<sup>37</sup> and in human AN patients<sup>35</sup>. A growing number of studies now attribute the beneficial effects of BMAT expansion to adiponectin production under restricted caloric conditions<sup>36,37,40</sup> and as such, elevated serum adiponectin levels could contribute to the improved metabolic phenotype of *Rptor<sub>ob</sub><sup>-/-</sup>* mice. Concordance in the phenotypes of starved rats, calorie-restricted mice and *Rptor<sub>ob</sub><sup>-/-</sup>* mice (i.e. hypoleptinemia, hypoinsulinemia, high corticosterone and an increase in ketone bodies) suggests that loss of mTORC1 function in OBs mimics a starvation response. Furthermore, a reduction in bone mass and an expansion of BMAT in the male *Rptor<sub>ob</sub><sup>-/-</sup>* mice previously reported in<sup>15</sup>, combined with elevated BMAT-derived adiponectin levels as evident in this study, suggest that suppression of mTORC1 function in OBs triggers a ‘starvation response’ in the bone which leads to starvation-induced BMAT formation and physiological adaptation to starvation.

In summary, these results suggest that the mTORC1 complex in OB plays an important role in the regulation of both skeletal development and skeletal regulation of whole-body energy homeostasis. The improvement in glucose metabolism in normal chow-fed *Rptor<sub>ob</sub><sup>-/-</sup>* mice also raises the possibility that these mice could be protected from deleterious consequences induced by a high-fat diet. Finally, these findings further highlight the important contribution of skeleton to whole-body glucose homeostasis.

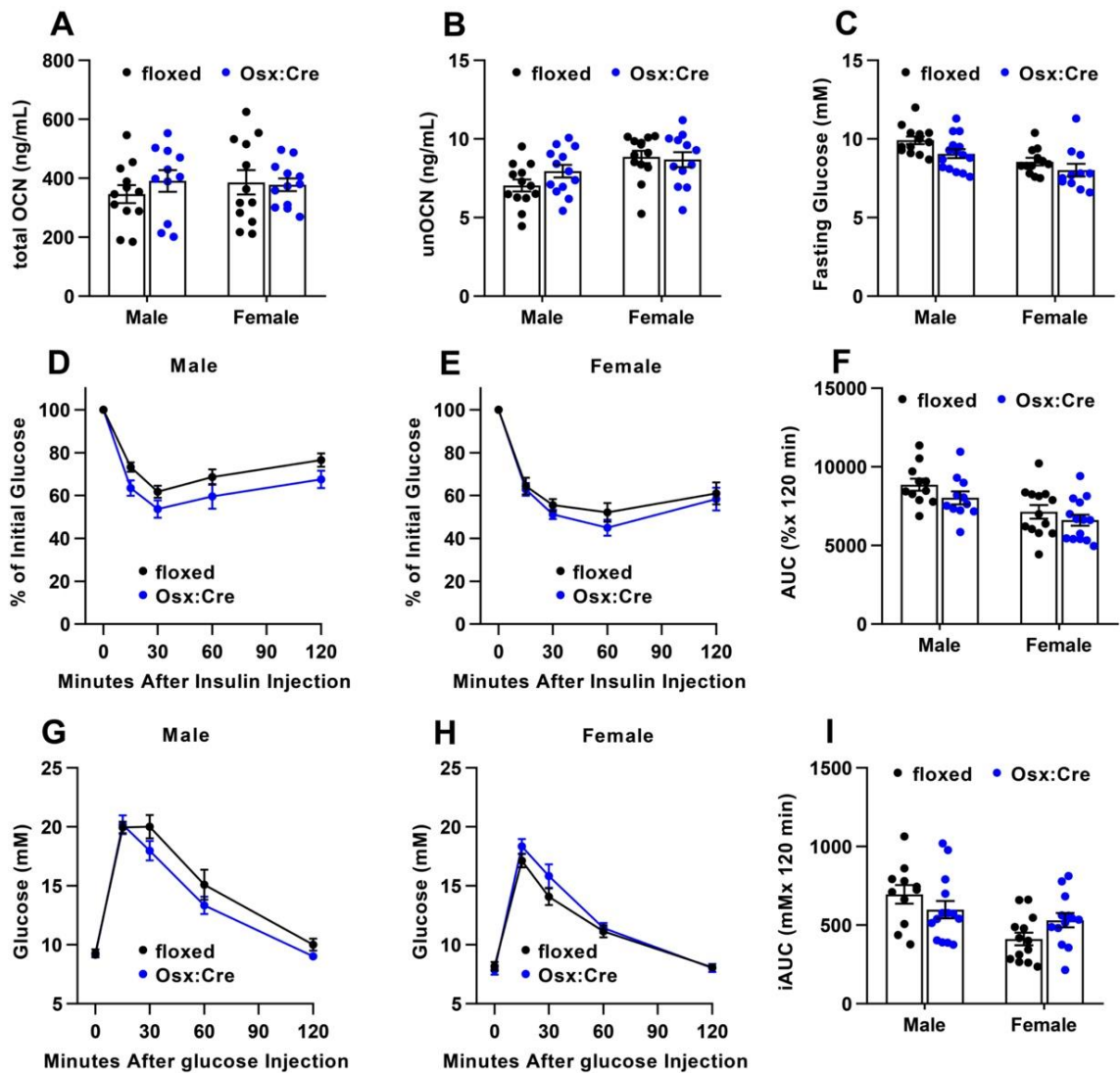
## **2.6 Acknowledgements**

The authors gratefully acknowledge Mrs Vicki Wilczek for assisting with mouse genotyping. This work was supported by grants from the National Health and Medical Research Council of Australia (APP1109207, awarded to ACWZ, PMB and CGP) and ARC (DP160100454, awarded to ACWZ and PMB) and an Australia Postgraduate Award (PT).

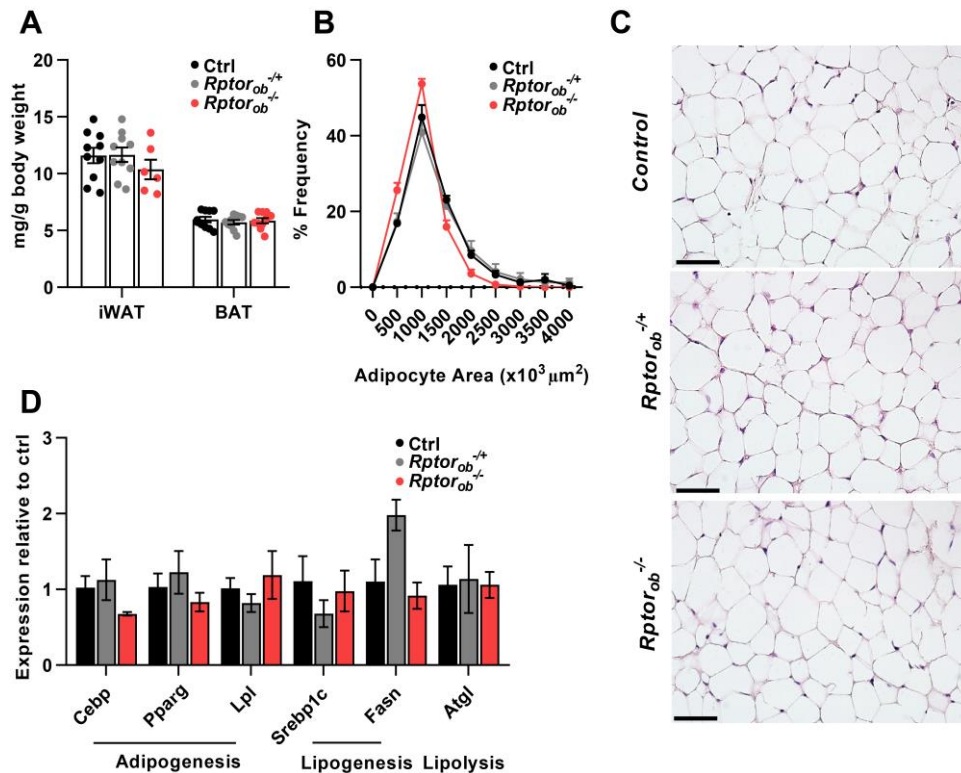
## **2.7 Supplementary data**

### ***2.7.1 Supplementary Figures***

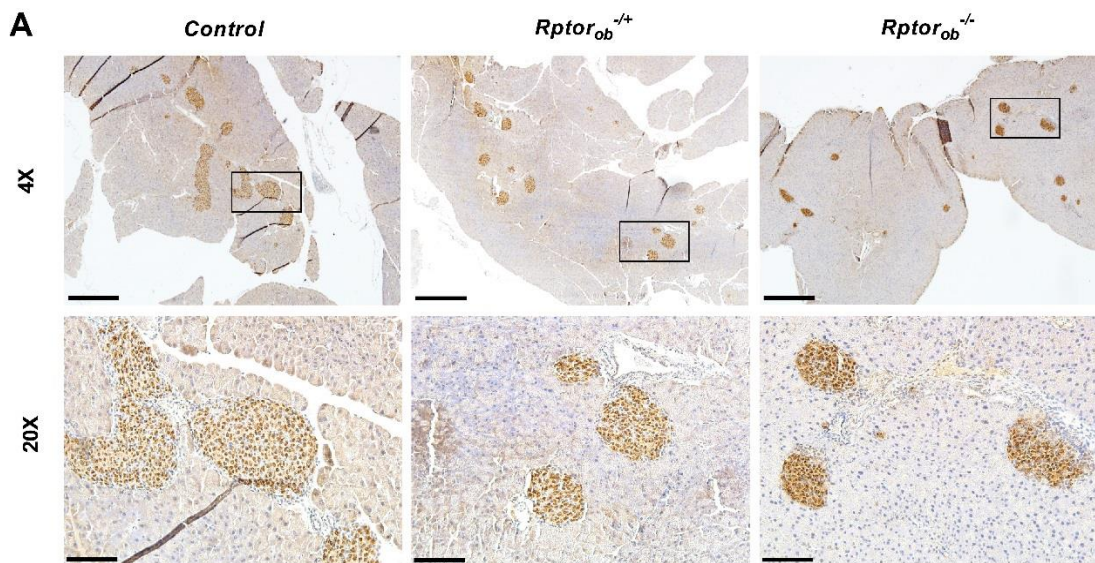




**Supplementary Fig. 2.1 *Osx:Cre* and floxed wild type mice display equivalent metabolic phenotypes.** (A) Serum OCN (total) levels in 9-week old male and female mice (n=12/genotype). (B) Serum unOCN levels (n=12-13/genotype). (C) Fasting glucose levels (n=11-15/genotype). (D-E) ITT blood glucose levels in male and female mice at 8-week of age, and (F) Area under the curve analysis (n=11-15/group). (G-H) GTT blood glucose levels in male and female mice at 9-week of age, and (I) area under the curve analysis (n=11-15/genotype). All panels: data are expressed as mean  $\pm$  SEM.



**Supplementary Fig. 2.2 Female *Rptor<sup>ob</sup>/-* mice display normal fat mass and adipocyte morphology.** (A) Body weight-adjusted inguinal white adipose tissue (iWAT) and interscapular brown adipose tissue (iBAT) mass in 9-week-old female mice (n=6-10/genotype). (B) Size distribution of iWAT adipocytes of female mice calculated from H&E stained sections using Image J (n=5 sections/mouse, n=4-6/genotype). (C) Representative H&E-stained iWAT section from female mice, scale bar = 50 $\mu\text{m}$ . (D) Relative expression of adipogenesis, lipogenesis and lipolysis genes, normalised to  $\beta$ -actin, in female iWAT samples (n=3-5/genotype). All panels: data are expressed as mean  $\pm$  SEM.



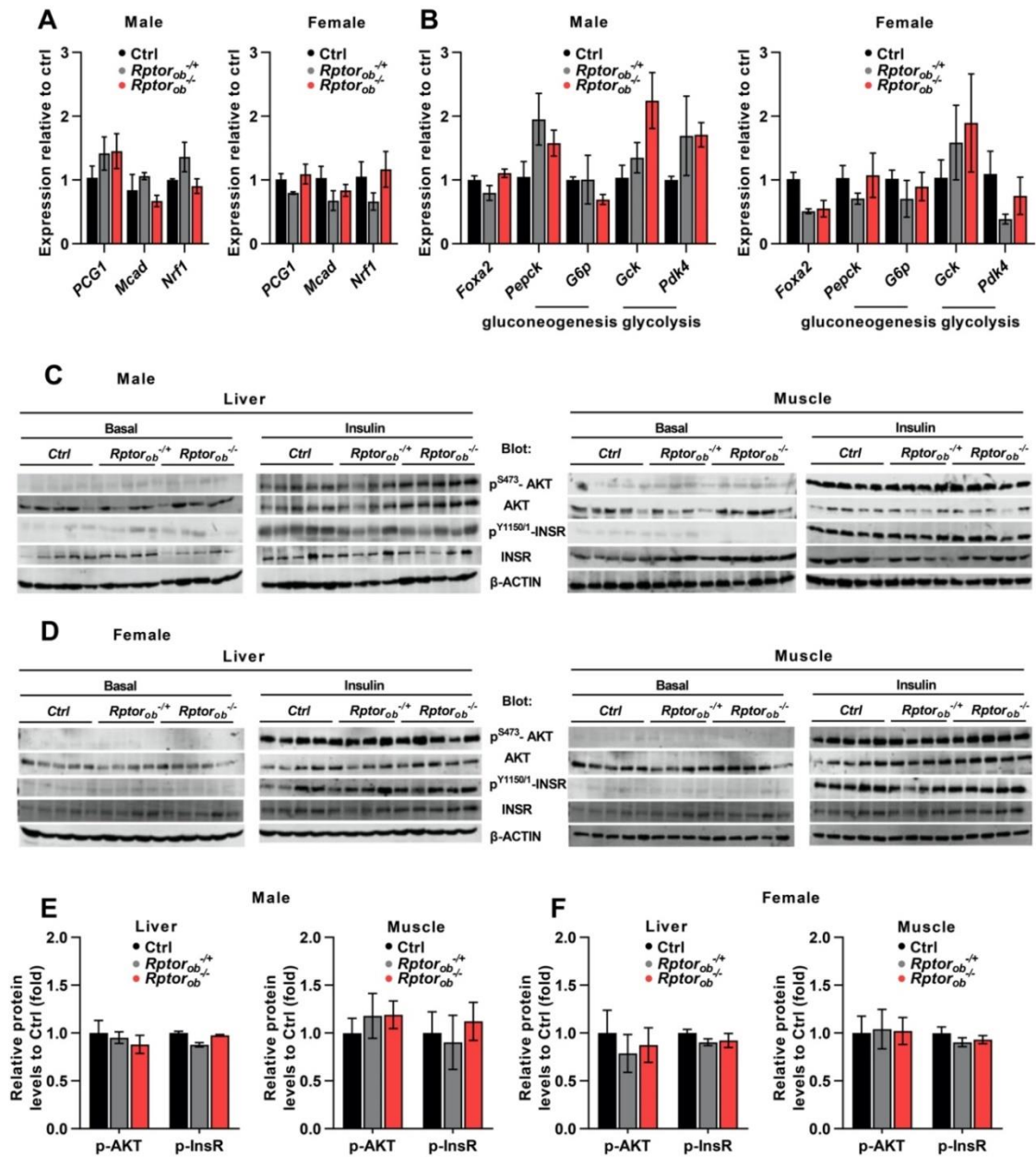
**B**

Male	Control	<i>Rptor<sub>ob</sub><sup>-/-</sup></i>	<i>Rptor<sub>ob</sub><sup>-/-</sup></i>	p-value
β-cell Area (%)	0.549 ± 0.123	0.240 ± 0.079	0.189 ± 0.049	0.065
No. of Islets	0.666 ± 0.039	0.457 ± 0.046	0.471 ± 0.091	0.151
Islet area/no. of Islets	0.008 ± 0.001	0.005 ± 0.001	0.004 ± 0.001	0.077

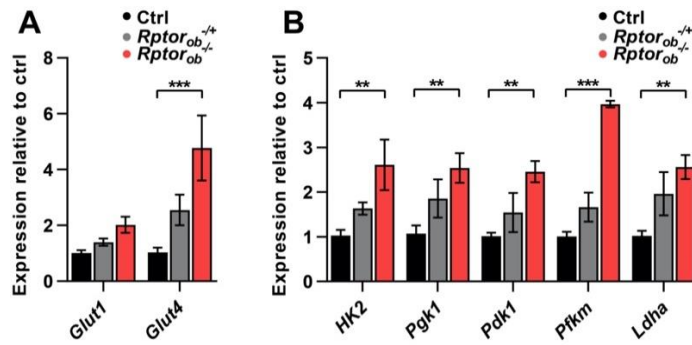
  

Female	Control	<i>Rptor<sub>ob</sub><sup>-/-</sup></i>	<i>Rptor<sub>ob</sub><sup>-/-</sup></i>	p-value
β-cell Area (%)	0.574 ± 0.233	0.409 ± 0.049	0.467 ± 0.044	0.855
No. of Islets	0.655 ± 0.143	0.561 ± 0.071	0.736 ± 0.114	0.871
Islet area/no. of Islets	0.008 ± 0.001	0.007 ± 0.001	0.007 ± 0.001	0.568

**Supplementary Fig. 2.3: *Rptor<sub>ob</sub><sup>-/-</sup>* mice display normal pancreatic morphology.** (A) Representative images of insulin immunostaining in pancreas samples from 9-week-old male mice. Boxes in 4X panels indicate the area depicted in the corresponding 20X panels. Scale bars: upper panels (4X) = 500μm; lower panels (20X) = 50μm. (B) Histomorphometric analysis of β-cell area, islet number and islet size (n=3/genotype). In Panel B, data are expressed as mean ± SEM, and p-values, *t*-test: *Rptor<sub>ob</sub><sup>-/-</sup>* vs control mice.



**Supplementary Fig. 2.4 Increased insulin sensitivity in *Rptor<sup>ob</sup><sup>-/-</sup>* mice is not due to changes in insulin signalling in the muscle or liver.** (A) Relative expression of genes involved in insulin sensitivity, normalised to  $\beta$ -actin, in liver samples from 9-week old male (*left*) and female (*right*) mice (n=3/genotype). (B) Relative expression of genes involved in insulin sensitivity, normalised to  $\alpha$ -actin, in skeletal muscle samples from 9-week old male (*left*) and female (*right*) mice (n=3/genotype). (C) Western immunoblot analysis of indicated proteins in liver (*left*) and muscle (*right*) samples harvested under basal (fasted + 20 minutes PBS) and insulin-stimulated (fasted + 20 minutes insulin) conditions in male mice (n=4-5/genotype). (D) Western immunoblot analysis of indicated proteins in liver (*left*) and muscle (*right*) samples harvested under basal (fasted + 20 minutes PBS) and insulin-stimulated (fasted + 20 minutes insulin) conditions in female mice (n=4-5/genotype). (E-F) Quantitative analysis of indicated protein levels from (C-D). Panels A, B, E, F: data are expressed as mean  $\pm$  SEM.



**Supplementary Fig. 2.5 Increased expression levels of genes involved in cellular glucose transportation and glycolysis in *Rptor<sup>ob</sup>/-* mice.** Gene expression analysis of (A) glucose transporters and (B) glycolysis in the flushed femur/tibia from 9-week old male mice (n=3-5/genotype). All panels: data are expressed as mean  $\pm$  SEM. \*\*p<0.01, \*\*\*p<0.001, two-way ANOVA with Tukey's post-hoc test.

## 2.7.2 Supplementary Tables

### Supplementary Table 2.1 Details of chow diet

2018



#### Teklad Global 18% Protein Rodent Diet

**Product Description-** 2018 is a fixed formula, non-autoclavable diet manufactured with high quality ingredients and designed to support gestation, lactation, and growth of rodents. 2018 does not contain alfalfa, thus lowering the occurrence of natural phytoestrogens. Typical isoflavone concentrations (daidzein + genistein aglycone equivalents) range from 150 to 250 mg/kg. Exclusion of alfalfa reduces chlorophyll, improving optical imaging clarity. Absence of animal protein and fish meal minimizes the presence of nitrosamines. **Also available certified (2018C) and irradiated (2918). For autoclavable diet, refer to 2018S (Sterilizable) or 2018SX (Extruded & Sterilizable).**

Macronutrients		
Crude Protein	%	18.6
Fat (ether extract) <sup>a</sup>	%	6.2
Carbohydrate (available) <sup>b</sup>	%	44.2
Crude Fiber	%	3.5
Neutral Detergent Fiber <sup>c</sup>	%	14.7
Ash	%	5.3
Energy Density <sup>d</sup>	kcal/g (kJ/g)	3.1 (13.0)
Calories from Protein	%	24
Calories from Fat	%	18
Calories from Carbohydrate	%	58
Minerals		
Calcium	%	1.0
Phosphorus	%	0.7
Non-Phytate Phosphorus	%	0.4
Sodium	%	0.2
Potassium	%	0.6
Chloride	%	0.4
Magnesium	%	0.2
Zinc	mg/kg	70
Manganese	mg/kg	100
Copper	mg/kg	15
Iodine	mg/kg	6
Iron	mg/kg	200
Selenium	mg/kg	0.23
Amino Acids		
Aspartic Acid	%	1.4
Glutamic Acid	%	3.4
Alanine	%	1.1
Glycine	%	0.8
Threonine	%	0.7
Proline	%	1.6
Serine	%	1.1
Leucine	%	1.8
Isoleucine	%	0.8
Valine	%	0.9
Phenylalanine	%	1.0
Tyrosine	%	0.6
Methionine	%	0.4
Cystine	%	0.3
Lysine	%	0.9
Histidine	%	0.4
Arginine	%	1.0
Tryptophan	%	0.2

Teklad Diets are designed and manufactured for research purposes only.



**Ingredients** (in descending order of inclusion)- Ground wheat, ground corn, wheat middlings, dehulled soybean meal, corn gluten meal, soybean oil, calcium carbonate, dicalcium phosphate, brewers dried yeast, iodized salt, L-lysine, DL-methionine, choline chloride, kaolin, magnesium oxide, vitamin E acetate, menadione sodium bisulfite complex (source of vitamin K activity), manganese oxide, ferrous sulfate, zinc oxide, niacin, calcium pantothenate, copper sulfate, pyridoxine hydrochloride, riboflavin, thiamin mononitrate, vitamin A acetate, calcium iodate, vitamin B<sub>12</sub> supplement, folic acid, biotin, vitamin D<sub>3</sub> supplement, cobalt carbonate.

Standard Product Form: **Pellet**

Vitamins		
Vitamin A <sup>e,f</sup>	IU/g	15.0
Vitamin D <sub>3</sub> <sup>e,g</sup>	IU/g	1.5
Vitamin E	IU/kg	110
Vitamin K <sub>3</sub> (menadione)	mg/kg	50
Vitamin B <sub>1</sub> (thiamin)	mg/kg	17
Vitamin B <sub>2</sub> (riboflavin)	mg/kg	15
Niacin (nicotinic acid)	mg/kg	70
Vitamin B <sub>6</sub> (pyridoxine)	mg/kg	18
Pantothenic Acid	mg/kg	33
Vitamin B <sub>12</sub> (cyanocobalamin)	mg/kg	0.08
Biotin	mg/kg	0.40
Folate	mg/kg	4
Choline	mg/kg	1200
Fatty Acids		
C16:0 Palmitic	%	0.7
C18:0 Stearic	%	0.2
C18:1ω9 Oleic	%	1.2
C18:2ω6 Linoleic	%	3.1
C18:3ω3 Linolenic	%	0.3
Total Saturated	%	0.9
Total Monounsaturated	%	1.3
Total Polyunsaturated	%	3.4
Other		
Cholesterol	mg/kg	--

<sup>a</sup> Ether extract is used to measure fat in pelleted diets, while an acid hydrolysis method is required to recover fat in extruded diets. Compared to ether extract, the fat value for acid hydrolysis will be approximately 1% point higher.

<sup>b</sup> Carbohydrate (available) is calculated by subtracting neutral detergent fiber from total carbohydrates.

<sup>c</sup> Neutral detergent fiber is an estimate of insoluble fiber, including cellulose, hemicellulose, and lignin. Crude fiber methodology underestimates total fiber.

<sup>d</sup> Energy density is a calculated estimate of *metabolizable energy* based on the Atwater factors assigning 4 kcal/g to protein, 9 kcal/g to fat, and 4 kcal/g to available carbohydrate.

<sup>e</sup> Indicates added amount but does not account for contribution from other ingredients.

<sup>f</sup> 1 IU vitamin A = 0.3 µg retinol

<sup>g</sup> 1 IU vitamin D = 25 ng cholecalciferol

For nutrients not listed, insufficient data is available to quantify.

Nutrient data represent the best information available, calculated from published values and direct analytical testing of raw materials and finished product. Nutrient values may vary due to the natural variations in the ingredients, analysis, and effects of processing.

**Supplementary Table 2.2. Oligonucleotides used for Real-time PCR (qRT-PCR)**

Gene	Accession	Forward (5' – 3')	Reverse (5' – 3')	Size (bp)
<i>Acaca</i>	NM_133360.2	ATGCGATCTATCCGTCGGTIG	CCAGCCCACTGCTTGT	224
<i>Acadl</i>	NM_007381.4	CCGCCGATGTCTCATTCT	CCCATTCTGTGTGGTIGAGGA	168
<i>Acadm</i>	NM_007382.5	TTCGAAGACGTCAGAGTGCC	CTGCGACTGTAGGTCTGGTT	103
<i>Acads</i>	NM_007383.3	TAGCCATGCAAACCCTGGAC	TTGCGGTTCTCGGCATACCT	106
<i>Acadvl</i>	NM_017366.3	ACAGGAATCGGCAGTGGTTT	ACTGCTCGTTGACAATCCCT	151
<i>Acox</i>	NM_015729.3	CATGTGGTTAAAAAECTGTGTC	GGCATGAAAGAAACGCTCCTG	123
<i>Acly</i>	NM_001199296.1	TTCCTCTTAATGCCAGCGG	GACTTGGGACTGAATCTTGGGG	136
<i>Actin</i>	NM_007393.5	TTGCTGACACGATGCAGGA	AAGGGTGTAAAACGCAGCTC	236
<i>Adipoq</i>	NM_009605.4	GATGCAGGTCTTCTTGGTCTTA	AGCGAATGGGTACATTGGGA	187
<i>Atgl</i>	NM_025802.3	CAACGCCACTCACATCTACGG	TCACCAGGTTGAAGGAGGGAT	161
<i>Axin2</i>	NM_015732.4	TAACAGCCCAAGAACCCGGGA	CAGCAATCGGCTTGGTCTCT	164
<i>Bdh1</i>	NM_175177.4	AGACACATCAAGCCCGGAGA	TCTGTGGTCTTATGCCAGTIG	159
<i>Bglap</i>	NM_001032298.3	AAGCGAGAGGGCAATAAGGT	TCAAGCCATACTGGTCTGATAGC	142
<i>Bmp7</i>	NM_007557.3	CAGCCAGAATCGTCCAAGA	TGCAATGATCCAGTCTGCC	154
<i>Birc</i>	NM_001037758.2	GCTCCCTTCTCGGACATAC	AACATTAACGAGTCTGGGCA	83
<i>Cebpa</i>	NM_007678.3	CAAAGCCAAGAACTCGGTGGACAA	TCAITGTGACTGGTCAACTCCAGC	150
<i>Cidea</i>	NM_007702.2	CAGTTCCTGTCTATCGGGG	AACCAGCCTTGGTGTAGG	92
<i>Col1a</i>	NM_007742.4	GCTCTCTTAGGGGCCACT	CCAGTCTCACCATTGGGG	103
<i>Cox7a</i>	NM_009944.3	AGACTGACATGACGCTGAC	GTGTCACTTCTTGTGGGGGAA	87
<i>Cpt1a</i>	NM_013495.2	GGACTCCGCTCGCTCATTC	AGCAGATCTGTGTGAGGGC	153
<i>Cpt1b</i>	NM_009948.2	CATGTATCGCCGAAACTGG	CCTGGATGCGTGTAGTGT	114
<i>Ctsk</i>	NM_007802.4	GCCACGCTTCTATCCGAAA	CGAGAGATTTATCCACCTTGC	188
<i>Cyp11a</i>	NM_019779.4	CCTTCTGAGCCCTACGTG	GCCAGCTTCTCCCTGTAAA	222
<i>Cyp17</i>	NM_007809.3	CAATGACCGGACTCACCTCC	TATCGTATGACAGTCCAG	176
<i>Cyp19</i>	NM_007810.4	TTCGCTGAGAGACGTGGAG	AGGATTGTGCTTCGACCTC	150
<i>Erol</i>	NM_015774.3	TTCGCGAGGTTAGTGGTACC	GTTTGACGGCACAGTCTCTC	202
<i>Erp44</i>	NM_029572.3	GACCCGTCGTTACCATGAA	TGAAACGACACCAGTACGCA	196
<i>Fasn</i>	NM_007988.3	TGGGTGTGGAAGTCTGTCAG	CTGTCGTGTCAGTAGCCGAG	132
<i>Fgf21</i>	NM_020013.4	CCTCCAGTTTGGGGGTCAAG	ACCACTGTTCCATCTCCCT	99
<i>Foxa2</i>	NM_001291065.1	CACTCGGCTTCCAGTATGC	GTTTCATGCCATTCATCCAG	138
<i>G6p</i>	NM_008061.4	TGAGACCGGACCCAGGAAGTC	GCAAGTAGATCCGGGACAG	195
<i>Gapgh</i>	NM_001289726.1	TGCACCACCAACTGCTTAG	GGATGCAGGGATGATGTT	177
<i>Gck</i>	NM_010292.5	CTGTTAGCAGGATGGCAGCTT	TTCTCTGGAGAGATGCTGTGG	82
<i>Glut1</i>	NM_011400.3	GCTACGGGGTCTTAAAGTGCG	CCTCCCAACAGCCAAACATGAG	169
<i>Glut4</i>	NM_009204.2	GGCTCTGACGATGGGGAAC	GCCACGTTGCATTGTAGCTC	157
<i>Gprc6a</i>	NM_153071.1	GGCATTATACTGAGCCGGAC	GGCAATAGTCCCATGGCT	134
<i>Hadha</i>	NM_178878.3	GTAGCACAGCAGTACGAGA	CCCAGACTTGCAGCCTAAGA	117
<i>Hk2</i>	NM_013820.3	TGATCGCCTGCTTATTCACGG	AACCGCTAGAAATCTCCAGA	112
<i>Hmgcl</i>	NM_008254.3	AGATGGCGTCAGTGGGAAAG	CTGGGGTGGGTACAATACTCTTT	165
<i>Hmgcs2</i>	NM_008256.4	TACTGGGATGGTGCCTATGC	ACCGCTTCTCCATGTGAGTT	166
<i>Hsd17</i>	NM_008292.4	AGCCACGTCAGGATTCGTTG	TGAAAGACAGCCAGGAACC	242
<i>Hsd3β1</i>	NM_008293.4	CTTGAAGTGCCTCTGATCT	CTTTATTCTGTGCAGCAGCC	120
<i>Hsl</i>	NM_010719.5	CTGCCAGGATGGATGGTIT	GAACGCTGAGGCTTGTATCTG	233
<i>Irisin</i>	NM_027402.4	CACGCGAGGCTGAAAAGATG	CATACTGGCGGAGAAAGAGA	156
<i>Ldha</i>	NM_010699.2	TGTCTCCAGCAAAGACTACTGT	GACTGTACTTGACAATGTGGGA	155
<i>Leptin</i>	NM_008493.3	CAAGCAGTGCCTATCCAGA	AAGCCAGGAATGAAGTCCA	141
<i>Lgr5</i>	NM_010195.2	TCTCTACATCGCTCTGCT	ATCTAGGCGCAGGGATTGAAG	187
<i>Lpl</i>	NM_008509.2	GGACGGTAAACGGAAATGTATG	ACGTTGTCTAGGGGTACTTAAA	214
<i>Nrf1</i>	NM_001164226.1	ATCTGGTGTGTCAGGTCC	CACTCGCTGCTGTACTCAT	170
<i>Opg</i>	NM_008764.3	TCATCCAAGACATTGACTCTGT	TCGCTCGATTGTCAGGCTTT	160
<i>Pcg-1α</i>	NM_008904.2	TGTGTGCTGTGTGTCAGAGT	ACCAGAGCAGCACACTCTATG	126
<i>Pdk1</i>	NM_172665.5	CCCCGATTCAGGTTACAG	CCCGGCTACTCATCTTACA	63
<i>Pdk4</i>	NM_013743.2	GATTGACATCTGCCTGACC	CATGGAATCCACCAAATCC	98
<i>Pepck</i>	NM_011044.3	ATCATCTTGGTGGCCGTAG	TGATGATCTTGGCCTTGTGT	136
<i>Pfkm1</i>	NM_001163487.1	GGTTCCCTGTACTCCATGC	TTCATCATCTGTGGTGCAGT	251
<i>Pgk1</i>	NM_008828.3	TTTGGACAAGCTGGACGTGA	AGCAGCTTGTATCCTTTGGTT	106
<i>Plin1</i>	NM_175640.2	GGCCTGGACGACAAAACC	CAGGATGGGCTCCATGAC	120
<i>Ppara</i>	NM_011144.6	GCAGTGCCCTGAACATCGA	CGCCGAAAGAACCCCTTAC	100
<i>Pparγ</i>	NM_001127330.2	TTTTCGGAAGAACCATCCGATT	ATGGCAATTTGAGACATCCCG	139
<i>Smurf1</i>	NM_001038627.1	TGAGGAGAGGAGGCCAGAC	CGCTGTAGAGCCTTGCAGA	92
<i>Sirt1</i>	NM_019812.3	GGCCGCGATAGGTCCA	AACAATCTGCCACAGCGTCA	137
<i>Sost</i>	NM_024449.6	GCCTCATCTGCTACTTGTG	CGGACACATCTTTGGCGT	201
<i>Sp7</i>	NM_130458.4	ATGGCGTCTCTTGTCTTG	GTCCATTGGTGTGAGAAAGG	211
<i>Sparc</i>	NM_009242.5	GATGGTACCTGTCCAGAC	AGCAGGAGGCGTGAACCTAG	199
<i>Srebf1</i>	NM_001313979.1	GTGGGCTAGTCCGAAGC	GAGCATGTCTTCGATGTGCTT	135
<i>StAR</i>	NM_011485.5	TCGCTACGTTCAAGCTGTGT	GCTTCCAGTTGAGAACCAAGC	184
<i>Tcirg</i>	NM_016921.3	CACAGGCTGTGCTTACAACCTG	CGTCTACCAGAAAGCGTCTC	110
<i>Ucp1</i>	NM_009463.3	TGGTGAACCCGACAACCTCC	GGCCTCACCTTGGATCTGAA	141
<i>Ucp2</i>	NM_011671.5	TGCGGTCCGGACACAATAGTA	CTCGTCTTCAAAGCTGCCG	111



## 2.8 References

1. Ferron M, *et al.* Insulin signaling in osteoblasts integrates bone remodeling and energy metabolism. *Cell* **142**, 296-308 (2010).
2. Fulzele K, *et al.* Insulin receptor signaling in osteoblasts regulates postnatal bone acquisition and body composition. *Cell* **142**, 309-319 (2010).
3. Rached MT, *et al.* FoxO1 is a positive regulator of bone formation by favoring protein synthesis and resistance to oxidative stress in osteoblasts. *Cell Metab* **11**, 147-160 (2010).
4. Yoshizawa T, *et al.* The transcription factor ATF4 regulates glucose metabolism in mice through its expression in osteoblasts. *J Clin Invest* **119**, 2807-2817 (2009).
5. Wei J, Hanna T, Suda N, Karsenty G, Ducy P. Osteocalcin promotes beta-cell proliferation during development and adulthood through Gprc6a. *Diabetes* **63**, 1021-1031 (2014).
6. Lee NK, *et al.* Endocrine regulation of energy metabolism by the skeleton. *Cell* **130**, 456-469 (2007).
7. Mizokami A, *et al.* Oral administration of osteocalcin improves glucose utilization by stimulating glucagon-like peptide-1 secretion. *Bone* **69**, 68-79 (2014).
8. Ferron M, Hinoi E, Karsenty G, Ducy P. Osteocalcin differentially regulates beta cell and adipocyte gene expression and affects the development of metabolic diseases in wild-type mice. *Proc Natl Acad Sci U S A* **105**, 5266-5270 (2008).
9. Ferron M, McKee MD, Levine RL, Ducy P, Karsenty G. Intermittent injections of osteocalcin improve glucose metabolism and prevent type 2 diabetes in mice. *Bone* **50**, 568-575 (2012).
10. Hsu PP, *et al.* The mTOR-regulated phosphoproteome reveals a mechanism of mTORC1-mediated inhibition of growth factor signaling. *Science* **332**, 1317-1322 (2011).
11. Polak P, Cybulski N, Feige JN, Auwerx J, Ruegg MA, Hall MN. Adipose-specific knockout of raptor results in lean mice with enhanced mitochondrial respiration. *Cell Metab* **8**, 399-410 (2008).
12. Lee PL, Tang Y, Li H, Guertin DA. Raptor/mTORC1 loss in adipocytes causes progressive lipodystrophy and fatty liver disease. *Molecular metabolism* **5**, 422-432 (2016).
13. Bentzinger CF, *et al.* Skeletal muscle-specific ablation of raptor, but not of rictor, causes metabolic changes and results in muscle dystrophy. *Cell Metab* **8**, 411-424 (2008).
14. Chen J, Long F. mTORC1 signaling promotes osteoblast differentiation from preosteoblasts. *PLoS One* **10**, e0130627 (2015).
15. Fitter S, *et al.* mTORC1 Plays an Important Role in Skeletal Development by Controlling Preosteoblast Differentiation. *Molecular and Cellular Biology* **37**, e00668-00616 (2017).
16. Wei J, *et al.* Glucose Uptake and Runx2 Synergize to Orchestrate Osteoblast Differentiation and Bone Formation. *Cell* **161**, 1576-1591 (2015).
17. Riddle R, *et al.* Tsc2 Is a Molecular Checkpoint Controlling Osteoblast Development and Glucose Homeostasis. *Molecular and Cellular Biology* **34**, 1850-1862 (2014).
18. Rodda SJ, McMahon AP. Distinct roles for Hedgehog and canonical Wnt signaling in specification, differentiation and maintenance of osteoblast progenitors. *Development* **133**, 3231 (2006).

19. Srinivas S, *et al.* Cre reporter strains produced by targeted insertion of EYFP and ECFP into the ROSA26 locus. *BMC Dev Biol* **1**, 4 (2001).
20. Dirckx N, *et al.* Vhl deletion in osteoblasts boosts cellular glycolysis and improves global glucose metabolism. *J Clin Invest* **128**, 1087-1105 (2018).
21. Huang W, Olsen BR. Skeletal defects in Osterix-Cre transgenic mice. *Transgenic research* **24**, 167-172 (2015).
22. Kraus D, Yang Q, Kahn BB. Lipid Extraction from Mouse Feces. *Bio-protocol* **5**, e1375 (2015).
23. Schneider CA, Rasband WS, Eliceiri KW. NIH Image to ImageJ: 25 years of image analysis. *Nat Methods* **9**, 671-675 (2012).
24. Livak KJ, Schmittgen TD. Analysis of relative gene expression data using real-time quantitative PCR and the 2(-Delta Delta C(T)) Method. *Methods* **25**, 402-408 (2001).
25. Martin SK, *et al.* mTORC1 plays an important role in osteoblastic regulation of B-lymphopoiesis. *Scientific Reports* **8**, 14501 (2018).
26. Ferron M, Lacombe J, Germain A, Oury F, Karsenty G. GGCX and VKORC1 inhibit osteocalcin endocrine functions. *J Cell Biol* **208**, 761-776 (2015).
27. Pi M, Wu Y, Quarles LD. GPRC6A mediates responses to osteocalcin in beta-cells in vitro and pancreas in vivo. *J Bone Miner Res* **26**, 1680-1683 (2011).
28. Mosialou I, *et al.* MC4R-dependent suppression of appetite by bone-derived lipocalin 2. *Nature* **543**, 385-390 (2017).
29. Lee NJ, *et al.* NPY signalling in early osteoblasts controls glucose homeostasis. *Mol Metab* **4**, 164-174 (2015).
30. Lee NJ, *et al.* Osteoglycin, a novel coordinator of bone and glucose homeostasis. *Molecular metabolism* **13**, 30-44 (2018).
31. Oury F, *et al.* Endocrine regulation of male fertility by the skeleton. *Cell* **144**, 796-809 (2011).
32. Matsubara M, Maruoka S, Katayose S. Inverse relationship between plasma adiponectin and leptin concentrations in normal-weight and obese women. *Eur J Endocrinol* **147**, 173-180 (2002).
33. Hara K, *et al.* Measurement of the high-molecular weight form of adiponectin in plasma is useful for the prediction of insulin resistance and metabolic syndrome. *Diabetes Care* **29**, 1357-1362 (2006).
34. Yatagai T, *et al.* Hypoadiponectinemia is associated with visceral fat accumulation and insulin resistance in Japanese men with type 2 diabetes mellitus. *Metabolism* **52**, 1274-1278 (2003).
35. Bredella MA, *et al.* Increased bone marrow fat in anorexia nervosa. *J Clin Endocrinol Metab* **94**, 2129-2136 (2009).
36. Cawthorn WP, *et al.* Bone marrow adipose tissue is an endocrine organ that contributes to increased circulating adiponectin during caloric restriction. *Cell Metab* **20**, 368-375 (2014).
37. Devlin MJ, *et al.* Caloric restriction leads to high marrow adiposity and low bone mass in growing mice. *J Bone Miner Res* **25**, 2078-2088 (2010).
38. Doucette CR, *et al.* A High Fat Diet Increases Bone Marrow Adipose Tissue (MAT) But Does Not Alter Trabecular or Cortical Bone Mass in C57BL/6J Mice. *J Cell Physiol* **230**, 2032-2037 (2015).
39. Hamrick MW, Pennington C, Newton D, Xie D, Isales C. Leptin deficiency produces contrasting phenotypes in bones of the limb and spine. *Bone* **34**, 376-383 (2004).
40. Cawthorn WP, *et al.* Expansion of Bone Marrow Adipose Tissue During Caloric Restriction Is Associated With Increased Circulating Glucocorticoids and Not With Hypoleptinemia. *Endocrinology* **157**, 508-521 (2016).

41. Dai Q, *et al.* mTOR/Raptor signaling is critical for skeletogenesis in mice through the regulation of Runx2 expression. *Cell Death and Differentiation* **24**, 1886-1899 (2017).
42. Tzatsos A, Kandror KV. Nutrients suppress phosphatidylinositol 3-kinase/Akt signaling via raptor-dependent mTOR-mediated insulin receptor substrate 1 phosphorylation. *Mol Cell Biol* **26**, 63-76 (2006).
43. Um SH, *et al.* Absence of S6K1 protects against age- and diet-induced obesity while enhancing insulin sensitivity. *Nature* **431**, 200-205 (2004).
44. Yu Y, *et al.* Phosphoproteomic Analysis Identifies Grb10 as an mTORC1 Substrate That Negatively Regulates Insulin Signaling. *Science* **332**, 1322-1326 (2011).
45. Rached MT, *et al.* FoxO1 expression in osteoblasts regulates glucose homeostasis through regulation of osteocalcin in mice. *J Clin Invest* **120**, 357-368 (2010).
46. Li Z, *et al.* Glucose Transporter-4 Facilitates Insulin-Stimulated Glucose Uptake in Osteoblasts. *Endocrinology* **157**, 4094-4103 (2016).
47. Risson V, *et al.* Muscle inactivation of mTOR causes metabolic and dystrophin defects leading to severe myopathy. *J Cell Biol* **187**, 859-874 (2009).
48. Pittas AG, Harris SS, Eliades M, Stark P, Dawson-Hughes B. Association between serum osteocalcin and markers of metabolic phenotype. *J Clin Endocrinol Metab* **94**, 827-832 (2009).
49. Singha UK, *et al.* Rapamycin inhibits osteoblast proliferation and differentiation in MC3T3-E1 cells and primary mouse bone marrow stromal cells. *J Cell Biochem* **103**, 434-446 (2008).
50. Yasutake Y, *et al.* Long-term oral administration of osteocalcin induces insulin resistance in male mice fed a high-fat, high-sucrose diet. *American journal of physiology Endocrinology and metabolism* **310**, E662-E675 (2016).
51. Pi M, *et al.* GPRC6A null mice exhibit osteopenia, feminization and metabolic syndrome. *PLoS One* **3**, e3858 (2008).
52. Mauvais-Jarvis F. Sex differences in metabolic homeostasis, diabetes, and obesity. *Biol Sex Differ* **6**, 14-14 (2015).
53. Kim SP, *et al.* Fatty acid oxidation by the osteoblast is required for normal bone acquisition in a sex- and diet-dependent manner. *JCI Insight* **2**, e92704 (2017).
54. Mitchell SJ, *et al.* Effects of Sex, Strain, and Energy Intake on Hallmarks of Aging in Mice. *Cell Metab* **23**, 1093-1112 (2016).
55. Perry RJ, *et al.* Leptin Mediates a Glucose-Fatty Acid Cycle to Maintain Glucose Homeostasis in Starvation. *Cell* **172**, 234-248 e217 (2018).

**CHAPTER 3:**

**LOSS OF BONE-SPECIFIC MTORC1 PROTECTS  
AGAINST DIET-INDUCED OBESITY AND  
ASSOCIATED METABOLIC DYSFUNCTION**

## **Loss of bone-specific mTORC1 protects against diet-induced obesity and associated metabolic dysfunction**

Pawanrat Tangseefa<sup>1,2</sup>, Sally K. Martin<sup>1,2</sup>, Peck Yin Chin<sup>3</sup>, Paul A. Baldock<sup>4</sup>, Gary A. Wittert<sup>1,5,6</sup>, Amanda J. Page<sup>1,6</sup>, Christopher G. Proud<sup>6,7</sup>, Stephen Fitter<sup>1,2,9\*</sup>, Andrew C.W. Zannettino<sup>1,2,8,9\*</sup>

<sup>1</sup>Adelaide Medical School, Faculty of Health and Medical Science, University of Adelaide, Adelaide, Australia.

<sup>2</sup>Cancer Program, Precision Medicine Theme, South Australian Health and Medical Research Institute, Adelaide, Australia.

<sup>3</sup>Research Centre for Reproductive Health, School of Paediatrics and Reproductive Health, University of Adelaide, Adelaide, SA, Australia.

<sup>4</sup>Skeletal Metabolism Group, Garvan Institute of Medical Research, Sydney, Australia.

<sup>5</sup>Freemasons Foundation Centre for Men's Health, University of Adelaide, Adelaide, Australia.

<sup>6</sup>Nutrition, Diabetes & Metabolism Program, Lifelong Health Theme, South Australian Health and Medical Research Institute, Adelaide, Australia.

<sup>7</sup>School of Biological Sciences, University of Adelaide, Adelaide, Australia.

<sup>8</sup>Central Adelaide Local Health Network, Adelaide, Australia

<sup>9</sup>contributed equally to this work

**Keywords:** mTORC1, osteoblasts, high fat diet, obesity, insulin resistance, browning of white adipose, UCP1

Running title: Loss of bone-specific mTORC1 protects against diet-induced obesity

Chapter 3 incorporates the following submitted article currently under review at Tangseefa P, Martin SK, Chin PY, Baldock PA, Wittert GA, Page AJ, Proud CG, Fitter S, Zannettino ACW. The mTORC1 complex in pre-osteoblasts regulates whole-body energy metabolism independently of osteocalcin.

### 3.1 Abstract

mTORC1 is the primary cellular nutrient-sensing hub that coordinates anabolic and catabolic processes to control cellular growth and metabolism. Importantly, mTORC1 is a critical mediator of insulin signalling and negatively regulates insulin signalling, via a negative feedback loop, to control insulin activity. Under states of nutrient overload, mTORC1 becomes hyper-activated, which leads to downregulation of insulin signalling and the development of insulin resistance. The skeleton has emerged as a critical insulin target tissue and recent studies have shown that modulating insulin signalling in OBs has a profound effect on systemic glucose metabolism. These findings suggest that dysregulation of insulin signalling in OBs, by hyperactivation of mTORC1 under states of nutrient overload, may contribute to the development of metabolic dysfunction. To address this question, mice in which mTORC1 function is impaired in OBs (*Rptor<sub>ob</sub><sup>-/-</sup>*) were generated.

The studies outlined herein show that *Rptor<sub>ob</sub><sup>-/-</sup>* mice are resistant to high-fat diet (HFD)-induced weight gain and display a significant reduction in fat mass and adipocyte hypertrophy in the gonadal and inguinal white adipose tissue (WAT). Metabolically, HFD-fed *Rptor<sub>ob</sub><sup>-/-</sup>* mice have significantly lower fasting glucose and insulin levels and exhibit increased glucose tolerance and insulin sensitivity compared to control mice. The obesity-resistant phenotype of *Rptor<sub>ob</sub><sup>-/-</sup>* mice is not attributable to changes in food intake, physical activity or lipid absorption. Instead, *Rptor<sub>ob</sub><sup>-/-</sup>* mice maintain the ability to switch between fuel sources of fat and carbohydrate and exhibit browning of WAT, as evidenced by increased UCP1 expression at both mRNA and protein levels. The browning of WAT is associated with elevated energy expenditure in the male, but not female, *Rptor<sub>ob</sub><sup>-/-</sup>* mice. Furthermore, RNA-sequencing and gene set enrichment analysis performed on RNA isolated from tibia revealed positively enriched gene sets for glucose uptake and metabolism and insulin signalling pathways as a result of OB-mTORC1 inhibition, suggesting potentiation of insulin signalling. This was confirmed by Western blotting both *in vivo* and using *Rptor*-null OBs *in vitro*. Notably, a profound increase in both basal and insulin-stimulated glucose uptake was also observed in *Rptor*-null OBs, suggesting that the low glycaemia and enhanced glucose tolerance in *Rptor<sub>ob</sub><sup>-/-</sup>* mice, were partially due to increased skeletal glucose uptake in these mice. Collectively, these data suggest that whole-body protection against diet-induced insulin resistance in response to OB-specific deletion of the Raptor/mTOR pathway is, at least

in part, attributable to a localised increase in responsiveness to insulin signalling leading to an increase in insulin-stimulated skeletal glucose uptake.

### 3.2 Introduction

Dysregulated insulin signalling and the development of insulin insensitivity are common features of many chronic disorders including obesity, diabetes and heart disease<sup>1</sup>. Furthermore over-nutrition, or excessive nutrient consumption, is a major contributing factor to the increasing prevalence of these metabolic diseases<sup>2</sup>. At the centre of nutritional challenges is mTORC1, the primary-nutrient-sensing hub involved in responding to changes in environmental nutrient availability to control cellular growth and metabolism. Binding of insulin to the insulin receptor (INSR) activates mTORC1, which in turn promotes mRNA translation, ribosome biogenesis and protein synthesis<sup>3</sup>. mTORC1 negatively regulates insulin signalling by disrupting the interaction between INSR and its adaptor protein, IRS1, via (i) activation of S6K1, which mediates IRS1 phosphorylation at Ser<sup>270/307/1101</sup> and thus induces ubiquitin mediated-proteasomal degradation of IRS1<sup>4,5,6</sup>; (ii) activation and stabilisation of the receptor tyrosine kinase (RTK) inhibitor growth factor receptor-bound protein 10 (Grb10), which inhibits IRS1 from binding to activated INSR<sup>7,8</sup>; or (iii) direct phosphorylation of IRS1 at Ser<sup>636/639</sup>, sites that lie in close proximity to the PI3-kinase activation motif, the phosphorylation of which suppresses IRS1-mediated PI3-kinase activation<sup>9</sup>.

In addition to insulin, multiple nutrient signals independently stimulate the mTORC1 pathway (reviewed in <sup>10</sup>). These include amino acids, in particular branched chain amino acids (BCAAs) via RAG GTPase-dependent signalling<sup>11</sup>. mTORC1 activity is also stimulated by glucose and fatty acids through cellular energy status, whereby high cellular energy levels (low AMP/ATP ratio) inactivates AMP-dependent kinase (AMPK), leading to suppression of the TSC1/2 complex, a negative regulator of mTORC1<sup>12,13</sup>. Consequently, in states of nutrient overload, mTORC1 is chronically activated, leading to sustained stimulation of S6K1 and S6K1-mediated phosphorylation and degradation of IRS1<sup>14</sup>. This eventually desensitises cellular insulin signalling and impairs the PI3K/AKT signalling pathway, thus rendering cells resistant to insulin<sup>15</sup>. In this insulin-resistant state, glucose uptake in muscle and glycogen synthesis in both liver and muscle are impaired, while gluconeogenesis in the liver is increased. Collectively, these conditions exacerbate the hyperglycaemic condition. Thus, as a consequence of chronically high nutrient levels in the circulation, mTORC1 remains active and maintains the negative feedback loop to the INSR, independently of insulin signalling, ultimately leading to systemic insulin insensitivity<sup>16</sup>.



Inhibition of mTORC1 or elements of the mTORC1 signalling pathway, either genetically or pharmacologically, is associated with an improved metabolic profile. Whole-body inactivation of S6K1 in mice protects against diet-induced insulin resistance and obesity due to elevated lipolysis and metabolic rate<sup>17</sup>, while pharmacological inhibition of S6K1 with PF-4708671 improves glucose tolerance in mice fed a HFD<sup>18</sup>. In these mice, the increased insulin sensitivity is associated with an enhanced insulin-induced AKT phosphorylation at Ser<sup>473</sup> and loss of the negative feedback loop from S6K1 to IRS1, as signified by a reduction of IRS1 phosphorylation at Ser<sup>307</sup> and Ser<sup>636/639</sup><sup>17</sup>. Conversely, combined disruption of 4E-BP1 and 4E-BP2, which are negatively regulated by mTORC1, has the opposite effect, with these mice displaying increased adiposity and sensitivity to both HFD-induced obesity and the development of insulin resistance<sup>19</sup>. An increase in insulin resistance in these mice was associated with increased S6K activity and impairment of AKT phosphorylation in muscle, liver and adipose tissues<sup>19</sup>.

The skeleton has recently emerged as a critical insulin target tissue. Importantly, insulin signalling in OBs, the bone-forming cells of skeleton, is necessary for whole-body glucose homeostasis, whereby OB-specific deletion of INSR (*INSR*<sup>OB-/-</sup> mice) causes elevated blood glucose, increased insulin resistance and increased peripheral fat mass in animals fed a normal diet<sup>20,21</sup>. Furthermore, in response to an obesogenic HFD, mice lacking one allele of INSR in OBs (*Coll1a1-INSR*<sup>+/-</sup>) have higher fasting glucose and insulin levels and develop exacerbated metabolic responses associated with severely impaired glucose and insulin tolerances<sup>22</sup>. Conversely, mice over-expressing the INSR in OBs (*Coll1a1-INSR*<sup>Tg</sup>) have smaller fat deposits, lower fasting glucose and insulin levels and are protected from HFD-induced glucose intolerance and insulin resistance<sup>22</sup>. Remarkably, bones isolated from HFD-fed wildtype mice exhibit features of insulin resistance such as reduced insulin-stimulated phosphorylation of AKT at Ser<sup>473</sup> and down-regulation of the INSR<sup>22</sup>. This reduction in insulin signalling in OBs was similar to that observed in other primary insulin target tissues such as liver, skeletal muscle and adipose tissues<sup>22</sup>. Collectively, these findings demonstrate that the skeleton plays an important role in the metabolic dysfunction associated with diet-induced insulin resistance and that restoration of insulin signalling in bone has systemic effects on insulin sensitivity. As aberrant activation of mTORC1 signalling leads to the development of insulin resistance, suppression of skeletal mTORC1 signalling may abrogate HFD-induced dysregulation of insulin signalling in the skeleton.

To investigate this question, mice with conditional deletion of *Rptor*, an essential component of mTORC1, in pre-OBs were utilised (*Rptor<sub>ob</sub><sup>-/-</sup>* mice). As shown in this Chapter, detailed metabolic analyses of these mice revealed that inactivation of OB-mTORC1 results in lean mice that are resistant to weight gain and are protected against the negative metabolic effects of HFD-induced obesity. Mechanistically, the protective phenotypes of *Rptor<sub>ob</sub><sup>-/-</sup>* mice are, at least in part, attributable to enhanced insulin signalling and thereby increased glucose uptake and glycolysis in the OBs of these mice.

### 3.3 Materials and Methods

For all other techniques previously outlined in Chapter 2, please refer to Section 2.2 for the detailed Materials and Methods

**3.3.1 High-fat diet studies.** All mice were bred and housed in pathogen-free conditions at the SAHMRI Bioresources Facility (SAHMRI, Adelaide, Australia), with *ad libitum* access to food (High fat diet: Specialty Feeds #SF16-096: 19.4% protein, 23% fat, WA, Australia; detailed in Supplementary Table 3.1) and water.

**3.3.2 Calculation of Food Quotient.** The food quotient (FQ), defined as an ideal diet-specific ratio of  $VCO_2/VO_2$ , was calculated using the following equation<sup>23</sup>:  $(0.835 \times \%protein) + (1.0 \times \%carbohydrate) + (0.71 \times \%fat)$ . The HFD contained 39.3% energy from protein, 43.4% energy from fat and 17.3% energy from carbohydrate resulting in a calculated FQ of 0.8093. Alternative FQ was estimated from linear regression analysis of change in body mass during the measurement period ( $\Delta M_b$ : *x*-axis) and 24-hour RQ (*y*-axis) as previously described<sup>24</sup> (Supplementary Fig. 3.1).

**3.3.3 Histology and Immunohistochemistry.** Immunohistochemistry was performed on interscapular brown adipose tissue using rabbit anti-UCP1 (ab209483, Abcam, Cambridge, MA, USA, 1:5000). For Oil red O staining, liver samples were mounted in Tissue-Tek Optimum Cutting Temperature compound (Sakura Finetek, The Netherlands). Cryosections were cut at 10  $\mu$ m and Oil red O staining procedure was performed as previously described<sup>25</sup>.

**3.3.4 Protein isolation and Western blotting.** Additional details of sources and concentrations of antibodies used in the immunoblotting are listed in Supplementary Table 3.2.

**3.3.5 RNA isolation and quantitative RT-PCR.** Additional details of forward and reverse primer pairs, designed to amplify across intron-exon boundaries, are listed in Supplementary Table 3.3.

**3.3.6 RNA high-throughput sequencing and gene expression analysis.** RNA isolated from marrow-flushed combined femora/tibiae was processed and sequenced through the low-input RNA-seq pipeline at The David Gunn Genomics Facility, SAHMRI (Illumina Nextseq, San Diego, CA, USA) using a 75 cycle v2 High Output sequencing kit. Analyses were then conducted by the SAHMRI Bioinformatics Facility. Initial raw read

processing was performed using an in-house pipeline developed at SAHMRI. Raw 75bp single-end FASTQ reads were assessed for quality using FastQC and results aggregated using R/Bioconductor package ngsReports<sup>26</sup>. Reads were then trimmed for sequence adapters using AdapterRemoval<sup>27</sup> and aligned to the GRCh38/mm10 version of the mouse genome using the RNA-seq alignment algorithm STAR<sup>28</sup>. After alignment, mapped sequence reads were summarised to the mm10 gene intervals using featureCounts<sup>29</sup>, and count table transferred to the R statistical programming environment for expression analysis.

Gene counts were filtered for low expression counts by removing genes with less than 1 count per million (cpm) in more than four samples and then normalised by the method of trimmed mean of M-values<sup>30</sup>. Differential gene expression was carried out on log-CPM counts and precision weights generated by the limma voom function<sup>31</sup> and edgeR<sup>32,33</sup>. Gene Set Enrichment Analysis (GSEA) was performed using the Molecular Signature Database (MSigDB) and other gene-sets were generated using the limma package<sup>34</sup>. Gene-sets returning an FDR adjusted p-value <25% were accepted as statistically enriched.

## 3.4 Results

### 3.4.1 *Rptor<sub>ob</sub><sup>-/-</sup>* mice are protected against high-fat diet-induced obesity

As outlined in Chapter 2, loss of mTORC1 function in pre-OBs is associated with improved glucose disposal and insulin sensitivity in mice fed a normal chow diet. These results suggest that mTORC1 signalling in OBs plays an important role in the regulation of glucose homeostasis. Furthermore, given that nutrient-overload leads to hyperactivation of mTORC1 signalling and the development of insulin resistance<sup>9</sup>, this led to the hypothesis that suppression of OBs-mTORC1 could protect animals from developing HFD-induced obesity and insulin resistance. To test this, *Rptor<sub>ob</sub><sup>-/-</sup>*, *Rptor<sub>ob</sub><sup>-/+</sup>* and littermate controls were placed on HFD (40% calories from fat) from 4-weeks of age and weight gain was monitored twice-weekly. Both male and female *Rptor<sub>ob</sub><sup>-/-</sup>* mice weighed significantly less than the control mice (Fig. 3.1A and B). As shown in Figure 3.1C and D, *Rptor<sub>ob</sub><sup>-/-</sup>* mice initially gained weight on the HFD at a similar rate to control and *Rptor<sub>ob</sub><sup>-/+</sup>* mice, and in the case of female mice, gained weight more rapidly. However, unlike the control and *Rptor<sub>ob</sub><sup>-/+</sup>* mice, which continued to gain weight in response to the obesogenic diet, weight gain in the *Rptor<sub>ob</sub><sup>-/-</sup>* mice plateaued after approximately 6 weeks and they gained only a small amount of additional weight thereafter (i.e. from 6-13 weeks on HFD, control mice gained 9.3g and 7.2g in male and female respectively, whereas *Rptor<sub>ob</sub><sup>-/-</sup>* mice gained only 1.7g; Fig. 3.1C-D).

The lower body weight of *Rptor<sub>ob</sub><sup>-/-</sup>* mice was independent of difference in their body length but rather due to the changes in the body composition as suggested by a significant lower BMI in the *Rptor<sub>ob</sub><sup>-/-</sup>* mice (Supplementary Fig. 3.2A-B). Further examination of body composition in these HFD-fed mice revealed that the difference in their body weight was largely attributable to a significant reduction in fat mass in *Rptor<sub>ob</sub><sup>-/-</sup>* mice (Fig. 3.1E), with a modest reduction in lean mass also observed (Supplementary Fig. 3.2C-D). When expressed as a percentage of total body mass, fat mass in male or female *Rptor<sub>ob</sub><sup>-/-</sup>* mice was 50% lower than that of the control mice (Fig. 3.1F). The total fat mass and % fat mass of HFD-fed *Rptor<sub>ob</sub><sup>-/+</sup>* mice was also found to be significantly lower than the controls in the male, but not female cohorts (Fig. 3.1E and F). Furthermore, the difference in fat mass in HFD-fed *Rptor<sub>ob</sub><sup>-/-</sup>* mice was clearly evident upon dissection and analysis of individual fat pad weights (Fig. 3.1G and H), whereas no such differences in lean organ weights (i.e. liver, heart, kidney, brain,

spleen; Supplementary Fig. 3.2E and F) were observed in *Rptor<sub>ob</sub><sup>-/-</sup>* mice compared to controls.

Metabolic phenotyping of control, *Rptor<sub>ob</sub><sup>+/+</sup>* and *Rptor<sub>ob</sub><sup>-/-</sup>* mice using Promethion cages revealed that the resistance of *Rptor<sub>ob</sub><sup>-/-</sup>* mice to HFD-induced weight gain and fat accumulation occurred independently of alterations in food intake, faecal lipid content and levels of physical activity (Supplementary Fig. 3.2G-K). Total energy expenditure (normalised to grams of lean mass, to account for the disproportionate HFD weight gaining between the genotypes) was similar between the genotypes during the light period, but was significantly higher in male *Rptor<sub>ob</sub><sup>-/-</sup>* mice during the dark cycle than the controls (Fig. 3.1I). Conversely, energy expenditure was equivalent across all genotypes during both light and dark cycles in the female cohort (Fig. 3.1J). Interestingly, while 24-h (daily) RQ values were similar across all three genotypes in both male and female cohorts, RQ patterns were noticeably different (Fig. 3.1K and L). To interrogate the hourly RQ patterns further, the food quotient (FQ), where FQ is the theoretical RQ produced by the diet, were calculated<sup>10</sup> and 24-h RQ≈FQ indicates a state of energy and macronutrient balance<sup>11</sup>. As detailed in Supplementary Fig 3.1A-C, the FQ of the HFD used in this study was calculated to be 0.7976, and is represented in Fig. 3.1K and L as a dotted line. Both *Rptor<sub>ob</sub><sup>-/-</sup>* and *Rptor<sub>ob</sub><sup>+/-</sup>* mice exhibited RQ>FQ during the dark cycle, relative to controls, whereas only in *Rptor<sub>ob</sub><sup>-/-</sup>* mice was RQ<FQ during the light cycle, culminating in a 24-h RQ close to the FQ. This suggests that *Rptor<sub>ob</sub><sup>-/-</sup>* mice maintain their constant weight and energy balance through greater substrate flexibility, with greater utilization of fat storage during the light cycle which provide a glycerol substrate for increased gluconeogenesis, thus resulting in higher carbohydrate oxidation in the dark cycle (Fig. 3.1K and L). Conversely, in *Rptor<sub>ob</sub><sup>+/-</sup>* mice, higher carbohydrate oxidation and lipid synthesis in the dark cycle was not offset by greater utilization of fat storage during the light cycle. Thus, even with greater substrate flexibility, as is evident in *Rptor<sub>ob</sub><sup>-/-</sup>* mice, higher energy storage during the dark cycle surpassed fat oxidation during the light cycle, resulting in overall continuous weight gain. In contrast, the average phasic RQ values of the control mice remained approximately constant, which is indicative of fewer shifts in their fat storage and oxidation and a more constant accumulation of adipose tissue mass.

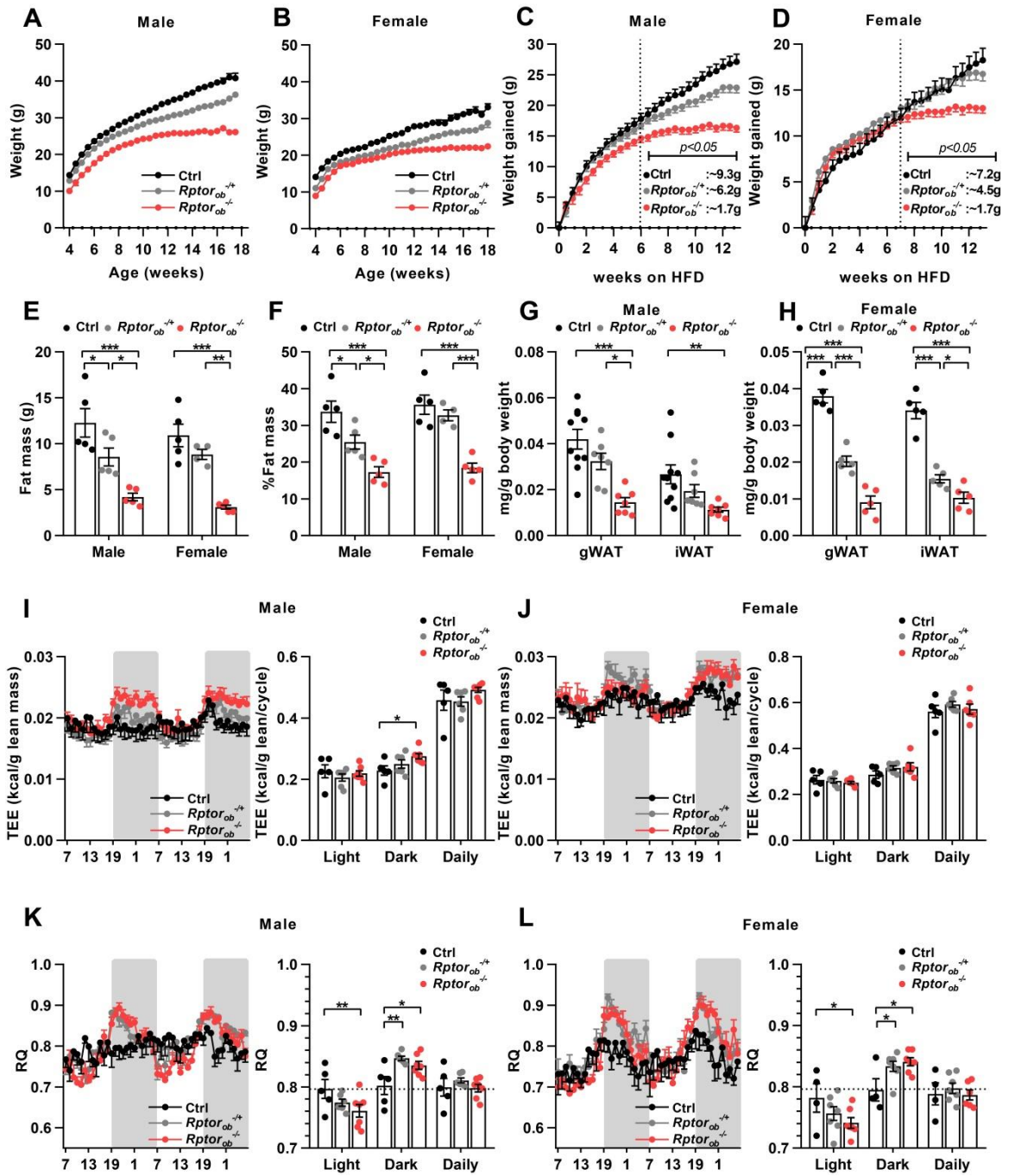


**Fig. 3.1 HFD-fed *Rptor<sub>ob</sub><sup>-/-</sup>* mice are protected against diet-induced obesity and exhibit greater substrate flexibility. (A-B)** Temporal body weight changes in male and female mice (n≥15/genotype). **(C-D)** Body weight gained in response to high fat diet (HFD) in male and female mice (n≥15/group). Dotted lines indicate the point at which *Rptor<sub>ob</sub><sup>-/-</sup>* mice became resistant to further weight gain. **(E-F)** DXA analysis of total fat mass and % fat mass normalised to total body weight in 18-week old HFD-fed mice (n=4-5/genotype). **(G-H)** gWAT and iWAT fat pad mass, normalised to body weight, in male and female mice at 18-week of age (n=4-9/genotype). **(I-J)** Total energy expenditure, normalised to lean mass, over a 48-h time course (*left*) and per light/dark cycle (*right*) in male and female HFD-fed mice (n=5-7/genotype). **(K-L)** Average respiratory quotient (RQ) over a 48-h time course (*left*) and per light and dark cycle (*right*) in male and female mice (n=5-7/genotype). All panels: data are expressed as mean ± SEM. \*p<0.05, \*\*p<0.01, \*\*\*p<0.001, two-way ANOVA with Tukey's post-hoc test. Panels H-K: shaded regions represent dark cycle.



### **3.4.2 *Rptor<sub>ob</sub><sup>-/-</sup>* mice are resistant to liver steatosis and adipocyte hypertrophy and exhibit increased browning of white adipose tissue**

On a systemic level, maintaining metabolic homeostasis during feeding or fasting relies on multi-organ coordinated control of available fuel. Fasting lowers the insulin-to-glucagon ratio, which stimulates hydrolysis of adipose tissue triacylglycerol (TG) (i.e. lipolysis) and thereby increases circulating levels of free fatty acids (FFAs) and their delivery to the periphery. Conversely, during postprandial states, high insulin levels favour glucose uptake, glycolysis, and pyruvate oxidation in liver and skeletal muscle while stimulating adipose *de novo* lipogenesis (DNL) from lipids and glucose. Furthermore, fatty acids derived from a meal also trigger adipose tissue to reduce FFA release and prompt hepatocytes to reduce endogenous TG release, which together stimulates the clearance of circulating TG<sup>38,39,40,41</sup>. The increased ability to switch metabolism between carbohydrate and fat oxidation in *Rptor<sub>ob</sub><sup>-/-</sup>* mice was associated with lower circulating TG levels in the male, but not the female mice, while FFA levels were higher in male *Rptor<sub>ob</sub><sup>+/-</sup>* mice relative to control and *Rptor<sub>ob</sub><sup>-/-</sup>* mice (Fig. 3.2A and B). Of note, significantly higher serum levels of  $\beta$ -hydroxybutyrate, the most abundant ketone<sup>42</sup>, which are typically produced under prolonged fasting, were observed in both HFD-fed male and female *Rptor<sub>ob</sub><sup>-/-</sup>* mice compared to controls (Supplementary Fig. 3.3A).

Both histological examination and quantification of lipid content in the liver revealed significantly less hepatic steatosis and lower levels of accumulated TG and FFA in the liver of HFD-fed *Rptor<sub>ob</sub><sup>-/-</sup>* mice compared to the controls (Fig. 3.3C-E) while expression analyses of genes involved in glucose or fatty acid metabolism failed to detect any changes in mRNA levels (Supplementary Fig. 3.3B and C). Analysis of adipocyte size and distribution revealed a significantly higher proportion of small adipocytes and a lower number of large adipocytes in both male *Rptor<sub>ob</sub><sup>-/-</sup>* gWAT and iWAT depots in response to the obesogenic diet (Fig. 3.2C, F and G). This reduction in adipocyte hypertrophy in *Rptor<sub>ob</sub><sup>-/-</sup>* mice was accompanied by an upregulation in the expression of adipogenic genes (*Cebpa*, *Ppar $\gamma$*  and *Lpl*) (Fig. 3.2H and I). An increase in adipose *de novo* lipogenesis, which promotes conversion of excessive carbohydrates to fatty acids for storage, has been reported to be beneficial to the body by sequestering excess TG thereby preventing lipotoxicity in other tissues (reviewed in<sup>43</sup>). Expression levels of DNL genes (*Fasn*, *Acc* and *Acyl*) were significantly upregulated in both fat depots of *Rptor<sub>ob</sub><sup>-/-</sup>* mice (Fig. 3.2H and I) suggesting that increased adipose DNL in the

*Rptor<sub>ob</sub><sup>-/-</sup>* mice could contribute to the lower levels of circulating and hepatic TG observed in these mice.

Strikingly, increased multilocularity of lipid droplets, a characteristic of brown adipocytes, was observed in iWAT of male HFD-fed *Rptor<sub>ob</sub><sup>-/-</sup>* mice suggesting “browning” of adipocytes (Fig. 3.2K). Consistent with these morphological observations, a strong upregulation in *Ucp1* mRNA and other genes associated with adipogenesis (e.g. *Pcg1a*, *Cidea* and *Cox7a*) was observed in *Rptor<sub>ob</sub><sup>-/-</sup>* iWAT samples compared to controls (Fig. 3.2J). Immunohistochemistry on the iWAT section and Western blotting of protein lysates made from iWAT confirmed the significant increase in protein levels of UCP1 in HFD-fed *Rptor<sub>ob</sub><sup>-/-</sup>* mice compared to the controls (Fig. 3.2J and L). In light of the observed browning of iWAT in HFD-fed *Rptor<sub>ob</sub><sup>-/-</sup>* mice, other adipose depots were also examined to determine whether they also displayed this effect. As shown in Supplementary Figure 3.3D-H, upregulation of *Ucp1* and *Pcg1a* expression was observed in the gWAT of *Rptor<sub>ob</sub><sup>-/-</sup>* mice at the mRNA level, but not at the protein level, whereas no changes in morphology, nor *Ucp1* expression, were observed in *Rptor<sub>ob</sub><sup>-/-</sup>* BAT. Similar data were obtained for the female mice (Supplementary Fig. 3.4A-M).

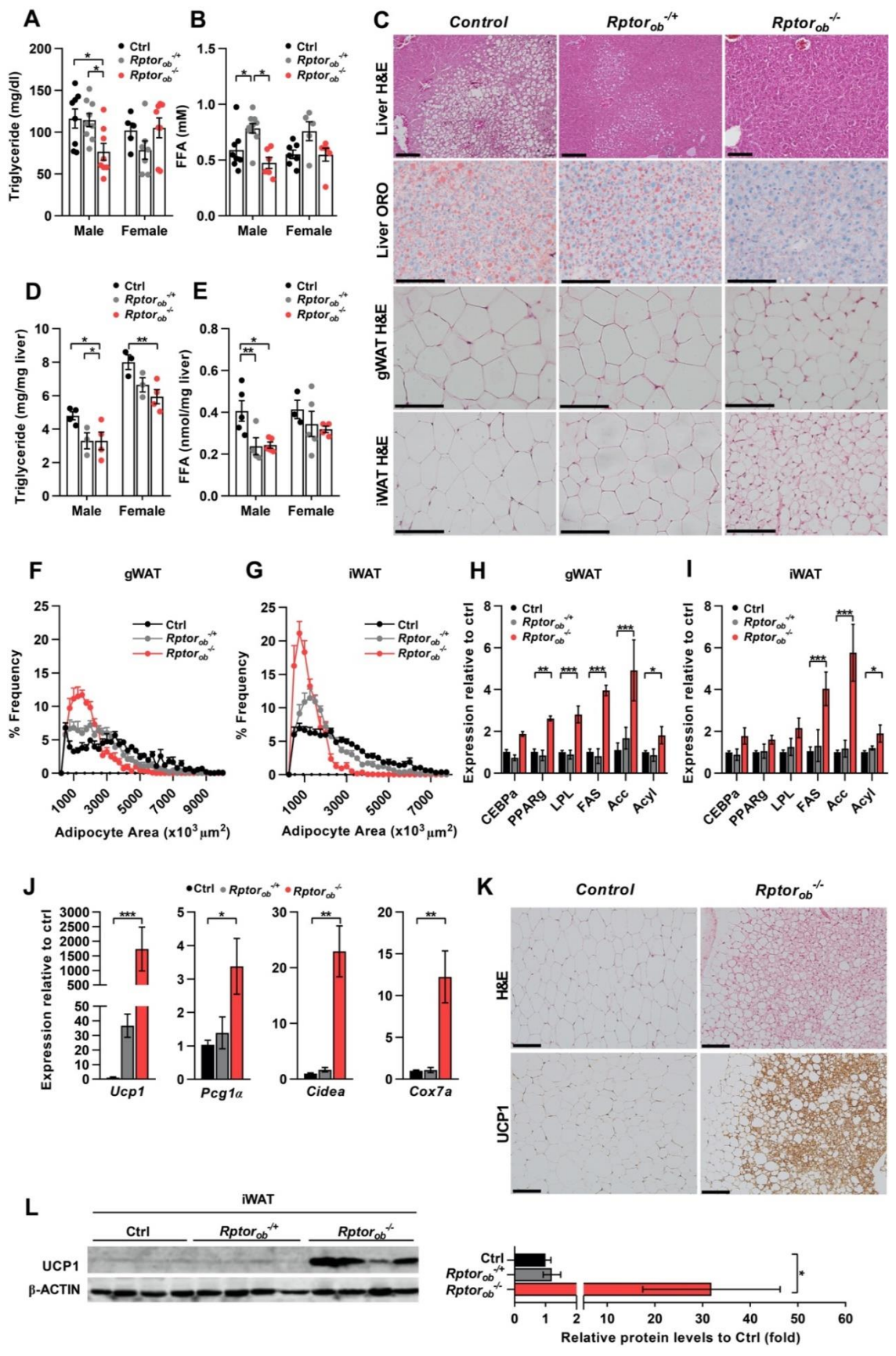


**Fig. 3.2 HFD-fed male *Rptor<sup>ob</sup><sup>-/-</sup>* mice exhibit browning of white adipose tissue.** (A) Serum triglyceride levels in HFD-fed mice at 18-week of age (n=6-9/genotype). (B) Serum free fatty acid levels (n=6-11/genotype). (C) Representative images of H&E and Oil red O-stained sections of liver and H&E section of gWAT and iWAT from HFD-fed male mice, scale bar = 100  $\mu$ m. (D) Hepatic triglyceride levels and (E) hepatic free fatty acid levels in 18-week old mice (n=3-4/genotype). (F-G) Size distribution of male gWAT and iWAT adipocytes calculated from H&E stained sections using Image J (n=5 sections/mouse, n=5-6/genotype). (H-I) Gene expression levels of adipogenesis and *de novo* lipogenesis markers in HFD-fed male gWAT and iWAT tissues, normalised to  $\beta$ -actin (n=3-5/genotype). (J) Representative images of H&E (*top*) and UCP1 immunostaining section (*bottom*) of iWAT from male mice, scale bar = 100 $\mu$ m. (K) Gene expression levels of brown adipose tissue markers in HFD-fed male iWAT tissue, normalised to  $\beta$ -actin (n=3-5/genotype). (L) Levels of UCP1 protein expression in HFD-fed male iWAT tissue (*left*) and quantitative analysis of protein levels relative to  $\beta$ -actin (*right*) (n=4/genotype). All panels except C and K: data are expressed as mean  $\pm$  SEM. \*p<0.05, \*\*p<0.01, \*\*\*p<0.001, two-way ANOVA with Tukey's post-hoc test.

The upregulation of protein levels of UCP1 only in the iWAT, but not the gWAT, suggested that browning of WAT in *Rptor<sub>ob</sub><sup>-/-</sup>* mice occurred in a depot-specific manner. Furthermore, even though proximal tibia regions (which are juxtaposed to trabecular bone) of BMAT have been reported to express markers of brown fat<sup>44,45</sup>, *Ucp1* levels were undetectable in the bone of *Rptor<sub>ob</sub><sup>-/-</sup>* mice (data not shown). Collectively these findings suggest that the mechanism(s) underlying this increase browning of white fat in *Rptor<sub>ob</sub><sup>-/-</sup>* mice may occur in an endocrine, not paracrine, manner. Recent studies have reported that skeletal muscle-secreted irisin<sup>46</sup> and fibroblast growth factor 21 (FGF21)<sup>47</sup> increase beige adipogenesis, raising the possibility that factors secreted from bone cells could alter the secretion of these factors. As shown in Fig. 3.3A and B, levels of *Fgf21* mRNA expression in the liver (the primary source of FGF21) were unchanged, and levels of skeletal muscle *Fndc5* expression (which encodes for Irisin) were significantly lower in both male and female *Rptor<sub>ob</sub><sup>-/-</sup>* mice. More recently, bone morphogenetic protein 7 (BMP7)<sup>48</sup> and the Wnt-signalling inhibitor, sclerostin<sup>49</sup> have been identified as additional regulators of WAT browning. As shown in Fig. 3.3C and D, mRNA expression levels of both *Bmp7* and *Sost* were significantly higher in flushed tibia/femur samples from male, but not female, *Rptor<sub>ob</sub><sup>-/-</sup>* mice. Consistent with the observed increase in *Sost* mRNA expression, sclerostin protein levels were also significantly elevated in the long bones of HFD-fed *Rptor<sub>ob</sub><sup>-/-</sup>* mice (Fig. 3.3E); however when expression levels of Axin2, a canonical Wnt signalling target gene, or total  $\beta$ -catenin levels were examined in the iWAT, there was no evidence of any inhibition of the Wnt signalling pathway (Fig. 3.3F and G). Given that browning of iWAT occurs in both sexes, this data suggests that increased *Bmp7* or *Sost* are not required for the beiging phenotype of the *Rptor<sub>ob</sub><sup>-/-</sup>* mice.

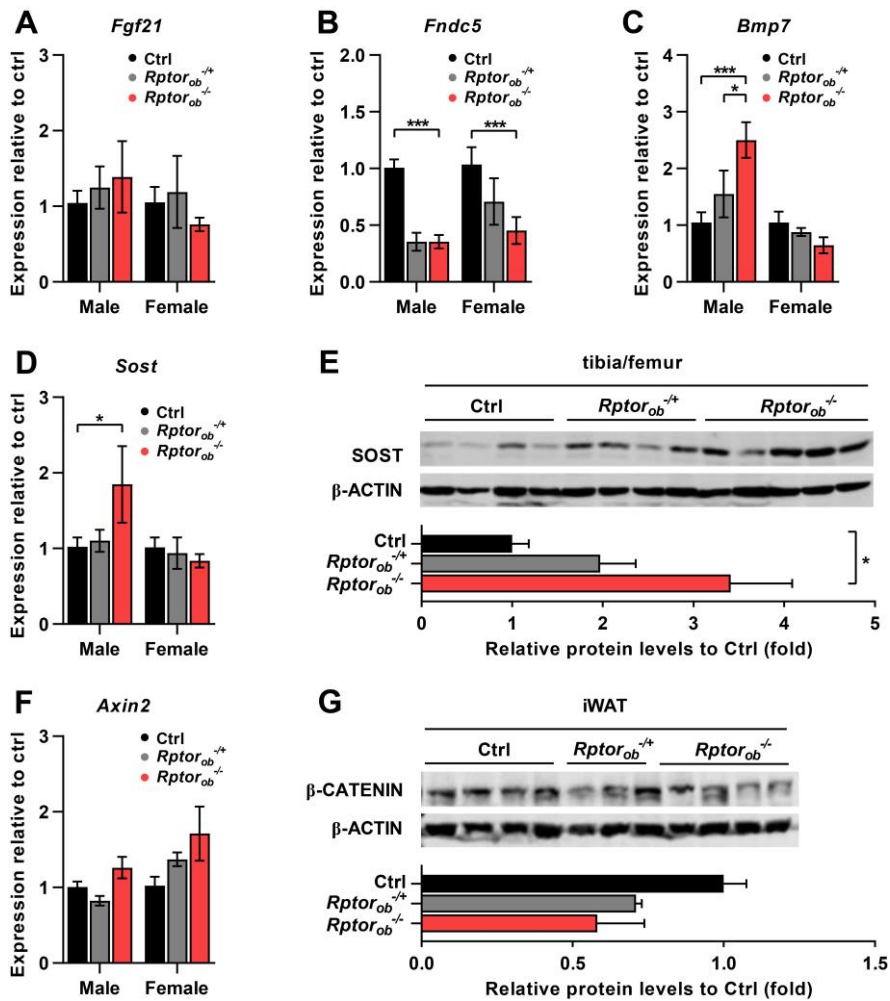


**Fig. 3.3 Browning of iWAT in HFD-fed *Rptor<sub>ob</sub><sup>-/-</sup>* mice occurs independent of known browning inducers.** (A) *Fgf21* gene expression, normalised to  $\beta$ -actin in liver (n=3-5/genotype). (B) *Fndc5* gene expression, normalised to  $\beta$ -actin in muscle (n=3-5/genotype). (C) *Bmp7* and (D) *Sost* gene expression, normalised to  $\beta$ -actin in bone samples (n=3-5/genotype). (E) Levels of Sclerostin protein expression in HFD-fed male bone tissue (top) and quantitative analysis of protein levels relative to  $\beta$ -actin (bottom) (n=4-5/genotype). (F) *Axin2* gene expression, normalised to  $\beta$ -actin in iWAT samples (n=3-5/genotype). (G) Levels of total  $\beta$ -catenin protein expression in HFD-fed male iWAT tissue (top) and quantitative analysis of protein levels relative to  $\beta$ -actin (bottom) (n=3-4/genotype). All panels: data are expressed as mean  $\pm$  SEM. \*p<0.05, \*\*p<0.01, \*\*\*p<0.001, two-way ANOVA with Tukey's post-hoc test.

### 3.4.3 *Rptor<sup>ob</sup><sup>-/-</sup>* mice are resistant to diet-induced insulin resistance

In addition to their role as an energy storage depot, adipose tissues play a crucial role in controlling energy metabolism via the actions of adipokines such as leptin and adiponectin<sup>50</sup>. Consistent with the lower fat mass observed in *Rptor<sup>ob</sup><sup>-/-</sup>* mice (Fig. 3.1D), serum leptin levels were greatly reduced in *Rptor<sup>ob</sup><sup>-/-</sup>* mice compared to both *Rptor<sup>ob</sup><sup>+/-</sup>* and control mice (Fig. 3.4A). Conversely, serum adiponectin levels were significantly higher in the *Rptor<sup>ob</sup><sup>-/-</sup>* mice compared to controls (Fig. 3.4B). Furthermore, analysis of adiponectin multimers showed a higher level of high molecular weight (HMW), the most bioactive, form of adiponectin in the serum of both male and female *Rptor<sup>ob</sup><sup>-/-</sup>* mice suggesting a greater sensitivity to insulin in *Rptor<sup>ob</sup><sup>-/-</sup>* mice (Fig. 3.4C and D).

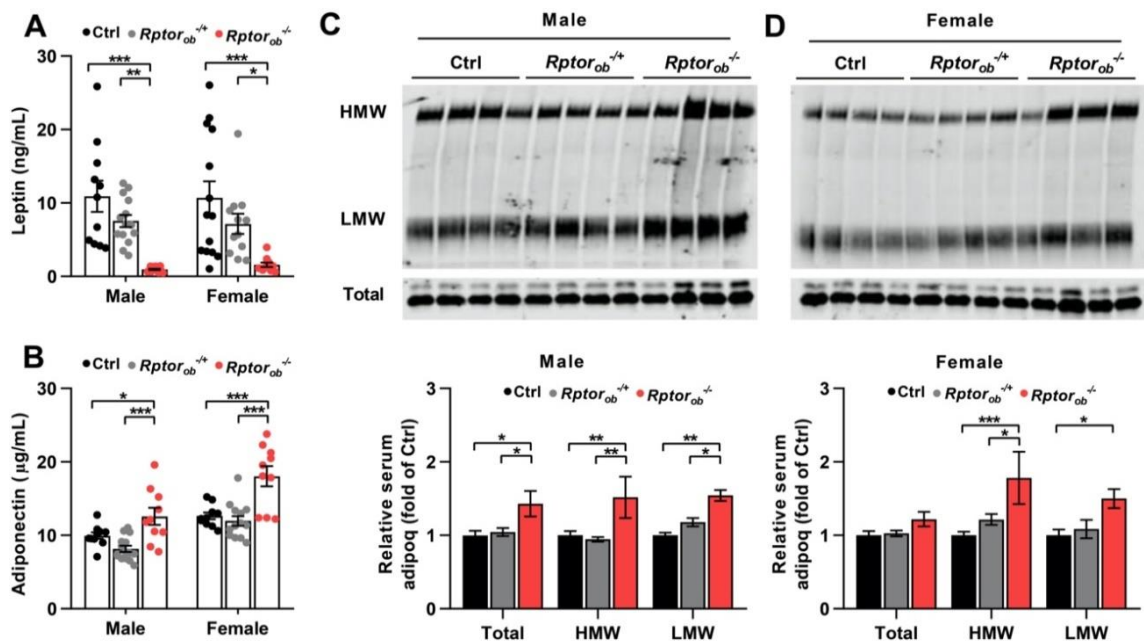


**Fig. 3.4 OB-specific deletion of *Rptor* affects serum adipokine levels.** (A) Serum leptin levels in HFD-fed mice at 18-week of age (n=11-14/genotype). (B) Serum adiponectin levels (n=10-15/genotype). (C-D) Western immunoblot analysis of high molecular weight (HMW), low molecular weight (LMW) and total adiponectin levels in sera from 18-week old HFD-fed male and female mice (*top*, n=4/genotype), and quantitative analysis of protein levels relative to  $\beta$ -actin (*bottom*). All panels: data are expressed as mean  $\pm$  SEM. \*p<0.05, \*\*p<0.01, \*\*\*p<0.001, two-way ANOVA with Tukey's post-hoc test.

Male *Rptor<sub>ob</sub><sup>-/-</sup>* mice showed a trend toward decreasing fasting glucose levels over the time course of HFD. Specifically, in 16-week old male *Rptor<sub>ob</sub><sup>-/-</sup>* mice, the fasting glucose levels were significantly lower than *Rptor<sub>ob</sub><sup>-/+</sup>* and control mice (Fig. 3.5A) while the fasting glucose levels of female *Rptor<sub>ob</sub><sup>-/-</sup>* mice were persistently lower than the control mice (Fig. 3.5B). The lower levels of fasting glucose in the *Rptor<sub>ob</sub><sup>-/-</sup>* mice were accompanied by a significant lower fasting insulin levels (Fig. 3.5C). As a result, calculation of homeostatic model assessment of insulin resistance (HOMA-IR) identify them as being more insulin-sensitive than both the *Rptor<sub>ob</sub><sup>-/+</sup>* and control mice (Fig. 3.3D).

Studies<sup>12</sup> suggest that in cases of significant difference in the fasting glucose levels, assessing glucose levels as a percentage of basal glucose for an ITT, can lead to erroneous interpretation of the results and thus all the ITT results were presented as absolute glucose levels. At 16 weeks of age, both male and female *Rptor<sub>ob</sub><sup>-/-</sup>* mice recapitulated all the key features of the metabolic profiles that were evident in the normal chow-fed studies, including the maintenance of higher glucose tolerance (Fig. 3.5E-G) as evidenced by with consistently lower glucose levels and significantly lower incremental area under the curve (iAUC) and higher responsiveness to insulin (Fig. 3.5H- J) compared to the controls. The improvements in glucose disposal in both male and female *Rptor<sub>ob</sub><sup>-/-</sup>* mice were associated with a higher fold change of insulin levels at 30 minutes post glucose injection, as measured by glucose-stimulated insulin secretion tests (Fig. 3.5K-N). Moreover, smaller  $\beta$ -cell islet hypertrophy was observed in male *Rptor<sub>ob</sub><sup>-/-</sup>* mice (Fig. 3.5N) which may have been a secondary effect of persistently low glucose levels.



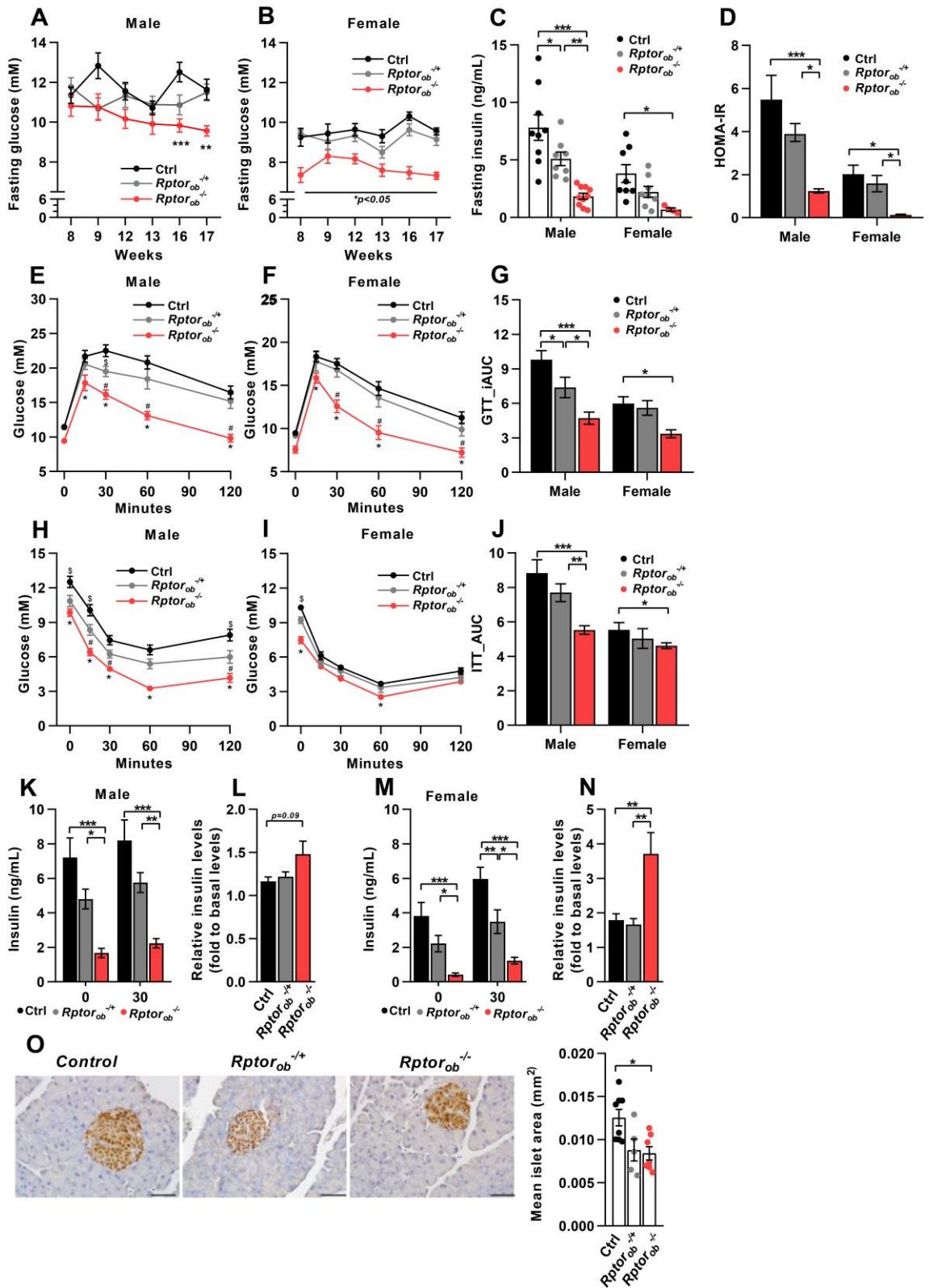


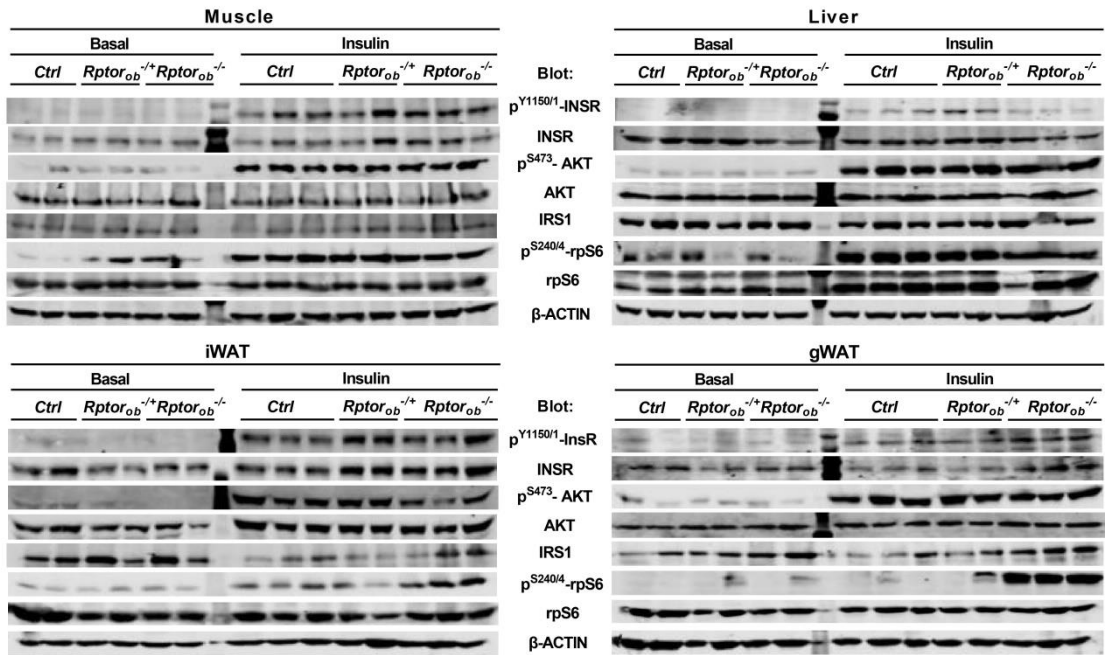
**Fig. 3.5 HFD-fed *Rptor<sub>ob</sub><sup>-/-</sup>* mice are protected against diet-induced insulin resistance.** (A-B) Fasting glucose levels over 8-17 weeks old male (A) and female (B) mice (n=5-15/genotype). (C) Fasting insulin levels (n=8-10/genotype). (D) HOMA-IR calculations of HFD-fed female mice (n=3-8/genotype). (E-F) Glucose tolerance tests (GTTs) in 17-week old male (E) and female (F) mice (n=6-15/genotype). (G) Incremental area under the curve analysis from (E-F). (H-I) Insulin tolerance tests (ITTs) in 16-week old male (H) and female (I) mice (n=6-15/genotype). (J) Area under the curve analysis from (H-I). (K-N) Insulin levels during a glucose-stimulated insulin secretion tests (GSIS) in male (K) and female (M) and Fold change in insulin levels at 30 minutes post glucose injection relative to basal levels (L and N) (n=8-10/genotypes). (O) Mean pancreatic islet area (n=5/genotype) and representative image of insulin immunostaining of pancreas at 18-week of age, scale bar=50µm. All panels except E, F, H and I: data are expressed as mean ± SEM. \*p<0.05, \*\*p<0.01, \*\*\*p<0.001, two-way ANOVA with Tukey's post-hoc test. For panel E, F, H and I: \*p<0.05 between *Rptor<sub>ob</sub><sup>-/-</sup>* and Ctrl, #p<0.05 between *Rptor<sub>ob</sub><sup>-/-</sup>* and *Rptor<sub>ob</sub><sup>-/+</sup>* and \$p<0.05 between *Rptor<sub>ob</sub><sup>-/+</sup>* and Ctrl, two-way ANOVA with Tukey's post-hoc test.

To further investigate the higher whole-body insulin sensitivity observed in HFD-fed *Rptor<sub>ob</sub><sup>-/-</sup>* mice, the insulin-induced phosphorylation of INSR at Tyr<sup>1150/1151</sup> and AKT at Ser<sup>473</sup> in the main insulin-target tissues: liver, skeletal muscle and adipose (iWAT and gWAT), was examined. Somewhat surprisingly, no significant difference in INSR or AKT phosphorylation was observed in either sex, with only a modest increase in AKT phosphorylation observed in skeletal muscle and INSR phosphorylation in iWAT from female HFD-fed *Rptor<sub>ob</sub><sup>-/-</sup>* mice (Fig. 3.7A-B). Of note, the levels of INSR phosphorylation in the male *Rptor<sub>ob</sub><sup>-/-</sup>* liver samples trended towards a decrease, compared to controls (Fig. 3.6A-D).

mTORC1 negatively regulates insulin signalling via a feedback loop where mTORC1 directly, and indirectly via S6K1 activation, leads to phosphorylation of IRS-1 and its subsequent ubiquitin-mediated degradation<sup>17,52</sup>. HFD feeding and obesity are associated with hyperactivation of the mTOR pathway, with increased S6K activity<sup>53</sup> and reduced IRS-1 protein levels<sup>35,54</sup> observed in the liver and skeletal muscle. To further interrogate the activation of the mTOR pathway in HFD-fed *Rptor<sub>ob</sub><sup>-/-</sup>* mice, the phosphorylation of rpS6 at Ser<sup>240/244</sup>, a substrate of S6K1, and total IRS-1 levels in the liver, skeletal muscle and adipose tissues was examined. Consistent with previously published studies<sup>53</sup>, basal phosphorylation of rpS6 was consistently detected in liver samples from all three genotypes, however basal phosphorylation of rpS6 at Ser<sup>240/244</sup> was detected only in the muscle of *Rptor<sub>ob</sub><sup>-/+</sup>* and *Rptor<sub>ob</sub><sup>-/-</sup>* mice, but not in the controls (Fig. 3.6A and B and 3.7A and B). Despite this, the levels of insulin-stimulated rpS6 phosphorylation in muscle and liver were similar across all three genotypes (Fig. 3.6A and B and 3.7A and B). While no significant difference was observed in basal S6 phosphorylation in the both fat depots, a significant induction in rpS6 phosphorylation was observed in response to insulin stimulation in gWAT of both male and female *Rptor<sub>ob</sub><sup>-/-</sup>* mice (Fig. 3.6A and B and 3.7A and B). In iWAT, rpS6 phosphorylation was significantly higher in male (Fig. 3.6A and B) and a trend toward significant (p=0.06) in the female *Rptor<sub>ob</sub><sup>-/-</sup>* mice (Fig. 3.7A and B), indicative of increased insulin-stimulated mTOR signalling. Increased IRS-1 protein levels were also observed in fat depots of *Rptor<sub>ob</sub><sup>-/-</sup>* mice under both basal conditions and in response to insulin stimulation (Fig. 3.6A and B and 3.7A and B). These results suggest that enhanced insulin signalling in the fat depots of *Rptor<sub>ob</sub><sup>-/-</sup>* mice may account for the higher peripheral sensitivity to insulin demonstrated by ITTs in the *Rptor<sub>ob</sub><sup>-/-</sup>* mice (as indicated by ITT data, Fig. 3.3F-H) and is attributable to changes in insulin signalling in adipose tissues and not the muscle or liver.

**A**

**Male**



**B**

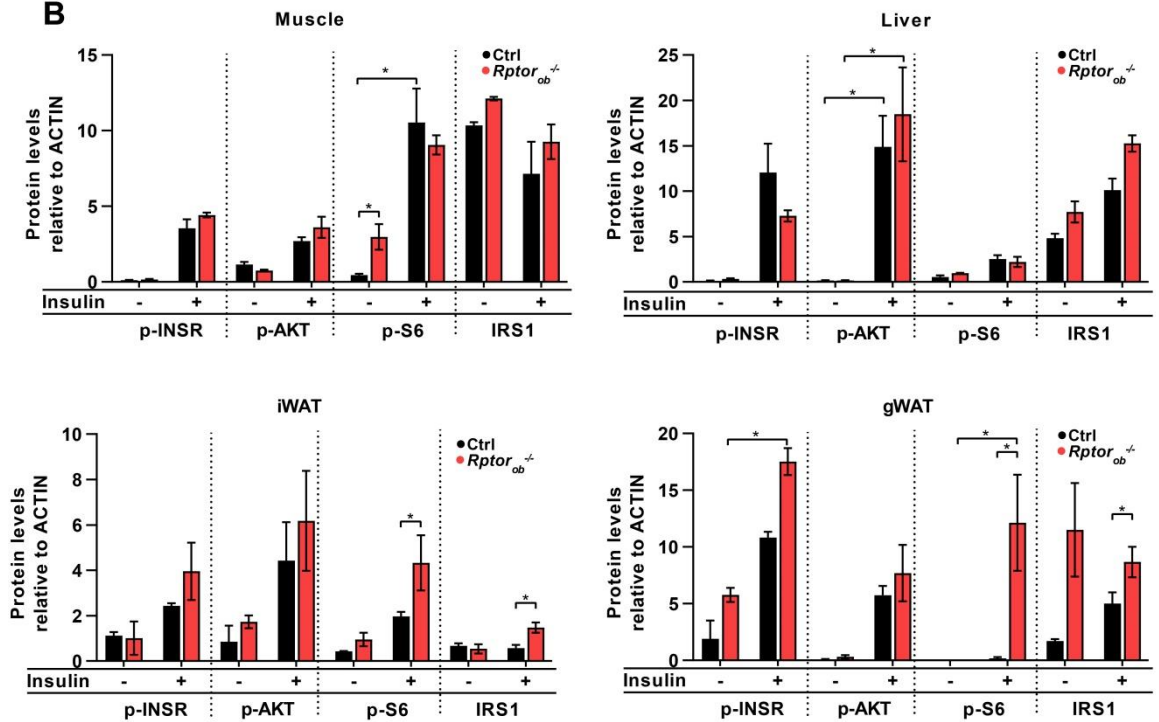
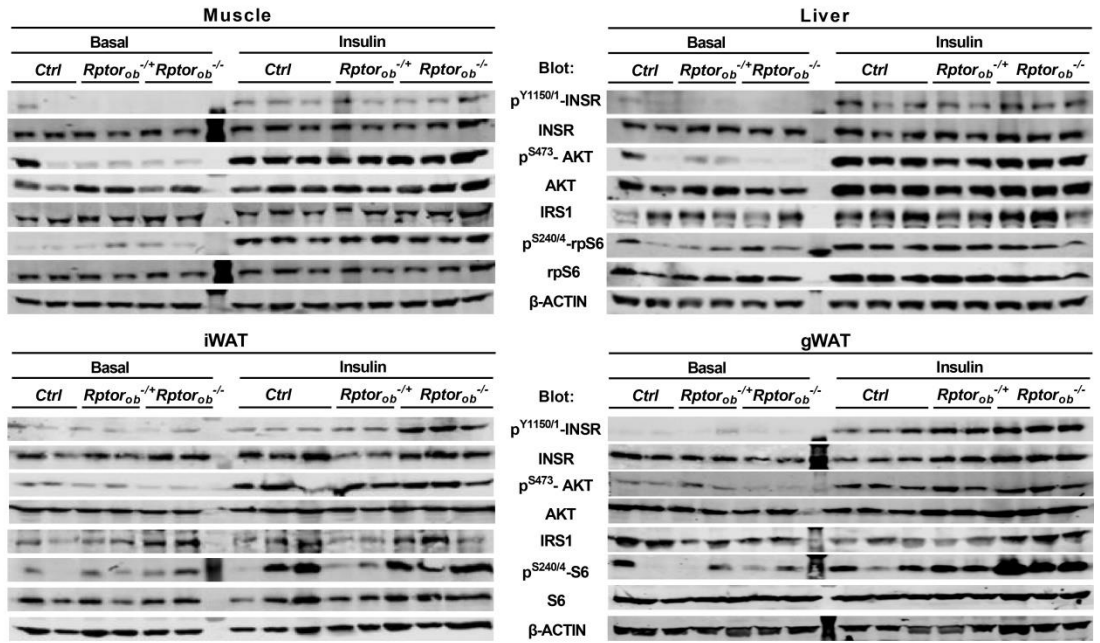


**Fig. 3.6 Insulin signalling in peripheral tissues in HFD-fed male mice.** (A) Western immunoblot analysis of indicated protein levels in skeletal muscle (*top left*), liver (*top right*), iWAT (*bottom left*), and gWAT (*bottom right*) tissues from 18-week old HFD-fed male mice collected after a 6 hour fast, under either basal (6 hr fast + PBS; n=2/genotype) or insulin-stimulated (6 hr fast + insulin stimulation; n=2-3/genotype) conditions. (B) Quantitative analysis of indicated protein levels from (A). Panels B: data are expressed as mean  $\pm$  SEM. \*p<0.05, two-way ANOVA with Tukey's post-hoc test.

**A**

Female



**B**

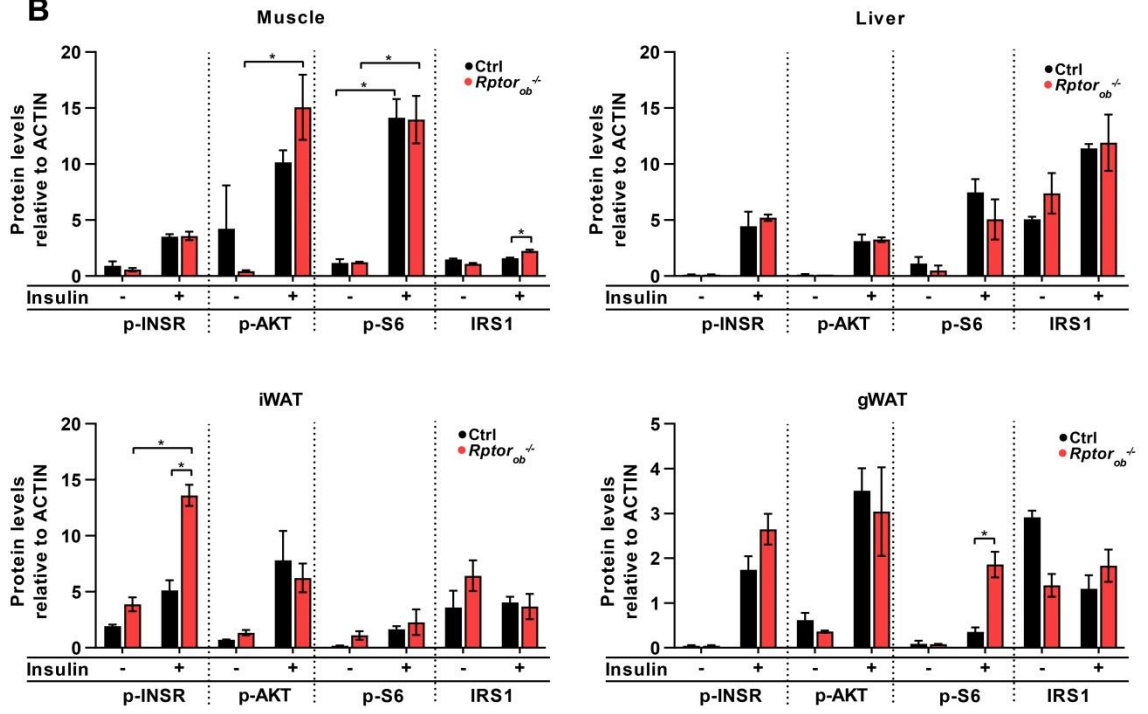


**Fig. 3.7 Insulin signalling in peripheral tissues in HFD-fed female mice.** (A) Western immunoblot analysis of indicated protein levels in skeletal muscle (*top left*), liver (*top right*), iWAT (*bottom left*), and gWAT (*bottom right*) tissues from 18-week old HFD-fed female mice collected after a 6 hour fast, under either basal (6 hr fast + PBS; n=2/genotype) or insulin-stimulated (6 hr fast + insulin stimulation; n=2-3/genotype) conditions. (B) Quantitative analysis of indicated protein levels from (A). Panels B: data are expressed as mean  $\pm$  SEM. \*p<0.05, two-way ANOVA with Tukey's post-hoc test.

### **3.4.6 Transcriptional changes associated with OB-specific *Rptor* deletion in male HFD-fed mice.**

To investigate how impaired mTORC1 function in pre-OBs contributes to systemic changes in metabolism, RNA-sequencing was used to identify transcriptional networks that are modulated in the bones of male *Rptor<sup>ob</sup><sup>-/-</sup>* mice. mTORC1 regulates transcription either directly, by controlling the nuclear import of transcription factors<sup>55,56</sup>, or indirectly through the translation of transcription factors<sup>57</sup>. To identify genes that are differentially regulated by mTORC1, RNA-seq analysis was performed to compare the transcriptomes of flushed long bone (tibia/femur) samples from control and *Rptor<sup>ob</sup><sup>-/-</sup>* mice. Gene set enrichment analysis (GSEA) of the whole transcriptome in the bone of *Rptor<sup>ob</sup><sup>-/-</sup>* mice identified an upregulation in gene sets associated with glucose uptake and oxidation, lipid oxidation pathways and insulin signalling (Fig. 3.8A). Furthermore, consistent with previously-published studies that have documented impaired B-cell development in *Rptor<sup>ob</sup><sup>-/-</sup>* mice<sup>58</sup>, pathways involved in B-cell development were down-regulated in the *Rptor<sup>ob</sup><sup>-/-</sup>* mice (Supplementary Fig. 3.6). A complete list of upregulated and downregulated pathways is detailed in Appendix I and II.

After data processing and filtering, 986 genes were found to be differentially expressed with 868 genes being significantly up-regulated and 118 genes significantly down-regulated in *Rptor<sup>ob</sup><sup>-/-</sup>* bones. These differentially-expressed genes (DEGs) were then mapped to the KEGG pathway enrichment analysis. Consistent with GSEA, DEGs were highly clustered towards glucose metabolism and response to insulin signalling including insulin signalling pathway (15/140 genes; enrichment FDR= 7.95E-04), Glycolysis / Gluconeogenesis pathway (9/67 genes; enrichment FDR= 1.87E-03), PI3K-Akt signalling pathway (25/357 genes; enrichment FDR= 8.65E-03), Starch and sucrose metabolism (5/33 genes; enrichment FDR=1.16E-02) and FoxO signalling pathway (11/131 genes; enrichment FDR= 2.23E-02).

Consistent with the enrichment of glycolysis pathway from GSEA (Fig. 3.8B) and KEGG pathway analysis, gene expression analyses revealed significantly higher expression levels of genes involved in glucose oxidation – e.g. hexokinase 2 (*HkII*), phosphoglycerate kinase 1 (*Pgk1*), lactate dehydrogenase A (*Ldha*), phosphoinositide-dependent kinase-1 (*Pdk1*) and 6-phosphofructokinase (*Pfkml1*) (Fig. 3.8C). OBs are known to express three glucose transporters (*Glut1*, 3 and 4)<sup>59,60,61</sup>. *Glut1*, predominantly expressed in undifferentiated OBs, is crucial for insulin-independent



glucose uptake for differentiation and proliferation<sup>62</sup> while *Glut4* mediates insulin-stimulated glucose uptake by mature OBs<sup>63</sup>. As shown in Figure 3.8C, levels of *Glut4* mRNA expression were 2-fold higher in the long bones of *Rptor<sub>ob</sub><sup>-/-</sup>* mice compared to the controls, whereas no change in *Glut1* expression was observed. The higher expression of *Glut4*, an insulin-dependent glucose transporter, together with upregulation of glycolysis and insulin signalling pathways suggests a potential increase in insulin-mediated glucose uptake in the bones of *Rptor<sub>ob</sub><sup>-/-</sup>* mice.

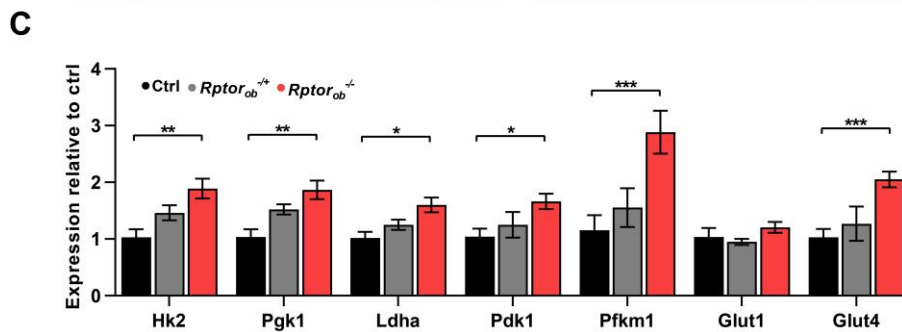
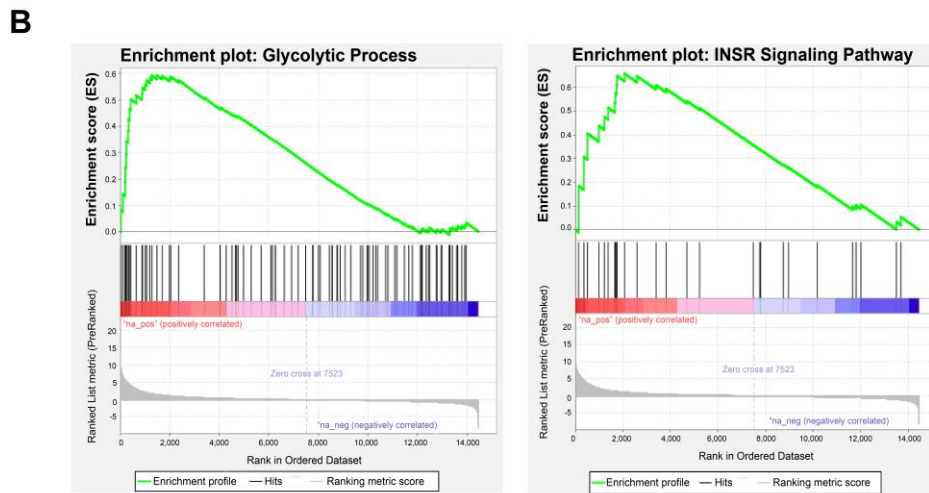
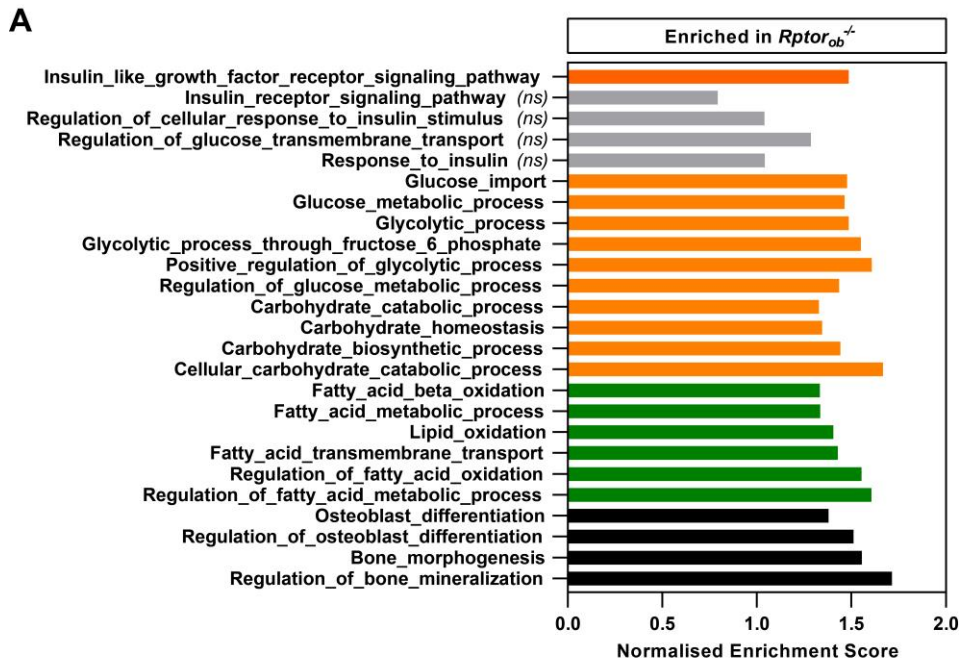


**Fig. 3.8 Increased glycolysis and insulin signalling pathways in the bone of HFD-fed male *Rptor<sub>ob</sub><sup>-/-</sup>* mice.** (A) Gene set enrichment analysis (GSEA) of positively-enriched pathways (upregulated) of RNA isolated from combined flushed femur and tibia (n=5; controls versus *Rptor<sub>ob</sub><sup>-/-</sup>*). (B) Enrichment plots of glycolysis (*left*) and insulin-like growth factor receptor signalling pathways (*right*). (C) Gene expressions of glycolysis (*HkII*, *Pgk1*, *Ldha*, *Pdk1* and *Pfkm1*) and glucose transporters (*Glut1* and *Glut4*) in the flushed femur/tibia from HFD-fed mice (n=3-5/genotype). Panel C: data are expressed as mean ± SEM. \*p<0.05, \*\*p<0.01, \*\*\*p<0.001, two-way ANOVA with Tukey's post-hoc test. Panels A: orange bar indicates pathways relating to glucose metabolism or insulin signalling, green bar indicates pathways relating to lipid metabolism, and black bar indicates pathways relating to bone development. Grey bar (*ns*) = not significant.

### **3.4.5 Increased insulin signalling and glycolysis in bone of *Rptor<sub>ob</sub><sup>-/-</sup>* mice**

In light of the RNA-seq data, we next interrogated if the systemic changes in glucose metabolism in *Rptor<sub>ob</sub><sup>-/-</sup>* mice, under HFD, was associated with an increase in insulin sensitivity in bone. Previous studies have shown that insulin resistance develops in the skeleton of HFD-fed mice and genetically increasing or decreasing insulin signalling in OBs protected or worsened whole-body glucose homeostasis in HFD-fed mice, which is partly due to the effects of insulin signalling on OCN activity<sup>22</sup>. Gene expression analysis of *Bglap* mRNA expression in the long bones of *Rptor<sub>ob</sub><sup>-/-</sup>* mice revealed a significant upregulation of *Bglap* expression in male, but not female, *Rptor<sub>ob</sub><sup>-/-</sup>* mice, compared to controls (Fig. 3.9A). However, at the protein level, circulating levels of both total and undercarboxylated OCN were found to be unchanged in both male and female *Rptor<sub>ob</sub><sup>-/-</sup>* mice compared to controls (Fig. 3.9B-C). Furthermore, the circulating levels of other reported osteokines, lipocalin 2 (LCN2)<sup>64</sup> and osteoglycin (OGN)<sup>65</sup>, were also unchanged between all three genotypes (Fig. 3.9D-E). An assessment of bone mineral density (BMD) using DEXA in HFD-fed *Rptor<sub>ob</sub><sup>-/-</sup>* mice revealed a significant reduction (8.7%) in the male, but not the female mice (Fig. 3.9F).

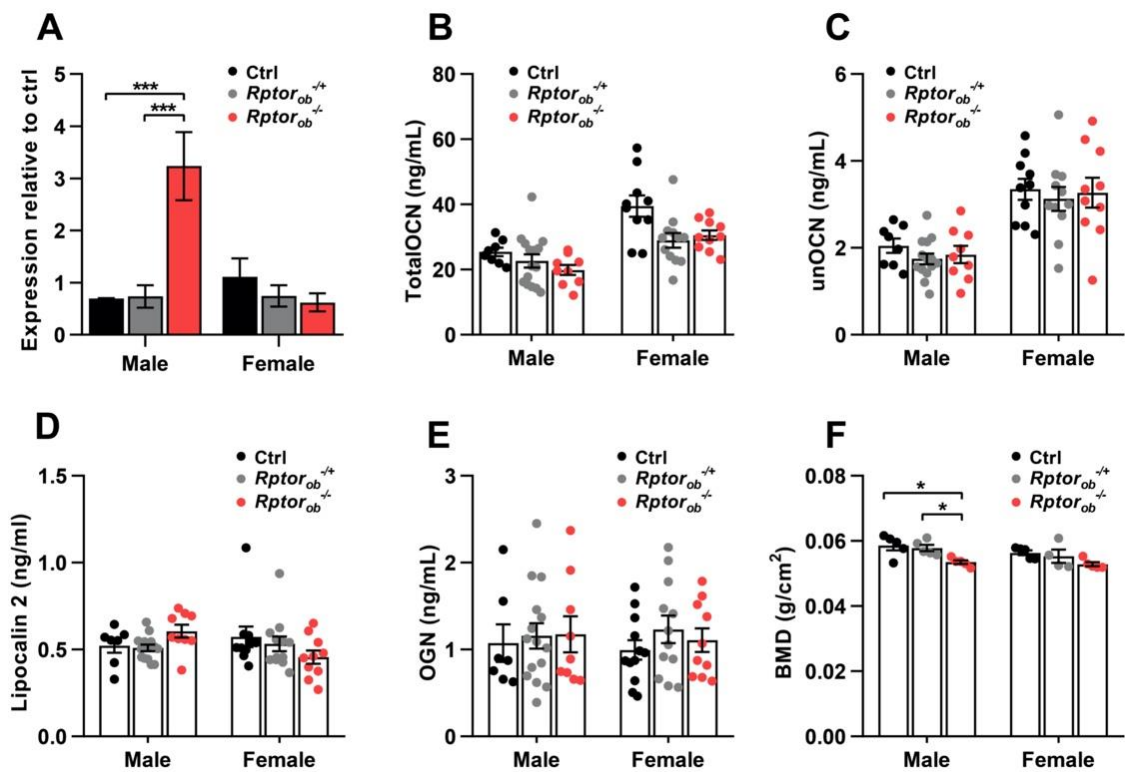


**Fig. 3.9 Improvements in glucose metabolism observed in HFD-fed *Rptor<sub>ob</sub><sup>-/-</sup>* mice occur independent of osteocalcin and other osteokines.** (A) Gene expression of *Bglap* in the flushed femur/tibia, normalised to  $\alpha$ -actin (n=3-4/genotype). (B) Serum levels of total osteocalcin, (C) undercarboxylated osteocalcin, (D) lipocalin-2 and (E) osteoglycin in HFD-fed mice at 18-weeks of age (n=7-15/genotype). All panels: data are expressed as mean  $\pm$  SEM. \*p<0.05, \*\*p<0.01, \*\*\*p<0.001, two-way ANOVA with Tukey's post-hoc test.

Insulin responsiveness in bone (calvaria) of *Rptor<sup>ob</sup><sup>-/-</sup>* mice was assessed biochemically following insulin stimulation. Initially, *Rptor* deletion was confirmed in calvaria by qRT-PCR, using primers specific to floxed exon 6. A significant reduction in *Rptor* gene expression was observed in *Rptor<sup>ob</sup><sup>-/-</sup>* mice consistent with Cre-mediated excision (Fig. 3.10A). Intracellular signalling events triggered by insulin, such as phosphorylation of insulin receptor at Tyr<sup>1150/1151</sup>, were significantly higher in the bone of *Rptor<sup>ob</sup><sup>-/-</sup>* mice (Fig. 3.10B). In contrast, insulin-stimulated phosphorylation of rpS6, a major effector protein downstream of mTOR1, at Ser<sup>240/244</sup> was blunted in the *Rptor<sup>ob</sup><sup>-/-</sup>* mice compared to controls, consistent with reduced mTORC1 activity. Importantly, both basal and insulin-stimulated levels of AKT (Thr<sup>308</sup> and Ser<sup>473</sup>) were significantly increased in *Rptor<sup>ob</sup><sup>-/-</sup>* mice (Fig. 3.10B). Concomitant with the increased activation of AKT, in both the basal and insulin-stimulated states, the phosphorylation levels of AKT substrates including glycogen synthases 3 $\beta$  (GSK3 $\beta$ ) at Ser<sup>9</sup> and AS160 at Thr<sup>642</sup>, a substrate of AKT that regulates insulin-stimulated Glut4 trafficking, at Thr<sup>642</sup> were increased (Fig. 3.10B). This data, in combination with the RNA-seq data, suggests that loss of mTORC1 function in OBs increases basal and insulin-dependent glucose uptake in *Rptor<sup>ob</sup><sup>-/-</sup>* mice.

To address this question, calvarial cells were isolated from newborn *Rptor<sup>fl/fl</sup>* mice and a tamoxifen-inducible Cre lentivirus was used to generate *Rptor* knockout OBs (*Rptor<sup>KO</sup>*) and wildtype control cells (*Rptor<sup>WT</sup>*). Deletion of *Rptor* in calvariae-derived OBs *in vitro* caused a reduction in basal and insulin-stimulated phosphorylation of the key mTORC1 substrates p70S6K and 4E-BP1 and ribosomal protein S6, a p70S6K substrate, findings consistent with reduced mTORC1 activity (Fig. 3.10C). Deletion of *Rptor* was also associated with an increase in basal and insulin-stimulated AKT activation and phosphorylation of GSK3 $\beta$  at Ser<sup>9</sup> (Fig. 3.10C), consistent with the *in vivo* insulin pulse experiments (Fig. 3.10B). Furthermore, qRT-PCR analysis revealed an increase in the expression of glycolytic genes in *Rptor<sup>KO</sup>* cells relative to wildtype control cells, mirroring the *in vivo* findings (Fig. 3.10D). Finally, using the accumulation of 2-deoxyglucose as a surrogate measure of glucose uptake, loss of mTORC1 function in OBs increased both basal and insulin-stimulated glucose uptake into OBs (Fig. 3.10E). Taken together, these findings support a central role for the mTORC1 complex in OBs in the control of systemic glucose metabolism and highlight the importance of this complex in bone in the development of systemic insulin resistance.

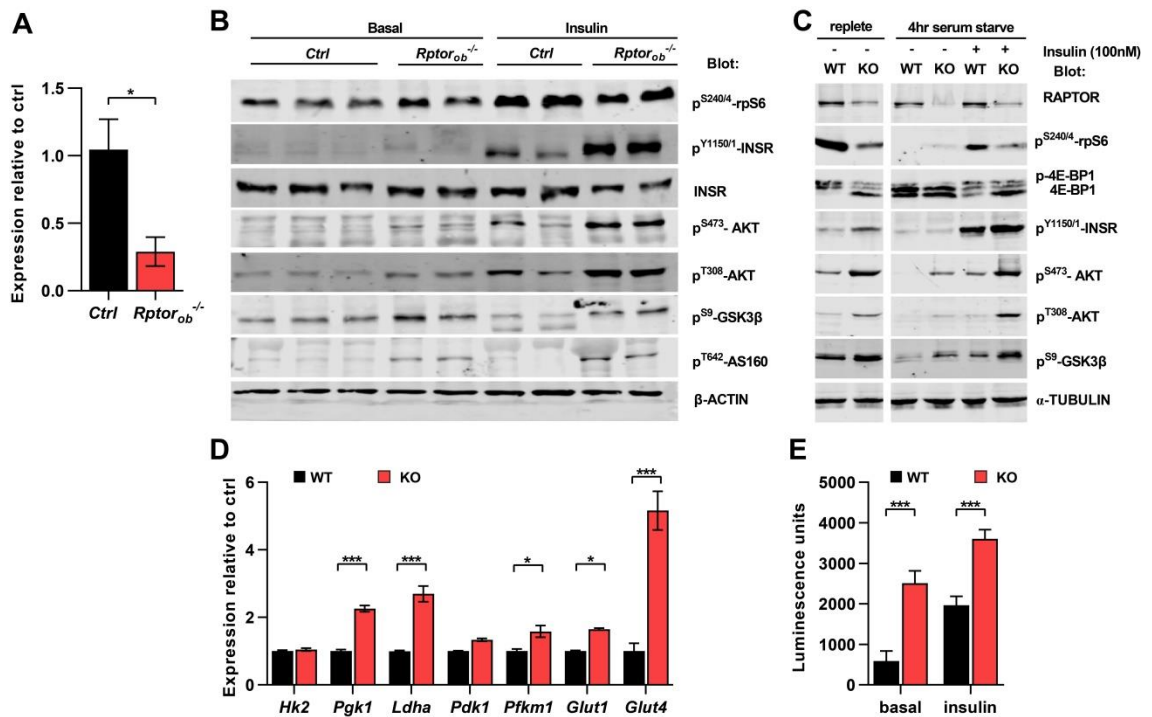


**Fig. 3.10 *In vivo* and *in vitro* loss of OB-mTORC1 lead to potentiation of OB insulin signalling.** (A) Gene expression of *Rptor* in the calvarial bone tissue, normalized to  $\beta$ -actin (n=3-4/genotype). Data are expressed as mean  $\pm$  SEM. \* $p < 0.05$ , unpaired Student's *t*-test. (B) Western immunoblot analysis of indicated protein levels in calvarial bone tissue from 18-week old HFD-fed mice collected after a 6 hour fast under either basal (6-hr fast + PBS; n=2-3/genotype) or insulin-stimulated (6-hr fast + insulin stimulation; n=2/genotype) conditions. (C) Western immunoblot analysis of indicated protein levels in wildtype (WT) and *Rptor* knockout (KO) cultured primary osteoblasts collected under normal growth and a 4-h serum starved conditions before or after stimulation with 100nM insulin. (D) Gene expression analysis of glycolysis and glucose transporters in WT or *Rptor* KO OBs (n=3). Data are expressed as mean  $\pm$  SD. \* $p < 0.05$ , \*\*\* $p < 0.001$ , unpaired Student's *t*-test. (E) 2-Deoxy-D-glucose uptake (measured as units of luminescence) of WT or *Rptor* KO OBs under either basal or insulin-stimulated conditions. Data are expressed as mean  $\pm$  SD. \*\*\* $p < 0.001$ , unpaired Student's *t*-test.

### 3.5 Discussion

The data presented in this study provide further mechanistic insight into how insulin signalling in the bone contributes to overall systemic glucose homeostasis. Under excessive nutrient conditions, suppression of skeletal mTORC1 signalling protects mice from developing diet-induced obesity and insulin resistance, which is associated with an enhancement in responsiveness to insulin and insulin-dependent glucose uptake in the OB of these mice.

#### 3.5.1 Increased OB insulin signalling

Previous studies have shown that modulation of insulin signalling in OBs, by genetically decreasing or increasing the levels of insulin receptor expression, either worsens or enhances glucose tolerance and insulin resistance in HFD-fed animals, respectively<sup>22</sup>. Furthermore, mice with OB-specific deletion of *FoxO1* (*FoxO1*<sup>OB-/-</sup>), a negative regulator of insulin signalling, are protected from HFD-induced obesity<sup>66</sup>. Consistent with these data, suppression of skeletal mTORC1 activity, a downstream mediator and negative regulator of insulin signalling, protects mice from diet-induced obesity. Of note, the lower fasting glucose levels, enhanced glucose tolerance and increased insulin sensitivity displayed by *Rptor<sub>ob</sub>*<sup>-/-</sup> mice mimics the metabolic phenotype of mice that overexpress the human insulin receptor in the OBs (*Colla1-INSR*<sup>Tg</sup> mice)<sup>22</sup>. At the molecular level, enhanced insulin signalling, or markers for insulin sensitivity, in the peripheral insulin target tissues (muscle, WAT and liver) was not observed in the *Rptor<sub>ob</sub>*<sup>-/-</sup> mice. As a side note, the dosage of insulin used for this intracellular signalling analysis of *Rptor<sub>ob</sub>*<sup>-/-</sup> mice was found to be significantly higher than other studies (150mU/g body weight vs 0.5mU/g body weight in<sup>22</sup> or 0.05mU/g body weight<sup>67</sup>) which could potentially lead to saturation of the insulin signalling in peripheral tissues<sup>68,69</sup>. Despite this, insulin signalling was found to be significantly enhanced in the bone of *Rptor<sub>ob</sub>*<sup>-/-</sup> mice. This response is similar to previously published studies in *Colla1-INSR*<sup>Tg</sup> mice, which reported enhanced insulin signalling in the bone (and not other tissues) under both normal chow and HFD conditions. Moreover, insulin-dependent activation of both INSR and AKT, in HFD-fed mice, was similar to normal chow-fed mice, suggesting insulin sensitivity is maintained in the bones of these mice under a HFD<sup>22</sup>. However, it is important to note that in this current study, the normal chow-fed (Chapter 2: 8-week old) and HFD-fed (16-week old) mice were not



age-matched, which prevents comparisons across diets with respect to insulin-sensitivity.

Mechanistically, the protective metabolic phenotype of *Colla1-INSR<sup>Tg</sup>* mice was attributed to an insulin-mediated increase in bone resorption, leading to an increase in OCN activity and its circulating levels (despite no difference in *Ocn* mRNA expression being observed)<sup>22</sup>. In contrast, both RNA-seq and qRT-PCR analysis of bone samples from *Rptor<sub>ob</sub><sup>-/-</sup>* mice revealed a downregulation of genes involved in bone resorption and osteoclast differentiation pathways, and an upregulation of genes associated with bone formation and OB differentiation. Despite detection of significantly higher *Ocn* mRNA expression levels in male *Rptor<sub>ob</sub><sup>-/-</sup>* mice, circulating levels of both total OCN and unOCN, for both male and female *Rptor<sub>ob</sub><sup>-/-</sup>* mice, were equivalent to those of the controls. This finding is in contrast to the normal chow study described in Chapter 2, where serum OCN levels were significantly reduced in *Rptor<sub>ob</sub><sup>-/-</sup>* mice. At this stage, the mechanisms underlying this disparity remain to be determined. OCN is expressed exclusively from mature OBs and low serum levels are used as a marker of reduced OB activity and bone mass<sup>70</sup>. Low serum OCN levels correlated with the low bone mass phenotype of normal chow-fed *Rptor<sub>ob</sub><sup>-/-</sup>* mice<sup>71</sup> whereas no difference in bone mineral content (BMC) was observed in HFD-fed *Rptor<sub>ob</sub><sup>-/-</sup>* mice of either sex relative to controls. It is important to note that the interpretation of these findings is unclear given an inability to directly compare bone mass with age-matched normal chow-fed control and *Rptor<sub>ob</sub><sup>-/-</sup>* mice, which would allow us to take into account the skeletal effects of a HFD. Previous studies have shown that HFD-fed WT mice have reduced total and unOCN levels<sup>22</sup>, suggesting that the apparent “normalisation” of OCN levels in HFD-fed *Rptor<sub>ob</sub><sup>-/-</sup>* mice may simply reflect this reduction. A full assessment of the skeletal phenotype of HFD-fed *Rptor<sub>ob</sub><sup>-/-</sup>* mice, using high-resolution micro Computed Tomography, would provide valuable insight into this question.

### **3.5.2 Osteoblast glucose uptake and utilisation**

Several lines of evidence point to the potentiation of insulin signalling as being an important mechanism in the metabolic phenotype of *Rptor<sub>ob</sub><sup>-/-</sup>* mice. Firstly, using bones isolated from HFD-fed mice, RNAseq and GSEA identified an increase in genes encoding proteins involved in glycolysis and carbohydrate metabolism. This gene expression pattern was also observed in the long bones of normal chow-fed *Rptor<sub>ob</sub><sup>-/-</sup>* mice (Supplementary Fig. 2.5B) and *Rptor* KO calvarial cells *in vitro*. Secondly, basal

and insulin-stimulated levels of AKT and AS160 (AKT-dependent phosphorylation of AS160 at Thr<sup>642</sup> is essential for GLUT4 translocation to the plasma membrane) were observed in calvarial cells of HFD-fed *Rptor<sub>ob</sub><sup>-/-</sup>* mice *in vivo*. Hyper-phosphorylation of AKT at Ser<sup>473</sup> and Thr<sup>308</sup> was also observed *in vitro* in *Rptor* KO OBs, in both basal and insulin-stimulated states. Thirdly, glucose uptake was significantly increased in *Rptor* KO cells *in vitro* in both basal and insulin-stimulated states, suggesting that constitutive activation of AKT leads to an increase in glucose transport in the absence of mTORC1 activity. Several studies have now recognised bone as a significant site of glucose uptake whereby at steady state, the skeleton accounts for almost 15% of glucose uptake from the circulation and the magnitude of glucose uptake by bone cells is sufficient to impact systemic glucose disposal in mice<sup>61,63,72</sup>. The higher basal phosphorylation levels of AKT and AS160 *in vivo* suggests that an increase in basal skeletal uptake of glucose could explain their low glycaemic phenotype.

### ***3.5.3 Whole-body metabolic flexibility***

In recent years, the effects of mTORC1 perturbation have been examined in a number of different metabolic tissues including WAT, skeletal muscle and liver, with each revealing a distinctive role for mTORC1 signalling in the tissue itself and in global metabolism as a whole. For example, hepatic knockdown of S6K1/2 in mice fed with HFD leads to improved systemic insulin sensitivity and glucose tolerance, and protection against hepatic steatosis<sup>73</sup>. In contrast, whilst deletion of raptor in WAT also protects against diet-induced obesity (via increased energy expenditure), these mice suffer from severe hepatic steatosis<sup>74,75</sup>. Similarly, inactivation of mTORC1 in the muscle causes resistance to HFD-induced metabolic dysfunction and improved glucose tolerance, but has no effect on insulin sensitivity<sup>76</sup>. Furthermore, systemic inhibition of mTORC1 signalling by deletion of S6K1<sup>17</sup> or rapamycin administration<sup>77</sup> results in mice that are resistant to weight gain due to elevated lipolysis and metabolic rate. Interestingly, despite the reported mechanistic differences in each of these models, one phenotype that is shared amongst these systemic and tissue-specific mTORC1 KO models is that they are resistant to HFD-induced weight gain. In this study, suppression of mTORC1 in OBs was also met with a resistance to HFD-induced weight gain, consistent with previous mTORC1 KO models.

Based on the data generated herein, the mechanisms underlying the obesity-resistance phenotype of *Rptor<sub>ob</sub><sup>-/-</sup>* mice likely include (i) their ability to switch substrate oxidation

during the light and dark period, and (ii) their ability to increase browning of iWAT via upregulation of *Ucp1* expression. The mechanism(s) underlying the browning of iWAT in *Rptor<sub>ob</sub><sup>-/-</sup>* mice remains unclear and appears to be independent of previously reported browning agents including FGF21 and irisin, as no changes in the expression levels of these factors were observed in tissues which contribute most to the serum levels of these factors (i.e. liver<sup>47</sup> and muscle<sup>46</sup>, respectively). It is interesting to note that upregulation of two bone-secreted factors, BMP7 and sclerostin<sup>48,49</sup> was observed in *Rptor<sub>ob</sub><sup>-/-</sup>* mice using RNA-seq. However, immunoblotting analysis of signalling pathways that are modulated in response to these factors (STAT1/3 for BMP7 and Wnt/ $\beta$ -catenin for sclerostin) in iWAT failed to detect any changes. With respect to sclerostin, the increase in *Sost* gene expression correlated with an increase in sclerostin protein levels in the long bones of *Rptor<sub>ob</sub><sup>-/-</sup>* mice, suggesting that mTORC1 plays a role in the regulation of *Sost*. Indeed, a recent study has shown that mTORC1 negatively regulates SOST in osteocytes via activation of SIRT1, a negative regulator of *Sost* gene expression<sup>78</sup> linking mTORC1 function in OBs/osteocytes with maintaining systemic energy balance.

While overfeeding promotes weight gain through fat storage shifting the 24-h RQ value above the FQ value (i.e. positive energy balance), underfeeding results in weight loss through lipid oxidation and a shift in 24-h RQ value below the FQ value (i.e. negative energy balance)<sup>37</sup>. In animals with balanced intake and expenditure, fat mass is constant and the 24-h RQ and FQ values are equal<sup>79</sup>. The energy intake in *Rptor<sub>ob</sub><sup>-/-</sup>* mice, which accounts for their smaller body size, suggests that they are slightly hyperphagic. However, they appear to offset their energy intake and maintain constant body weight through greater substrate flexibility; their excess energy is efficiently stored during the dark period (RQ>FQ), and stored fat readily oxidized during the light period (RQ<FQ). Conversely, the 24-h RQ>FQ in *Rptor<sub>ob</sub><sup>+/-</sup>* mice suggests that they are in positive energy balance and thus even with their greater substrate flexibility, overfeeding and energy storage during the dark cycle surpasses fat oxidation during the light cycle and thus results in continued weight gain. Even though the control animals appear to be in an energy balanced state, they have lost the ability to switch substrate between fat and carbohydrate oxidation. In other words, maximal HFD-induced fat oxidation during the light period (where animals are less active) is reduced and predictably, they continue to gain significant fat.

Of note, while metabolic flexibility is typically defined as an increase in RQ between fasting and postprandial states, the fact that *Rptor<sub>ob</sub><sup>-/-</sup>* mice exhibit greater plasticity in switching between fatty acid and carbohydrate oxidation during light and dark periods under *ad libitum* feeding suggests that they are capable of maintaining metabolic flexibility. Consistent with this, clinical studies in humans have reported lower fat oxidation and higher RQ in the subjects with family history of diabetes<sup>80</sup> and in particular, a lesser decrease in RQ during the sleeping period in these subjects<sup>81</sup>. Furthermore, impairment in metabolic flexibility has been associated with metabolic syndromes including obesity, insulin resistance and diabetes (reviewed in <sup>82</sup>). These results, combined with the impaired glucose metabolism observed in the control mice, indicate a correlation between metabolic inflexibility and abnormality in glucose homeostasis. As such, the flexibility in substrate switching in *Rptor<sub>ob</sub><sup>-/-</sup>* mice could produce the systemic metabolic protection phenotype observed in these mice.

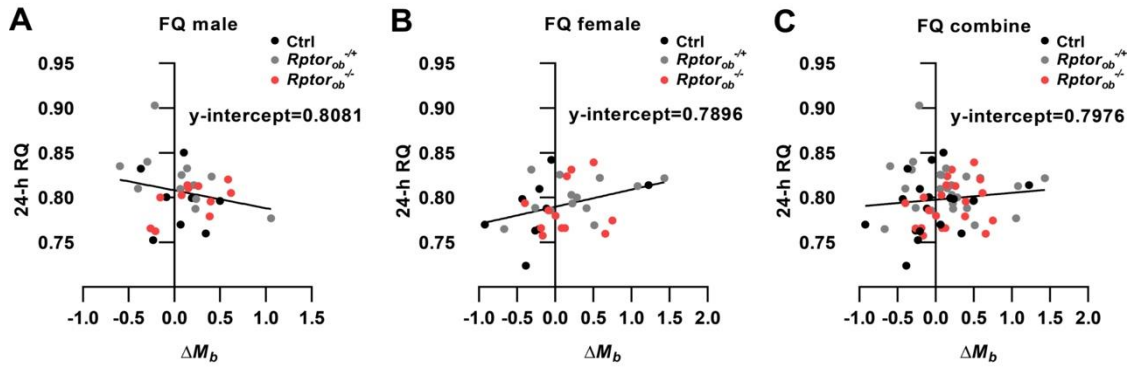
In summary, inactivation of bone-specific mTORC1 in mice protects against diet-induced obesity and insulin resistance. These phenotypes are associated with locally enhanced responsiveness to insulin and skeletal insulin-dependent glucose uptake, and a systemic increase in substrate flexibility and browning of white fat. These studies highlight the beneficial systemic consequences of reducing mTORC1 function in OBs under nutrient excess revealing skeletal mTORC1 as a potential target for anti-obesity and diabetes drugs.

### **3.6 Acknowledgements**

The authors gratefully acknowledge Mrs Vicki Wilczek for assisting with mouse genotyping. This work was supported by grants from the National Health and Medical Research Council of Australia (APP1109207, awarded to ACWZ, PMB and CGP) and ARC (DP160100454, awarded to ACWZ and PMB) and an Australia Postgraduate Award (PT).

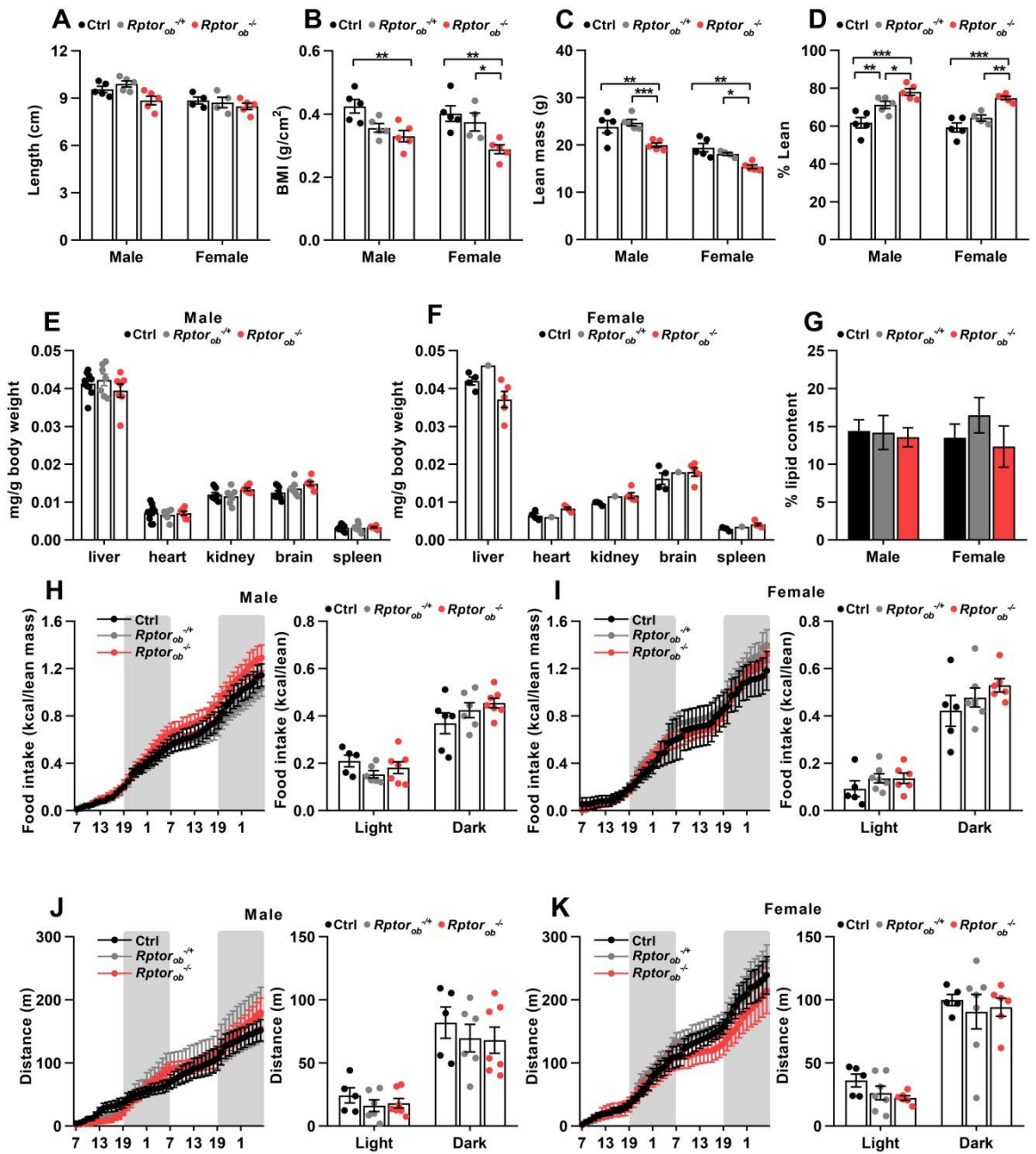
## 3.7 Supplementary data

### 3.7.1 Supplementary Figures

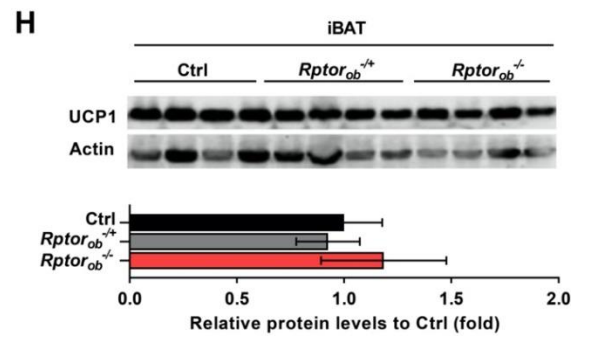
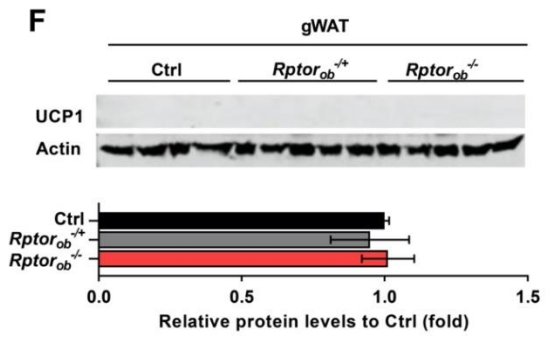
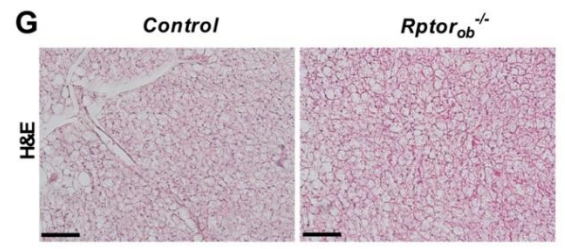
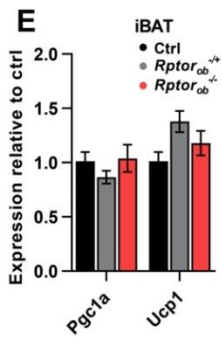
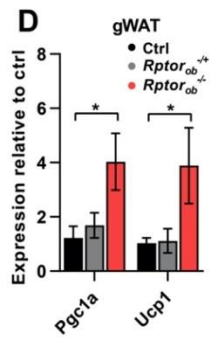
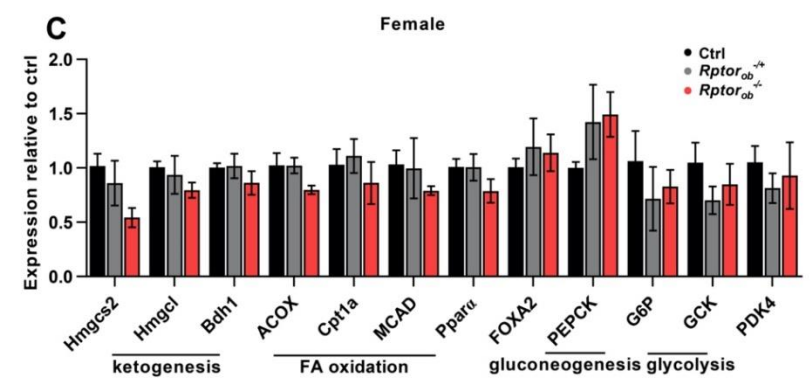
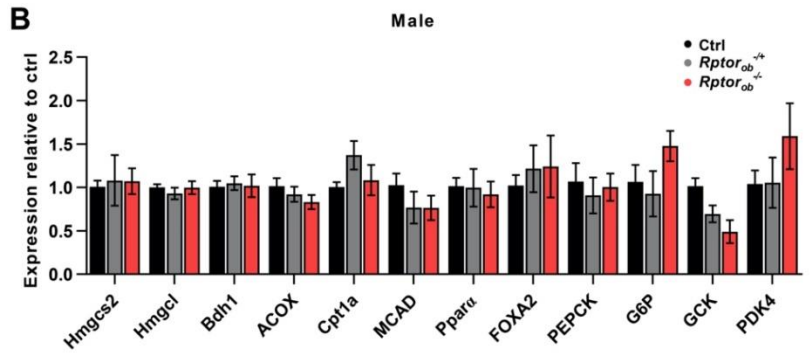
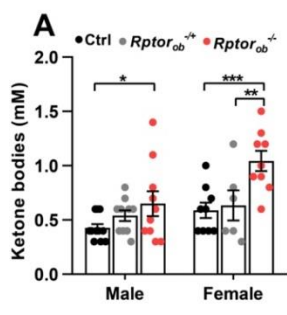


#### Supplementary Fig. 3.1 Alternative food quotient (theoretical FQ) calculation.

Linear regression analysis of change in body mass during the 48-h measurement period ( $\Delta M_b$ : x-axis) and 24-hour RQ (y-axis) were used to estimate alternative FQ whereby the y-intercepts were the 24-h RQ when  $\Delta M_b$  equalled zero or theoretical FQ in (A) male, (B) female and (C) combined sexes (n=5-7/genotype for each sex).

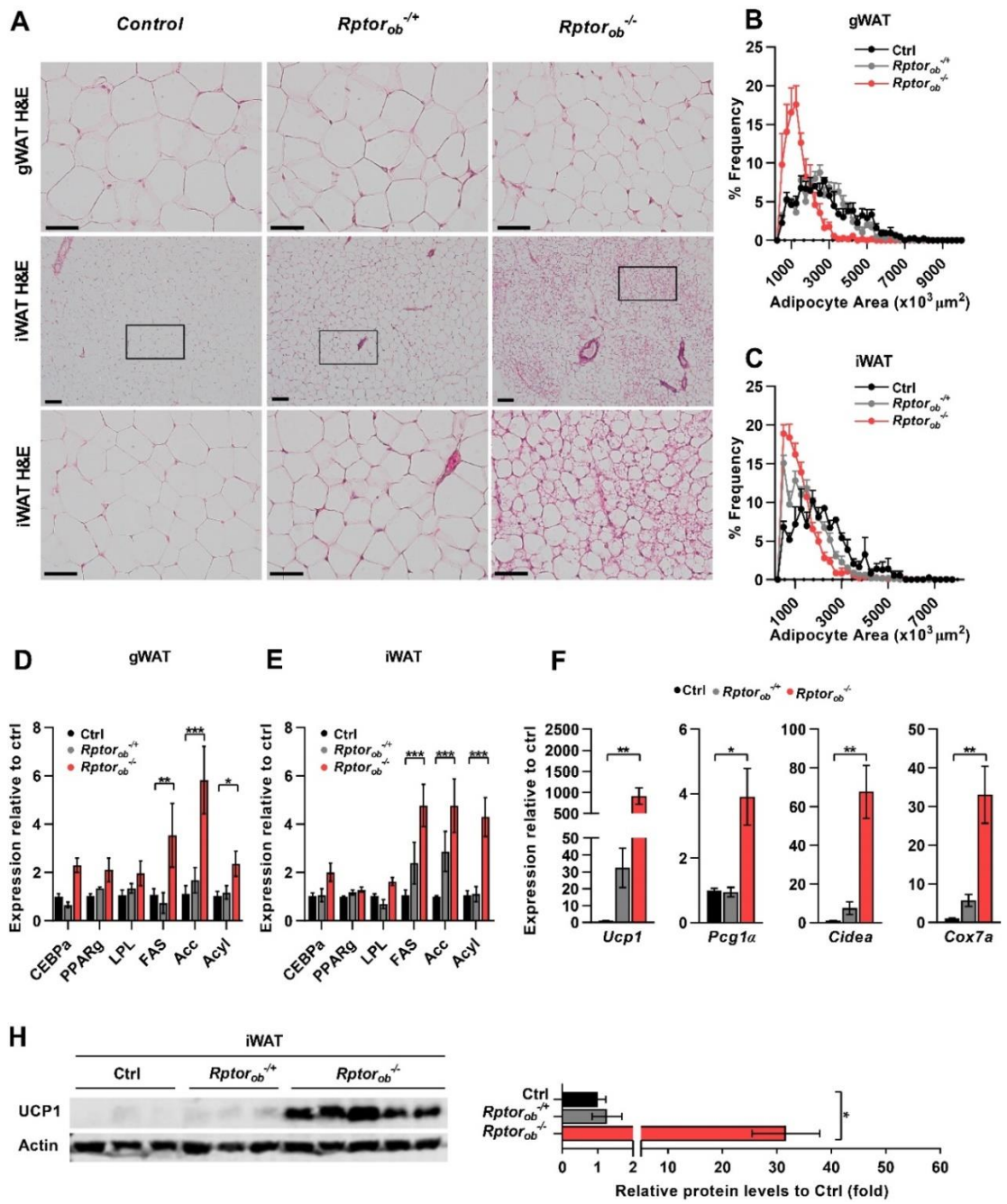


**Supplementary Fig. 3.2 Daily food intake, physical activities and % of fecal lipid are normal in HFD-fed *Rptor<sup>ob</sup><sup>-/-</sup>* mice.** (A) Body length of 18-week old mice, as measured from nose to anus (n=4-5/genotype). (D) Body mass index (BMI) (n=4-5/genotype). (B-D) DXA analysis of total lean mass and % lean mass in male and female HFD-fed mice (n=4-5/genotype). (E-F) Lean organ weights, normalised to total body weight, in 18-week-old HFD-fed male and female mice (n=4-9/genotype). (G) %lipid content of 1g faeces collected from male and female HFD-fed mice (n=9-10/genotype). (E-F) Food intake normalised to lean mass (kcal/g lean mass), measured over a 48-h period (*left*) and per 12-h light/dark cycle (*right*) in HFD-fed male and female mice (n=5-7/genotype). (H-I) Total activity (distance of movement) measured over a 48-h period (*left*) and per 12-h light/dark cycle (*right*) in HFD-fed male and female mice (n=5-7/genotype). All panels: data are expressed as mean  $\pm$  SEM. \*p<0.05, two-way ANOVA with Tukey's post-hoc test. Panels E-H: shaded regions represent dark cycle.



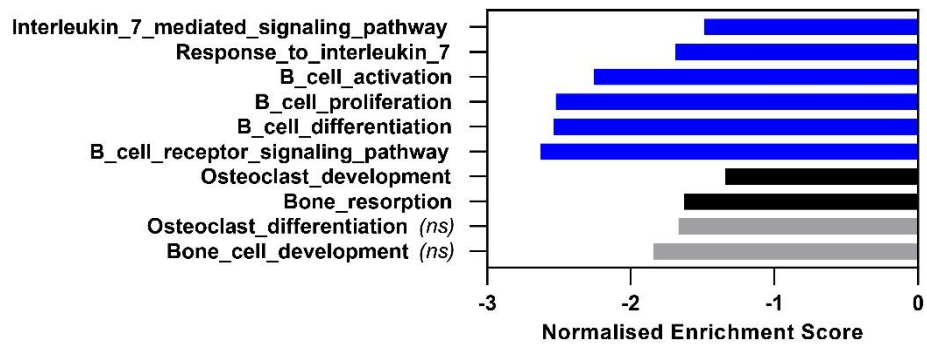


**Supplementary Fig. 3.3 Serum ketone bodies, hepatic gene expression and UCP1 gene expression and UCP1 protein levels in other fat depots of HFD-fed *Rptor<sup>ob</sup><sup>-/-</sup>* mice.** (A) Serum ketone bodies levels in HFD-fed mice at 18 weeks of age (n=5-10/genotype). (B-C) Gene expression levels of ketogenesis, fatty acid oxidation, gluconeogenesis and glycolysis genes in HFD-fed male (B) and female (C) liver tissue samples, normalised to  $\beta$ -actin (n=3-5/genotype). (D-E) Gene expression levels of brown adipose tissue markers in HFD-fed male gWAT and interscapular BAT (iBAT) samples, normalised to  $\beta$ -actin (n=3-5/genotype). (F) Levels of UCP1 protein expression in HFD-fed male gWAT (*top*) and quantitative analysis of protein levels relative to  $\beta$ -actin (*bottom*) (n=4/genotype). (G) Representative images of H&E of iBAT from male mice, scale bar = 100 $\mu$ m. (H) Levels of UCP1 protein expression in HFD-fed male gWAT (*top*) and quantitative analysis of protein levels relative to  $\beta$ -actin (*bottom*) (n=4/genotype). All panels except G: data are expressed as mean  $\pm$  SEM. \*p<0.05, \*\*p<0.01, \*\*\*p<0.001, one-way ANOVA with Tukey's post-hoc test.



**Supplementary Fig. 3.4 Adipocyte hypotrophy and browning of iWAT are also observed in HFD-fed female *Rptor<sup>ob</sup><sup>-/-</sup>* mice.**

(A) Representative images of H&E section of gWAT and iWAT from HFD-fed female mice. Boxes in middle panels indicate the area depicted in the corresponding bottom panels. Scale bars: top and bottom panels = 50 $\mu$ m; middle panels = 100 $\mu$ m. (B-C) Size distribution of gWAT (B) and iWAT (C) adipocytes from HFD-fed female mice was calculated using H&E stained sections using Image J (n=5 sections/mouse, n=5-6/genotype). (D-E) Gene expression levels of adipogenesis and *de novo* lipogenesis markers in HFD-fed male gWAT and iWAT tissues, normalised to  $\beta$ -actin (n=3-5/genotype). (F) Brown adipose tissue markers gene expression in iWAT (n=3-5/genotype). (G) Levels of UCP1 protein in iWAT and quantitative analysis assessed by Western blot analysis female mice (n=3-5/genotype). All panels except A: data are expressed as mean  $\pm$  SEM. \*p<0.05, \*\*p<0.01, \*\*\*p<0.001, one-way ANOVA with Tukey's post-hoc test.



**Supplementary Fig. 3.5 Down regulation of pathways involved in B-cell developments in *Rptor<sup>ob</sup><sup>-/-</sup>* mice.** Gene set enrichment analysis (GSEA) of negatively enriched pathways (down-regulated) of RNA isolated from combined flushed femur and tibia (n=5; only controls and *Rptor<sup>ob</sup><sup>-/-</sup>*). Blue bar indicates pathways relating to B-cell development and/or interleukin 7 signalling and black bar indicates pathways relating to bone development. Grey bar (*ns*) = not significant.

### 3.7.2 Supplementary Table

**Supplementary Table 3.1** High fat diet details and composition



**Specialty Feeds**

3150 Great Eastern Hwy  
Glen Forrest  
Western Australia 6071  
p: +61 8 9298 8111  
F: +61 8 9298 8700  
Email: [info@specialtyfeeds.com](mailto:info@specialtyfeeds.com)

**Diet**  
**SF16-096 SF03-020 with increased vitamins for irradiation**




A semi-pure diet formulation for laboratory rats and mice based on AIN-93G.

- The fat content has been increased to 23%, sucrose content has been increased to improve pellet strength and starch content has been reduced.
- Cholesterol has been added at 0.19%.
- Vitamin inclusion has been increased to account for some losses that may occur during the irradiation process.

Calculated Nutritional Parameters as Fed		Ingredients	
Protein	19.70%	Casein (Acid)	200 g/Kg
Total Fat	23.00%	Sucrose	418 g/Kg
Crude Fibre	4.70%	Canola Oil	50 g/Kg
AD Fibre	4.70%	Cocoa Butter	50 g/Kg
Digestible Energy	19.7 MJ / Kg	Hydrogenated Vegetable Oil (Copha)	131 g/Kg
% Total calculated digestible energy from lipids	43.40%	Cellulose	50 g/Kg
% Total calculated digestible energy from protein	17.30%	Pregelged Wheat Starch	50 g/Kg
		L Methionine	3.0 g/Kg
		Calcium Carbonate	13.1 g/Kg
		Sodium Chloride	2.6 g/Kg
		AIN93 Trace Minerals	1.4 g/Kg
		Potassium Citrate	2.5 g/Kg
		Potassium Dihydrogen Phosphate	6.9 g/Kg
		Potassium Sulphate	1.6 g/Kg
		Choline Chloride (75%)	2.5 g/Kg
		AIN93 Vitamins	15 g/Kg
		Vitamin K 0.23%	0.87g / Kg
		Cholesterol USP	1.9 g/Kg

**Diet Form and Features**

- Semi pure diet. 12 mm diameter pellets.
- Pack size 1.5 Kg, vacuum packed in oxygen- impermeable plastic bags, under nitrogen. Bags are packed into cardboard cartons to protect them during transit. Smaller pack quantity on request.
- Diet suitable for irradiation but not suitable for autoclave. Note, Irradiation can soften pellets.
- Lead time 2 weeks for non-irradiation or 4 weeks for irradiation.

VS SF16-096 Page 1 of 2 21/09/16

Calculated Amino Acids as Fed		Calculated Total Vitamins as Fed				
Valine	1.25%	Vitamin A (Retinol)	6 000 IU/Kg			
Leucine	1.71%	Vitamin D (Cholecalciferol)	1 500 IU/Kg			
Isoleucine	0.94%	Vitamin E (a Tocopherol acetate)	116 mg/Kg			
Threonine	0.79%	Vitamin K (Menadione)	3.5 mg/Kg			
Methionine	0.83%	Vitamin C (Ascorbic acid)	None added			
Cysteine	0.08%	Vitamin B1 (Thiamine)	9.1 mg/Kg			
Lysine	1.42%	Vitamin B2 (Riboflavin)	9.3 mg/Kg			
Phenylalanine	0.93%	Niacin (Nicotinic acid)	45 mg/Kg			
Tyrosine	0.99%	Vitamin B6 (Pryridoxine)	10.7 mg/Kg			
Tryptophan	0.17%	Pantothenic Acid	24.5 mg/Kg			
Histidine	0.52%	Biotin	300 ug/Kg			
<th>Calculated Total Minerals as Fed</th> <td>Folic Acid</td> <td>3 mg/Kg</td>		Calculated Total Minerals as Fed	Folic Acid	3 mg/Kg		
		Inositol	None added			
		Calcium	0.69%	Vitamin B12 (Cyancobalamin)	153 ug/Kg	
		Phosphorous	0.32%	Choline	1 980 mg/Kg	
		Magnesium	0.05%	<th>Calculated Fatty Acid Composition</th>		Calculated Fatty Acid Composition
		Sodium	0.12%	Saturated fats C12 or Less	7.65%	
		Chloride	0.16%	Myristic Acid 14:0	2.37%	
		Potassium	0.39%	Palmitic Acid 16:0	2.75%	
		Sulphur	0.22%	Stearic Acid 18:0	3.51%	
		Iron	48 mg/Kg	Oleic Acid 18:1	4.45%	
		Copper	7.2 mg/Kg	Gadoleic Acid 20:1	0.06%	
		Iodine	0.2 mg/Kg	Linoleic Acid 18:2 n6	1.31%	
Manganese	16 mg/Kg	a Linolenic Acid 18:3 n3	0.71%			
Cobalt	No data	EPA 20:5 n3	No data			
Zinc	52 mg/Kg	DHA 22:6 n3	No data			
Molybdenum	0.15 mg/Kg	Total n3	0.71%			
Selenium	0.3 mg/Kg	Total n6	1.31%			
Cadmium	No data	Total Saturated Fats	16.50%			
Chromium	1.0 mg/Kg	Total Monosaturated Fats	4.54%			
Fluoride	1.0 mg/Kg	Total Polyunsaturated Fat	2.03%			
Lithium	0.1 mg/Kg	Cholesterol	0.19%			
Boron	2.1 mg/Kg					
Nickel	0.5 mg/Kg					
Vanadium	0.1 mg/Kg					

Calculated data uses information from typical raw material composition. It could be expected that individual batches of diet will vary from this figure. **Diet post treatment by irradiation or autoclave could change these parameters.** We are happy to provide full calculated nutritional information for all of our products, however we would like to emphasise that these diets have been specifically designed for manufacture by Specialty Feeds.

**Supplementary Table 3.2 Antibodies used for immunoblotting**

<b>Antibody</b>	<b>Species</b>	<b>Dilution</b>	<b>Company and Catalogue #</b>
ACTIN	Mouse	1:1000	A5441
ADIPONECTIN	Rabbit	1:1000	A6354
AKT	Rabbit	1:1000	CST4691S
INSR	Rabbit	1:1000	CST3025
Phospho-AKT (Ser473)	Mouse	1:1000	CST4060
Phospho-AS160 (Thr642)	Rabbit	1:1000	CST4288
Phospho-GSK3 $\beta$ (Ser9)	Rabbit	1:1000	CST9336
Phospho-INSR (Tyr1150/1151)	Rabbit	1:1000	CST3024
Phospho-rpS6 (Ser240/244)	Rabbit	1:1000	CST2215S
rpS6	Mouse	1:1000	CST2317
UCP1	Rabbit	1:5000	ab209483

**Supplementary Table 3.3. Oligonucleotides used for Real-time PCR (qRT-PCR)**

Gene	Accession	Forward (5' – 3')	Reverse (5' – 3')	Size (bp)
<i>Acaca</i>	NM_133360.2	ATGCATCTATCCGTCGGTG	CCAGCCCACACTGCTTGT	224
<i>Acadl</i>	NM_007381.4	CCGCCGATGTTCATCTCT	CCCATTCTGTGTGGTGAGGA	168
<i>Acadm</i>	NM_007382.5	TTCCGAAGACGTAGAGTGGC	CTGGACTGTAGGTCTGGTT	103
<i>Acads</i>	NM_007383.3	TAGCCATGCAAAACCTTGGAC	TTGCGGTCTCGGCATACTT	106
<i>Acadvl</i>	NM_017366.3	ACAGGAATCGGCAGTGGTTT	ACTGCTCGTGGACAATCCCT	151
<i>Acox</i>	NM_015729.3	CATGTGGTTTAAAACTCTGTGC	GGCATGAAGAAACGCTCCTG	123
<i>Achy</i>	NM_001199296.1	TTCTCTTAATGCCAGCGG	GACTTGGGACTGAACTTGGGG	136
<i>Actin</i>	NM_007393.5	TTGCTGACACGATGCAGGA	AAGGGTGAAAACGCAGCTC	236
<i>Adipoq</i>	NM_009605.4	GATGCAGGTCTCTTGGTCCTA	AGCGAATGGGTACATGGGA	187
<i>Aigl</i>	NM_025802.3	CAACGCCACTCACATCTACGG	TCACCAGGTGAAAGAGGGAT	161
<i>Axin2</i>	NM_015732.4	TAAACAGCCCAAGAACCGGGA	CAGCAATCGGCTTGGTCTCT	164
<i>Bdh1</i>	NM_175177.4	AGACACATCAAGCCCGGAGA	TTCTGGTGGCTCTTAGCCAGTG	159
<i>Bglap</i>	NM_001032298.3	AAGCGAGAGGGCAATAAGGI	TCAAGCCATCTGGTCTGATAGC	142
<i>Bmp7</i>	NM_007557.3	CAGCCAGAATCGCTCCAAGA	TGCAATGATCCAGCTCCTCC	154
<i>Btre</i>	NM_001037758.2	GCTCCCTTCTCGGACATAC	AACATTAAACGAGTCTTGGGCA	83
<i>Cebpa</i>	NM_007678.3	CAAAGCCAAAGAAGTCGGTGGACAA	TCATTGACTGGTCAACTCCAGC	150
<i>Cidea</i>	NM_007702.2	CAGTTCCTGGTCTATGCGGG	AACCAGCCTTGGTGTCTAGG	92
<i>Col1a</i>	NM_007742.4	GCTCTCTTAGGGCCACT	CCACGTCTACCATTGGGG	103
<i>Cox7a</i>	NM_009944.3	AGACTGACCATGACCTGAC	GTGTCACTTCTTGGGGGAA	87
<i>Cpt1a</i>	NM_013495.2	GGACTCCGCTCGCTCATT	AGGCAGATCTGTTTGGGGC	153
<i>Cpt1b</i>	NM_009948.2	CATGTATCGCCGAAACTGG	CCTGGGATCGGTGTAGTGT	114
<i>Ctsk</i>	NM_007802.4	GCCACGCTTCCATCCGAAA	CGAGAGATTTCATCCACCTTGC	188
<i>Cyp11a</i>	NM_019779.4	CCTTCTGAGCCCTACGTG	GCCCAGTCTTCCCTGTAAA	222
<i>Cyp17</i>	NM_007809.3	CAATGACCCGACTCACCTCC	TATCGTGAATGACAGTCCAG	176
<i>Cyp19</i>	NM_007810.4	TTTCGCTGAGAGACGTGGAG	AGGATTGCTGCTTCGACCTC	150
<i>Erol</i>	NM_015774.3	TTCGCGAGGTAGTGGTACC	GTCTGACGGCACAGTCTTCT	202
<i>Erfp44</i>	NM_029572.3	GACCCGCTGTTACCATGAA	TGAAAACGACACCAGTACGA	196
<i>Fasn</i>	NM_007988.3	TGGGTGTGGAAGTCTGTCAG	CTGTCTGTGTCAGTACCCGAG	132
<i>Fgf21</i>	NM_020013.4	CCTCCAGTTTGGGGTCAAG	ACCAGTGTCCATCCCTCCT	99
<i>Foxa2</i>	NM_001291065.1	CATTCGGCTTCCAGTATGC	GTTCATGCCATTCAATCCCAG	138
<i>G6p</i>	NM_008061.4	TGAGACCGGACCAGGAAGTC	GCAAGGTAGATCCGGGACAG	195
<i>Gapgh</i>	NM_001289726.1	TGACACCACAACTGCTTAG	GGATGCAGGGATGATGTT	177
<i>Gck</i>	NM_010292.5	CTGTTAGCAGGATGGCAGCTT	TTTCTTGGAGAGATGCTGTGG	82
<i>Glut1</i>	NM_011400.3	GCTACGGGTCTTAAAGTGGC	CCTCCACAGCCAAACATGAG	169
<i>Glut4</i>	NM_009204.2	GGCTCTGACGATGGGGAAC	GCCACGTTGCAATGTAGCTC	157
<i>Gpre6a</i>	NM_153071.1	GGCATTATACTGAGCCGGGAC	GGCAAGTACTGCCATGGCT	134
<i>Hadha</i>	NM_178878.3	GTAGCACAGCACGTAGCAGA	CCCAGACTTGGCACCIAAGA	117
<i>Hh2</i>	NM_013820.3	TGATCGCTGCTTATTCACGG	AACCGCTAGAAATCTCCAGA	112
<i>Hmgcl</i>	NM_008254.3	AGATGGCGTCAAGTGGGAAAG	CTGGGGTGGGTACAATACTTCT	165
<i>Hmgcs2</i>	NM_008256.4	TACTGGGATGGTGCATGTC	ACCGGTTCTCCATGTGAGTT	166
<i>Hsd17</i>	NM_008292.4	AGCCACGTCAGGATTCGTTG	TGAATGACAGCCCAAGGAACC	242
<i>Hsd3β1</i>	NM_008293.4	CTTGAAGCTGCCCTGATCT	CTTATTCCTGTGACAGAGCC	120
<i>Hsl</i>	NM_010719.5	CTGCCAGGATGGATGGTTT	GAACGCTGAGGCTTTGATCTTG	233
<i>Irisin</i>	NM_027402.4	CACGCGAGGC1GAAAGATG	CAIAC1GGCGGCAGAAGAGA	156
<i>Idha</i>	NM_010699.2	TGTCTCCAGCAAAAGCTACTGT	GACTGTACTTGACAATGTTGGGA	155
<i>Leptin</i>	NM_008493.3	CAAGCAGTGCCTATCCAGA	AAGCCAGGAATGAAGTCCA	141
<i>Lgr5</i>	NM_010195.2	TCTCTACATCGCCTCTGCT	ATCTAGGCGCAGGGATTGAAG	187
<i>Lpl</i>	NM_008509.2	GGACGTTAAACGGGAATGTATG	ACGTTGTCTAGGGGTACTTAAA	214
<i>Nfj1</i>	NM_001164226.1	ATCTGGCTGCTGCAGGTCC	CACCTCGGCTGTGACTACTC	170
<i>Opg</i>	NM_008764.3	TCATCCAAGACATGACCTCTGT	TCCGTCGATTTGACAGGTCTT	160
<i>Pcg-1α</i>	NM_008904.2	TGTGTGCTGTGTGTCAGAGT	ACCAGAGCAGCACACTCTATG	126
<i>Pdk1</i>	NM_172665.5	CCCAGATTCAGGTTACAG	CCCGGTCACTCATCTTACA	63
<i>Pdk4</i>	NM_013743.2	GATTGACATCCTGCCTGACC	CATGGAACCTCCACCAATCC	98
<i>Pepck</i>	NM_011044.3	ATCATCTTTGGTGGCCGTAG	TGATGATCTTGGCTTGTGT	136
<i>Pfkm1</i>	NM_001163487.1	GGTTTCCCTGTACTCCATGC	TTCAATCATGTTGGTGCAGAT	251
<i>Pgkl</i>	NM_008828.3	TTTGGACAAGCTGGACGTGA	AGCAGCCTTGATCCTTTGGTT	106
<i>Plin1</i>	NM_175640.2	GGCC1GGACGACAAAACC	CAGGATGGGC1CCA1GAC	120
<i>Pparaα</i>	NM_011144.6	GCAGTGCCTGAACATCGA	CGCCGAAAAGAACCCCTTAC	100
<i>Pparγ</i>	NM_001127330.2	TTTTCGGAAAGAACCATCCGAT	ATGGCATTTGTGAGACATCCCG	139
<i>Smurf1</i>	NM_001038627.1	TGAGGAGAGGAGAGCCAGAC	CGCCTGTAGAGCCTTGACA	92
<i>Sirt1</i>	NM_019812.3	GGCCGCGGATAGGTCCA	AACAATCTGCCACAGCGTCA	137
<i>Sost</i>	NM_024449.6	GCCTCATCTGCCTACTTGTG	CGGACACATCTTTGGCGT	201
<i>Sp7</i>	NM_130458.4	ATGGCGTCTCTCTGCTTGT	GTCCATTGGTGTCTTGGAGAAGG	211
<i>Sparc</i>	NM_009242.5	GATGGGTACTGTCCAGAC	AGCAGGAGGCGTGAACCTAG	199
<i>Srebf1</i>	NM_001313979.1	GTGGGCTAGTCCGAAGC	GAGCATGCTCTCGATGCTGTT	135
<i>StAR</i>	NM_011485.5	TCGCTACGTTCAAGCTGTGT	GCTTCCAGTTGAGAACCAAGC	184
<i>Tcirg</i>	NM_016921.3	CACAGGGTCTGTCTACAACCTG	CGTCTACCAGAAAGCGTCTC	110
<i>Ucp1</i>	NM_009463.3	TGGTGAACCCGACAACCTCC	GGCCTTCACTTGGATCTGAA	141
<i>Ucp2</i>	NM_011671.5	TGCGGTCCGGACACAATAGTA	CTCGTCTTCAAAGTGGCCG	111



### 3.8 References

1. Roberts CK, Hevener AL, Barnard RJ. Metabolic syndrome and insulin resistance: underlying causes and modification by exercise training. *Compr Physiol* **3**, 1-58 (2013).
2. Keller KB, Lemberg L. Obesity and the metabolic syndrome. *Am J Crit Care* **12**, 167-170 (2003).
3. Ma X. M. BJ. Molecular mechanisms of mTOR-mediated translational control. *Cell Mol Biol* **10**, 307-318 (2009).
4. Zhang J, Gao Z, Yin J, Quon MJ, Ye J. S6K directly phosphorylates IRS-1 on Ser-270 to promote insulin resistance in response to TNF-(alpha) signaling through IKK2. *J Biol Chem* **283**, 35375-35382 (2008).
5. Shah OJ, Hunter T. Turnover of the active fraction of IRS1 involves raptor-mTOR- and S6K1-dependent serine phosphorylation in cell culture models of tuberous sclerosis. *Mol Cell Biol* **26**, 6425-6434 (2006).
6. Tremblay F, *et al.* Identification of IRS-1 Ser-1101 as a target of S6K1 in nutrient- and obesity-induced insulin resistance. *Proc Natl Acad Sci U S A* **104**, 14056-14061 (2007).
7. Hsu PP, *et al.* The mTOR-regulated phosphoproteome reveals a mechanism of mTORC1-mediated inhibition of growth factor signaling. *Science* **332**, 1317-1322 (2011).
8. Yu Y, *et al.* Phosphoproteomic Analysis Identifies Grb10 as an mTORC1 Substrate That Negatively Regulates Insulin Signaling. *Science* **332**, 1322-1326 (2011).
9. Tzatsos A, Kandror KV. Nutrients suppress phosphatidylinositol 3-kinase/Akt signaling via raptor-dependent mTOR-mediated insulin receptor substrate 1 phosphorylation. *Mol Cell Biol* **26**, 63-76 (2006).
10. Ali M, Bukhari SA, Ali M, Lee H-W. Upstream signalling of mTORC1 and its hyperactivation in type 2 diabetes (T2D). *BMB reports* **50**, 601-609 (2017).
11. Sancak Y, *et al.* The Rag GTPases bind raptor and mediate amino acid signaling to mTORC1. *Science* **320**, 1496-1501 (2008).
12. Kim J, Kundu M, Viollet B, Guan KL. AMPK and mTOR regulate autophagy through direct phosphorylation of Ulk1. *Nat Cell Biol* **13**, 132-141 (2011).
13. Gwinn DM, *et al.* AMPK phosphorylation of raptor mediates a metabolic checkpoint. *Mol Cell* **30**, 214-226 (2008).
14. Gual P, Le Marchand-Brustel Y, Tanti JF. Positive and negative regulation of insulin signaling through IRS-1 phosphorylation. *Biochimie* **87**, 99-109 (2005).
15. Tanti JF, Jager J. Cellular mechanisms of insulin resistance: role of stress-regulated serine kinases and insulin receptor substrates (IRS) serine phosphorylation. *Curr Opin Pharmacol* **9**, 753-762 (2009).
16. Newgard CB, *et al.* A branched-chain amino acid-related metabolic signature that differentiates obese and lean humans and contributes to insulin resistance. *Cell Metab* **9**, 311-326 (2009).
17. Um SH, *et al.* Absence of S6K1 protects against age- and diet-induced obesity while enhancing insulin sensitivity. *Nature* **431**, 200-205 (2004).

18. Shum M, Bellmann K, St-Pierre P, Marette A. Pharmacological inhibition of S6K1 increases glucose metabolism and Akt signalling in vitro and in diet-induced obese mice. *Diabetologia* **59**, 592-603 (2016).
19. Le Bacquer O, *et al.* Elevated sensitivity to diet-induced obesity and insulin resistance in mice lacking 4E-BP1 and 4E-BP2. *J Clin Invest* **117**, 387-396 (2007).
20. Ferron M, *et al.* Insulin signaling in osteoblasts integrates bone remodeling and energy metabolism. *Cell* **142**, 296-308 (2010).
21. Fulzele K, *et al.* Insulin receptor signaling in osteoblasts regulates postnatal bone acquisition and body composition. *Cell* **142**, 309-319 (2010).
22. Wei J, *et al.* Bone-specific insulin resistance disrupts whole-body glucose homeostasis via decreased osteocalcin activation. *The Journal of Clinical Investigation* **124**, 1781-1793 (2014).
23. Livesey G, Elia M. Estimation of energy expenditure, net carbohydrate utilization, and net fat oxidation and synthesis by indirect calorimetry: evaluation of errors with special reference to the detailed composition of fuels. *The American Journal of Clinical Nutrition* **47**, 608-628 (1988).
24. Longo KA, *et al.* The 24-hour respiratory quotient predicts energy intake and changes in body mass. *American Journal of Physiology-Regulatory, Integrative and Comparative Physiology* **298**, R747-R754 (2010).
25. Mehlem A, Hagberg CE, Muhl L, Eriksson U, Falkevall A. Imaging of neutral lipids by oil red O for analyzing the metabolic status in health and disease. *Nature Protocols* **8**, 1149 (2013).
26. Ward CM, Thu-Hien T, Pederson SM. ngsReports: A Bioconductor package for managing FastQC reports and other NGS related log files. *Bioinformatics*, (2019).
27. Schubert M, Lindgreen S, Orlando L. AdapterRemoval v2: rapid adapter trimming, identification, and read merging. *BMC Res Notes* **9**, 88-88 (2016).
28. Dobin A, *et al.* STAR: ultrafast universal RNA-seq aligner. *Bioinformatics* **29**, 15-21 (2012).
29. Liao Y, Smyth GK, Shi W. featureCounts: an efficient general purpose program for assigning sequence reads to genomic features. *Bioinformatics* **30**, 923-930 (2013).
30. Zhou Y, Zhu J, Tong T, Wang J, Lin B, Zhang J. A statistical normalization method and differential expression analysis for RNA-seq data between different species. *BMC Bioinformatics* **20**, 163 (2019).
31. Law CW, Chen Y, Shi W, Smyth GK. voom: precision weights unlock linear model analysis tools for RNA-seq read counts. *Genome Biology* **15**, R29 (2014).
32. McCarthy DJ, Chen Y, Smyth GK. Differential expression analysis of multifactor RNA-Seq experiments with respect to biological variation. *Nucleic Acids Res* **40**, 4288-4297 (2012).
33. Robinson MD, McCarthy DJ, Smyth GK. edgeR: a Bioconductor package for differential expression analysis of digital gene expression data. *Bioinformatics* **26**, 139-140 (2010).

34. Smyth GK. Limma: Linear Models for Microarray Data. . In: *Bioinformatics and computational biology solutions using R and Bioconductor* (eds Gentleman R, Carey VJ, Huber W, Irizarry RA, Dudoit S). springer (2005).
35. Shah OJ, Wang Z, Hunter T. Inappropriate activation of the TSC/Rheb/mTOR/S6K cassette induces IRS1/2 depletion, insulin resistance, and cell survival deficiencies. *Current biology : CB* **14**, 1650-1656 (2004).
36. Flatt JP. Dietary fat, carbohydrate balance, and weight maintenance. *Annals of the New York Academy of Sciences* **683**, 122-140 (1993).
37. Westerterp KR. Food quotient, respiratory quotient, and energy balance. *Am J Clin Nutr* **57**, 759S-764S; discussion 764S-765S (1993).
38. Muoio Deborah M. Metabolic Inflexibility: When Mitochondrial Indecision Leads to Metabolic Gridlock. *Cell* **159**, 1253-1262 (2014).
39. Jung TW, Yoo HJ, Choi KM. Implication of hepatokines in metabolic disorders and cardiovascular diseases. *BBA Clin* **5**, 108-113 (2016).
40. Luo L, Liu M. Adipose tissue in control of metabolism. *J Endocrinol* **231**, R77-R99 (2016).
41. Frayn KN. Adipose tissue as a buffer for daily lipid flux. *Diabetologia* **45**, 1201-1210 (2002).
42. Newman JC, Verdin E.  $\beta$ -Hydroxybutyrate: A Signaling Metabolite. *Annu Rev Nutr* **37**, 51-76 (2017).
43. Solinas G, Borén J, Dulloo AG. De novo lipogenesis in metabolic homeostasis: More friend than foe? *Molecular metabolism* **4**, 367-377 (2015).
44. Krings A, Rahman S, Huang S, Lu Y, Czernik PJ, Lecka-Czernik B. Bone marrow fat has brown adipose tissue characteristics, which are attenuated with aging and diabetes. *Bone* **50**, 546-552 (2012).
45. Lecka-Czernik B, Stechschulte LA, Czernik PJ, Sherman SB, Huang S, Krings A. Marrow Adipose Tissue: Skeletal Location, Sexual Dimorphism, and Response to Sex Steroid Deficiency. *Front Endocrinol (Lausanne)* **8**, 188 (2017).
46. Bostrom P, *et al.* A PGC1- $\alpha$ -dependent myokine that drives brown-fat-like development of white fat and thermogenesis. *Nature* **481**, (2012).
47. Fisher FM, *et al.* FGF21 regulates PGC-1 $\alpha$  and browning of white adipose tissues in adaptive thermogenesis. *Genes & development* **26**, 271-281 (2012).
48. Brun J, Berthou F, Trajkovski M, Maechler P, Foti M, Bonnet N. Bone Regulates Browning and Energy Metabolism Through Mature Osteoblast/Osteocyte PPAR $\gamma$  Expression. *Diabetes* **66**, 2541-2554 (2017).
49. Fulzele K, *et al.* Osteocyte-Secreted Wnt Signaling Inhibitor Sclerostin Contributes to Beige Adipogenesis in Peripheral Fat Depots. *J Bone Miner Res* **32**, 373-384 (2017).
50. Kershaw EE, Flier JS. Adipose tissue as an endocrine organ. *J Clin Endocrinol Metab* **89**, 2548-2556 (2004).
51. Ayala JE, *et al.* Standard operating procedures for describing and performing metabolic tests of glucose homeostasis in mice. *Disease Models & Mechanisms* **3**, 525-534 (2010).

52. Harrington LS, *et al.* The TSC1-2 tumor suppressor controls insulin-PI3K signaling via regulation of IRS proteins. *J Cell Biol* **166**, 213-223 (2004).
53. Khamzina L, Veilleux A, Bergeron S, Marette A. Increased activation of the mammalian target of rapamycin pathway in liver and skeletal muscle of obese rats: possible involvement in obesity-linked insulin resistance. *Endocrinology* **146**, 1473-1481 (2005).
54. Liu Z, *et al.* High-fat diet induces hepatic insulin resistance and impairment of synaptic plasticity. *PLoS One* **10**, e0128274-e0128274 (2015).
55. Yan B, *et al.* mTORC1 regulates PTHrP to coordinate chondrocyte growth, proliferation and differentiation. *Nature Communications* **7**, 11151 (2016).
56. Huang B, *et al.* mTORC1 prevents preosteoblast differentiation through the notch signaling pathway. *PLoS genetics* **11**, e1005426 (2015).
57. Thoreen CC, Chantranupong L, Keys HR, Wang T, Gray NS, Sabatini DM. A unifying model for mTORC1-mediated regulation of mRNA translation. *Nature* **485**, 109-113 (2012).
58. Martin SK, *et al.* mTORC1 plays an important role in osteoblastic regulation of B-lymphopoiesis. *Scientific reports* **8**, 14501-14501 (2018).
59. Thomas DM, Rogers SD, Ng KW, Best JD. Dexamethasone modulates insulin receptor expression and subcellular distribution of the glucose transporter GLUT 1 in UMR 106-01, a clonal osteogenic sarcoma cell line. *J Mol Endocrinol* **17**, 7-17 (1996).
60. Thomas DM, Maher F, Rogers SD, Best JD. Expression and regulation by insulin of GLUT 3 in UMR 106-01, a clonal rat osteosarcoma cell line. *Biochem Biophys Res Commun* **218**, 789-793 (1996).
61. Zoch ML, Abou DS, Clemens TL, Thorek DLJ, Riddle RC. In vivo radiometric analysis of glucose uptake and distribution in mouse bone. *Bone Research* **4**, 16004 (2016).
62. Wei J, *et al.* Glucose Uptake and Runx2 Synergize to Orchestrate Osteoblast Differentiation and Bone Formation. *Cell* **161**, 1576-1591 (2015).
63. Li Z, *et al.* Glucose Transporter-4 Facilitates Insulin-Stimulated Glucose Uptake in Osteoblasts. *Endocrinology* **157**, 4094-4103 (2016).
64. Mosialou I, *et al.* MC4R-dependent suppression of appetite by bone-derived lipocalin 2. *Nature* **543**, 385-390 (2017).
65. Lee NJ, *et al.* Osteoglycin, a novel coordinator of bone and glucose homeostasis. *Molecular metabolism* **13**, 30-44 (2018).
66. Rached MT, *et al.* FoxO1 expression in osteoblasts regulates glucose homeostasis through regulation of osteocalcin in mice. *J Clin Invest* **120**, 357-368 (2010).
67. Yoshizawa T, *et al.* The transcription factor ATF4 regulates glucose metabolism in mice through its expression in osteoblasts. *J Clin Invest* **119**, 2807-2817 (2009).
68. Ryan NT, Blackburn GL, Clowes HA, Jr. Differential tissue sensitivity to elevated endogenous insulin levels during experimental peritonitis in rats. *Metabolism* **23**, 1081-1089 (1974).

69. Agouni A, Owen C, Czopek A, Mody N, Delibegovic M. In vivo differential effects of fasting, re-feeding, insulin and insulin stimulation time course on insulin signaling pathway components in peripheral tissues. *Biochem Biophys Res Commun* **401**, 104-111 (2010).
70. Kuo T-R, Chen C-H. Bone biomarker for the clinical assessment of osteoporosis: recent developments and future perspectives. *Biomarker Research* **5**, 18 (2017).
71. Fitter S, *et al.* mTORC1 Plays an Important Role in Skeletal Development by Controlling Preosteoblast Differentiation. *Molecular and Cellular Biology* **37**, e00668-00616 (2017).
72. Dirckx N, *et al.* Vhl deletion in osteoblasts boosts cellular glycolysis and improves global glucose metabolism. *J Clin Invest* **128**, 1087-1105 (2018).
73. Bae EJ, *et al.* Liver-specific p70 S6 kinase depletion protects against hepatic steatosis and systemic insulin resistance. *The Journal of biological chemistry* **287**, 18769-18780 (2012).
74. Polak P, Cybulski N, Feige JN, Auwerx J, Ruegg MA, Hall MN. Adipose-specific knockout of raptor results in lean mice with enhanced mitochondrial respiration. *Cell Metab* **8**, 399-410 (2008).
75. Lee PL, Tang Y, Li H, Guertin DA. Raptor/mTORC1 loss in adipocytes causes progressive lipodystrophy and fatty liver disease. *Molecular metabolism* **5**, 422-432 (2016).
76. Guridi M, *et al.* Alterations to mTORC1 signaling in the skeletal muscle differentially affect whole-body metabolism. *Skelet Muscle* **6**, 13-13 (2016).
77. Chang GR, *et al.* Rapamycin protects against high fat diet-induced obesity in C57BL/6J mice. *J Pharmacol Sci* **109**, 496-503 (2009).
78. Liu W, *et al.* Osteocyte TSC1 promotes sclerostin secretion to restrain osteogenesis in mice. *Open Biol* **9**, 180262-180262 (2019).
79. Weigle DS. Appetite and the regulation of body composition. *FASEB journal : official publication of the Federation of American Societies for Experimental Biology* **8**, 302-310 (1994).
80. De Pergola G, Pannacciulli N, Minenna A, Martina RA, Cannito F, Giorgino R. Fuel metabolism in adult individuals with a wide range of body mass index: effect of a family history of type 2 diabetes. *Diabetes, nutrition & metabolism* **16**, 41-47 (2003).
81. Ukropcova B, *et al.* Family History of Diabetes Links Impaired Substrate Switching and Reduced Mitochondrial Content in Skeletal Muscle. *Diabetes* **56**, 720-727 (2007).
82. Goodpaster BH, Sparks LM. Metabolic Flexibility in Health and Disease. *Cell Metab* **25**, 1027-1036 (2017).

**CHAPTER 4:**  
**DISCUSSION AND CONCLUSION**

## 4.1 General Discussion

Diabetes is a chronic disease that occurs when the pancreas cannot produce sufficient insulin or when the body cannot respond to insulin effectively. Type 2 diabetes (T2DM) is by far the most prevalent form of diabetes and arises from genetic and environmental factors such as obesity and physical inactivity. Over the past three decades, the number of people with T2DM has doubled globally, making it one of the most important public health challenges currently facing healthcare systems<sup>1</sup>. Loss of postprandial glycaemic control, followed by fasting hyperglycaemia, is the hallmark of T2DM<sup>2</sup>. Thus, much attention has been directed towards gaining an understanding of the underlying mechanisms responsible for T2DM and identifying how insulin-responsive tissues interact to control glucose homeostasis.

Under normal physiological conditions, insulin regulates glucose utilisation by binding to the insulin receptor (INSR). The INSR is expressed by several tissues, including the heart, liver, skeletal muscle and adipose tissue; INSR activation in these tissues leads to an increase in glucose uptake or conversion of glucose to glycogen in the liver. Under obesogenic conditions, excessive caloric intake increases serum glucose levels, which leads to an increase in insulin production from the pancreas, and chronic exposure of insulin-responsive tissues to insulin results in them becoming insulin resistant<sup>3</sup>.

More-recent studies have shown, somewhat surprisingly, that the skeleton also plays a central role in regulating glucose levels in the body. Specifically, studies have identified the OB-specific protein, OCN, as a novel hormone that stimulates pancreatic  $\beta$ -cell proliferation and insulin secretion and promotes insulin sensitivity in peripheral tissues such as muscle, liver and adipose tissues<sup>4,5</sup>. Notably, deletion of the INSR in skeletal OBs results in elevated blood glucose and reduced serum insulin levels in normal-chow fed mice<sup>6</sup> while overexpression or downregulation of INSR in OBs results in profound changes in systemic glucose metabolism in response to an obesogenic diet<sup>7</sup>. These results suggest that dysregulated insulin signalling in bone could play an important role in the development of systemic insulin resistance and that restoration of insulin signalling in the bone alone could potentially protect against the negative systemic metabolic effects arising from an obesogenic diet.

Mechanistically, binding of insulin to its receptor activates the PI3K pathway. This eventually leads to activation of mTORC1 pathways, which results in cell growth and

proliferation by promoting protein synthesis, lipid biogenesis and metabolism<sup>8</sup>. Additionally, mTORC1 directly, and indirectly via activation of S6K1, negatively regulates insulin signalling by disrupting the interaction between INSR and its adaptor protein, IRS1. In response to excessive nutrients, mTORC1 becomes hyper-activated and turns off insulin signalling inappropriately, rendering cells unresponsive to insulin. Based on several lines of evidence, it was hypothesised that mTORC1 function in OBs plays an important role in skeletal regulation of systemic glucose homeostasis and that inhibition of OB-mTORC1 could protect against the development of systemic HFD-induced insulin resistance. To investigate this hypothesis, a loss-of-function mouse model was generated in which *Rptor*, which encodes RAPTOR, a defining and essential component of mTORC1, was specifically deleted in pre-OBs (*Rptor<sub>ob</sub><sup>-/-</sup>*). Using an array of metabolic tests, and detailed assessment of insulin and mTORC1 signalling pathways in insulin-target tissues, the studies outlined in this thesis have characterised the metabolic consequences of OB-mTORC1 impairment in mice fed either normal chow or obesogenic HFD.

In Chapter 2, OB-specific deletion of *Rptor* was shown to have a profound effect on body composition, whole-body glucose metabolism, and the male reproductive system in mice fed a normal diet. While both sexes of *Rptor<sub>ob</sub><sup>-/-</sup>* mice were markedly lean and showed a preference for fat utilisation and elevated ketone body levels, sex-dependent differences in body composition and energy metabolism were observed. Specifically, a significant decrease in fat mass and white adipocyte size and a significant increase in glucose tolerance were observed in male, but not female, *Rptor<sub>ob</sub><sup>-/-</sup>* mice compared to controls. Notwithstanding these differences, both male and female *Rptor<sub>ob</sub><sup>-/-</sup>* mice exhibited higher sensitivity to insulin and lower levels of fasting glucose and insulin.

#### *Inactivation of OB-specific nutrient sensing mTORC1 results in DR-like phenotypes*

Interestingly, while the low glucose levels and increased insulin sensitivity in *Rptor<sub>ob</sub><sup>-/-</sup>* mice could not be explained by increased levels of OCN, nor increased insulin production, they were associated with a dramatic elevation in circulating adiponectin levels. Notably, data presented in this thesis suggest that the increased adiponectin levels in *Rptor<sub>ob</sub><sup>-/-</sup>* mice arises from the newly-characterised bone marrow adipocytes (BMAds, which are dramatically increased in these mice<sup>9</sup>) rather than the classical WAT depots. Although the physiological role of BMAT remains largely unknown, its expansion has been reported in response to changes in nutrient availability including



starvation (reviewed in <sup>10</sup>), under dietary restriction (DR) in mice<sup>11</sup> and anorexic nervosa in humans<sup>12</sup>, HFD feeding<sup>13</sup> and leptin deficiency<sup>14</sup>. Furthermore, a growing body of literature suggests that BMAT expansion under restricted dietary conditions increases production of adiponectin to promote systemic improvements in glucose metabolism<sup>12,15,16</sup>. In this regard, the expansion of BMAT, the elevation of BMAT-derived adiponectin production, and hypoleptinemia observed in *Rptor<sub>ob</sub><sup>-/-</sup>* mice, suggest that suppression of mTORC1 in OBs could lead to DR-induced BMAT expansion and subsequent systemic adaptation to DR via increased secretion of BMAT-derived adiponectin.

DR has been shown to extend lifespan in a wide spectrum of organisms spanning from yeast to vertebrates<sup>17</sup>. Moreover, it has been shown to reduce or delay the development of age-related diseases such as cardiovascular disease, cancer, metabolic diseases and muscle atrophy<sup>18,19,20</sup>. During DR, low nutrient and high AMP/ATP ratios activate AMP-activated protein kinase (AMPK), which inhibits mTORC1 by stimulating TSC2<sup>21</sup>, a negative regulator of mTORC1, and/or by phosphorylating RAPTOR<sup>22</sup>. Consistent with this view, pharmaceutical inhibition of TOR signalling (via rapamycin treatment) extends lifespan<sup>23,24,25</sup> and genetic ablation of S6K1 in mice (*S6K1<sup>-/-</sup>*) leads to a gene expression profile similar to that of DR mice. Of note, female *S6K1<sup>-/-</sup>* are long-lived and have reduced incidence of age-related diseases<sup>26</sup>. In this context, it is interesting to note that the *Rptor<sub>ob</sub><sup>-/-</sup>* mice share a number of metabolic phenotypes with DR mice (i.e. low basal glucose levels, low insulin levels, high adiponectin levels, low leptin levels, increased insulin sensitivity and BMAT expansion), which suggests that suppression of mTORC1 activity in the skeleton could play an important role in the physiological response to DR.

#### *Roles of OCN beyond regulation of glucose metabolism and sex dimorphism*

In keeping with this, low circulating leptin and testosterone levels observed in *Rptor<sub>ob</sub><sup>-/-</sup>* mice could be part of their metabolic adaptation in response to DR. Under DR conditions, leptin can exert a strong effect on the reproductive axis<sup>27</sup>. Low leptin directly reduces gonadotropin-releasing hormone (GnRH) secretion from the hypothalamus, which itself reduces secretion of luteinizing hormone (LH) from the pituitary and a subsequent decreased release of gonadal sex steroid hormones (GH: testosterone and estradiol)<sup>28,29</sup>. Thus, the impaired reproductive function of male *Rptor<sub>ob</sub><sup>-/-</sup>* mice could be due to the combined effects of low leptin and OCN levels.

Given that the effect of OCN on reproductive function is limited to male mice (the putative OCN receptor, GRPC6A, is only expressed in testicular Leydig cells and not in the ovary<sup>30</sup>) while DR affects reproductive function in both genders, further investigation of female reproductive function is required to determine if altered reproductive function in *Rptor<sub>ob</sub><sup>-/-</sup>* mice is the consequence of an mTORC1-mediated response to DR.

OCN has also shown to regulate brain development and function, whereby *Ocn<sup>-/-</sup>* mice were found to be more passive and suffer from increased anxiety and decreased memory compared to their control littermates<sup>31</sup>. While both male and female *Rptor<sub>ob</sub><sup>-/-</sup>* mice exhibit low circulating OCN levels, only female *Rptor<sub>ob</sub><sup>-/-</sup>* mice were more passive than the controls. It is noteworthy that given *ad libitum* access to food, the food intake (either with or without normalisation) is still reduced in female *Rptor<sub>ob</sub><sup>-/-</sup>* mice, suggesting a “self-imposed” DR or possibly equivalent to ‘anorexic’ phenotype in these mice. Depression and anxiety are the common comorbidities of anorexia<sup>32</sup> and drastic change in feeding and activity behaviours are the early signs of depression-like phenotypes in mice<sup>33</sup>. It would be interesting to investigate further if female *Rptor<sub>ob</sub><sup>-/-</sup>* mice display other anorexic and/or depression-like behaviours or their passivity is a secondary effect of low circulating OCN levels.

In light of the advantageous metabolic phenotypes of *Rptor<sub>ob</sub><sup>-/-</sup>* mice, including improved glucose disposal and insulin sensitivity under normal chow diet feeding (as outlined in Chapter 2) and previous data demonstrating that nutrient-overload leads to hyper-activation of mTORC1 signalling and the development of insulin resistance<sup>34</sup>, this led to the investigation of metabolic responses of *Rptor<sub>ob</sub><sup>-/-</sup>* mice to an obesogenic HFD diet (which is well-established to induce insulin resistance in mice) as detailed in Chapter 3. Consistent with other studies<sup>35,36,37</sup>, HFD-feeding resulted in significant weight gain in the control mice, with more pronounced weight gain observed in males. Notably, both male and female *Rptor<sub>ob</sub><sup>-/-</sup>* mice were resistant to HFD-induced weight gain and maintained a constant body weight after 6 weeks of HFD, despite consuming similar amounts of food to the controls. Body composition analyses confirmed a significant reduction in %fat mass and adipocyte hypertrophy in both gonadal and inguinal WAT depots. Remarkably, *Rptor<sub>ob</sub><sup>-/-</sup>* mice were able to maintain the favourable metabolic phenotypes observed with chow diet feeding (Chapter 2) and were thus protected against the negative effects of HFD-feeding on glycaemia (e.g. lower fasting

glucose and insulin levels, increased glucose tolerance and enhanced insulin sensitivity).

It is important to note that, while the severe hypoglycaemia observed in the female *Rptor<sub>ob</sub><sup>-/-</sup>* mice during the ITTs suggests that they are hypersensitive to exogenous insulin administration, it is also possible that they have difficulty in recovering from insulin-induced hypoglycaemia. This could arise from a defect in the counter-regulatory responses which, in mice, are activated when blood glucose levels fall below ~80 mg/dL (~4.4mM)<sup>38</sup>. Further assessment of these glucose counter-regulatory mechanisms by hypoglycaemic clamp studies and measurement of hormones such as glucagon, corticosterone and epinephrine in these mice could provide further clarification<sup>39,40</sup>.

#### Metabolic phenotypes independent of OCN

Notably, protection from HFD-induced glucose intolerance and insulin resistance has been observed in other mouse models in which an increase in OB insulin signalling is observed. These include mice in which there is an OB-specific deletion of *FoxO1* (*FoxO1<sup>OB-/-</sup>*)<sup>41</sup>, a negative regulator of insulin signalling, and mice in which there is an OB-specific overexpression of INSR (*Coll1a1-INSR<sup>Tg</sup>*)<sup>7</sup>. These phenotypes are consistent with the data for *Rptor<sub>ob</sub><sup>-/-</sup>* mice reported in Chapter 3. The protected phenotypes of both *FoxO1<sup>OB-/-</sup>* and *Coll1a1-INSR<sup>Tg</sup>* mice were, however, attributed to an insulin-mediated increase in bone resorption leading to an increase in OCN activity and serum levels (although no difference in *Bglap2* mRNA expression was observed)<sup>7</sup>. In contrast, both RNA-seq and qRT-PCR analysis of bone samples from HFD-fed *Rptor<sub>ob</sub><sup>-/-</sup>* mice revealed a downregulation of genes involved in bone resorption and osteoclast differentiation pathways, and upregulation of genes associated with bone formation and OB differentiation. Intriguingly, despite detection of significantly higher *Ocn* mRNA expression levels in male HFD-fed *Rptor<sub>ob</sub><sup>-/-</sup>* mice, circulating levels of both total and unOCN protein were equivalent to those of the controls. Furthermore, the significantly lower levels of total and undercarboxylated forms of OCN have been observed in the normal-chow-diet-fed *Rptor<sub>ob</sub><sup>-/-</sup>* mice compared to the control mice, despite their improved metabolic phenotype. Of note, the normal chow studies (8-week old mice: Chapter 2) and HFD studies (16-week old mice: Chapter 3) were performed at different ages, which precludes any direct inter-diet comparison. It is possible that the discrepancy in the OCN levels of *FoxO1<sup>OB-/-</sup>*, *Coll1a1-INSR<sup>Tg</sup>* and *Rptor<sub>ob</sub><sup>-/-</sup>* mice is attributable to a lowering of OCN levels in response to HFD feeding in the control

mice<sup>42</sup>, whereas in *Rptor<sub>ob</sub><sup>-/-</sup>* mice, OCN levels were already-low and their HFD-resistant phenotype prevented any further fall in the OCN levels. Another possibility is that OB-mTORC1 is a negative regulator of *Bglap2* (which encodes OCN) gene expression and possibly required for *Bglap2* translation.

Notwithstanding this, an important finding of this present study is the observation that the beneficial metabolic effects associated with OB-mTORC1 inhibition occur independently of OCN. Several studies have implicated OCN-independent mechanisms in the bone-metabolism interplay. For example, genetic ablation of OBs, or conditional OB-specific inactivation of glycogen synthase kinase (GSK)-3 $\beta$ ,  $\beta$ -catenin or *Vhl*, a regulator of Hypoxia-inducible factors (HIFs), leads to systemic metabolic alterations that cannot be fully rescued or explained by congruent changes in serum OCN<sup>43,44,45,46</sup>. These studies suggest the existence of additional, as yet unidentified, bone secretagogues, amongst other factors, that influence global glucose homeostasis and energy metabolism.

#### Potential molecular mechanism underlying suppression of OB-mTORC1

Both *in vitro* and *in vivo* data suggest that suppression of OB-mTORC1 activity results in relaxation of mTORC1-dependent negative feedback controls, which leads to potentiation of insulin signalling in OBs. These are evident by (i) *in vivo* insulin-stimulated phosphorylation levels of INSR, AKT and subsequent phosphorylation of its substrate, AS160 at Thr<sup>642</sup> and GSK3 $\beta$  at Ser<sup>9</sup>, are significantly higher in calvarial cells of HFD-fed *Rptor<sub>ob</sub><sup>-/-</sup>* mice compared to the controls; (ii) at the basal levels, phosphorylation of AKT at Ser<sup>473</sup> and Thr<sup>308</sup> and its two substrates is observed in calvarial cells of HFD-fed *Rptor<sub>ob</sub><sup>-/-</sup>* mice, but not in the controls; and (iii) hyperphosphorylation of AKT at Ser<sup>473</sup> and Thr<sup>308</sup> is observed *in vitro* in *Rptor* KO OBs, in both basal and insulin-stimulated states. AKT-mediated phosphorylation of AS160 at Thr<sup>642</sup> has been reported to attenuate its inhibitory effects (i.e. AKT-mediated phospho-AS160 inhibits its GAP (GTPase-activating protein) activity leading to elevation of the ‘active’ GTP-bound form of RAB required for GLUT4 translocation: Fig. 4.1) on RAB, leading to GLUT4 membrane translocation and thus cellular glucose uptake<sup>47,48</sup>. The hyperphosphorylation of AKT observed both *in vivo* and *in vitro*, hyperphosphorylation of AS160 observed *in vivo*, and significantly increased glucose uptake in *Rptor* KO cell *in vitro* in both basal and insulin-stimulated states point to the mechanism in which

enhanced and prolonged insulin signalling leads to an increase in glucose transport in the absence of mTORC1 activity.

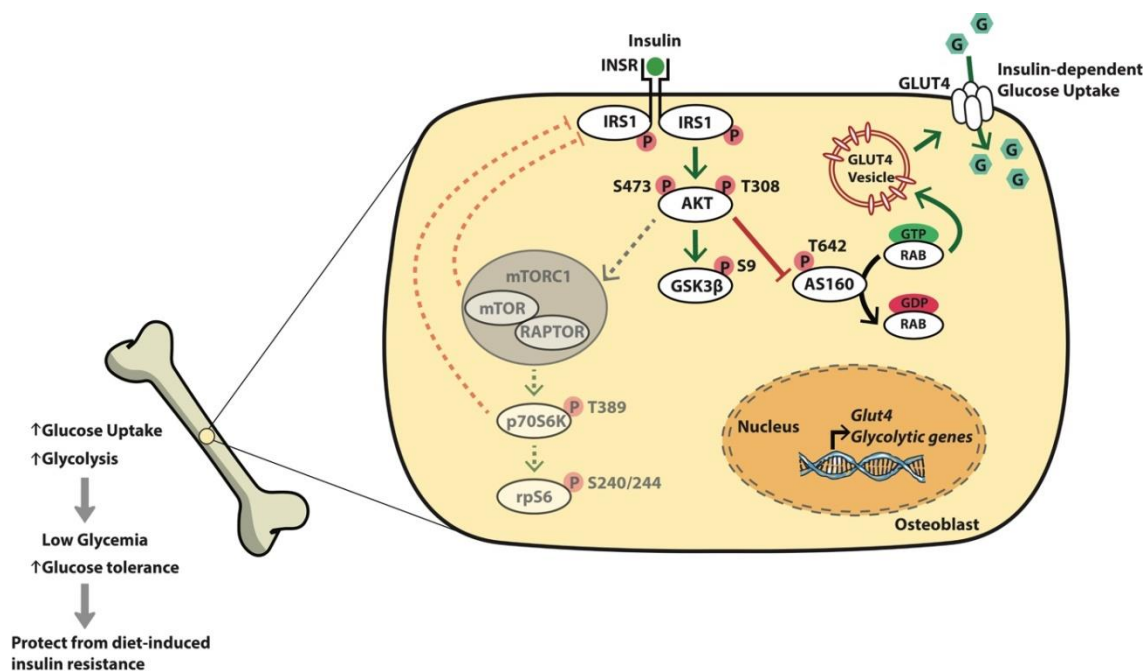


**Figure 4.1 Schematic summary.**

Suppression of mTORC1 activity in pre-OBs results in relaxation of mTORC1-dependent negative feedback controls (both directly and indirectly via activation of p70S6K) on insulin signalling by disrupting the interaction between IRS1 and INSR. This leads to enhanced and prolonged insulin signalling as indicated by hyperactivation of AKT at Ser<sup>473</sup> and Thr<sup>308</sup> in both basal and insulin-stimulated states. AKT hyperactivation attenuates the inhibitory effects of AS160 on RAB, leading to GLUT4 membrane translocation. These molecular changes are associated with increased cellular glucose uptake in *Rptor*-deficient OBs and upregulation of the insulin-dependent glucose transporter 4 (*Glut4*) and glycolysis-promoting enzymes in the skeleton of *Rptor<sub>ob</sub><sup>-/-</sup>* mice. Systemically, *Rptor<sub>ob</sub><sup>-/-</sup>* mice show persistently low fasting glucose levels and significantly increased tolerance to glucose; metabolic phenotypes that are, at least in part, attributable to an enhanced responsiveness to insulin and insulin-dependent glucose uptake in OBs.

*Skeletal glucose uptake and utilisation as determinants of whole-body glucose metabolism*

Glucose is a primary source of energy for osteogenic cells, with osteogenic cells being highly glycolytic in both aerobic and anaerobic environments<sup>49,50</sup>. OB cells express three high-affinity glucose transporters: *Glut1*, *Glut3*, and *Glut4*<sup>51,52,53</sup>, which are expressed at different stages of OB differentiation. GLUT4 mediates insulin-dependent glucose uptake in mature osteoblasts and its expression rises in parallel with the increased insulin-stimulated glucose oxidation<sup>54</sup>. *Glut4* ablation in OBs *in vitro* abolishes insulin-stimulated glucose uptake, while mice with OB-specific *Glut4* deletion ( $\Delta$ Glut4) are insulin-resistant with no detectable skeletal changes as measured using high resolution micro-computed tomography (microCT)<sup>54</sup>.

GLUT1, on the other hand, is a major glucose transporter in primary OBs. It mediates glucose uptake in an insulin-independent manner and favours OB differentiation and bone formation by suppressing AMPK-dependent proteasomal degradation of RUNX2<sup>55</sup>. Importantly, accumulation of RUNX2 leads to transcriptional activation of *Glut1*, thereby forming a feed-forward regulation between GLUT1-mediated glucose uptake and RUNX2-coordinated OB differentiation and bone formation<sup>55</sup>.

Expression of *Glut1* is also regulated by other transcription factors e.g. hypoxia-inducible transcription factor 1 $\alpha$  (HIF-1 $\alpha$ ) under hypoxia<sup>56,57</sup>, c-Myc<sup>58</sup> and un-controlled KRAS<sup>59</sup> in cancer cells. In this context, the bone is a particularly hypoxic tissue with pressure of oxygen levels below 1% in hypoxic regions and up to 6% in sinusoidal cavities<sup>60</sup>. Consequently, HIF-1 $\alpha$  has been shown to play a crucial role in the promotion of angiogenesis and coupling between osteogenic and angiogenic processes (reviewed in<sup>61,62</sup>). Under normoxic condition, HIF prolyl hydroxylases hydroxylate specific residues in the HIF- $\alpha$  protein, rendering it a substrate for the E3 ubiquitin ligase von Hippel–Lindau (VHL) and thus a target for proteasomal degradation<sup>63</sup>. Conversely, under hypoxic condition, HIF-1 $\alpha$  serves as a molecular switch diverting energy production from oxidative to glycolytic metabolism by up-regulating HIF target genes such as *Vegf*, *Glut1* and *Epo*.

In regard to mTORC1, activation of HIF upregulates REDD1 (also known as DDIT4/RTP801/Dig1), which induces mTORC1 inhibition via activation of the TSC1/2 complex<sup>64,65</sup>. Consistent with this, stabilisation of HIF via deletion of *Vhl* in OBs (*Vhl*

cKO) results in mice with low glycaemia and increased glucose tolerance and high bone mass; this metabolic phenotype resembles *Rptor<sub>ob</sub><sup>-/-</sup>* mice while the bone phenotypes that are similar to mice overexpressing GLUT1 in OBs<sup>46,55</sup>. Furthermore, both *Vhl* cKO mice and mice harbouring *Vhl*-deficient OBs display an approximately 20% and 40% increase in glucose uptake, respectively, and a significant upregulation of glycolysis genes compared to the controls. Of note, basal glucose uptake is increased both *in vivo* and *in vitro* in these *Vhl*-deficient OBs. This increased basal glucose uptake was also associated with elevated expression of *Glut1* and increase extracellular acidification rates (ECARs: reflect lactic acid production and thus glycolysis) while basal oxygen consumption rates (OCRs: generation of ATP by mitochondrial therefore oxidative phosphorylation) were decreased. These findings suggest increased glycolysis but not glucose oxidation; a phenomenon akin to the Warburg effect<sup>46,66</sup>. Furthermore, expression levels of RUNX2 in the *Vhl* cKO mice were 3-fold higher than in the control mice, suggesting that the mechanism underlying their high bone mass may be due to the feed-forward relationship of *Glut1-Runx2* as previously described by Wei et al<sup>55</sup>.

Consistent with the similarities in their metabolic phenotypes *in vivo*, *Rptor*-null OBs also exhibited an increase in basal glucose uptake and an upregulation of glycolytic genes (as indicated by RNA-seq and GSEA and confirmed with qRT-PCR), with a moderate increase in *Glut1* expression. On the other hand, the increased basal and insulin-stimulated glucose uptake in the *Rptor* KO OBs was associated with a significant upregulation of *Glut4* mRNA and the metabolic phenotype of *Rptor<sub>ob</sub><sup>-/-</sup>* mice was indeed the opposite to that observed in the  $\Delta$ Glut4 mice. Furthermore, the upregulation of *Glut4* is also observed *in vivo* in the bones of *Rptor<sub>ob</sub><sup>-/-</sup>* mice irrespective of diet feeding, suggesting that glucose uptake could be increased in the OBs of *Rptor<sub>ob</sub><sup>-/-</sup>* mice and this increase in glucose uptake is, at least in part, attributable to their enhanced systemic glucose tolerance.

#### *OBs Bioenergetics and whole-body energy metabolism*

While the bioenergetics of the *Rptor*-null OBs would require further investigation, GSEA showed an upregulation of other intermediary metabolic pathways in addition to glycolysis, including conversion of pyruvate from acetyl-coA, tricarboxylic acid (TCA), oxidative phosphorylation and respiratory electron transport chain, which argues against the Warburg effect in these cells.



Apart from glucose, fatty acids and amino acids represent the additional fuel substrates that can be processed and oxidised through the TCA cycle. In this regard, GSEA has identified upregulation of gene sets involved in fatty acid oxidation and transportation, cellular amino acid transport and cellular amino acid catabolism. In the bone, amino acids not only provide energy but also serve as substrates for synthesis of collagen and other matrix proteins (reviewed in <sup>67</sup>). Mechanistically, phosphorylation of ATF4 by RSK2, a kinase inactivated in Coffin-Lowry Syndrome, promotes its transcriptional activity, leading to synthesis of type 1 collagen by favouring amino acid import<sup>68</sup>. Moreover, a high protein diet could rescue the skeletal defects in the Coffin-Lowry mice lacking RSK2, which are characterised by decreased ATF function<sup>69</sup>. A growing number of studies have identified fatty acids as being important fuel substrates for OBs. For example, deletion of a fatty acid transporter, CD36, or CPT2, an obligate enzyme for fatty acid oxidation, in OBs results in mice with low bone mass and reduced OBs number and activity<sup>70,71</sup>. Furthermore, mice with OB-specific deletion of *Lrp5*, a Wnt co-receptor, exhibited a reduction in bone mass while peripheral fat mass and serum TG and FFA were significantly increased when fed a normal chow diet<sup>72,73</sup>. Collectively, these studies highlight a significant contribution of the skeleton, and in particular the choice of fuel substrate by OBs, in the regulation of whole-body energy metabolism.

#### *Inhibition of mTORC1 as a novel therapeutic approach to treat T2DM*

The studies presented in this thesis are the first to characterise the effects of skeletal mTORC1 inactivation on the whole-body energy and glucose metabolism. Since the consequences of mTORC1 perturbation have also been described in other metabolic tissues such as muscle, adipose or liver, it is evident that mTORC1 has tissue-specific effects on whole-body metabolism. For example, inactivation of *Rptor* in skeletal muscle (RAMKO mice) results in resistance to weight-gain and enhanced tolerance to glucose compared to controls, but no improvement in insulin sensitivity<sup>74</sup>. These phenotypes are associated with increased muscle glycogen levels due to AKT-mediated activation of glycogen synthesis and a down-regulation of genes involved in glucose transport and glycolysis<sup>74,75</sup>. Conversely, liver-specific *Rptor* ablation (*Raptor*<sup>Ahep</sup> mice) results in severe liver damage with augmented inflammation and fibrosis, with improved glucose tolerance observed in low fat-fed *Raptor*<sup>Ahep</sup> mice but not in HFD-fed *Raptor*<sup>Ahep</sup> mice<sup>76</sup>. In the context of adipose tissue, mice lacking adipose *Rptor* using *Ap2-Cre* (*raptor*<sup>ad-/-</sup>) were found to be lean and resistant to HFD-induced metabolic dysfunction, due to the abolition of HFD-induced hyperphosphorylation of S6K1 and

restoration of AKT activation in response to insulin<sup>77</sup>. However, recent data has indicated that the *Ap2-Cre* line has a mosaic expression of *Cre* in adipose tissue and is not specific to adipocytes, with extra-adipose *Cre* activity observed in other cell types including endothelial cells in the heart and skeletal muscle<sup>78,79,80</sup>. A more-specific and efficient *Adiponectin-Cre*, which targets mature adipocytes, found that loss of *Rptor* in adipose tissue leads to lipodystrophy and insulin resistance, and a significant increase in liver mass and ectopic lipid accumulation<sup>81</sup>.

These tissue-specific functions and responses to mTORC1 inhibition are further highlighted in studies where administration of rapamycin has been shown to have both beneficial and detrimental effects on metabolism. For example, *in vitro* acute rapamycin treatment improves muscle insulin sensitivity<sup>82</sup> while 16-week treatment with rapamycin protects against HFD-induced obesity in C57BL/6J mice<sup>83</sup>. Conversely, rapamycin has been shown to impair glucose tolerance and insulin sensitivity in both inbred and genetically heterogeneous mice<sup>84</sup>, to exacerbate glucose intolerance in HFD-fed KK/HIJ mice<sup>85</sup>, decrease hepatic insulin sensitivity<sup>86</sup> and promote insulin resistance and hyperlipidemia in rats<sup>87</sup>. These contradictory effects of rapamycin could possibly be explained by the duration of the treatment, the off-target inhibition of closely-related mTORC2<sup>86,88</sup>, or the tissue-specific responses to rapamycin<sup>89</sup>. Together, this suggests that sustained systemic suppression of mTORC1 function has significant limitations. As previously discussed, even though ablation of *Rptor* in these insulin-targeted tissues protects these mice from diet-induced obesity, they suffer from other adverse effects (i.e. liver damage, increase hepatic steatosis or insulin resistance). Conversely, deletion of *Rptor* in OBs results in enhanced glucose tolerance and increased insulin sensitivity irrespective of diet (phenotypes of *Rptor<sub>ob</sub><sup>-/-</sup>* mice are summarised in Table 4.1).

The unique phenotypes of *Rptor<sub>ob</sub><sup>-/-</sup>* mice have revealed OB-mTORC1 as a target for the development of antidiabetic drugs, whereby localised inhibition of skeletal mTORC1 could have favourable metabolic outcomes in patients with T2DM. However, it is important to note that *Rptor<sub>ob</sub><sup>-/-</sup>* mice are a developmental model where the *Osx-Cre* driver is expressed from E14.5<sup>90</sup>. Further investigations, in a more clinically relevant setting (i.e. inhibition of OB-mTORC1 postnatally or pharmaceutically using a bone-specific mTORC1 inhibitor), are therefore required to confirm the therapeutic potential of the current findings. There are several ways that this could be achieved. Firstly, the tetracycline-repressible nature of the tTA:Osx:Cre driver in these mice<sup>90</sup> could be exploited by administering tetracycline to dams to suppress Cre expression during

development (via chow and drinking water)<sup>91</sup>. Once the doxycycline is removed, *Osx-I*- driven Cre expression will resume and temporal and spatial deletion of *Rptor* will occur in OBs (as the *Osx-I* promoter is active throughout post-natal skeletal development in mice)<sup>92</sup>. Following postnatal OB-specific deletion of *Rptor*, animals could then be challenged with an obesogenic HFD to assess whether they are protected against developing T2DM.

A pharmaceutical approach, using a bone-specific mTORC1-specific inhibitor, could also be developed. NR1, is a newly-identified small molecule that binds to the switch II domain of the small G-protein, RHEB and potently inhibits mTORC1 activity without affecting mTORC2<sup>93</sup>. Localised drug delivery to bone is readily attainable using a bone-targeting bisphosphonate<sup>94</sup> (alendronate, ALN), which binds avidly to hydroxyapatite and has been used very successfully as a vehicle to deliver agents to bone<sup>95</sup>. Therefore, conjugation of an mTORC1 inhibitor such as NR1 with the ALN could represent a novel therapeutic approach to treat T2DM.

**Table 4.1 Summary of normal chow and high fat diet-fed male and female *Rptor<sup>ob</sup><sup>-/-</sup>* mice phenotypes**

	Chow-fed_8wks		High fat diet-fed_16wks	
	Female	Male	Female	Male
Weight gain	constant after 6wk on HFD			
Body weight	↓	↓	↓	↓
% Fat	↔	↓	↓	↓
%Lean	↔	↑	↑	↑
BMD	↓	↓	↔	↓
BMC	↓	↓	↔	↔
iWAT (g/gBW)	↓	↔	↓	↓
gWAT (g/gBW)	↓	↓	↓	↓
BAT (g/gBW)	↔	↔	↓	↔
Energy expenditure (kcal/g lean mass)	↔	↑	↔	↑ dark
Food intake (g/g BW)	↓	↔	↔	↔
RQ	↔	↓	↓ light ↑ dark	↓ light ↑ dark
Activity	↓	↔	↔	↔
%fecal lipid	↔	↔	↔	↔
<u>Metabolic phenotype</u>				
Fasting glucose	↓	↓	↓	↓
Insulin sensitivity	↑	↑	↑	↑
Glucose tolerance	↔	↑	↑	↑
Glucose-stimulated insulin secretion	↑	↑	↑	↑
<u>Serum analysis</u>				
Fasting insulin	↓	↓	↓	↓
Fasting Ketone bodies	↑	↑	↑	↑
Fasting peptide	↓	↓	↓	↓
Leptin	↓	↓	↓	↓
Adiponectin	↑	↑	↑	↑
totalOCN	↓	↓	↓	↔
unOCN	↓	↓	↔	↔
TG	↔	↓	↔	↓
FFA	↔	↔	↔	↔
<u>Histological analysis</u>				
Liver steatosis			↓	↓
Liver TG			↓	↔
Liver FFA			↔	↓
Liver glycogen			n/a	↑
iWAT adipocyte	↔	↓	↓	↓
gWAT adipocyte	n/a	↓	↓	↓
Browning of WAT			√	√

## 4.2 Future directions

The studies outlined in this thesis have identified an important role for the mTORC1 pathway in the skeletal regulation of glucose metabolism, and provide strong evidence to support the concept that dysregulated insulin signalling and changes in glucose uptake in OBs have systemic effects on gluco-regulation and energy homeostasis. In particular, as described in Chapter 3, the bone-specific inactivation of mTORC1 protected the mice against diet-induced insulin resistance which, at least in part, may be attributable to changes in skeletal glucose uptake. As outlined below, these findings have generated several new avenues of research that remain to be fully interrogated in order to fully understand this complex metabolic phenotype.

*Is the improvement in glucose disposal and insulin sensitivity in  $Rptor_{ob}^{-/-}$  mice due to elevated adiponectin levels?*

Both chow-fed and HFD-fed  $Rptor_{ob}^{-/-}$  mice have significantly higher serum levels of adiponectin, which may account for their increased insulin sensitivity. In particular, levels of the most bio-active HMW form of adiponectin are significantly higher in these mice and BMAT appears to be the major source of adiponectin in these mice. Genetic manipulation in mice has been extensively used to interrogate molecular mechanisms and cellular pathways in the biomedical research. For example, compound mice with heterozygous deletions of *Ocn* and *Adipoq* were used to provide the genetic evidence that OCN regulates insulin sensitivity, partially, via adiponectin<sup>4</sup>. To determine whether adiponectin is responsible for insulin-sensitizing effects of *Raptor* deletion in OBs, compound mice in which one allele of *Adipoq* is deleted in  $Rptor_{ob}^{-/-}$  ( $Rptor_{ob}^{-/-}; Adipoq^{+/-}$  mice) could be utilised and their metabolic phenotype compared to that of  $Rptor_{ob}^{-/-}$ ,  $Adipoq^{+/-}$  and control mice. This will provide the genetic evidence to determine if the increased insulin sensitivity in the  $Rptor_{ob}^{-/-}$  mice occurs, at least in part, through adiponectin.

*Does the phenotype observed in  $Rptor_{ob}^{-/-}$  mice mimic a DR-type response and is OB-mTORC1-inhibition a DR mimetic?*

The phenotypes observed in  $Rptor_{ob}^{-/-}$  mice are similar to physiological changes associated with DR (e.g. change in body composition resulting in total body weight and fat mass reduction but paradoxically elevated BMAT and circulating adiponectin levels,

reduced leptin levels and improved glucose metabolism). Furthermore, the reproductive phenotypes observed in the male *Rptor<sub>ob</sub><sup>-/-</sup>* mice (e.g. low circulating testosterone levels and lower sperm counts) are similar to those observed in mice subject to DR<sup>28</sup> suggesting that impaired mTORC1 function in bone mimics a dietary restriction phenotype. DR has been shown to disturb the hypothalamic-pituitary-gonadal axis in which disturbed GnRH, a high ratio of FSH/LH and low growth hormone are observed. Furthermore, female rats subjected to DR exhibit decreased reproductive organ weight, abnormal reproductive cycle and aberrant hormonal levels<sup>96</sup>. To characterise the ‘DR-like’ phenotypes of *Rptor<sub>ob</sub><sup>-/-</sup>* mice, pair-feeding and dietary-restricted control animals coupled with their body composition and metabolic analyses could be performed. Moreover, determinants of female reproductive functions (hormone measurements, reproductive organ weights, ovarian morphology and follicle classification, and gene expression analysis for genes related to ovarian follicle growth and degradation (i.e. *Sfrp4*, *Sgk*, *Lhcgr*, and *Cyp11a1*) might offer further support the hypothesis that mTORC1 in OBs plays an important role in the DR response.

*What are the mechanism(s) responsible for the observed browning of WAT in Rptor<sub>ob</sub><sup>-/-</sup> mice?*

As discussed in Chapter 3, the mechanism(s) underlying the browning of iWAT in *Rptor<sub>ob</sub><sup>-/-</sup>* mice appears to be independent of previously reported browning agents including FGF21<sup>97</sup>, irisin<sup>98</sup>, sclerostin<sup>99</sup> and BMP7<sup>100</sup>. These findings suggest the existence of other mechanisms or unknown factors which could serve as browning inducers.

- *Lactate as by-product of increased skeletal glycolysis?*

Previous studies by Carriere *et al.* have shown that lactate, an important intermediary metabolite, strongly induces thermogenic gene expression in mouse and human WAT cells via intracellular redox modifications. Furthermore,  $\beta$ -hydroxybutyrate, a primary ketone body that has a similar impact on redox state, is also capable of inducing the browning of mouse primary white adipocytes<sup>101</sup>. Serum  $\beta$ -hydroxybutyrate levels are higher in the *Rptor<sub>ob</sub><sup>-/-</sup>* mice irrespective of diet. From this, it is speculated that an increase in glycolysis in the *Rptor<sub>ob</sub><sup>-/-</sup>* mice, with a concomitant upregulation of lactate dehydrogenase (which catalyses the inter-conversion of pyruvate and lactate, the last step of anaerobic glycolysis) could lead to a higher output of lactate from the bone into the circulation. In support of this, *in vitro* studies have shown that bone consumes a

large amount of glucose, and that >80% of the glucose consumed is converted to lactate<sup>49,102</sup>. Measurement of circulating lactate levels in *Rptor<sub>ob</sub><sup>-/-</sup>* mice and ECARs of *Rptor* KO OBs could be used to examine this further.

- *Are there any other novel 'osteokines'?*

It is also interesting to note that the upregulation of UCP1 in *Rptor<sub>ob</sub><sup>-/-</sup>* mice appears to be depot-specific, with marked induction observed only in the iWAT, while upregulation of *Ucp1* mRNA, but not at the protein levels, was observed in the gWAT. Furthermore, even though proximal tibial regions (which are juxtaposed to trabecular bone) of BMAT have been reported to express markers of brown fat<sup>103,104</sup>, undetectable levels of *Ucp1* were observed in the bone of *Rptor<sub>ob</sub><sup>-/-</sup>* mice. Collectively, these results suggest that the mechanism(s) underlying this increased browning of white fat in *Rptor<sub>ob</sub><sup>-/-</sup>* mice is likely to occur in an endocrine, not paracrine, manner. Further studies integrating RNAseq data to identify translated genes that encode secreted proteins and non-targeted metabolomic profiling of serum<sup>105</sup>, involving the use of nuclear magnetic resonance mass spectrometry or complementary technologies, would be helpful to identify novel factor(s) underlying the metabolic phenotypes of *Rptor<sub>ob</sub><sup>-/-</sup>* mice.

*Does potentiated insulin signalling in the bone of *Rptor<sub>ob</sub><sup>-/-</sup>* mice protect them from deterioration in bone quality that would otherwise occur under HFD feeding?*

Several lines of evidence demonstrate that increased marrow adiposity is associated with lower BMD and increased skeletal fragility<sup>106</sup> in HFD-fed rodents<sup>13</sup> and obese or diabetic human patients<sup>107,108</sup>. Importantly, a decrease in number and differentiation of OBs and diminished quantities of osteoid lead to a poorly organised bone structure and decreased bone quality and increased fracture risk – a phenotype often observed in T2DM patients<sup>109,110,111</sup>. It is interesting to note that mice with OB-specific deletion of TSC2 (and hence hyperactivation of mTORC1) have high bone mass that is associated with the accumulation of poorly differentiated OBs that are insulin-resistant<sup>112</sup>. This phenotype is completely opposite to that of *Rptor<sub>ob</sub><sup>-/-</sup>* mice which, on normal chow, are osteopenic<sup>9</sup> and insulin-sensitive as shown in this study. Collectively, these results suggest that excess caloric intake, as often occur in T2DM, activates mTORC1-dependent anabolic processes and that hyper-activation of mTORC1 drives insulin resistance in the OBs, leading to formation of poorly formed bone. At the mRNA level, RNA-seq and qRT-PCR analyses of bones from HFD-fed *Rptor<sub>ob</sub><sup>-/-</sup>* mice showed strong upregulation of the expression of markers of bone formation and OB differentiation (i.e.

*Sp7, Ocn, Sparc, Col1a1*) and a concomitant downregulation of osteoclast markers (i.e. *Ctsk, Rank, Trap*). To characterise the bone phenotype of HFD-fed *Rptor<sub>ob</sub><sup>-/-</sup>* mice, micro-CT could be used to analyse bone microarchitecture and structure. Furthermore, histomorphometry could be used to assess the effects of potentiation of local insulin signalling, as a result of mTORC1 inhibition, on bone modelling and remodelling or bone microenvironment, including marrow adiposity, mesenchymal stromal cell fate and local inflammation.

*What other potential mechanisms are revealed by the RNA-seq data?*

RNA-sequencing and GSEA have identified critical pathways that are involved in mTORC1-dependent skeletal regulation of glucose homeostasis, including upregulation of glycolysis and glucose oxidation pathways in the bone of *Rptor<sub>ob</sub><sup>-/-</sup>* mice. Somewhat surprisingly, muscle-related pathways (Supplementary Table 3.4) were found to be significantly enriched (i.e. upregulated) in the long bones of *Rptor<sub>ob</sub><sup>-/-</sup>* mice, despite all the muscle having been stripped from the tibia/femur during dissection such that no muscle was present when RNA was isolated from the flushed cortical and trabecular bone. Upon examination of the literature, at least two studies have reported expressions of muscle-related genes in the bone cell population. In the first study, the authors utilised a dual GFP reporter to selectively isolate mature OBs and osteocytes and, using RNA-seq, identified muscle-related genes as being highly expressed in pre-osteocytes and osteocytes compared to osteoblasts<sup>113</sup>. In another study, an examination of gene expression patterns in the rat ulnae, following mechanical loading, revealed a downregulation of muscle-related genes, together with TGF- $\beta$  and Wnt/ $\beta$ -catenin signalling, during the synthetic phase of bone formation<sup>114</sup>. In *Rptor<sub>ob</sub><sup>-/-</sup>* mice, RNA-seq and GSEA have identified the coincident upregulation of bone formation and muscle-related genes, which appears to contradict previous reports<sup>114</sup>. As the involvement of muscle-related genes in bone biology is still unclear, this disparity could be due to the condition of the animals (subjected to mechanical loading) or heterogeneity of the bone cell populations whereby the RNA of *Rptor<sub>ob</sub><sup>-/-</sup>* mice could contain a higher proportion of osteocytes.

Another interesting positively enriched pathway identified in the long bones of *Rptor<sub>ob</sub><sup>-/-</sup>* mice were calcium signalling pathways, in particular, Sarco/Endo-plasmic reticulum (SR/ER) Ca<sup>2+</sup>-ATPase (SERCA) which transfers Ca<sup>2+</sup> from the sarcoplasm into the lumen of the sarcoplasmic reticulum, hydrolysing ATP and generating heat in the



process<sup>115</sup>. It is possible that the upregulation of this pathway in the bone of *Rptor<sub>ob</sub><sup>-/-</sup>* mice could provide an additional mechanism underlying their resistance to obesity in addition to the increase browning of their white adipose depots.

While there are three distinct genes that encode SERCA isoforms and the physiological function of each isoform remains unclear, SERCA1 gene is expressed exclusively in fast skeletal muscle and is essential for non-shivering thermogenesis. In contrast, SERCA3 and SERCA2b genes are expressed in blood platelets and lymphoid tissues<sup>116,117,118</sup>. A recent study has reported a role for SERCA2b, in beige adipocytes, in the elevation of energy expenditure and glucose oxidation in an UCP1-independent manner<sup>119</sup>. RNA-seq analysis revealed significant upregulation of the *Atp2a1* gene, which encodes for SERCA1, while GSEA identifies positive enrichment of pathways involved in SR-Ca<sup>2+</sup> transport, release of Ca<sup>2+</sup> and cardiac muscle contraction in the bone of *Rptor<sub>ob</sub><sup>-/-</sup>* mice. In regard to mTORC1, rapamycin-mediated inhibition of mTORC1 has been shown to enhance autophagy by remodelling of intracellular Ca<sup>2+</sup> signalling machinery<sup>120</sup> and attenuated ER-stressed induced apoptosis in IRE1-JNK signalling manner<sup>121,122</sup>. Furthermore, activation of the SERCA pump has been reported in response to ER stress<sup>123,124</sup> and is involved in the initial phase of autophagy<sup>125</sup> suggesting the potential molecular connection between mTORC1 and SERCAs. The expression and specific function of SERCA1 in bone cells is currently unknown. Western blot could be used to confirm the increase of SERCA1 at the protein levels in the bone of *Rptor<sub>ob</sub><sup>-/-</sup>* mice while *in vitro* confirmation of *Atp2a1* expression and its cellular location (by qRT-PCR and immunocytochemistry) could be performed on *Rptor* KO OBs. Depletion of SERCA1 in primary OBs culture by lentivirus shRNA or CRISPR/Cas9 genome editing, followed by functional assays including oxygen consumption assays, intracellular Ca<sup>2+</sup> flux assays, and glucose uptake and oxidation assays could be performed to gain further understanding of the role of SERCA1 in OB biology and potential novel roles for the skeleton in non-shivering thermogenesis.

### 4.3 Conclusion

Over-nutrition causes hyper-activation of mTORC1-dependent negative feedback loops leading to down-regulation of insulin signalling and development of insulin resistance. In OBs, insulin signalling plays a crucial role in the control of systemic glucose homeostasis. To investigate a role of OB-mTORC1 in the regulation of glucose metabolism, mice with an OB-specific deletion of *Rptor* (*Rptor<sub>ob</sub><sup>-/-</sup>*) were generated. Compared to the controls, *Rptor<sub>ob</sub><sup>-/-</sup>* mice had substantially less fat mass and exhibited adipocyte hyperplasia. Remarkably, they were also protected from diet-induced obesity and exhibited improved glucose metabolism with lower fasting glucose and insulin levels, increased glucose tolerance and insulin sensitivity. This leanness and resistance to weight gain was not attributable to changes in food intake, physical activity or lipid absorption but instead was due to increased energy expenditure and greater whole-body substrate flexibility. RNA-seq revealed an increase in glycolysis and skeletal insulin signalling pathways, which correlated with potentiation of insulin signalling and increased insulin-dependent glucose uptake in *Rptor*-knockout osteoblasts. Collectively, these findings point to a critical role for the mTORC1 complex in the skeletal regulation of whole-body glucose metabolism and the skeletal development of insulin resistance.

#### 4.4 References

1. Wild S, Roglic G, Green A, Sicree R, King H. Global prevalence of diabetes: estimates for the year 2000 and projections for 2030. *Diabetes Care* **27**, 1047-1053 (2004).
2. Fonseca VA. Defining and characterizing the progression of type 2 diabetes. *Diabetes care* **32 Suppl 2**, S151-S156 (2009).
3. Muoio DM, Newgard CB. Mechanisms of disease: Molecular and metabolic mechanisms of insulin resistance and beta-cell failure in type 2 diabetes. *Nat Rev Mol Cell Biol* **9**, 193-205 (2008).
4. Lee NK, *et al.* Endocrine regulation of energy metabolism by the skeleton. *Cell* **130**, 456-469 (2007).
5. Ferron M, Hinoi E, Karsenty G, Ducy P. Osteocalcin differentially regulates beta cell and adipocyte gene expression and affects the development of metabolic diseases in wild-type mice. *Proc Natl Acad Sci U S A* **105**, 5266-5270 (2008).
6. Ferron M, *et al.* Insulin signaling in osteoblasts integrates bone remodeling and energy metabolism. *Cell* **142**, 296-308 (2010).
7. Wei J, *et al.* Bone-specific insulin resistance disrupts whole-body glucose homeostasis via decreased osteocalcin activation. *The Journal of Clinical Investigation* **124**, 1781-1793 (2014).
8. Ma X. M. B.J. Molecular mechanisms of mTOR-mediated translational control. *Cell Mol Biol* **10**, 307-318 (2009).
9. Fitter S, *et al.* mTORC1 Plays an Important Role in Skeletal Development by Controlling Preosteoblast Differentiation. *Molecular and Cellular Biology* **37**, e00668-00616 (2017).
10. Devlin MJ. Why does starvation make bones fat? *Am J Hum Biol* **23**, 577-585 (2011).
11. Devlin MJ, *et al.* Caloric restriction leads to high marrow adiposity and low bone mass in growing mice. *J Bone Miner Res* **25**, 2078-2088 (2010).
12. Bredella MA, *et al.* Increased bone marrow fat in anorexia nervosa. *J Clin Endocrinol Metab* **94**, 2129-2136 (2009).
13. Doucette CR, *et al.* A High Fat Diet Increases Bone Marrow Adipose Tissue (MAT) But Does Not Alter Trabecular or Cortical Bone Mass in C57BL/6J Mice. *J Cell Physiol* **230**, 2032-2037 (2015).
14. Hamrick MW, Pennington C, Newton D, Xie D, Isaacs C. Leptin deficiency produces contrasting phenotypes in bones of the limb and spine. *Bone* **34**, 376-383 (2004).
15. Cawthorn WP, *et al.* Bone marrow adipose tissue is an endocrine organ that contributes to increased circulating adiponectin during caloric restriction. *Cell Metab* **20**, 368-375 (2014).
16. Cawthorn WP, *et al.* Expansion of Bone Marrow Adipose Tissue During Caloric Restriction Is Associated With Increased Circulating Glucocorticoids and Not With Hypoleptinemia. *Endocrinology* **157**, 508-521 (2016).
17. Anderson RM, Weindruch R. Metabolic reprogramming, caloric restriction and aging. *Trends in endocrinology and metabolism: TEM* **21**, 134-141 (2010).
18. Lefevre M, *et al.* Caloric restriction alone and with exercise improves CVD risk in healthy non-obese individuals. *Atherosclerosis* **203**, 206-213 (2009).
19. Larson-Meyer DE, *et al.* Effect of calorie restriction with or without exercise on insulin sensitivity, beta-cell function, fat cell size, and ectopic lipid in overweight subjects. *Diabetes Care* **29**, 1337-1344 (2006).

20. Cerletti M, Jang YC, Finley LW, Haigis MC, Wagers AJ. Short-term calorie restriction enhances skeletal muscle stem cell function. *Cell Stem Cell* **10**, 515-519 (2012).
21. Inoki K, Zhu T, Guan KL. TSC2 mediates cellular energy response to control cell growth and survival. *Cell* **115**, 577-590 (2003).
22. Gwinn DM, *et al.* AMPK phosphorylation of raptor mediates a metabolic checkpoint. *Mol Cell* **30**, 214-226 (2008).
23. Harrison DE, *et al.* Rapamycin fed late in life extends lifespan in genetically heterogeneous mice. *Nature* **460**, 392-395 (2009).
24. Neff F, *et al.* Rapamycin extends murine lifespan but has limited effects on aging. *J Clin Invest* **123**, 3272-3291 (2013).
25. Bitto A, *et al.* Transient rapamycin treatment can increase lifespan and healthspan in middle-aged mice. *Elife* **5**, (2016).
26. Selman C, *et al.* Ribosomal protein S6 kinase 1 signaling regulates mammalian life span. *Science* **326**, 140-144 (2009).
27. Henry BA, Goding JW, Tilbrook AJ, Dunshea FR, Clarke IJ. Intracerebroventricular infusion of leptin elevates the secretion of luteinising hormone without affecting food intake in long-term food-restricted sheep, but increases growth hormone irrespective of bodyweight. *J Endocrinol* **168**, 67-77 (2001).
28. Govic A, Levay EA, Hazi A, Penman J, Kent S, Paolini AG. Alterations in male sexual behaviour, attractiveness and testosterone levels induced by an adult-onset calorie restriction regimen. *Behavioural Brain Research* **190**, 140-146 (2008).
29. Sirotkin AV, *et al.* Effects of chronic food restriction and treatments with leptin or ghrelin on different reproductive parameters of male rats. *Peptides* **29**, 1362-1368 (2008).
30. Oury F, *et al.* Endocrine regulation of male fertility by the skeleton. *Cell* **144**, 796-809 (2011).
31. Oury F, *et al.* Maternal and offspring pools of osteocalcin influence brain development and functions. *Cell* **155**, 228-241 (2013).
32. Godart N, *et al.* Mood disorders in eating disorder patients: Prevalence and chronology of ONSET. *J Affect Disord* **185**, 115-122 (2015).
33. Cryan JF, Mombereau C. In search of a depressed mouse: utility of models for studying depression-related behavior in genetically modified mice. *Mol Psychiatry* **9**, 326-357 (2004).
34. Shah OJ, Wang Z, Hunter T. Inappropriate activation of the TSC/Rheb/mTOR/S6K cassette induces IRS1/2 depletion, insulin resistance, and cell survival deficiencies. *Current biology : CB* **14**, 1650-1656 (2004).
35. Toniazzo AP, *et al.* Sex-specific effects of prepubertal stress and high-fat diet on leptin signaling in rats. *Nutrition (Burbank, Los Angeles County, Calif)* **50**, 18-25 (2018).
36. Morselli E, Criollo A, Rodriguez-Navas C, Clegg DJ. Chronic High Fat Diet Consumption Impairs Metabolic Health of Male Mice. *Inflammation and cell signaling* **1**, e561 (2014).
37. Asha GV, Raja Gopal Reddy M, Mahesh M, Vajreswari A, Jeyakumar SM. Male mice are susceptible to high fat diet-induced hyperglycaemia and display increased circulatory retinol binding protein 4 (RBP4) levels and its expression in visceral adipose depots. *Archives of physiology and biochemistry* **122**, 19-26 (2016).
38. Jacobson L, Ansari T, McGuinness OP. Counterregulatory deficits occur within 24 h of a single hypoglycemic episode in conscious, unrestrained, chronically

- cannulated mice. *American journal of physiology Endocrinology and metabolism* **290**, E678-E684 (2006).
39. Berglund ED, *et al.* Glucose metabolism in vivo in four commonly used inbred mouse strains. *Diabetes* **57**, 1790-1799 (2008).
  40. Ayala JE, *et al.* Standard operating procedures for describing and performing metabolic tests of glucose homeostasis in mice. *Disease Models & Mechanisms* **3**, 525-534 (2010).
  41. Rached MT, *et al.* FoxO1 expression in osteoblasts regulates glucose homeostasis through regulation of osteocalcin in mice. *J Clin Invest* **120**, 357-368 (2010).
  42. Cao JJ, Sun L, Gao H. Diet-induced obesity alters bone remodeling leading to decreased femoral trabecular bone mass in mice. *Annals of the New York Academy of Sciences* **1192**, 292-297 (2010).
  43. Yoshikawa Y, *et al.* Genetic evidence points to an osteocalcin-independent influence of osteoblasts on energy metabolism. *J Bone Miner Res* **26**, 2012-2025 (2011).
  44. Gillespie JR, *et al.* GSK-3 $\beta$  Function in Bone Regulates Skeletal Development, Whole-Body Metabolism, and Male Life Span. *Endocrinology* **154**, 3702-3718 (2013).
  45. Yao Q, Yu C, Zhang X, Zhang K, Guo J, Song L. Wnt/beta-catenin signaling in osteoblasts regulates global energy metabolism. *Bone* **97**, 175-183 (2017).
  46. Dirckx N, *et al.* Vhl deletion in osteoblasts boosts cellular glycolysis and improves global glucose metabolism. *J Clin Invest* **128**, 1087-1105 (2018).
  47. Sano H, *et al.* Insulin-stimulated phosphorylation of a Rab GTPase-activating protein regulates GLUT4 translocation. *J Biol Chem* **278**, 14599-14602 (2003).
  48. Miinea CP, *et al.* AS160, the Akt substrate regulating GLUT4 translocation, has a functional Rab GTPase-activating protein domain. *Biochem J* **391**, 87-93 (2005).
  49. Borle AB, Nichols N, Nichols G, Jr. Metabolic studies of bone in vitro. I. Normal bone. *J Biol Chem* **235**, 1206-1210 (1960).
  50. Felix R, Neuman WF, Fleisch H. Aerobic glycolysis in bone: lactic acid production by rat calvaria cells in culture. *Am J Physiol* **234**, C51-55 (1978).
  51. Thomas DM, Rogers SD, Ng KW, Best JD. Dexamethasone modulates insulin receptor expression and subcellular distribution of the glucose transporter GLUT 1 in UMR 106-01, a clonal osteogenic sarcoma cell line. *J Mol Endocrinol* **17**, 7-17 (1996).
  52. Thomas DM, Maher F, Rogers SD, Best JD. Expression and regulation by insulin of GLUT 3 in UMR 106-01, a clonal rat osteosarcoma cell line. *Biochem Biophys Res Commun* **218**, 789-793 (1996).
  53. Zoch ML, Abou DS, Clemens TL, Thorek DLJ, Riddle RC. In vivo radiometric analysis of glucose uptake and distribution in mouse bone. *Bone Research* **4**, 16004 (2016).
  54. Li Z, *et al.* Glucose Transporter-4 Facilitates Insulin-Stimulated Glucose Uptake in Osteoblasts. *Endocrinology* **157**, 4094-4103 (2016).
  55. Wei J, *et al.* Glucose Uptake and Runx2 Synergize to Orchestrate Osteoblast Differentiation and Bone Formation. *Cell* **161**, 1576-1591 (2015).
  56. Ebert BL, Firth JD, Ratcliffe PJ. Hypoxia and mitochondrial inhibitors regulate expression of glucose transporter-1 via distinct Cis-acting sequences. *J Biol Chem* **270**, 29083-29089 (1995).
  57. Semenza GL. Hypoxia-inducible factors in physiology and medicine. *Cell* **148**, 399-408 (2012).

58. Osthus RC, *et al.* Deregulation of glucose transporter 1 and glycolytic gene expression by c-Myc. *J Biol Chem* **275**, 21797-21800 (2000).
59. Yun J, *et al.* Glucose deprivation contributes to the development of KRAS pathway mutations in tumor cells. *Science* **325**, 1555-1559 (2009).
60. Mohyeldin A, Garzon-Muvdi T, Quinones-Hinojosa A. Oxygen in stem cell biology: a critical component of the stem cell niche. *Cell Stem Cell* **7**, 150-161 (2010).
61. Riddle RC, Khatri R, Schipani E, Clemens TL. Role of hypoxia-inducible factor-1alpha in angiogenic-osteogenic coupling. *J Mol Med (Berl)* **87**, 583-590 (2009).
62. Schipani E, Maes C, Carmeliet G, Semenza GL. Regulation of osteogenesis-angiogenesis coupling by HIFs and VEGF. *J Bone Miner Res* **24**, 1347-1353 (2009).
63. Jaakkola P, *et al.* Targeting of HIF-alpha to the von Hippel-Lindau ubiquitylation complex by O<sub>2</sub>-regulated prolyl hydroxylation. *Science* **292**, 468-472 (2001).
64. Kucejova B, *et al.* Interplay between pVHL and mTORC1 pathways in clear-cell renal cell carcinoma. *Mol Cancer Res* **9**, 1255-1265 (2011).
65. DeYoung MP, Horak P, Sofer A, Sgroi D, Ellisen LW. Hypoxia regulates TSC1/2-mTOR signaling and tumor suppression through REDD1-mediated 14-3-3 shuttling. *Genes & development* **22**, 239-251 (2008).
66. Warburg O. On the origin of cancer cells. *Science* **123**, 309-314 (1956).
67. Conigrave AD, Brown EM, Rizzoli R. Dietary protein and bone health: roles of amino acid-sensing receptors in the control of calcium metabolism and bone homeostasis. *Annu Rev Nutr* **28**, 131-155 (2008).
68. Yang X, *et al.* ATF4 is a substrate of RSK2 and an essential regulator of osteoblast biology; implication for Coffin-Lowry Syndrome. *Cell* **117**, 387-398 (2004).
69. Eleftheriou F, *et al.* ATF4 mediation of NF1 functions in osteoblast reveals a nutritional basis for congenital skeletal dysplasias. *Cell Metab* **4**, 441-451 (2006).
70. Kevorkova O, Martineau C, Martin-Falstra L, Sanchez-Dardon J, Brissette L, Moreau R. Low-bone-mass phenotype of deficient mice for the cluster of differentiation 36 (CD36). *PLoS One* **8**, e77701 (2013).
71. Kim SP, *et al.* Fatty acid oxidation by the osteoblast is required for normal bone acquisition in a sex- and diet-dependent manner. *JCI Insight* **2**, e92704 (2017).
72. Frey JL, *et al.* Wnt-Lrp5 signaling regulates fatty acid metabolism in the osteoblast. *Mol Cell Biol* **35**, 1979-1991 (2015).
73. Kim SP, Frey JL, Li Z, Goh BC, Riddle RC. Lack of Lrp5 Signaling in Osteoblasts Sensitizes Male Mice to Diet-Induced Disturbances in Glucose Metabolism. *Endocrinology* **158**, 3805-3816 (2017).
74. Guridi M, *et al.* Alterations to mTORC1 signaling in the skeletal muscle differentially affect whole-body metabolism. *Skelet Muscle* **6**, 13-13 (2016).
75. Bentzinger CF, *et al.* Skeletal muscle-specific ablation of raptor, but not of rictor, causes metabolic changes and results in muscle dystrophy. *Cell Metab* **8**, 411-424 (2008).
76. Umemura A, *et al.* Liver Damage, Inflammation, and Enhanced Tumorigenesis after Persistent mTORC1 Inhibition. *Cell Metab* **20**, 133-144 (2014).
77. Polak P, Cybulski N, Feige JN, Auwerx J, Ruegg MA, Hall MN. Adipose-specific knockout of raptor results in lean mice with enhanced mitochondrial respiration. *Cell Metab* **8**, 399-410 (2008).

78. Lee KY, *et al.* Lessons on Conditional Gene Targeting in Mouse Adipose Tissue. *Diabetes* **62**, 864-874 (2013).
79. Jeffery E, *et al.* Characterization of Cre recombinase models for the study of adipose tissue. *Adipocyte* **3**, 206-211 (2014).
80. Mullican SE, Tomaru T, Gaddis CA, Peed LC, Sundaram A, Lazar MA. A Novel Adipose-Specific Gene Deletion Model Demonstrates Potential Pitfalls of Existing Methods. *Molecular Endocrinology* **27**, 127-134 (2013).
81. Lee PL, Tang Y, Li H, Guertin DA. Raptor/mTORC1 loss in adipocytes causes progressive lipodystrophy and fatty liver disease. *Molecular metabolism* **5**, 422-432 (2016).
82. Tremblay F, Marette A. Amino acid and insulin signaling via the mTOR/p70 S6 kinase pathway. A negative feedback mechanism leading to insulin resistance in skeletal muscle cells. *J Biol Chem* **276**, 38052-38060 (2001).
83. Chang GR, *et al.* Rapamycin protects against high fat diet-induced obesity in C57BL/6J mice. *J Pharmacol Sci* **109**, 496-503 (2009).
84. Liu Y, *et al.* Rapamycin-induced metabolic defects are reversible in both lean and obese mice. *Aging (Albany NY)* **6**, 742-754 (2014).
85. Chang GR, *et al.* Long-term administration of rapamycin reduces adiposity, but impairs glucose tolerance in high-fat diet-fed KK/HIJ mice. *Basic Clin Pharmacol Toxicol* **105**, 188-198 (2009).
86. Lamming DW, *et al.* Rapamycin-induced insulin resistance is mediated by mTORC2 loss and uncoupled from longevity. *Science (New York, NY)* **335**, 1638-1643 (2012).
87. Houde VP, *et al.* Chronic rapamycin treatment causes glucose intolerance and hyperlipidemia by upregulating hepatic gluconeogenesis and impairing lipid deposition in adipose tissue. *Diabetes* **59**, 1338-1348 (2010).
88. Sarbassov DD, *et al.* Prolonged Rapamycin Treatment Inhibits mTORC2 Assembly and Akt/PKB. *Molecular Cell* **22**, 159-168 (2006).
89. Rodriguez KA, Dodds SG, Strong R, Galvan V, Sharp ZD, Buffenstein R. Divergent tissue and sex effects of rapamycin on the proteasome-chaperone network of old mice. *Frontiers in Molecular Neuroscience* **7**, (2014).
90. Rodda SJ, McMahon AP. Distinct roles for Hedgehog and canonical Wnt signaling in specification, differentiation and maintenance of osteoblast progenitors. *Development* **133**, 3231 (2006).
91. Schöning K, Schwenk F, Rajewsky K, Bujard H. Stringent doxycycline dependent control of CRE recombinase in vivo. *Nucleic acids research* **30**, e134-e134 (2002).
92. Zhou X, *et al.* Multiple functions of Osterix are required for bone growth and homeostasis in postnatal mice. *Proc Natl Acad Sci U S A* **107**, 12919-12924 (2010).
93. Mahoney SJ, *et al.* A small molecule inhibitor of Rheb selectively targets mTORC1 signaling. *Nat Commun* **9**, 548 (2018).
94. Drake MT, Clarke BL, Khosla S. Bisphosphonates: mechanism of action and role in clinical practice. *Mayo Clin Proc* **83**, 1032-1045 (2008).
95. Cole LE, Vargo-Gogola T, Roeder RK. Targeted delivery to bone and mineral deposits using bisphosphonate ligands. *Adv Drug Deliv Rev* **99**, 12-27 (2016).
96. Martin B, *et al.* Sex-dependent metabolic, neuroendocrine, and cognitive responses to dietary energy restriction and excess. *Endocrinology* **148**, 4318-4333 (2007).
97. Fisher FM, *et al.* FGF21 regulates PGC-1alpha and browning of white adipose tissues in adaptive thermogenesis. *Genes & development* **26**, 271-281 (2012).

98. Bostrom P, *et al.* A PGC1-alpha-dependent myokine that drives brown-fat-like development of white fat and thermogenesis. *Nature* **481**, (2012).
99. Fulzele K, *et al.* Osteocyte-Secreted Wnt Signaling Inhibitor Sclerostin Contributes to Beige Adipogenesis in Peripheral Fat Depots. *J Bone Miner Res* **32**, 373-384 (2017).
100. Brun J, Berthou F, Trajkovski M, Maechler P, Foti M, Bonnet N. Bone Regulates Browning and Energy Metabolism Through Mature Osteoblast/Osteocyte PPARgamma Expression. *Diabetes* **66**, 2541-2554 (2017).
101. Carriere A, *et al.* Browning of white adipose cells by intermediate metabolites: an adaptive mechanism to alleviate redox pressure. *Diabetes* **63**, 3253-3265 (2014).
102. Flanagan B, Nichols G, Jr. METABOLIC STUDIES OF BONE IN VITRO. V. GLUCOSE METABOLISM AND COLLAGEN BIOSYNTHESIS. *J Biol Chem* **239**, 1261-1265 (1964).
103. Krings A, Rahman S, Huang S, Lu Y, Czernik PJ, Lecka-Czernik B. Bone marrow fat has brown adipose tissue characteristics, which are attenuated with aging and diabetes. *Bone* **50**, 546-552 (2012).
104. Lecka-Czernik B, Stechschulte LA, Czernik PJ, Sherman SB, Huang S, Krings A. Marrow Adipose Tissue: Skeletal Location, Sexual Dimorphism, and Response to Sex Steroid Deficiency. *Front Endocrinol (Lausanne)* **8**, 188 (2017).
105. Bain JR, Stevens RD, Wenner BR, Ilkayeva O, Muoio DM, Newgard CB. Metabolomics applied to diabetes research: moving from information to knowledge. *Diabetes* **58**, 2429-2443 (2009).
106. Sheu Y, *et al.* Vertebral bone marrow fat, bone mineral density and diabetes: The Osteoporotic Fractures in Men (MrOS) study. *Bone* **97**, 299-305 (2017).
107. Cohen A, *et al.* Abdominal fat is associated with lower bone formation and inferior bone quality in healthy premenopausal women: a transiliac bone biopsy study. *J Clin Endocrinol Metab* **98**, 2562-2572 (2013).
108. Baum T, *et al.* Does vertebral bone marrow fat content correlate with abdominal adipose tissue, lumbar spine bone mineral density, and blood biomarkers in women with type 2 diabetes mellitus? *J Magn Reson Imaging* **35**, 117-124 (2012).
109. Moayeri A, Mohamadpour M, Mousavi SF, Shirzadpour E, Mohamadpour S, Amraei M. Fracture risk in patients with type 2 diabetes mellitus and possible risk factors: a systematic review and meta-analysis. *Ther Clin Risk Manag* **13**, 455-468 (2017).
110. Vestergaard P. Discrepancies in bone mineral density and fracture risk in patients with type 1 and type 2 diabetes--a meta-analysis. *Osteoporosis international : a journal established as result of cooperation between the European Foundation for Osteoporosis and the National Osteoporosis Foundation of the USA* **18**, 427-444 (2007).
111. Leite Duarte ME, da Silva RD. [Histomorphometric analysis of the bone tissue in patients with non-insulin-dependent diabetes (DMNID)]. *Revista do Hospital das Clinicas* **51**, 7-11 (1996).
112. Riddle R, *et al.* Tsc2 Is a Molecular Checkpoint Controlling Osteoblast Development and Glucose Homeostasis. *Molecular and Cellular Biology* **34**, 1850-1862 (2014).
113. Paic F, *et al.* Identification of differentially expressed genes between osteoblasts and osteocytes. *Bone* **45**, 682-692 (2009).
114. Mantila Roosa SM, Liu Y, Turner CH. Gene expression patterns in bone following mechanical loading. *Journal of bone and mineral research : the*



- official journal of the American Society for Bone and Mineral Research* **26**, 100-112 (2011).
115. MEIS LD. Energy interconversion by the sarcoplasmic reticulum Ca<sup>2+</sup>-ATPase: ATP hydrolysis, Ca<sup>2+</sup> transport, ATP synthesis and heat production. *Anais da Academia Brasileira de Ciências* **72**, 365-379 (2000).
  116. Wuytack F, *et al.* A sarco/endoplasmic reticulum Ca(2+)-ATPase 3-type Ca<sup>2+</sup> pump is expressed in platelets, in lymphoid cells, and in mast cells. *J Biol Chem* **269**, 1410-1416 (1994).
  117. MacLennan DH, Brandl CJ, Korczak B, Green NM. Amino-acid sequence of a Ca<sup>2+</sup> + Mg<sup>2+</sup>-dependent ATPase from rabbit muscle sarcoplasmic reticulum, deduced from its complementary DNA sequence. *Nature* **316**, 696-700 (1985).
  118. Lytton J, Westlin M, Burk SE, Shull GE, MacLennan DH. Functional comparisons between isoforms of the sarcoplasmic or endoplasmic reticulum family of calcium pumps. *J Biol Chem* **267**, 14483-14489 (1992).
  119. Ikeda K, *et al.* UCP1-independent signaling involving SERCA2b-mediated calcium cycling regulates beige fat thermogenesis and systemic glucose homeostasis. *Nat Med* **23**, 1454-1465 (2017).
  120. Decuyper J-P, *et al.* mTOR-Controlled Autophagy Requires Intracellular Ca<sup>2+</sup> Signaling. *PLoS One* **8**, e61020 (2013).
  121. Kato H, Nakajima S, Saito Y, Takahashi S, Katoh R, Kitamura M. mTORC1 serves ER stress-triggered apoptosis via selective activation of the IRE1–JNK pathway. *Cell Death & Differentiation* **19**, 310-320 (2012).
  122. Ozcan U, *et al.* Loss of the Tuberous Sclerosis Complex Tumor Suppressors Triggers the Unfolded Protein Response to Regulate Insulin Signaling and Apoptosis. *Molecular Cell* **29**, 541-551 (2008).
  123. Højmann Larsen A, Frandsen A, Treiman M. Upregulation of the SERCA-type Ca<sup>2+</sup> pump activity in response to endoplasmic reticulum stress in PC12 cells. *BMC Biochem* **2**, 4-4 (2001).
  124. Caspersen C, Pedersen PS, Treiman M. The sarco/endoplasmic reticulum calcium-ATPase 2b is an endoplasmic reticulum stress-inducible protein. *J Biol Chem* **275**, 22363-22372 (2000).
  125. Zhao YG, *et al.* The ER-Localized Transmembrane Protein EPG-3/VMP1 Regulates SERCA Activity to Control ER-Isolation Membrane Contacts for Autophagosome Formation. *Mol Cell* **67**, 974-989 e976 (2017).

# APPENDIX I: GSEA REPORT FOR POSITIVELY ENRICHED GENE SETS

NAME	SIZE	ES	NES	NOM p-val	FDR q-val	FWER p-val	RANK AT MAX	LEADING EDGE
GO_MYOFIBRIL_ASSEMBLY	58	0.874524	2.135557	0	0	0	1065	tags=71%, list=7%, signal=76%
GO_CELLULAR_COMPONENT_ASSEMBLY_INVOLVED_IN_MORPHOGENESIS	88	0.827517	2.073096	0	0	0	1065	tags=51%, list=7%, signal=55%
GO_MULTICELLULAR_ORGANISMAL_MOVEMENT	44	0.86768	2.072549	0	0	0	1021	tags=57%, list=7%, signal=61%
GO_SARCOMERE_ORGANIZATION	37	0.881661	2.051726	0	0	0	1065	tags=76%, list=7%, signal=81%
GO_MUSCLE_FILAMENT_SLIDING	35	0.884341	2.020663	0	0	0	1021	tags=74%, list=7%, signal=80%
GO_SKELETAL_MUSCLE_CONTRACTION	34	0.879661	2.011898	0	0	0	1021	tags=68%, list=7%, signal=73%
GO_MUSCLE_CELL_DEVELOPMENT	143	0.787669	2.009729	0	0	0	1232	tags=46%, list=9%, signal=50%
GO_MUSCLE_CONTRACTION	259	0.760367	1.99408	0	0	0	1356	tags=40%, list=9%, signal=44%
GO_MUSCLE_FIBER_DEVELOPMENT	60	0.806744	1.96499	0	0	0	1232	tags=55%, list=9%, signal=60%
GO_STRIATED_MUSCLE_CONTRACTION	131	0.768407	1.961853	0	0	0	1132	tags=42%, list=8%, signal=45%
GO_ACTIN_MEDIATED_CELL_CONTRACTION	91	0.778766	1.956403	0	0	0	1132	tags=47%, list=8%, signal=51%
GO_MUSCLE_SYSTEM_PROCESS	336	0.731569	1.926685	0	0	0	1565	tags=37%, list=11%, signal=40%
GO_CARDIAC_CELL_DEVELOPMENT	67	0.773606	1.920179	0	0	0	1141	tags=37%, list=8%, signal=40%
GO_CARDIAC_MYOFIBRIL_ASSEMBLY	23	0.878425	1.909077	0	0	0	1065	tags=65%, list=7%, signal=70%
GO_STRIATED_MUSCLE_CELL_DIFFERENTIATION	213	0.734499	1.908431	0	0	0	1634	tags=40%, list=11%, signal=44%
GO_MUSCLE_CELL_DIFFERENTIATION	278	0.728558	1.908281	0	0	0	1634	tags=38%, list=11%, signal=42%
GO_SARCOPLASMIC_RETICULUM_CALCIIUM_ION_TRANSPORT	33	0.841039	1.902377	0	4.49E-05	0.001	879	tags=45%, list=6%, signal=48%
GO_RELEASE_OF_SEQUESTERED_CALCIIUM_ION_INTO_CYTOSOL_BY_ENDOPLASMIC_RETICULUM	29	0.831656	1.88302	0	8.49E-05	0.002	879	tags=45%, list=6%, signal=48%
GO_HEART_PROCESS	190	0.730881	1.868629	0	2.42E-04	0.006	1132	tags=35%, list=8%, signal=38%
GO_REGULATION_OF_MUSCLE_CONTRACTION	111	0.724481	1.864766	0	2.29E-04	0.006	1183	tags=34%, list=8%, signal=37%
GO_CARDIAC_MUSCLE_CONTRACTION	102	0.727263	1.850618	0	4.72E-04	0.013	1132	tags=35%, list=8%, signal=38%
GO_CARDIAC_CONDUCTION	9	0.737995	1.845661	0	5.20E-04	0.015	1613	tags=40%, list=11%, signal=45%
GO_CARDIAC_MUSCLE_FIBER_DEVELOPMENT	16	0.90331	1.844665	0	4.97E-04	0.015	1141	tags=75%, list=8%, signal=81%
GO_CARDIAC_MUSCLE_TISSUE_MORPHOGENESIS	51	0.767312	1.839425	0	6.36E-04	0.02	1065	tags=41%, list=7%, signal=44%
GO_MULTICELLULAR_ORGANISMAL_SIGNALING	117	0.721578	1.83437	0	7.03E-04	0.023	1613	tags=39%, list=11%, signal=43%
GO_REGULATION_OF_STRIATED_MUSCLE_CONTRACTION	70	0.731078	1.833024	0	6.76E-04	0.023	1094	tags=37%, list=8%, signal=40%
GO_EMBRYONIC_SKELETAL_SYSTEM_DEVELOPMENT	90	0.720108	1.832808	0	6.51E-04	0.023	1646	tags=43%, list=11%, signal=49%
GO_MUSCLE_ORGAN_DEVELOPMENT	311	0.699469	1.830396	0	6.82E-04	0.025	1656	tags=35%, list=11%, signal=39%
GO_CARDIAC_MUSCLE_CELL_DIFFERENTIATION	90	0.717582	1.828934	0	6.58E-04	0.025	1943	tags=38%, list=13%, signal=43%
GO_ACTIN_FILAMENT_BASED_MOVEMENT	113	0.72123	1.819367	0	8.15E-04	0.032	1540	tags=43%, list=11%, signal=48%
GO_ACTINMYOSIN_STRUCTURE_ORGANIZATION	163	0.69983	1.81429	0	9.86E-04	0.04	1226	tags=31%, list=8%, signal=33%
GO_SKELETAL_MUSCLE_ADAPTATION	25	0.813331	1.811976	0	0.001003	0.042	1733	tags=56%, list=12%, signal=64%
GO_STRIATED_MUSCLE_ADAPTATION	41	0.780036	1.808718	0	0.001042	0.045	1882	tags=49%, list=13%, signal=56%
GO_MUSCLE_STRUCTURE_DEVELOPMENT	497	0.684107	1.802102	0	0.001281	0.056	1656	tags=34%, list=11%, signal=37%
GO_SKELETAL_MUSCLE_ORGAN_DEVELOPMENT	140	0.692397	1.797582	0	0.001485	0.066	1569	tags=36%, list=11%, signal=40%
GO_MYOTUBE_DIFFERENTIATION	79	0.721135	1.796398	0	0.001465	0.066	1569	tags=35%, list=11%, signal=40%
GO_REGULATION_OF_BLOOD_CIRCULATION	182	0.692022	1.7945	0	0.001487	0.069	1735	tags=36%, list=12%, signal=41%
GO_MUSCLE_TISSUE_DEVELOPMENT	310	0.682255	1.784846	0	0.002111	0.1	1634	tags=34%, list=11%, signal=37%
GO_REGULATION_OF_CARDIAC_CONDUCTION	52	0.738143	1.77388	0	0.003037	0.144	1222	tags=37%, list=8%, signal=40%
GO_RESPONSE_TO_CAFFEINE	15	0.874776	1.772527	0	0.003114	0.149	484	tags=40%, list=3%, signal=41%
GO_EMBRYONIC_SKELETAL_SYSTEM_MORPHOGENESIS	70	0.712911	1.770351	0	0.003187	0.156	2119	tags=50%, list=15%, signal=58%
GO_REGULATION_OF_MUSCLE_SYSTEM_PROCESS	171	0.682166	1.769001	0	0.00322	0.161	1183	tags=28%, list=8%, signal=30%
GO_MUSCLE_ORGAN_MORPHOGENESIS	63	0.724217	1.768146	0	0.003287	0.167	1754	tags=43%, list=12%, signal=49%
GO_MEMBRANE_DEPOLARIZATION_DURING_ACTION_POTENTIAL	27	0.799384	1.768055	0	0.003212	0.167	1208	tags=48%, list=8%, signal=52%
GO_CARDIAC_MUSCLE_TISSUE_DEVELOPMENT	165	0.685795	1.766839	0	0.003243	0.172	1634	tags=33%, list=11%, signal=37%
GO_REGULATION_OF_RYANODINE_SENSITIVE_CALCIIUM_RELEASE_CHANNEL_ACTIVITY	23	0.814936	1.764524	0	0.003405	0.184	484	tags=39%, list=3%, signal=40%
GO_COLLAGEN_FIBRIL_ORGANIZATION	48	0.735943	1.763084	0	0.00343	0.189	2418	tags=58%, list=17%, signal=70%
GO_MYOTUBE_CELL_DEVELOPMENT	32	0.762613	1.7609	0	0.003613	0.203	561	tags=31%, list=4%, signal=32%
GO_REGULATION_OF_MEMBRANE_REPOLARIZATION	24	0.802829	1.759001	0	0.003804	0.218	1094	tags=46%, list=8%, signal=50%
GO_REGULATION_OF_HEART_RATE	59	0.720655	1.755107	0	0.00408	0.234	1094	tags=36%, list=8%, signal=38%
GO_RESPIRATORY_ELECTRON_TRANSPORT_CHAIN	104	0.691583	1.753816	0	0.004225	0.247	3428	tags=66%, list=24%, signal=86%
GO_REGULATION_OF_CARDIAC_MUSCLE_CELL_MEMBRANE_REPOLARIZATION	17	0.845133	1.749579	0.001321	0.004893	0.285	879	tags=47%, list=6%, signal=50%
GO_ATP_SYNTHESIS_COUPLED_ELECTRON_TRANSPORT	86	0.699424	1.748337	0	0.004973	0.294	3428	tags=70%, list=24%, signal=91%
GO_REGULATION_OF_SKELETAL_MUSCLE_TISSUE_DEVELOPMENT	44	0.727556	1.745708	0	0.005178	0.309	2245	tags=52%, list=16%, signal=62%
GO_SPECIFICATION_OF_ANIMAL_ORGAN_IDENTITY	22	0.790665	1.745286	0	0.00514	0.311	1965	tags=55%, list=14%, signal=63%
GO_REGULATION_OF_CARDIAC_MUSCLE_CONTRACTION_BY_REGULATION_OF_THE_RELEASE_OF_SEQUESTERED_CALCIIUM_ION	18	0.83624	1.743846	0	0.005226	0.319	879	tags=44%, list=6%, signal=47%
GO_CARDIOCYTE_DIFFERENTIATION	114	0.67798	1.738629	0	0.006086	0.363	1943	tags=37%, list=13%, signal=42%
GO_REGULATION_OF_MYOTUBE_DIFFERENTIATION	44	0.728449	1.73691	0	0.006271	0.38	1569	tags=36%, list=11%, signal=41%
GO_OXIDATIVE_PHOSPHORYLATION	110	0.682384	1.727708	0	0.007759	0.455	3428	tags=64%, list=24%, signal=83%
GO_MITOCHONDRIAL_ELECTRON_TRANSPORT_NADH_TO_UBIQUINONE	49	0.716854	1.726762	0	0.007807	0.464	3428	tags=80%, list=24%, signal=104%
GO_MEMBRANE_REPOLARIZATION	31	0.751839	1.71881	0.002296	0.009384	0.529	1094	tags=39%, list=8%, signal=42%
GO_REGULATION_OF_BONE_MINERALIZATION	56	0.703961	1.715205	0	0.010279	0.569	2036	tags=46%, list=14%, signal=54%
GO_SKELETAL_SYSTEM_MORPHOGENESIS	181	0.658703	1.710685	0	0.011292	0.605	2119	tags=41%, list=15%, signal=47%
GO_POSITIVE_REGULATION_OF_OSTEOBLAST_DIFFERENTIATION	48	0.714156	1.708808	0	0.011665	0.626	2025	tags=44%, list=14%, signal=51%
GO_GLYCAN_METABOLIC_PROCESS	56	0.694625	1.703249	0	0.013143	0.675	1919	tags=34%, list=13%, signal=39%
GO_VENTRICULAR_CARDIAC_MUSCLE_CELL_MEMBRANE_REPOLARIZATION	17	0.821188	1.701771	0	0.013372	0.68	879	tags=47%, list=6%, signal=50%
GO_REGULATION_OF_RELEASE_OF_SEQUESTERED_CALCIIUM_ION_INTO_CYTOSOL	65	0.687602	1.698466	0	0.014541	0.721	879	tags=28%, list=6%, signal=29%
GO_REGULATION_OF_BIOMINERAL_TISSUE_DEVELOPMENT	66	0.687594	1.696248	0	0.014911	0.738	2036	tags=44%, list=14%, signal=51%
GO_MEMBRANE_DEPOLARIZATION_DURING_CARDIAC_MUSCLE_CELL_ACTION_POTENTIAL	20	0.791178	1.694679	0.001242	0.015359	0.755	1208	tags=45%, list=8%, signal=49%
GO_REGULATION_OF_SYSTEM_PROCESS	370	0.645761	1.689712	0	0.01694	0.795	1896	tags=31%, list=13%, signal=35%
GO_REGULATION_OF_CATION_CHANNEL_ACTIVITY	99	0.6631	1.689368	0	0.01682	0.8	1613	tags=32%, list=11%, signal=36%
GO_NEGATIVE_REGULATION_OF_POTASSIUM_ION_TRANSPORT	22	0.781462	1.687621	0	0.017341	0.808	1208	tags=45%, list=8%, signal=50%
GO_REGULATION_OF_SKELETAL_MUSCLE_CELL_DIFFERENTIATION	18	0.787478	1.687115	0.005	0.017302	0.809	1569	tags=56%, list=11%, signal=62%
GO_POSITIVE_REGULATION_OF_BONE_MINERALIZATION	29	0.750386	1.684616	0	0.018059	0.826	2025	tags=55%, list=14%, signal=64%
GO_NADH_DEHYDROGENASE_COMPLEX_ASSEMBLY	61	0.69009	1.683767	0	0.018185	0.831	3659	tags=74%, list=25%, signal=98%
GO_HEART_MORPHOGENESIS	197	0.652064	1.683007	0	0.018238	0.834	1943	tags=36%, list=13%, signal=40%
GO_PROXIMAL_DISTAL_PATTERN_FORMATION	18	0.807013	1.682516	0.001307	0.0182	0.837	1965	tags=61%, list=14%, signal=71%
GO_CARDIAC_MUSCLE_CELL_CONTRACTION	49	0.695931	1.672381	0	0.022413	0.9	1735	tags=41%, list=12%, signal=46%
GO_NEURAL_CREST_CELL_MIGRATION	39	0.713935	1.671032	0	0.022826	0.902	1569	tags=44%, list=11%, signal=49%
GO_POSITIVE_REGULATION_OF_MUSCLE_CELL_DIFFERENTIATION	69	0.668741	1.669604	0	0.023314	0.906	1879	tags=32%, list=13%, signal=36%
GO_POTASSIUM_ION_TRANSPORT	129	0.647245	1.669121	0	0.023272	0.914	1606	tags=29%, list=11%, signal=33%
GO_CELLULAR_CARBOHYDRATE_CATABOLIC_PROCESS	37	0.718089	1.667764	0	0.023631	0.917	902	tags=27%, list=6%, signal=29%
GO_REGULATION_OF_CARDIAC_MUSCLE_CONTRACTION_BY_CALCIIUM_ION_SIGNALING	23	0.773742	1.667255	0.002475	0.02353	0.92	879	tags=35%, list=6%, signal=37%
GO_CELLULAR_RESPONSE_TO_ALKALOID	23	0.768383	1.666581	0	0.023605	0.924	484	tags=26%, list=3%, signal=27%
GO_POSITIVE_REGULATION_OF_HEART_GROWTH	25	0.746515	1.666015	0.001199	0.023598	0.926	1879	tags=36%, list=13%, signal=41%
GO_CALCIIUM_ION_IMPORT	54	0.678389	1.664688	0.002183	0.023998	0.928	1526	tags=31%, list=11%, signal=35%
GO_MEMBRANE_DEPOLARIZATION	62	0.681425	1.664466	0	0.023871	0.929	1735	tags=37%, list=12%, signal=42%
GO_NEURON_PROJECTION_EXTENSION_INVOLVED_IN_NEURON_PROJECTION_GUIDANCE	32	0.723798	1.664199	0.001171	0.023696	0.931	1777	tags=44%, list=12%, signal=50%
GO_NEGATIVE_REGULATION_OF_CALCIIUM_ION_TRANSPORT	43	0.69958	1.664139	0.001114	0.023464	0.932	1232	tags=35%, list=9%, signal=38%
GO_REGULATION_OF_CALCIIUM_ION_TRANSMEMBRANE_TRANSPORTER_ACTIVITY	67	0.675473	1.663606	0	0.023797	0.936	1232	tags=30%, list=9%, signal=32%
GO_MONOSACCHARIDE_BIOSYNTHETIC_PROCESS	75	0.663614	1.662976	0	0.023619	0.936	1793	tags=25%, list=12%, signal=29%
GO_MITOCHONDRIAL_RESPIRATORY_CHAIN_COMPLEX_ASSEMBLY	91	0.652603	1.657615	0	0.026145	0.952	3707	tags=65%, list=26%, signal=87%
GO_POSITIVE_REGULATION_OF_BIOMINERAL_TISSUE_DEVELOPMENT	32	0.723896	1.657541	0.002345	0.025914	0.952	2025	tags=50%, list=14%, signal=58%
GO_TISSUE_REGENERATION	46	0.699566	1.656683	0	0.026068	0.954	1232	tags=30%, list=9%, signal=33%
GO_RESPONSE_TO_MUSCLE_ACTIVITY	21	0.769875	1.65516	0.003812	0.026703	0.961	909	tags=38%, list=6%, signal=41%
GO_GLYCAN_CATABOLIC_PROCESS	21	0.774295	1.654983	0.001248	0.026504	0.961	826	tags=38%, list=6%, signal=40%
GO_NEGATIVE_REGULATION_OF_POTASSIUM_ION_TRANSMEMBRANE_TRANSPORT	17	0.793466	1.654223	0	0.026625	0.964	1208	tags=47%, list=8%, signal=51%
GO_SKELETAL_MUSCLE_CELL_DIFFERENTIATION	56	0.679143	1.65318	0	0.026938	0.969	1569	tags=39%, list=11%, signal=44%
GO_SKELETAL_MUSCLE_TISSUE_REGENERATION	28	0.740599	1.652472	0.001212	0.027052	0.97	1565	tags=36%, list=11%, signal=40%
GO_CELLULAR_RESPIRATION	173	0.635242	1.650799	0	0.027699	0.976	3375	tags=53%, list=23%, signal=69%
GO_DETECTION_OF_MECHANICAL_STIMULUS	24	0.754501	1.648095					

NAME	SIZE	ES	NES	NOM p-val	FDR q-val	FWER p-val	RANK AT MAX	LEADING EDGE
GO_CELL_CELL_SIGNALING_INVOLVED_IN_CARDIAC_CONDUCTION	20	0.763775	1.635443	0.003764	0.035285	0.995	1735	tags=50%, list=12%, signal=57%
GO_RESPONSE_TO_ACTIVITY	54	0.675979	1.635514	0	0.035154	0.995	1891	tags=31%, list=13%, signal=36%
GO_POLYSACCHARIDE_CATABOLIC_PROCESS	24	0.742925	1.63386	0.007566	0.035647	0.997	826	tags=33%, list=6%, signal=35%
GO_COLLAGEN_BIOSYNTHETIC_PROCESS	35	0.707438	1.633439	0.003468	0.03565	0.997	1655	tags=40%, list=11%, signal=45%
GO_CIRCULATORY_SYSTEM_PROCESS	348	0.625237	1.632562	0	0.035897	0.997	1821	tags=29%, list=13%, signal=33%
GO_ELECTRON_TRANSPORT_CHAIN	153	0.635223	1.631563	0	0.036175	0.997	3428	tags=55%, list=24%, signal=71%
GO_POSITIVE_REGULATION_OF_MYOTUBE_DIFFERENTIATION	26	0.73713	1.628319	0.007117	0.03808	0.998	397	tags=27%, list=3%, signal=28%
GO_CARDIAC_MUSCLE_CELL_ACTION_POTENTIAL	48	0.682496	1.627037	0.001094	0.03873	0.998	1735	tags=40%, list=12%, signal=45%
GO_REGULATION_OF_ACTIN_FILAMENT_BASED_MOVEMENT	33	0.710741	1.626865	0.00453	0.038502	0.998	1356	tags=39%, list=9%, signal=43%
GO_NEGATIVE_REGULATION_OF_CALCIUM_MEDIATED_SIGNALING	29	0.725008	1.626569	0.002381	0.038372	0.998	1526	tags=31%, list=11%, signal=37%
GO_SYNAPTIC_MEMBRANE_ADHESION	15	0.791094	1.625272	0.005479	0.038909	0.998	1185	tags=40%, list=8%, signal=44%
GO_CARDIAC_MUSCLE_CELL_MEMBRANE_REPOLARIZATION	23	0.761783	1.624845	0.003741	0.038923	0.998	879	tags=35%, list=6%, signal=37%
GO_RESPONSE_TO_BMP	108	0.635909	1.624572	0	0.03876	0.998	2458	tags=38%, list=17%, signal=45%
GO_POSITIVE_REGULATION_OF_MUSCLE_TISSUE_DEVELOPMENT	55	0.671152	1.62447	0	0.03851	0.998	1916	tags=35%, list=13%, signal=40%
GO_MUSCLE_ADAPTATION	94	0.646	1.622006	0	0.039958	0.999	1882	tags=30%, list=13%, signal=34%
GO_CARDIAC_MUSCLE_CELL_ACTION_POTENTIAL_INVOLVED_IN_CONTRACTION	34	0.70663	1.621741	0.001164	0.039855	0.999	1540	tags=41%, list=11%, signal=46%
GO_NEGATIVE_CHEMOTAXIS	38	0.696704	1.620947	0.002237	0.040056	0.999	1451	tags=37%, list=10%, signal=41%
GO_ENERGY_DERIVATION_BY_OXIDATION_OF_ORGANIC_COMPOUNDS	240	0.624024	1.620275	0	0.040172	0.999	3077	tags=46%, list=21%, signal=58%
GO_POSITIVE_REGULATION_OF_CARDIAC_MUSCLE_CELL_PROLIFERATION	17	0.79289	1.620061	0.004005	0.040044	0.999	1382	tags=41%, list=10%, signal=45%
GO_POSITIVE_REGULATION_OF_OSSIFICATION	64	0.659493	1.619815	0	0.039924	0.999	2025	tags=38%, list=14%, signal=43%
GO_RESPIRATORY_SYSTEM_PROCESS	21	0.742469	1.618936	0.002525	0.040302	0.999	2587	tags=48%, list=18%, signal=58%
GO_POSITIVE_REGULATION_OF_CARTILAGE_DEVELOPMENT	24	0.740228	1.618345	0	0.040395	0.999	2243	tags=46%, list=16%, signal=54%
GO_DORSAL_VENTRAL_PATTERN_FORMATION	46	0.687797	1.618277	0.002278	0.040143	0.999	1425	tags=28%, list=10%, signal=31%
GO_CARTILAGE_DEVELOPMENT	153	0.624017	1.617841	0	0.040109	0.999	2078	tags=39%, list=14%, signal=45%
GO_REGULATION_OF_CALCIUM_ION_TRANSMEMBRANE_TRANSPORT	110	0.632666	1.617447	0	0.040089	1	1232	tags=26%, list=9%, signal=29%
GO_ACTION_POTENTIAL	84	0.640168	1.616388	0	0.040468	1	1735	tags=36%, list=12%, signal=40%
GO TRABECULA MORPHOGENESIS	43	0.689428	1.614299	0.003382	0.041758	1	1487	tags=33%, list=10%, signal=36%
GO_HEART_GROWTH	62	0.662636	1.614094	0.002132	0.041574	1	1382	tags=26%, list=10%, signal=28%
GO_REGULATION_OF_CARDIAC_MUSCLE_CONTRACTION	56	0.663656	1.613227	0.001111	0.041795	1	1356	tags=30%, list=9%, signal=33%
GO TRABECULA FORMATION	21	0.755456	1.612264	0.006112	0.042197	1	785	tags=33%, list=5%, signal=35%
GO_POSITIVE_REGULATION_OF_GLYCOLYTIC_PROCESS	17	0.772689	1.608448	0.010512	0.04467	1	1281	tags=29%, list=9%, signal=32%
GO_HEART_DEVELOPMENT	437	0.611667	1.607455	0	0.045043	1	2659	tags=35%, list=18%, signal=43%
GO_REGULATION_OF_MYOBLAST_DIFFERENTIATION	44	0.679864	1.606196	0.001096	0.045535	1	1952	tags=36%, list=13%, signal=42%
GO_REGULATION_OF_FATTY_ACID_METABOLIC_PROCESS	41	0.681823	1.606176	0.004469	0.045216	1	1549	tags=39%, list=11%, signal=44%
GO_POSITIVE_REGULATION_OF_CATION_CHANNEL_ACTIVITY	43	0.685311	1.606131	0.004484	0.044962	1	1208	tags=33%, list=8%, signal=35%
GO_CELL_FATE_SPECIFICATION	40	0.686753	1.605419	0.002257	0.045225	1	2080	tags=45%, list=14%, signal=52%
GO_ANIMAL_ORGAN_FORMATION	42	0.675091	1.605183	0.001114	0.045083	1	2581	tags=48%, list=18%, signal=58%
GO_NEURAL_CRESCENT_CELL_DIFFERENTIATION	65	0.652843	1.602838	0.001065	0.046542	1	1569	tags=35%, list=11%, signal=40%
GO_NEGATIVE_REGULATION_OF_AXON_GUIDANCE	24	0.733476	1.59452	0.00618	0.053058	1	1777	tags=46%, list=12%, signal=52%
GO_CALCIUM_ION_TRANSMEMBRANE_IMPORT_INTO_CYTOSOL	101	0.636924	1.594006	0	0.053141	1	1292	tags=26%, list=9%, signal=28%
GO_POSITIVE_REGULATION_OF_TRANSPORTER_ACTIVITY	73	0.631461	1.593036	0	0.055915	1	1526	tags=27%, list=11%, signal=30%
GO_REGULATION_OF_VOLTAGE_GATED_CALCIUM_CHANNEL_ACTIVITY	25	0.724321	1.588591	0.008505	0.057165	1	1232	tags=32%, list=9%, signal=35%
GO_ENDOCHONDRAL_BONE_MORPHOGENESIS	60	0.648606	1.588026	0	0.057311	1	2078	tags=43%, list=14%, signal=50%
GO_ENDOCARDIAL_CUSHION_DEVELOPMENT	34	0.689494	1.587096	0.003405	0.057859	1	1931	tags=44%, list=13%, signal=51%
GO_CHONDROCYTE_DIFFERENTIATION	92	0.626557	1.586507	0	0.057978	1	2078	tags=38%, list=14%, signal=44%
GO_REGULATION_OF_MEMBRANE_POTENTIAL	251	0.605577	1.58393	0	0.060235	1	1606	tags=28%, list=11%, signal=31%
GO_APPENDAGE_MORPHOGENESIS	105	0.625218	1.583195	0.001028	0.060601	1	1965	tags=36%, list=14%, signal=42%
GO_EMBRYONIC_FORELIMB_MORPHOGENESIS	19	0.734295	1.580521	0.008963	0.062862	1	2144	tags=53%, list=15%, signal=62%
GO_CONNECTIVE_TISSUE_DEVELOPMENT	199	0.609942	1.579522	0	0.063445	1	2078	tags=35%, list=14%, signal=41%
GO_REGULATION_OF_ANIMAL_ORGAN_FORMATION	24	0.72016	1.578956	0.017073	0.063714	1	2581	tags=54%, list=18%, signal=66%
GO_REGULATION_OF_MUSCLE_ORGAN_DEVELOPMENT	109	0.619606	1.578741	0	0.063509	1	1943	tags=31%, list=13%, signal=36%
GO_AEROBIC_ELECTRON_TRANSPORT_CHAIN	18	0.758472	1.577746	0.007557	0.064106	1	2835	tags=61%, list=20%, signal=76%
GO_MUSCLE_HYPERTROPHY_IN_RESPONSE_TO_STRESS	18	0.75732	1.575944	0.005083	0.065484	1	1882	tags=39%, list=13%, signal=45%
GO_BONE_MINERALIZATION	91	0.626696	1.575921	0.001029	0.065074	1	2036	tags=40%, list=14%, signal=46%
GO_REGULATION_OF_ION_TRANSMEMBRANE_TRANSPORT	282	0.602374	1.57577	0	0.064843	1	1620	tags=26%, list=11%, signal=29%
GO_RELAXATION_OF_MUSCLE	25	0.703891	1.574343	0.006061	0.065956	1	851	tags=24%, list=6%, signal=25%
GO_OVULATION_CYCLE_PROCESS	32	0.701842	1.573907	0.00237	0.065931	1	1777	tags=31%, list=12%, signal=36%
GO_REGULATION_OF_ACTION_POTENTIAL	37	0.670598	1.573629	0.007937	0.065755	1	1356	tags=35%, list=9%, signal=39%
GO_ENERGY_RESERVE_METABOLIC_PROCESS	64	0.643169	1.57334	0.002153	0.065628	1	1919	tags=31%, list=13%, signal=36%
GO_POSITIVE_REGULATION_OF_SKELETAL_MUSCLE_TISSUE_DEVELOPMENT	22	0.73639	1.572597	0.01125	0.06602	1	2125	tags=55%, list=15%, signal=64%
GO_ACYLGLYCEROL_HOMEOSTASIS	18	0.744729	1.571709	0.011613	0.066598	1	1246	tags=39%, list=9%, signal=43%
GO_POSITIVE_REGULATION_OF_POTASSIUM_ION_TRANSPORT	27	0.693884	1.57043	0.010539	0.067468	1	965	tags=30%, list=7%, signal=32%
GO_CELLULAR_RESPONSE_TO_XENOBIOTIC_STIMULUS	96	0.618483	1.570199	0.001035	0.067274	1	1224	tags=22%, list=8%, signal=24%
GO_REPLACEMENT_OSSIFICATION	26	0.71791	1.570036	0.004751	0.067119	1	1544	tags=42%, list=11%, signal=47%
GO PEPTIDYL ARGININE MODIFICATION	21	0.734033	1.569525	0.017588	0.067279	1	304	tags=14%, list=2%, signal=15%
GO_REGULATION_OF_CALCIUM_MEDIATED_SIGNALING	86	0.628164	1.568386	0.001036	0.06816	1	1128	tags=24%, list=8%, signal=26%
GO_POSITIVE_REGULATION_OF_HEART_CONTRACTION	18	0.757272	1.567439	0.007605	0.068874	1	803	tags=28%, list=6%, signal=29%
GO_SODIUM_ION_TRANSMEMBRANE_TRANSPORT	80	0.624584	1.564442	0.003155	0.071455	1	1807	tags=31%, list=12%, signal=36%
GO_REGULATION_OF_SODIUM_ION_TRANSMEMBRANE_TRANSPORT	48	0.647581	1.563818	0.001112	0.071704	1	738	tags=23%, list=5%, signal=24%
GO_REGULATION_OF_AXON_GUIDANCE	35	0.682102	1.563662	0.008055	0.071503	1	1777	tags=37%, list=12%, signal=42%
GO_REGULATION_OF_AMINO_ACID_TRANSPORT	20	0.739312	1.563358	0.012739	0.071444	1	851	tags=15%, list=6%, signal=16%
GO_REGULATION_OF_STRIATED_MUSCLE_CELL_DIFFERENTIATION	77	0.62689	1.562955	0.003138	0.071503	1	1943	tags=27%, list=13%, signal=31%
GO_CELL_COMMUNICATION_INVOLVED_IN_CARDIAC_CONDUCTION	39	0.670226	1.562627	0.004484	0.0715	1	1735	tags=36%, list=12%, signal=41%
GO_REGULATION_OF_CATION_TRANSMEMBRANE_TRANSPORT	213	0.603094	1.561579	0	0.072257	1	1613	tags=26%, list=11%, signal=29%
GO_REGIONALIZATION	211	0.602363	1.560662	0	0.072886	1	2119	tags=32%, list=15%, signal=37%
GO_GLYCOGEN_BIOSYNTHETIC_PROCESS	36	0.668147	1.560043	0.002294	0.073165	1	1919	tags=33%, list=13%, signal=38%
GO_MESENCHYMAL_CELL_PROLIFERATION	34	0.675036	1.558238	0.009227	0.074766	1	2453	tags=53%, list=17%, signal=64%
GO_ENDOCARDIAL_CUSHION_MORPHOGENESIS	27	0.698374	1.557663	0.011876	0.075004	1	1931	tags=48%, list=13%, signal=55%
GO_NEGATIVE_REGULATION_OF_ION_TRANSPORT	98	0.610591	1.556725	0.001026	0.075782	1	1620	tags=30%, list=11%, signal=33%
GO_MITOCHONDRIAL_CALCIUM_ION_HOMEOSTASIS	21	0.725547	1.556189	0.003659	0.075923	1	712	tags=19%, list=5%, signal=20%
GO_NEGATIVE_REGULATION_OF_CALCINEURIN_MEDIATED_SIGNALING	15	0.766707	1.556112	0.009333	0.075583	1	1128	tags=33%, list=8%, signal=36%
GO_BONE_MORPHOGENESIS	86	0.618808	1.555766	0.001036	0.075575	1	2078	tags=41%, list=14%, signal=47%
GO_BROWN_FAT_CELL_DIFFERENTIATION	34	0.68399	1.555261	0.008083	0.075799	1	2168	tags=44%, list=15%, signal=52%
GO_PROTEIN_ADP_RIBOSYLATION	29	0.694234	1.554789	0.013237	0.075969	1	490	tags=14%, list=3%, signal=14%
GO_REGULATION_OF_FATTY_ACID_OXIDATION	27	0.691742	1.553963	0.00949	0.076534	1	1441	tags=37%, list=10%, signal=41%
GO_APPENDAGE_DEVELOPMENT	127	0.610047	1.553855	0	0.076231	1	1965	tags=34%, list=14%, signal=39%
GO_REGULATION_OF_CALCIUM_ION_TRANSPORT_INTO_CYTOSOL	80	0.627089	1.553703	0.001046	0.076036	1	1104	tags=26%, list=8%, signal=28%
GO_CARDIAC_CHAMBER_MORPHOGENESIS	97	0.61313	1.553519	0	0.075851	1	2476	tags=40%, list=17%, signal=48%
GO_POSITIVE_REGULATION_OF_SMOOTHENED_SIGNALING_PATHWAY	27	0.700825	1.552821	0.009627	0.076242	1	1219	tags=33%, list=8%, signal=36%
GO_MUSCLE_CELL_CELLULAR_HOMEOSTASIS	18	0.740953	1.552681	0.014157	0.075986	1	714	tags=39%, list=5%, signal=41%
GO_GLYCOLYTIC_PROCESS_THROUGH_FRUCTOSE_6_PHOSPHATE	23	0.70591	1.550459	0.014706	0.078203	1	1698	tags=30%, list=12%, signal=34%
GO_AMINE_TRANSPORT	47	0.650529	1.550257	0.009989	0.078003	1	851	tags=17%, list=6%, signal=18%
GO_REGULATION_OF_TRANSPORTER_ACTIVITY	171	0.604026	1.549664	0	0.078238	1	1620	tags=27%, list=11%, signal=27%
GO_MONOVALENT_INORGANIC_CATION_TRANSPORT	296	0.591144	1.549197	0	0.078333	1	1526	tags=25%, list=11%, signal=27%
GO_OUTFLOW_TRACT_SEPTUM_MORPHOGENESIS	19	0.740918	1.549194	0.014031	0.077994	1	1836	tags=53%, list=13%, signal=60%
GO_HEART_FORMATION	21	0.718556	1.5467	0.017263	0.080473	1	1943	tags=38%, list=13%, signal=44%
GO_POSITIVE_REGULATION_OF_ION_TRANSMEMBRANE_TRANSPORT	101	0.611313	1.546688	0.001026	0.080008	1	1605	tags=26%, list=11%, signal=29%
GO_SKELETAL_SYSTEM_DEVELOPMENT	394	0.588475	1.544173	0	0.082525	1	2078	tags=34%, list=14%, signal=38%
GO_MELANOCYTE_DIFFERENTIATION	18	0.738205	1.543676	0.014944	0.082691	1	1452	tags=39%, list=10%, signal=43%
GO_THYROID_GLAND_DEVELOPMENT	16</							

NAME	SIZE	ES	NES	NOM p-val	FDR q-val	FWER p-val	RANK AT MAX	LEADING EDGE
GO_CRANIAL_NERVE_MORPHOGENESIS	20	0.720727	1.531842	0.02551	0.09141	1	1656	tags=50%, list=11%, signal=56%
GO_CELLULAR_AMINO_ACID_CATABOLIC_PROCESS	61	0.623573	1.531802	0.006637	0.091043	1	3106	tags=46%, list=21%, signal=58%
GO_POSITIVE_REGULATION_OF_EMBRYONIC_DEVELOPMENT	24	0.699557	1.531425	0.01836	0.091061	1	1615	tags=33%, list=11%, signal=37%
GO_NEGATIVE_REGULATION_OF_CHEMOTAXIS	50	0.63641	1.531077	0.01105	0.091071	1	2735	tags=42%, list=19%, signal=52%
GO_SEQUESTERING_OF_CALCIIUM_IION	101	0.60373	1.529988	0	0.092027	1	1605	tags=25%, list=11%, signal=28%
GO_CYTOSOLIC_CALCIIUM_IION_TRANSPORT	128	0.60082	1.528107	0	0.094246	1	1605	tags=26%, list=11%, signal=29%
GO_BIOMINERAL_TISSUE_DEVELOPMENT	116	0.592512	1.527128	0.003064	0.09505	1	2036	tags=37%, list=14%, signal=43%
GO_MYOBLAST_DIFFERENTIATION	69	0.614503	1.527055	0.003158	0.094731	1	1952	tags=29%, list=13%, signal=33%
GO_VENTRICULAR_CARDIAC_MUSCLE_CELL_ACTION_POTENTIAL	21	0.716871	1.524683	0.018382	0.09744	1	1094	tags=43%, list=8%, signal=46%
GO_MESENOPHRIC_TUBULE_MORPHOGENESIS	43	0.65052	1.52388	0.00904	0.098128	1	2458	tags=47%, list=17%, signal=56%
GO_MITOCHONDRIAL_FISSION	33	0.678087	1.523717	0.01479	0.097877	1	853	tags=21%, list=6%, signal=22%
GO_POSITIVE_REGULATION_OF_STRIATED_MUSCLE_CELL_DIFFERENTIATION	43	0.650546	1.523605	0.013245	0.097592	1	1569	tags=26%, list=11%, signal=29%
GO_POSITIVE_REGULATION_OF_CALCIIUM_IION_TRANSMEMBRANE_TRANSPORTER_ACTIVITY	32	0.668077	1.522254	0.010381	0.098878	1	879	tags=28%, list=6%, signal=30%
GO_GENERATION_OF_PRECURSOR_METABOLITES_AND_ENERGY	397	0.581339	1.52206	0	0.09873	1	2390	tags=31%, list=17%, signal=36%
GO_ROOF_OF_MOUTH_DEVELOPMENT	68	0.607922	1.521608	0.006431	0.098961	1	2418	tags=49%, list=17%, signal=58%
GO_EMBRYONIC_ORGAN_MORPHOGENESIS	191	0.585886	1.52159	0	0.098554	1	2458	tags=38%, list=17%, signal=45%
GO_REGULATION_OF_MITOCHONDRIAL_FISSION	22	0.703579	1.521387	0.018541	0.098361	1	712	tags=23%, list=5%, signal=24%
GO_REGULATION_OF_CALCIIUM_IION_TRANSPORT	175	0.583314	1.518651	0	0.101666	1	1232	tags=23%, list=9%, signal=25%
GO_SODIUM_IION_TRANSPORT	120	0.595942	1.51845	0	0.101529	1	1807	tags=28%, list=12%, signal=32%
GO_NEGATIVE_REGULATION_OF_CATION_CHANNEL_ACTIVITY	27	0.681855	1.518194	0.010676	0.101458	1	1526	tags=37%, list=11%, signal=41%
GO_DOPAMINE_TRANSPORT	24	0.694077	1.517035	0.021765	0.102558	1	2128	tags=29%, list=15%, signal=34%
GO_NEPHRON_EPITHELIUM_DEVELOPMENT	73	0.611042	1.516317	0.00523	0.103052	1	2458	tags=42%, list=17%, signal=51%
GO_AEROBIC_RESPIRATION	79	0.607116	1.515484	0.004154	0.103707	1	3342	tags=48%, list=23%, signal=62%
GO_NOTOCHORD_DEVELOPMENT	15	0.74112	1.51465	0.028226	0.104367	1	2243	tags=60%, list=16%, signal=71%
GO_REGULATION_OF_OSTEOBLAST_DIFFERENTIATION	92	0.596292	1.512216	0.007261	0.107508	1	2025	tags=30%, list=14%, signal=35%
GO_NEGATIVE_REGULATION_OF_ANIMAL_ORGAN_MORPHOGENESIS	27	0.685473	1.511373	0.016807	0.108223	1	1487	tags=33%, list=10%, signal=37%
GO_MUSCLE_HYPERTROPHY	71	0.600485	1.510812	0.006336	0.108459	1	923	tags=17%, list=6%, signal=18%
GO_RESPIRATORY_GASEOUS_EXCHANGE	44	0.63328	1.510332	0.014461	0.108797	1	2678	tags=39%, list=19%, signal=47%
GO_REGULATION_OF_GASTRULATION	27	0.680989	1.509348	0.015029	0.109741	1	1943	tags=41%, list=13%, signal=44%
GO_NEUROMUSCULAR_JUNCTION_DEVELOPMENT	40	0.647321	1.508859	0.012195	0.109993	1	2109	tags=40%, list=15%, signal=47%
GO_REGULATION_OF_METAL_IION_TRANSPORT	256	0.580466	1.507339	0	0.111828	1	1232	tags=22%, list=9%, signal=24%
GO_REGULATION_OF_HEART_MORPHOGENESIS	29	0.664774	1.507001	0.023419	0.111916	1	2458	tags=48%, list=17%, signal=58%
GO_REGULATION_OF_MUSCLE_ADAPTATION	73	0.613383	1.505582	0.006363	0.113636	1	1882	tags=27%, list=13%, signal=31%
GO_DRUG_TRANSPORT	115	0.589718	1.502469	0.002043	0.117677	1	1905	tags=22%, list=13%, signal=25%
GO_NEGATIVE_REGULATION_OF_MUSCLE_CONTRACTION	21	0.70039	1.499889	0.026022	0.121202	1	1021	tags=29%, list=7%, signal=31%
GO_POSITIVE_REGULATION_OF_TRANSMEMBRANE_TRANSPORT	136	0.585536	1.49935	0	0.121316	1	1605	tags=23%, list=11%, signal=25%
GO_COLLAGEN_METABOLIC_PROCESS	16	0.733851	1.499171	0.03251	0.121115	1	2073	tags=50%, list=14%, signal=61%
GO_REGULATION_OF_IION_TRANSPORT	409	0.570849	1.499151	0	0.120677	1	1620	tags=24%, list=11%, signal=26%
GO_ASPARTATE_FAMILY_AMINO_ACID_CATABOLIC_PROCESS	17	0.719984	1.498477	0.030928	0.121187	1	1768	tags=35%, list=12%, signal=40%
GO_EMBRYONIC_CRANIAL_SKELETON_MORPHOGENESIS	37	0.644299	1.497714	0.013605	0.121916	1	1587	tags=32%, list=11%, signal=36%
GO_REGULATION_OF_MESENCHYMAL_CELL_PROLIFERATION	27	0.670795	1.496911	0.015495	0.122643	1	1798	tags=41%, list=12%, signal=46%
GO_MESENCHYME_DEVELOPMENT	192	0.577771	1.496486	0	0.122721	1	1754	tags=27%, list=12%, signal=30%
GO_EXTRACELLULAR_STRUCTURE_ORGANIZATION	323	0.573635	1.496366	0	0.122416	1	2614	tags=38%, list=18%, signal=46%
GO_NEGATIVE_REGULATION_OF_SMOOTH_MUSCLE_CELL_PROLIFERATION	39	0.641368	1.495187	0.019451	0.123847	1	1817	tags=33%, list=13%, signal=38%
GO_POSITIVE_REGULATION_OF_SODIUM_IION_TRANSPORT	27	0.680028	1.494805	0.015815	0.123925	1	542	tags=22%, list=4%, signal=23%
GO_CRANIAL_NERVE_DEVELOPMENT	30	0.661441	1.494421	0.019767	0.124018	1	1656	tags=43%, list=11%, signal=49%
GO_REGULATION_OF_SODIUM_IION_TRANSMEMBRANE_TRANSPORTER_ACTIVITY	40	0.641365	1.494259	0.016816	0.123794	1	1735	tags=30%, list=12%, signal=34%
GO_INORGANIC_IION_IMPORT_ACROSS_PLASMA_MEMBRANE	53	0.624236	1.493591	0.008715	0.12435	1	1482	tags=25%, list=10%, signal=27%
GO_KIDNEY_EPITHELIUM_DEVELOPMENT	102	0.585392	1.493148	0.00715	0.124589	1	2458	tags=40%, list=17%, signal=48%
GO_CELL_COMMUNICATION_VIA_ELECTRICAL_COUPLING	25	0.674667	1.492291	0.021687	0.125555	1	1540	tags=36%, list=11%, signal=40%
GO_REGULATION_OF_HEART_GROWTH	44	0.631171	1.489774	0.014509	0.129014	1	1382	tags=25%, list=10%, signal=28%
GO_POSITIVE_REGULATION_OF_MYOBLAST_DIFFERENTIATION	18	0.710349	1.488871	0.03939	0.129973	1	1740	tags=44%, list=12%, signal=50%
GO_MESENCHYME_MORPHOGENESIS	39	0.643016	1.488372	0.021469	0.130288	1	2315	tags=49%, list=16%, signal=58%
GO_OUTFLOW_TRACT_MORPHOGENESIS	59	0.612072	1.487842	0.006501	0.130668	1	2458	tags=42%, list=17%, signal=51%
GO_POSITIVE_REGULATION_OF_ANIMAL_ORGAN_MORPHOGENESIS	56	0.603098	1.487374	0.016411	0.130941	1	1965	tags=39%, list=14%, signal=45%
GO_GLYCOLYTIC_PROCESS	89	0.592939	1.486159	0.003195	0.132441	1	1281	tags=19%, list=9%, signal=21%
GO_CALCIIUM_IION_TRANSMEMBRANE_TRANSPORT	214	0.573675	1.485668	0	0.132675	1	1613	tags=22%, list=11%, signal=24%
GO_INSULIN_LIKE_GROWTH_FACTOR_RECEPTOR_SIGNALING_PATHWAY	27	0.695927	1.485632	0.02303	0.132261	1	2072	tags=41%, list=14%, signal=47%
GO_CARDIAC_CHAMBER_DEVELOPMENT	130	0.574598	1.48244	0	0.137143	1	2480	tags=35%, list=17%, signal=42%
GO_NEGATIVE_REGULATION_OF_AXON_EXTENSION	36	0.631176	1.481716	0.021764	0.137903	1	1451	tags=31%, list=10%, signal=34%
GO_STRIATED_MUSCLE_CELL_PROLIFERATION	49	0.623258	1.478815	0.019502	0.142188	1	1382	tags=27%, list=10%, signal=29%
GO_PHOSPHATIDYLSERINE_METABOLIC_PROCESS	15	0.727875	1.478587	0.026385	0.142048	1	446	tags=20%, list=3%, signal=21%
GO_CALCIIUM_MEDIATED_SIGNALING	169	0.572909	1.478458	0	0.141758	1	1183	tags=21%, list=8%, signal=22%
GO_GLUCCOSE_IMPORT	50	0.614974	1.478129	0.019934	0.141825	1	1919	tags=24%, list=13%, signal=28%
GO_DOPAMINE_SECRETION	19	0.707217	1.477299	0.032051	0.142776	1	2128	tags=32%, list=15%, signal=37%
GO_SOMITE_DEVELOPMENT	62	0.603674	1.474719	0.012848	0.146957	1	2628	tags=37%, list=18%, signal=45%
GO_ANTERIOR_POSTERIOR_PATTERN_SPECIFICATION	134	0.574564	1.474226	0.003046	0.147315	1	2458	tags=37%, list=17%, signal=44%
GO_POSITIVE_REGULATION_OF STEM_CELL_DIFFERENTIATION	15	0.718622	1.4739	0.044678	0.147426	1	1906	tags=47%, list=13%, signal=54%
GO_LABYRINTHINE_LAYER_BLOOD_VESSEL_DEVELOPMENT	17	0.717154	1.473646	0.03875	0.147286	1	389	tags=18%, list=3%, signal=18%
GO_REGULATION_OF_MESENOPHRUS_DEVELOPMENT	16	0.709495	1.472177	0.038961	0.149352	1	1210	tags=38%, list=8%, signal=41%
GO_GLUTAMATE_RECEPTOR_SIGNALING_PATHWAY	44	0.627219	1.472087	0.021253	0.149002	1	1613	tags=27%, list=11%, signal=31%
GO_POSITIVE_REGULATION_OF_PROTEIN_TARGETING_TO_MEMBRANE	28	0.695939	1.47154	0.023364	0.149517	1	1669	tags=32%, list=12%, signal=36%
GO_HEART TRABECULA_MORPHOGENESIS	29	0.66191	1.470579	0.02662	0.150692	1	1467	tags=28%, list=10%, signal=31%
GO_HIPPO_SIGNALING	34	0.632466	1.470107	0.029412	0.151028	1	1812	tags=29%, list=13%, signal=34%
GO_REGENERATION	143	0.569424	1.469852	0.001008	0.150942	1	1417	tags=22%, list=10%, signal=24%
GO_REGULATION_OF_FIBROBLAST_GROWTH_FACTOR_RECEPTOR_SIGNALING_PATHWAY	24	0.672866	1.469616	0.027711	0.151572	1	2243	tags=38%, list=16%, signal=44%
GO_MESENOPHRUS_DEVELOPMENT	71	0.595427	1.467575	0.005342	0.153889	1	2670	tags=41%, list=18%, signal=50%
GO_RENAL_TUBULE_DEVELOPMENT	63	0.592961	1.464572	0.009667	0.15888	1	2458	tags=43%, list=17%, signal=51%
GO_GLUCCOSE_METABOLIC_PROCESS	94	0.582706	1.464493	0.004124	0.158497	1	1919	tags=27%, list=13%, signal=30%
GO_REGULATION_OF_OSSIFICATION	146	0.566293	1.463595	0.001012	0.159529	1	2036	tags=28%, list=14%, signal=32%
GO_NEPHRON_MORPHOGENESIS	52	0.615321	1.463276	0.019459	0.159591	1	2458	tags=42%, list=17%, signal=51%
GO_HOMOPHILIC_CELL_ADHESION_VIA_PLASMA_MEMBRANE_ADHESION_MOLECULES	75	0.591977	1.462429	0.007384	0.160633	1	2889	tags=36%, list=20%, signal=45%
GO_CARTILAGE_MORPHOGENESIS	20	0.67292	1.461722	0.051833	0.161346	1	3608	tags=75%, list=25%, signal=100%
GO_SYNAPTIC_TRANSMISSION_GLUTAMATERGIC	45	0.615609	1.461224	0.019934	0.161778	1	2269	tags=38%, list=16%, signal=45%
GO_CARDIAC_VENTRICLE_MORPHOGENESIS	49	0.612474	1.460044	0.025247	0.16356	1	1453	tags=31%, list=10%, signal=34%
GO_PROTEIN_HYDROXYLATION	22	0.683768	1.459935	0.031592	0.163218	1	2813	tags=45%, list=18%, signal=56%
GO_METANEPHRUS_DEVELOPMENT	59	0.606672	1.458204	0.015038	0.166607	1	2581	tags=42%, list=18%, signal=51%
GO_TRANSMISSION_OF_NERVE_IMPULSE	30	0.645013	1.457859	0.02907	0.166167	1	1613	tags=37%, list=11%, signal=41%
GO_WATER_HOMEOSTASIS	38	0.62636	1.457213	0.030682	0.166683	1	1577	tags=16%, list=11%, signal=18%
GO_REGULATION_OF_SODIUM_IION_TRANSPORT	63	0.597295	1.4566	0.014737	0.167443	1	738	tags=21%, list=5%, signal=22%
GO_RETINA_DEVELOPMENT_IN_CAMERA_TYPE_EYE	87	0.577028	1.456358	0.010395	0.167388	1	1798	tags=25%, list=12%, signal=29%
GO_GLOMERULUS_DEVELOPMENT	45	0.607537	1.456303	0.028729	0.166949	1	2458	tags=47%, list=17%, signal=56%
GO_POSITIVE_REGULATION_OF_MESENCHYMAL_CELL_PROLIFERATION	20	0.667794	1.454502	0.04804	0.169806	1	1569	tags=45%, list=11%, signal=50%
GO_REGULATION_OF_CARTILAGE_DEVELOPMENT	52	0.607227	1.454134	0.017316	0.169896	1	1965	tags=37%, list=14%, signal=42%
GO_POSITIVE_REGULATION_OF_CALCIIUM_IION_TRANSMEMBRANE_TRANSPORT	51	0.604237	1.453438	0.015054	0.170569	1	879	tags=22%, list=6%, signal=23%
GO_NEGATIVE_REGULATION_OF_SMOOTH_MUSCLE_CELL_MIGRATION	21	0.67565	1.452712	0.041509	0.171411	1	2435	tags=48%, list=17%, signal=57%
GO_PROTEIN_O_LINKED_MANNOSYLATION	17	0.701585	1.452294	0.043709	0.171688	1	2931	tags=53%, list=20%, signal=66%
GO_REGULATION_OF_CELL_FATE_COMMITMENT	17	0.692791	1.451505	0.047375	0.172636	1	2418	tags=47%, list=17%, signal=56%
GO_INORGANIC_IION_TRANSMEMBRANE_TRANSPORT	493	0.551984	1.451047	0				

NAME	SIZE	ES	NES	NOM p-val	FDR q-val	FWER p-val	RANK AT MAX	LEADING EDGE
GO_VASODILATION	24	0.659134	1.442953	0.050307	0.183419	1	1347	tags=25%, list=9%, signal=28%
GO_LIPID_DROPLET_ORGANIZATION	16	0.706254	1.442705	0.044814	0.183348	1	2398	tags=44%, list=17%, signal=52%
GO_CARBOHYDRATE_BIOSYNTHETIC_PROCESS	161	0.553749	1.442547	0.002016	0.183096	1	1919	tags=23%, list=13%, signal=26%
GO_REGULATION_OF_COLLAGEN_BIOSYNTHETIC_PROCESS	27	0.652723	1.441798	0.047736	0.183987	1	1615	tags=30%, list=11%, signal=33%
GO_CENTRAL_NERVOUS_SYSTEM_PROJECTION_NEURON_AXONOGENESIS	21	0.67237	1.440691	0.042945	0.185636	1	1777	tags=38%, list=12%, signal=43%
GO_RENAL_WATER_HOMEOSTASIS	22	0.660698	1.440623	0.041872	0.185205	1	1577	tags=18%, list=11%, signal=20%
GO_ENERGY_HOMEOSTASIS	30	0.625023	1.440147	0.042303	0.185664	1	1667	tags=23%, list=12%, signal=26%
GO_QUINONE_BIOSYNTHETIC_PROCESS	16	0.706492	1.43993	0.055851	0.185558	1	1445	tags=25%, list=10%, signal=28%
GO_REGULATION_OF_ENDOCRINE_PROCESS	23	0.663919	1.439527	0.046683	0.185873	1	877	tags=17%, list=6%, signal=18%
GO_MUSCLE_CELL_MIGRATION	77	0.580299	1.438984	0.012592	0.186421	1	2435	tags=32%, list=17%, signal=39%
GO_POSITIVE_REGULATION_OF_BLOOD_CIRCULATION	35	0.616752	1.438818	0.033839	0.186558	1	1094	tags=20%, list=8%, signal=22%
GO_NEGATIVE_REGULATION_OF_STRIATED_MUSCLE_CELL_DIFFERENTIATION	28	0.650924	1.438167	0.031542	0.186896	1	1943	tags=32%, list=13%, signal=37%
GO_DOPAMINERGIC_NEURON_DIFFERENTIATION	19	0.6937	1.437794	0.050932	0.187104	1	2243	tags=42%, list=16%, signal=50%
GO_SMOOTH_MUSCLE_CELL_DIFFERENTIATION	45	0.604576	1.437312	0.027211	0.187466	1	1634	tags=33%, list=11%, signal=37%
GO_POSITIVE_REGULATION_OF_PROTEIN_COMPLEX_DISASSEMBLY	29	0.63862	1.43701	0.0363	0.187565	1	1231	tags=24%, list=9%, signal=26%
GO_MITOCHONDRIAL_TRANSMEMBRANE_TRANSPORT	69	0.583172	1.436471	0.017039	0.188115	1	3298	tags=32%, list=23%, signal=41%
GO_VENTRICULAR_CARDIAC_MUSCLE_TISSUE_DEVELOPMENT	39	0.618656	1.435856	0.039063	0.188789	1	1425	tags=28%, list=10%, signal=31%
GO_ODONTOGENESIS	80	0.569286	1.43582	0.024416	0.188308	1	1754	tags=34%, list=12%, signal=38%
GO_REGULATION_OF_GLUCOSE_METABOLIC_PROCESS	58	0.592329	1.435539	0.015267	0.188336	1	1919	tags=29%, list=13%, signal=34%
GO_KIDNEY_MORPHOGENESIS	62	0.592681	1.435342	0.018143	0.188224	1	2670	tags=42%, list=18%, signal=51%
GO_CIRCADIAN_REGULATION_OF_GENE_EXPRESSION	49	0.592642	1.433816	0.030168	0.190762	1	2191	tags=29%, list=15%, signal=34%
GO_POLYSACCHARIDE_METABOLIC_PROCESS	82	0.574933	1.433766	0.012618	0.190305	1	1919	tags=27%, list=13%, signal=31%
GO_ALPHA_AMINO_ACID_CATABOLIC_PROCESS	54	0.595945	1.433729	0.022752	0.189832	1	3106	tags=41%, list=21%, signal=52%
GO_IMPORT_ACROSS_PLASMA_MEMBRANE	73	0.578141	1.433156	0.011542	0.190489	1	1482	tags=21%, list=10%, signal=25%
GO_RESPONSE_TO_PURINE_CONTAINING_COMPOUND	118	0.561468	1.432471	0.007136	0.191327	1	1549	tags=23%, list=11%, signal=25%
GO_NEURON_RECOGNITION	34	0.625062	1.431927	0.042353	0.191855	1	2507	tags=41%, list=17%, signal=50%
GO_PYRIDINE_CONTAINING_COMPOUND_BIOSYNTHETIC_PROCESS	29	0.62922	1.429835	0.05	0.195561	1	2420	tags=24%, list=17%, signal=29%
GO_REGULATION_OF_SMOOTHED_SIGNALING_PATHWAY	66	0.57942	1.42906	0.012889	0.196573	1	1646	tags=23%, list=11%, signal=29%
GO_FATTY_ACID_TRANSMEMBRANE_TRANSPORT	16	0.680351	1.428353	0.069677	0.197454	1	942	tags=25%, list=7%, signal=27%
GO_SENSORY_ORGAN_MORPHOGENESIS	158	0.551898	1.427248	0.004057	0.199197	1	1798	tags=28%, list=12%, signal=31%
GO_RENAL_SYSTEM_DEVELOPMENT	224	0.544851	1.425908	0.001001	0.201602	1	2508	tags=33%, list=17%, signal=39%
GO_POSITIVE_REGULATION_OF_ION_TRANSPORT	180	0.548173	1.424219	0.003018	0.204734	1	1094	tags=19%, list=8%, signal=20%
GO_EXPORT_ACROSS_PLASMA_MEMBRANE	18	0.680707	1.422847	0.063211	0.207135	1	1482	tags=33%, list=10%, signal=37%
GO_RESPONSE_TO_XENOBIOTIC_STIMULUS	166	0.545859	1.421948	0.004024	0.208497	1	1224	tags=17%, list=8%, signal=19%
GO_REGULATION_OF_PROTEIN_TARGETING_TO_MEMBRANE	32	0.626842	1.421841	0.025791	0.208129	1	1669	tags=28%, list=12%, signal=32%
GO_SYNAPSE_ASSEMBLY	104	0.567533	1.421678	0.009221	0.207914	1	2419	tags=38%, list=17%, signal=46%
GO_METANEPHRIC_EPITHELIAL_DEVELOPMENT	16	0.690405	1.421651	0.065217	0.207401	1	1786	tags=56%, list=12%, signal=64%
GO_STEM_CELL_PROLIFERATION	80	0.568048	1.420811	0.019895	0.208601	1	2428	tags=34%, list=17%, signal=40%
GO_CELL_FATE_DETERMINATION	22	0.665729	1.420658	0.054591	0.208332	1	1916	tags=36%, list=13%, signal=42%
GO_NEGATIVE_REGULATION_OF_EPITHELIAL_CELL_PROLIFERATION	95	0.565516	1.420568	0.005165	0.207957	1	1798	tags=25%, list=12%, signal=29%
GO_RELAXATION_OF_CARDIAC_MUSCLE	15	0.688544	1.420427	0.059974	0.207733	1	257	tags=20%, list=2%, signal=20%
GO_REGULATION_OF_SYNAPSE_ASSEMBLY	67	0.572763	1.418977	0.027897	0.210208	1	2419	tags=36%, list=17%, signal=43%
GO_REGULATION_OF_PROTEIN_TARGETING	73	0.572171	1.418296	0.017857	0.21102	1	1669	tags=19%, list=12%, signal=22%
GO_REGULATION_OF_POSITIVE_CHEMOTAXIS	17	0.679233	1.418052	0.062663	0.21097	1	3441	tags=71%, list=24%, signal=93%
GO_MEMBRANE_REPOLARIZATION_DURING_ACTION_POTENTIAL	15	0.696913	1.417086	0.068548	0.212453	1	1094	tags=33%, list=8%, signal=36%
GO_LUNG_EPITHELIAL_DEVELOPMENT	21	0.652171	1.416559	0.066667	0.213009	1	1730	tags=38%, list=12%, signal=43%
GO_XENOBIOTIC_METABOLIC_PROCESS	51	0.59712	1.416272	0.033408	0.213106	1	1218	tags=20%, list=8%, signal=21%
GO_NERVE_DEVELOPMENT	49	0.586746	1.415841	0.033259	0.213457	1	1692	tags=33%, list=12%, signal=37%
GO_FOREBRAIN_NEURON_DEVELOPMENT	19	0.663479	1.41441	0.071608	0.216155	1	2735	tags=42%, list=19%, signal=52%
GO_REGULATION_OF_SYNAPSE_STRUCTURE_OR_ACTIVITY	158	0.546836	1.414386	0.005061	0.215612	1	2419	tags=32%, list=17%, signal=38%
GO_POSITIVE_REGULATION_OF_PROTEIN_DEPOLYMERIZATION	15	0.696817	1.414055	0.063187	0.215662	1	1231	tags=33%, list=9%, signal=36%
GO_REGULATION_OF_CHONDROCYTE_DIFFERENTIATION	37	0.601001	1.413745	0.045249	0.215812	1	1965	tags=35%, list=14%, signal=41%
GO_ENDODERM_FORMATION	39	0.603847	1.412705	0.04447	0.217551	1	1943	tags=33%, list=13%, signal=38%
GO_POSITIVE_REGULATION_OF_AMINE_TRANSPORT	16	0.685196	1.412118	0.064085	0.218291	1	496	tags=13%, list=3%, signal=13%
GO_NEGATIVE_REGULATION_OF_ENDOTHELIAL_CELL_PROLIFERATION	29	0.631773	1.411695	0.049941	0.218667	1	1659	tags=34%, list=11%, signal=39%
GO_REGULATION_OF_POTASSIUM_ION_TRANSMEMBRANE_TRANSPORTER_ACTIVITY	35	0.611622	1.410442	0.04638	0.220815	1	1208	tags=29%, list=8%, signal=31%
GO_ENDOCRINE_HORMONE_SECRETION	26	0.649565	1.409739	0.06401	0.22182	1	999	tags=19%, list=7%, signal=21%
GO_ACETYL_COA_BIOSYNTHETIC_PROCESS_FROM_PYRUVATE	15	0.688873	1.408952	0.060288	0.223063	1	3349	tags=67%, list=23%, signal=87%
GO_CELL_COMMUNICATION_BY_ELECTRICAL_COUPLING_INVOLVED_IN_CARDIAC_CONDUCTIO N	22	0.651477	1.40806	0.068238	0.22448	1	1540	tags=32%, list=11%, signal=36%
GO_FORMATION_OF_PRIMARY_GERM_LAYER	87	0.564106	1.406662	0.021672	0.227065	1	1965	tags=26%, list=14%, signal=30%
GO_LIPID_OXIDATION	87	0.561771	1.404126	0.020812	0.232366	1	1974	tags=25%, list=14%, signal=29%
GO_REGULATION_OF_THE_FORCE_OF_HEART_CONTRACTION	23	0.641247	1.403905	0.0743	0.232203	1	1094	tags=30%, list=8%, signal=33%
GO_HEART_VALVE_DEVELOPMENT	51	0.585965	1.403869	0.037158	0.231696	1	1931	tags=37%, list=13%, signal=43%
GO_REGULATION_OF_CARDIAC_MUSCLE_CELL_ACTION_POTENTIAL	22	0.648975	1.403271	0.069682	0.232501	1	1735	tags=41%, list=12%, signal=46%
GO_REGULATION_OF_BMP_SIGNALING_PATHWAY	61	0.582592	1.402876	0.030655	0.232752	1	2458	tags=31%, list=17%, signal=37%
GO_REGULATION_OF_SIGNALING_RECEPTOR_ACTIVITY	249	0.536019	1.399845	0	0.239203	1	2280	tags=29%, list=16%, signal=34%
GO_DETECTION_OF ABIOTIC STIMULUS	61	0.57053	1.39893	0.034115	0.24076	1	851	tags=15%, list=6%, signal=16%
GO_COCHLEA_MORPHOGENESIS	16	0.681293	1.397941	0.081925	0.242436	1	2243	tags=50%, list=16%, signal=59%
GO_REGULATION_OF_PROTEIN_COMPLEX_DISASSEMBLY	97	0.549166	1.397217	0.015353	0.243471	1	1460	tags=19%, list=10%, signal=21%
GO_PROTEIN_DEPOLYMERIZATION	91	0.556106	1.397028	0.019669	0.243282	1	1512	tags=20%, list=10%, signal=22%
GO_OSSIFICATION	305	0.533438	1.395407	0	0.246436	1	1943	tags=28%, list=13%, signal=32%
GO_NEGATIVE_REGULATION_OF_CHONDROCYTE_DIFFERENTIATION	15	0.685202	1.394569	0.078273	0.247903	1	1614	tags=40%, list=11%, signal=45%
GO_CARTILAGE_DEVELOPMENT_INVOLVED_IN_ENDOCHONDRAL_BONE_MORPHOGENESIS	37	0.602491	1.393704	0.058625	0.249225	1	2078	tags=46%, list=14%, signal=54%

## APPENDIX II: GSEA REPORT FOR NEGATIVELY ENRICHED GENE SETS

NAME	SIZE	ES	NES	NOM p-val	FDR q-val	FWER p-val	RANK AT MAX	LEADING EDGE
GO_REGULATION_OF_CELL_ACTIVATION	442	-0.3849			1	0	2407 tags=34%, list=17%, signal=39%	
GO_RIBOSOME_BIOGENESIS	260	-0.23279			1	0	4557 tags=32%, list=32%, signal=46%	
GO_LEUKOCYTE_DIFFERENTIATION	412	-0.46123			1	0	2412 tags=39%, list=17%, signal=45%	
GO_REGULATION_OF_INNATE_IMMUNE_RESPONSE	343	-0.42914			1	0	2913 tags=36%, list=20%, signal=43%	
GO_LEUKOCYTE_MIGRATION	334	-0.31513			1	0	2167 tags=31%, list=15%, signal=35%	
GO_REGULATION_OF_HEMOPOIESIS	378	-0.38669			1	0	2833 tags=37%, list=20%, signal=44%	
GO_NCRNA_PROCESSING	342	-0.23001			1	0	2963 tags=20%, list=20%, signal=24%	
GO_DNA_REPAIR	481	-0.18039			1	0	3421 tags=23%, list=24%, signal=29%	
GO_RESPONSE_TO_BACTERIUM	408	-0.28691			1	0	2050 tags=25%, list=14%, signal=29%	
GO_PROTEIN_POLYUBIQUITINATION	270	-0.13888			1	0	2684 tags=17%, list=19%, signal=21%	
GO_NCRNA_METABOLIC_PROCESS	404	-0.19525			1	0	2984 tags=19%, list=21%, signal=23%	
GO_POSITIVE_REGULATION_OF_CELL_ACTIVATION	268	-0.45419			1	0	2407 tags=36%, list=17%, signal=42%	
GO_RNA_SPLICING_VIA_TRANSESTERIFICATION_REACTIONS	304	-0.18573			1	0	2787 tags=24%, list=19%, signal=28%	
GO_INFLAMMATORY_RESPONSE	492	-0.27039			1	0	2197 tags=27%, list=15%, signal=31%	
GO_VIRAL_LIFE_CYCLE	266	-0.30039			1	0	3453 tags=38%, list=24%, signal=49%	
GO_REGULATION_OF_DNA_METABOLIC_PROCESS	244	-0.21249			1	0	3387 tags=29%, list=23%, signal=37%	
GO_ACTIVATION_OF_IMMUNE_RESPONSE	480	-0.43955			1	0	2970 tags=41%, list=21%, signal=50%	
GO_MYELOID_LEUKOCYTE_MEDIATED_IMMUNITY	443	-0.46739			1	0	2653 tags=41%, list=18%, signal=49%	
GO_REGULATION_OF_CELL_CELL_ADHESION	304	-0.37811			1	0	2969 tags=39%, list=21%, signal=48%	
GO_RIBONUCLEOPROTEIN_COMPLEX_BIOGENESIS	409	-0.20499			1	0	4013 tags=30%, list=28%, signal=40%	
GO_LEUKOCYTE_CELL_CELL_ADHESION	260	-0.44251			1	0	2969 tags=43%, list=21%, signal=53%	
GO_POSITIVE_REGULATION_OF_CYTOKINE_PRODUCTION	340	-0.40181			1	0	3489 tags=46%, list=24%, signal=59%	
GO_REGULATION_OF_MULTIORGANISM_PROCESS	299	-0.32705			1	0	2947 tags=32%, list=20%, signal=40%	
GO_REGULATION_OF_CHROMOSOME_ORGANIZATION	293	-0.26693			1	0	3356 tags=31%, list=23%, signal=39%	
GO_PROTEIN_DNA_COMPLEX_SUBUNIT_ORGANIZATION	194	-0.23756			1	0	3695 tags=30%, list=26%, signal=40%	
GO_MYELOID_CELL_DIFFERENTIATION	330	-0.37617			1	0	2412 tags=35%, list=17%, signal=41%	
GO_NEGATIVE_REGULATION_OF_IMMUNE_SYSTEM_PROCESS	338	-0.31446			1	0	2412 tags=32%, list=17%, signal=37%	
GO_IMMUNE_RESPONSE_REGULATING_CELL_SURFACE_RECEPTOR_SIGNALING_PATHWAY	324	-0.49892			1	0	2969 tags=41%, list=21%, signal=51%	
GO_METHYLATION	286	-0.19463			1	0	3028 tags=24%, list=21%, signal=30%	
GO_RNA_CATABOLIC_PROCESS	357	-0.25823			1	0	3900 tags=30%, list=27%, signal=40%	
GO_REGULATION_OF_GENE_EXPRESSION_EPIGENETIC	274	-0.27512			1	0	2858 tags=31%, list=20%, signal=37%	
GO_POSITIVE_REGULATION_OF_DEFENSE_RESPONSE	375	-0.38045			1	0	3135 tags=38%, list=22%, signal=47%	
GO_DNA_REPLICATION	247	-0.15827			1	0	3617 tags=24%, list=25%, signal=31%	
GO_RESPONSE_TO_MOLECULE_OF_BACTERIAL_ORIGIN	253	-0.31981			1	0	2353 tags=32%, list=16%, signal=37%	
GO_IMMUNE_RESPONSE_REGULATING_SIGNALING_PATHWAY	464	-0.47532			1	0	2969 tags=41%, list=21%, signal=50%	
GO_REGULATION_OF_NUCLEOBASE_CONTAINING_COMPOUND_METABOLIC_PROCESS	436	-0.18092			1	0	3188 tags=27%, list=22%, signal=34%	
GO_REGULATION_OF_T_CELL_ACTIVATION	242	-0.44039			1	0	2969 tags=43%, list=21%, signal=53%	
GO_REGULATION_OF_LYMPHOCYTE_ACTIVATION	341	-0.45279			1	0	2407 tags=36%, list=17%, signal=42%	
GO_B_CELL_RECEPTOR_SIGNALING_PATHWAY	65	-0.69149	-2.63119	0	0	0	1998 tags=55%, list=14%, signal=64%	
GO_B_CELL_DIFFERENTIATION	98	-0.63401	-2.53522	0	0	0	3691 tags=64%, list=26%, signal=86%	
GO_B_CELL_PROLIFERATION	64	-0.70808	-2.52059	0	0	0	1632 tags=47%, list=11%, signal=53%	
GO_LYMPHOCYTE_DIFFERENTIATION	279	-0.4968	-2.40966	0	0	0	3058 tags=48%, list=21%, signal=60%	
GO_MYELOID_DENDRITIC_CELL_ACTIVATION	23	-0.81072	-2.40144	0	0	0	1529 tags=61%, list=11%, signal=68%	
GO_LEUKOCYTE_PROLIFERATION	208	-0.50769	-2.39197	0	0	0	2756 tags=44%, list=19%, signal=53%	
GO_REGULATION_OF_B_CELL_RECEPTOR_SIGNALING_PATHWAY	25	-0.79972	-2.38965	0	0	0	1888 tags=68%, list=13%, signal=78%	
GO_ADAPTIVE_IMMUNE_RESPONSE	283	-0.51077	-2.36535	0	0	0	1541 tags=29%, list=11%, signal=32%	
GO_POSITIVE_REGULATION_OF_LEUKOCYTE_DIFFERENTIATION	116	-0.57848	-2.36269	0	0	0	2816 tags=51%, list=19%, signal=63%	
GO_REGULATION_OF_ANTIGEN_RECEPTOR_MEDIATED_SIGNALING_PATHWAY	53	-0.64567	-2.34787	0	0	0	2401 tags=55%, list=17%, signal=65%	
GO_POSITIVE_REGULATION_OF_LYMPHOCYTE_DIFFERENTIATION	74	-0.58925	-2.33391	0	0	0	2816 tags=51%, list=19%, signal=63%	
GO_ANTIGEN_RECEPTOR_MEDIATED_SIGNALING_PATHWAY	213	-0.52514	-2.30391	0	0	0	2407 tags=34%, list=17%, signal=40%	
GO_REGULATION_OF_B_CELL_PROLIFERATION	50	-0.65218	-2.2921	0	0	0	2401 tags=52%, list=17%, signal=62%	
GO_LYMPHOCYTE_HOMEOSTASIS	57	-0.61598	-2.27587	0	0	0	3046 tags=56%, list=21%, signal=71%	
GO_INTERLEUKIN_12_PRODUCTION	40	-0.6851	-2.27024	0	0	0	992 tags=40%, list=7%, signal=43%	
GO_B_CELL_ACTIVATION	206	-0.59037	-2.25408	0	4.92E-05	0.001	3449 tags=56%, list=24%, signal=72%	
GO_REGULATION_OF_ALPHA_BETA_T_CELL_DIFFERENTIATION	50	-0.6288	-2.25323	0	4.83E-05	0.001	2491 tags=50%, list=17%, signal=60%	
GO_POSITIVE_REGULATION_OF_ALPHA_BETA_T_CELL_DIFFERENTIATION	36	-0.66504	-2.23526	0	1.47E-04	0.003	2491 tags=58%, list=17%, signal=70%	
GO_LEUKOCYTE_HOMEOSTASIS	77	-0.59794	-2.21894	0	1.97E-04	0.004	2933 tags=55%, list=20%, signal=68%	
GO_INTERLEUKIN_4_PRODUCTION	25	-0.74816	-2.21872	0	1.93E-04	0.004	1762 tags=52%, list=12%, signal=59%	
GO_DENDRITIC_CELL_DIFFERENTIATION	33	-0.68216	-2.18312	0	3.93E-04	0.007	1529 tags=45%, list=11%, signal=51%	
GO_REGULATION_OF_INTERLEUKIN_4_PRODUCTION	21	-0.76291	-2.17827	0	3.86E-04	0.007	1762 tags=57%, list=12%, signal=65%	
GO_POSITIVE_REGULATION_OF_HEMOPOIESIS	150	-0.53416	-2.16371	0	4.69E-04	0.009	2816 tags=47%, list=19%, signal=58%	
GO_REGULATION_OF_B_CELL_ACTIVATION	116	-0.53517	-2.1561	0	5.06E-04	0.01	1719 tags=34%, list=12%, signal=38%	
GO_PHAGOCYTOSIS	232	-0.47176	-2.1547	0	5.45E-04	0.011	2962 tags=47%, list=20%, signal=58%	
GO_POSITIVE_REGULATION_OF_MYELOID_LEUKOCYTE_DIFFERENTIATION	42	-0.63387	-2.13723	0	7.62E-04	0.016	1855 tags=50%, list=13%, signal=57%	
GO_REGULATION_OF_DEFENSE_RESPONSE_TO_VIRUS_BY_VIRUS	28	-0.68011	-2.13449	0	7.50E-04	0.016	3991 tags=75%, list=28%, signal=103%	
GO_REGULATION_OF_CD4_POSITIVE_ALPHA_BETA_T_CELL_DIFFERENTIATION	37	-0.65522	-2.12035	0	9.09E-04	0.02	2491 tags=51%, list=17%, signal=62%	
GO_REGULATION_OF_LEUKOCYTE_APOPTOTIC_PROCESS	68	-0.56601	-2.11831	0	9.38E-04	0.021	3046 tags=51%, list=21%, signal=65%	
GO_REGULATION_OF_LEUKOCYTE_DIFFERENTIATION	217	-0.4686	-2.10667	0	0.001292	0.03	2773 tags=45%, list=19%, signal=54%	
GO_POSITIVE_REGULATION_OF_LYMPHOCYTE_ACTIVATION	222	-0.48774	-2.1019	0	0.001396	0.033	3058 tags=44%, list=21%, signal=55%	
GO_LEUKOCYTE_APOPTOTIC_PROCESS	85	-0.56118	-2.0967	0	0.001534	0.037	2825 tags=48%, list=20%, signal=60%	
GO_NATURAL_KILLER_CELL_ACTIVATION	46	-0.60399	-2.09438	0	0.001587	0.039	3711 tags=61%, list=26%, signal=82%	
GO_MAST_CELL_MEDIATED_IMMUNITY	37	-0.65415	-2.09368	0	0.001565	0.039	1739 tags=43%, list=12%, signal=49%	
GO_POSITIVE_REGULATION_OF_B_CELL_ACTIVATION	78	-0.55337	-2.0831	0	0.001853	0.046	1632 tags=28%, list=11%, signal=32%	
GO_FC_RECEPTOR_MEDIATED_STIMULATORY_SIGNALING_PATHWAY	87	-0.54253	-2.07828	0	0.001869	0.047	2962 tags=54%, list=20%, signal=68%	
GO_MYELOID_LEUKOCYTE_DIFFERENTIATION	166	-0.46889	-2.07531	0	0.001957	0.05	1892 tags=38%, list=13%, signal=43%	
GO_FC_RECEPTOR_SIGNALING_PATHWAY	177	-0.48202	-2.06783	0	0.002227	0.058	2962 tags=40%, list=20%, signal=49%	
GO_TOLERANCE_INDUCTION	16	-0.76862	-2.06509	0	0.002305	0.061	1105 tags=44%, list=8%, signal=47%	
GO_LYMPHOCYTE_COSTIMULATION	43	-0.58673	-2.06025	0	0.00235	0.062	1139 tags=33%, list=8%, signal=35%	
GO_NEGATIVE_REGULATION_OF_LEUKOCYTE_CELL_CELL_ADHESION	89	-0.50552	-2.05969	0	0.00239	0.063	3711 tags=54%, list=26%, signal=72%	
GO_NEGATIVE_REGULATION_OF_REGULATED_SECRETORY_PATHWAY	20	-0.73178	-2.04906	0	0.00261	0.069	1620 tags=50%, list=11%, signal=56%	
GO_REGULATION_OF_LEUKOCYTE_PROLIFERATION	158	-0.48849	-2.04104	0	0.002884	0.078	2756 tags=44%, list=19%, signal=53%	
GO_REGULATION_OF_CD4_POSITIVE_ALPHA_BETA_T_CELL_ACTIVATION	48	-0.57274	-2.03873	0	0.00299	0.082	2491 tags=48%, list=17%, signal=58%	
GO_INTERLEUKIN_10_PRODUCTION	37	-0.63044	-2.03787	0	0.002987	0.083	1469 tags=41%, list=10%, signal=45%	
GO_REGULATION_OF_MYELOID_LEUKOCYTE_MEDIATED_IMMUNITY	41	-0.58769	-2.03418	0	0.003087	0.087	2091 tags=41%, list=14%, signal=48%	
GO_REGULATION_OF_LYMPHOCYTE_DIFFERENTIATION	133	-0.48674	-2.03303	0	0.003154	0.09	2816 tags=45%, list=19%, signal=56%	
GO_LYMPHOCYTE_APOPTOTIC_PROCESS	57	-0.57373	-2.03252	0	0.003117	0.09	1594 tags=35%, list=11%, signal=39%	
GO_T_CELL_LINEAGE_COMMITMENT	20	-0.71068	-2.0234	0	0.003572	0.103	1762 tags=50%, list=12%, signal=57%	
GO_POSITIVE_REGULATION_OF_INTERLEUKIN_10_PRODUCTION	23	-0.69129	-2.02199	0	0.003596	0.105	1175 tags=43%, list=8%, signal=47%	
GO_POSITIVE_REGULATION_OF_CYTOKINE_BIOSYNTHETIC_PROCESS	55	-0.59164	-2.016	0	0.003856	0.114	1880 tags=55%, list=13%, signal=62%	
GO_B_CELL_HOMEOSTASIS	29	-0.63313	-2.00764	0	0.004284	0.129	2933 tags=62%, list=20%, signal=78%	
GO_POSITIVE_REGULATION_OF_MYELOID_CELL_DIFFERENTIATION	73	-0.53254	-2.00255	0	0.00448	0.137	2756 tags=51%, list=19%, signal=62%	
GO_POSITIVE_REGULATION_OF_LEUKOCYTE_CELL_CELL_ADHESION	168	-0.47177	-2.00118	0	0.004464	0.138	2969 tags=44%, list=21%, signal=55%	
GO_POSITIVE_REGULATION_OF_TYPE_I_INTERFERON_PRODUCTION	73	-0.53548	-1.98953	0	0.005254	0.163	3421 tags=47%, list=24%, signal=61%	
GO_NEGATIVE_REGULATION_OF_INTERLEUKIN_6_PRODUCTION	33	-0.60553	-1.98815	0	0.005383	0.169	2600 tags=45%, list=18%, signal=55%	
GO_NEGATIVE_REGULATION_OF_LEUKOCYTE_APOPTOTIC_PROCESS	40	-0.59991	-1.98543	0	0.005473	0.172	3046 tags=52%, list=21%, signal=66%	
GO_T_CELL_HOMEOSTASIS	33	-0.62065	-1.98366	0	0.005566	0.176	3046 tags=52%, list=21%, signal=65%	
GO_B_CELL_MEDIATED_IMMUNITY	91	-0.49978	-1.98083	0	0.005686	0.181	1541 tags=26%, list=11%, signal=29%	
GO_REGULATION_OF_LYMPHOCYTE_APOPTOTIC_PROCESS	44	-0.56019	-1.97894	0	0.005769	0.185	3046 tags=48%, list=21%, signal=60%	
GO_TYPE_2_IMMUNE_RESPONSE	24	-0.67189	-1.96883	0	0.006572	0.209	3629 tags=63%, list=25%, signal=83%	
GO_POSITIVE_REGULATION_OF_INTERFERON_BETA_PRODUCTION	30	-0.61198	-1.96756	0	0.006563	0.211	2875 tags=47%, list=20%, signal=58%	
GO_T_HELPER_1_TYPE_IMMUNE_RESPONSE	33	-0.60388	-1.96561	0	0.006721	0.218	3711 tags=55%, list=26%, signal=73%	

NAME	SIZE	ES	NES	NOM p-val	FDR q-val	FWER p-val	RANK AT IMAX	LEADING EDGE
GO_MATURE_B_CELL_DIFFERENTIATION	22	-0.68469	-1.96232	0	0.006876	0.225	2211	tags=50%, list=15%, signal=59%
GO_REGULATION_OF_DNA_METHYLATION	17	-0.72484	-1.95964	0.004348	0.00698	0.231	536	tags=24%, list=4%, signal=24%
GO_POSITIVE_T_CELL_SELECTION	28	-0.62102	-1.95601	0	0.007269	0.239	3863	tags=64%, list=27%, signal=88%
GO_REGULATION_OF_LEUKOCYTE_DEGRANULATION	35	-0.59347	-1.95448	0	0.007254	0.24	2407	tags=46%, list=17%, signal=55%
GO_REGULATION_OF_VIRAL_TRANSCRIPTION	58	-0.53079	-1.95257	0	0.007507	0.249	3212	tags=45%, list=22%, signal=57%
GO_REGULATION_OF_ALPHA_BETA_T_CELL_ACTIVATION	76	-0.52526	-1.94251	0	0.008645	0.281	2491	tags=42%, list=17%, signal=51%
GO_MEMBRANE_INVAGINATION	73	-0.50679	-1.93671	0	0.009209	0.299	2088	tags=34%, list=14%, signal=40%
GO_POSITIVE_REGULATION_OF_VIRAL_TRANSCRIPTION	38	-0.59705	-1.93274	0	0.00953	0.309	3212	tags=45%, list=22%, signal=57%
GO_POSITIVE_REGULATION_OF_ANTIGEN_RECEPTOR_MEDIATED_SIGNALING_PATHWAY	21	-0.66739	-1.92819	0	0.010087	0.328	4076	tags=76%, list=28%, signal=106%
GO_POSITIVE_REGULATION_OF_INTERFERON_GAMMA_PRODUCTION	48	-0.56247	-1.92817	0	0.009996	0.328	2313	tags=44%, list=16%, signal=52%
GO_TYPE_1_INTERFERON_PRODUCTION	114	-0.48707	-1.92707	0	0.009984	0.33	3429	tags=46%, list=24%, signal=60%
GO_ALPHA_BETA_T_CELL_DIFFERENTIATION	84	-0.50518	-1.92663	0	0.009946	0.332	2491	tags=45%, list=17%, signal=54%
GO_MACROPHAGE_DIFFERENTIATION	39	-0.57606	-1.92554	0	0.00998	0.337	1728	tags=49%, list=12%, signal=55%
GO_MODULATION_OF_TRANSCRIPTION_IN_OTHER_ORGANISM_INVOLVED_IN_SYMBIOTIC_INTERACTION	24	-0.66192	-1.92449	0	0.009942	0.339	2844	tags=54%, list=20%, signal=67%
GO_CYTOKINE_METABOLIC_PROCESS	89	-0.49	-1.92444	0	0.009857	0.339	2094	tags=44%, list=14%, signal=51%
GO_T_CELL_DIFFERENTIATION	196	-0.4361	-1.92181	0	0.00992	0.343	2825	tags=42%, list=20%, signal=51%
GO_POSITIVE_REGULATION_OF_ALPHA_BETA_T_CELL_ACTIVATION	49	-0.55976	-1.91965	0	0.010054	0.351	2491	tags=47%, list=17%, signal=57%
GO_POSITIVE_REGULATION_OF_GENE_EXPRESSION_EPIGENETIC	52	-0.54895	-1.90813	0	0.011326	0.383	3106	tags=44%, list=21%, signal=56%
GO_POSITIVE_REGULATION_OF_INTERLEUKIN_4_PRODUCTION	17	-0.71716	-1.90715	0.004464	0.011423	0.388	882	tags=41%, list=6%, signal=44%
GO_REGULATION_OF_T_CELL_DIFFERENTIATION	107	-0.46668	-1.90378	0	0.011753	0.398	2969	tags=45%, list=21%, signal=56%
GO_TUMOR_NECROSIS_FACTOR_SUPERFAMILY_CYTOKINE_PRODUCTION	115	-0.46821	-1.90349	0	0.01168	0.399	2942	tags=46%, list=20%, signal=57%
GO_REGULATION_OF_MYELOID_LEUKOCYTE_DIFFERENTIATION	93	-0.48708	-1.90257	0	0.011629	0.399	2199	tags=45%, list=15%, signal=53%
GO_REGULATION_OF_NATURAL_KILLER_CELL_ACTIVATION	22	-0.67902	-1.90179	0	0.011676	0.402	2816	tags=55%, list=19%, signal=68%
GO_ALPHA_BETA_T_CELL_ACTIVATION	112	-0.47268	-1.90149	0	0.011605	0.403	2491	tags=41%, list=17%, signal=49%
GO_T_CELL_ACTIVATION	357	-0.4343	-1.90024	0	0.011599	0.406	3058	tags=44%, list=21%, signal=54%
GO_MATURE_B_CELL_DIFFERENTIATION_INVOLVED_IN_IMMUNE_RESPONSE	16	-0.70236	-1.89695	0.004405	0.011909	0.419	891	tags=38%, list=6%, signal=40%
GO_INTERFERON_BETA_PRODUCTION	48	-0.53574	-1.89521	0	0.01204	0.424	2913	tags=52%, list=20%, signal=65%
GO_POSITIVE_REGULATION_OF_LEUKOCYTE_MEDIATED_IMMUNITY	86	-0.49046	-1.89302	0	0.012223	0.432	4090	tags=49%, list=28%, signal=68%
GO_CELLULAR_DEFENSE_RESPONSE	37	-0.57414	-1.88677	0	0.012757	0.445	3665	tags=54%, list=25%, signal=72%
GO_POSITIVE_REGULATION_OF_INTERFERON_ALPHA_PRODUCTION	21	-0.66887	-1.8852	0.005348	0.013047	0.455	2734	tags=48%, list=19%, signal=59%
GO_LYMPHOCTE_MEDIATED_IMMUNITY	178	-0.45665	-1.88133	0	0.013589	0.472	1609	tags=24%, list=11%, signal=27%
GO_GNANULOCYTE_DIFFERENTIATION	28	-0.61045	-1.8766	0	0.014471	0.496	1762	tags=46%, list=12%, signal=53%
GO_REGULATION_OF_GENE_SILENCING	107	-0.45431	-1.87467	0	0.014795	0.509	3371	tags=47%, list=23%, signal=60%
GO_POSITIVE_REGULATION_OF_B_CELL_PROLIFERATION	33	-0.59157	-1.87405	0	0.01477	0.51	1632	tags=36%, list=11%, signal=41%
GO_T_CELL_PROLIFERATION	131	-0.45253	-1.87355	0	0.014767	0.513	3053	tags=44%, list=21%, signal=56%
GO_POSITIVE_REGULATION_OF_CD4_POSITIVE_ALPHA_BETA_T_CELL_ACTIVATION	26	-0.61785	-1.87293	0	0.014742	0.515	2491	tags=54%, list=17%, signal=65%
GO_NATURAL_KILLER_CELL_MEDIATED_IMMUNITY	40	-0.55785	-1.87197	0	0.014819	0.52	4108	tags=58%, list=28%, signal=80%
GO_REGULATION_OF_TYPE_2_IMMUNE_RESPONSE	20	-0.6678	-1.86914	0	0.015098	0.528	3629	tags=60%, list=25%, signal=80%
GO_POSITIVE_REGULATION_OF_SUBSTRATE_ADHESION_DEPENDENT_CELL_SPREADING	31	-0.58827	-1.86878	0	0.015053	0.53	3867	tags=65%, list=27%, signal=88%
GO_RESPONSE_TO_INTERLEUKIN_12	44	-0.53646	-1.86708	0.009804	0.015085	0.533	3183	tags=55%, list=22%, signal=70%
GO_POSITIVE_REGULATION_BY_HOST_OF_VIRAL_TRANSCRIPTION	16	-0.69379	-1.86464	0.00431	0.015342	0.54	3162	tags=63%, list=22%, signal=80%
GO_DEFENSE_RESPONSE_TO_BACTERIUM	130	-0.45288	-1.86439	0	0.015295	0.541	3025	tags=38%, list=21%, signal=47%
GO_INTERLEUKIN_1_BETA_SECRETION	34	-0.57856	-1.86438	0	0.015188	0.541	2690	tags=50%, list=19%, signal=61%
GO_POSITIVE_REGULATION_OF_VIRAL_PROCESS	91	-0.4768	-1.86223	0	0.015369	0.547	3390	tags=40%, list=23%, signal=51%
GO_POSITIVE_REGULATION_OF_INTERLEUKIN_2_PRODUCTION	29	-0.61344	-1.85603	0.006897	0.01611	0.567	2930	tags=52%, list=20%, signal=65%
GO_B_CELL_APOPTOTIC_PROCESS	22	-0.64312	-1.85552	0	0.016152	0.57	2143	tags=45%, list=15%, signal=53%
GO_POSITIVE_REGULATION_OF_LEUKOCYTE_PROLIFERATION	95	-0.46359	-1.85382	0	0.01633	0.576	3053	tags=42%, list=21%, signal=53%
GO_N_TERMINAL_PROTEIN_AMINO_ACID_ACETYLATION	15	-0.71601	-1.85285	0.003906	0.016439	0.58	2257	tags=47%, list=16%, signal=55%
GO_HUMORAL_IMMUNE_RESPONSE_MEDIATED_BY_CIRCULATING_IMMUNOGLOBULIN	38	-0.56616	-1.85206	0.008333	0.016483	0.584	1541	tags=32%, list=11%, signal=35%
GO_T_CELL_APOPTOTIC_PROCESS	38	-0.56929	-1.84815	0	0.017122	0.6	1445	tags=34%, list=10%, signal=38%
GO_POSITIVE_REGULATION_OF_INTERLEUKIN_12_PRODUCTION	22	-0.6283	-1.84452	0.005618	0.017616	0.607	2313	tags=55%, list=16%, signal=65%
GO_T_CELL_RECEPTOR_SIGNALING_PATHWAY	161	-0.41211	-1.84131	0	0.018061	0.618	2969	tags=32%, list=21%, signal=40%
GO_BONE_CELL_DEVELOPMENT	30	-0.57338	-1.83945	0	0.018478	0.629	2085	tags=53%, list=14%, signal=62%
GO_REGULATION_OF_CHROMATIN_SILENCING	25	-0.61644	-1.83711	0.006098	0.018787	0.637	1945	tags=44%, list=13%, signal=51%
GO_NEGATIVE_REGULATION_OF_T_CELL_PROLIFERATION	41	-0.52427	-1.83683	0	0.01872	0.639	2491	tags=44%, list=17%, signal=53%
GO_LYMPHOCTE_ACTIVATION_INVOLVED_IN_IMMUNE_RESPONSE	126	-0.44559	-1.83229	0	0.019295	0.659	3058	tags=45%, list=21%, signal=57%
GO_NEGATIVE_REGULATION_OF_GENE_SILENCING	24	-0.62489	-1.83104	0.005128	0.019369	0.662	2275	tags=42%, list=16%, signal=49%
GO_FIBROBLAST_APOPTOTIC_PROCESS	17	-0.65941	-1.83102	0.020243	0.019247	0.662	1600	tags=35%, list=11%, signal=40%
GO_INTERFERON_GAMMA_PRODUCTION	80	-0.47594	-1.82979	0	0.019265	0.664	1990	tags=33%, list=14%, signal=37%
GO_WALKING_BEHAVIOR	16	-0.69514	-1.8248	0	0.020365	0.686	1507	tags=38%, list=10%, signal=42%
GO_HISTONE_H4_ACETYLATION	63	-0.49263	-1.82021	0	0.021232	0.705	2022	tags=33%, list=14%, signal=39%
GO_LOW_DENSITY_LIPOPROTEIN_PARTICLE_CLEARANCE	27	-0.58635	-1.82015	0	0.021102	0.705	2241	tags=48%, list=15%, signal=57%
GO_IMMUNOGLOBULIN_PRODUCTION	76	-0.48939	-1.81578	0	0.021626	0.719	1529	tags=28%, list=11%, signal=31%
GO_FC_EPSILON_RECEPTOR_SIGNALING_PATHWAY	113	-0.44932	-1.81487	0	0.021803	0.724	2841	tags=31%, list=20%, signal=38%
GO_SOMATIC_DIVERSIFICATION_OF_IMMUNE_RECEPTORS	56	-0.50217	-1.81043	0	0.022577	0.732	1152	tags=18%, list=8%, signal=19%
GO_ALPHA_BETA_T_CELL_LINEAGE_COMMITMENT	15	-0.68142	-1.80286	0.008621	0.024298	0.759	1762	tags=53%, list=12%, signal=61%
GO_DEFENSE_RESPONSE_TO_OTHER_ORGANISM	305	-0.41713	-1.80177	0	0.024452	0.762	2973	tags=34%, list=21%, signal=42%
GO_PATTERN_RECOGNITION_RECEPTOR_SIGNALING_PATHWAY	163	-0.4248	-1.79623	0	0.025595	0.778	2736	tags=39%, list=19%, signal=48%
GO_SNRNA_PROCESSING	24	-0.6028	-1.79534	0	0.025607	0.78	2963	tags=54%, list=20%, signal=68%
GO_ACTIVATION_OF_INNATE_IMMUNE_RESPONSE	257	-0.42392	-1.79164	0	0.026563	0.796	2913	tags=37%, list=20%, signal=46%
GO_B_CELL_ACTIVATION_INVOLVED_IN_IMMUNE_RESPONSE	60	-0.47703	-1.79134	0	0.026506	0.796	1497	tags=27%, list=10%, signal=30%
GO_REGULATION_OF_MONOCYTE_DIFFERENTIATION	18	-0.62947	-1.78865	0.008511	0.027156	0.807	2143	tags=56%, list=15%, signal=65%
GO_HISTONE_UBIQUITINATION	44	-0.521	-1.78592	0.012658	0.027777	0.814	2837	tags=34%, list=20%, signal=42%
GO_LIPOPOLYSACCHARIDE_MEDIATED_SIGNALING_PATHWAY	52	-0.5204	-1.78541	0.01087	0.027666	0.814	3026	tags=50%, list=21%, signal=63%
GO_POSITIVE_REGULATION_OF_CELL_CELL_ADHESION	193	-0.40798	-1.78517	0	0.027637	0.815	2969	tags=42%, list=21%, signal=53%
GO_CD4_POSITIVE_ALPHA_BETA_T_CELL_ACTIVATION	73	-0.47727	-1.78503	0	0.027526	0.815	2491	tags=45%, list=17%, signal=54%
GO_NUCLEAR_TRANSCRIBED_MRNA_CATABOLIC_PROCESS	193	-0.35006	-1.78363	0	0.027654	0.818	3900	tags=31%, list=27%, signal=42%
GO_ALPHA_BETA_T_CELL_PROLIFERATION	28	-0.58431	-1.78321	0	0.02761	0.82	3991	tags=68%, list=28%, signal=94%
GO_POSITIVE_REGULATION_OF_ADAPTIVE_IMMUNE_RESPONSE	74	-0.47624	-1.783	0	0.027582	0.82	4591	tags=53%, list=32%, signal=77%
GO_REGULATION_OF_NEUROINFLAMMATORY_RESPONSE	26	-0.59045	-1.78261	0.006289	0.027492	0.821	2088	tags=42%, list=14%, signal=49%
GO_NEGATIVE_REGULATION_OF_LEUKOCYTE_PROLIFERATION	56	-0.50046	-1.77948	0	0.028152	0.829	1620	tags=38%, list=11%, signal=42%
GO_BARBED_END_ACTIN_FILAMENT_CAPPING	16	-0.68168	-1.77807	0.013575	0.028262	0.833	2452	tags=56%, list=17%, signal=68%
GO_MAST_CELL_ACTIVATION	46	-0.53525	-1.77666	0	0.028569	0.838	1739	tags=41%, list=12%, signal=47%
GO_LIPOPOLYSACCHARIDE_METABOLIC_PROCESS	44	-0.52593	-1.77528	0	0.028755	0.843	1535	tags=39%, list=11%, signal=43%
GO_VIRAL_GENE_EXPRESSION	179	-0.42328	-1.77448	0	0.028832	0.847	3371	tags=30%, list=23%, signal=38%
GO_SOMATIC_DIVERSIFICATION_OF_IMMUNE_RECEPTORS_VIA_GERMLINE_RECOMBINATION_WITHIN_A_SINGLE_LOCUS	50	-0.51579	-1.77403	0.010753	0.028825	0.849	1151	tags=18%, list=8%, signal=19%
GO_TOLL_LIKE_RECEPTOR_SIGNALING_PATHWAY	121	-0.42992	-1.76847	0	0.029937	0.859	2470	tags=38%, list=17%, signal=45%
GO_NEGATIVE_REGULATION_OF_LYMPHOCTE_ACTIVATION	108	-0.46492	-1.76713	0	0.030123	0.86	2491	tags=40%, list=17%, signal=48%
GO_MYD88_DEPENDENT_TOLL_LIKE_RECEPTOR_SIGNALING_PATHWAY	34	-0.54811	-1.76281	0.007299	0.03127	0.873	1880	tags=35%, list=13%, signal=40%
GO_PLATELET_MORPHOGENESIS	20	-0.61927	-1.76229	0	0.031313	0.876	2236	tags=60%, list=15%, signal=71%
GO_HISTONE_H3_ACETYLATION	53	-0.47718	-1.75499	0	0.033237	0.888	3162	tags=40%, list=22%, signal=51%
GO_HISTONE_MONOUBIQUITINATION	28	-0.58084	-1.75303	0.006289	0.033742	0.892	1886	tags=32%, list=13%, signal=37%
GO_INTERLEUKIN_6_PRODUCTION	107	-0.44474	-1.75204	0	0.033827	0.894	3234	tags=48%, list=22%, signal=61%
GO_NEGATIVE_REGULATION_OF_HISTONE_METHYLATION	19	-0.60282	-1.74879	0.009132	0.034661	0.89	3895	tags=63%, list=27%, signal=86%
GO_NEGATIVE_REGULATION_OF_EXOCYTOSIS	26	-0.55431	-1.74636	0.00578	0.035211	0.903	1620	tags=38%, list=11%, signal=43%
GO_POSITIVE_REGULATION_OF_TUMOR_NECROSIS_FACTOR_SUPERFAMILY_CYTOKINE_PRODUCTION	69	-0.43967	-1.74442	0	0.035612	0.905	1587	tags=35%, list=11%, signal=39%

NAME	SIZE	ES	NES	NOM p-val	FDR q-val	FWER p-val	RANK AT MAX	LEADING EDGE
GO_ADAPTIVE_IMMUNE_RESPONSE_BASED_ON_SOMATIC_RECOMBINATION_OF_IMMUNE_RECEPTORS_BUILT_FROM_IMMUNOGLOBULIN_SUPERFAMILY_DOMAINS	194	-0.42794	-1.74173	0	0.036302	0.913	1541	tags=24%, list=11%, signal=27%
GO_REGULATION_OF_B_CELL_APOPTOTIC_PROCESS	16	-0.63863	-1.74035	0	0.036528	0.917	2143	tags=44%, list=15%, signal=51%
GO_T_HELPER_1_CELL_DIFFERENTIATION	15	-0.65931	-1.73944	0.017094	0.036719	0.919	3629	tags=60%, list=25%, signal=80%
GO_LYMPHOID_PROGENITOR_CELL_DIFFERENTIATION	17	-0.63137	-1.73778	0.021739	0.03727	0.923	1632	tags=41%, list=11%, signal=46%
GO_INTERLEUKIN_6_MEDIATED_SIGNALING_PATHWAY	17	-0.62936	-1.7348	0	0.038036	0.929	2874	tags=53%, list=20%, signal=66%
GO_I_KAPPAB_PHOSPHORYLATION	18	-0.62143	-1.73363	0.013333	0.038227	0.932	957	tags=33%, list=7%, signal=36%
GO_CD4_POSITIVE_OR_CD8_POSITIVE_ALPHA_BETA_T_CELL_LINEAGE_COMMITMENT	16	-0.64675	-1.72435	0.021834	0.041239	0.942	1762	tags=44%, list=12%, signal=50%
GO_POSITIVE_REGULATION_OF_INTERLEUKIN_8_PRODUCTION	40	-0.49501	-1.7243	0	0.041038	0.942	1445	tags=33%, list=10%, signal=36%
GO_MEMBRANE_PROTEIN_INTRACELLULAR_DOMAIN_PROTEOLYSIS	18	-0.64177	-1.72373	0.009346	0.040984	0.943	3486	tags=56%, list=24%, signal=73%
GO_NEGATIVE_REGULATION_OF_LYMPHOCYTE_APOPTOTIC_PROCESS	27	-0.56326	-1.72137	0.012903	0.041552	0.946	1594	tags=33%, list=11%, signal=37%
GO_HUMORAL_IMMUNE_RESPONSE	120	-0.40602	-1.71995	0	0.041919	0.946	2130	tags=32%, list=15%, signal=37%
GO_POSITIVE_REGULATION_OF_MYELOID_LEUKOCYTE_MEDIATED_IMMUNITY	23	-0.58302	-1.71868	0.010256	0.042249	0.947	2091	tags=43%, list=14%, signal=51%
GO_POSITIVE_REGULATION_OF_LEUKOCYTE_DEGRANULATION	17	-0.63062	-1.71491	0.008547	0.043581	0.954	4090	tags=76%, list=28%, signal=107%
GO_INTERLEUKIN_2_BIOSYNTHETIC_PROCESS	20	-0.58002	-1.71359	0.005525	0.043816	0.955	3991	tags=60%, list=28%, signal=83%
GO_MYELOID_CELL_DEVELOPMENT	58	-0.47163	-1.70771	0	0.045652	0.958	2390	tags=40%, list=17%, signal=47%
GO_T_CELL_SELECTION	39	-0.52078	-1.70302	0	0.047325	0.962	1855	tags=41%, list=13%, signal=47%
GO_REGULATION_OF_T_CELL_APOPTOTIC_PROCESS	27	-0.54151	-1.6974	0.018634	0.049453	0.971	836	tags=26%, list=6%, signal=27%
GO_REGULATION_OF_T_CELL_RECEPTOR_SIGNALING_PATHWAY	32	-0.51877	-1.69579	0.012658	0.049893	0.972	2401	tags=47%, list=17%, signal=56%
GO_CD8_POSITIVE_ALPHA_BETA_T_CELL_ACTIVATION	18	-0.61394	-1.69363	0.009804	0.050803	0.974	3373	tags=67%, list=23%, signal=87%
GO_SPHINGOLIPID_METABOLIC_PROCESS	63	-0.44612	-1.69291	0	0.050892	0.976	2115	tags=35%, list=15%, signal=41%
GO_POSITIVE_REGULATION_OF_T_CELL_MEDIATED_IMMUNITY	27	-0.54594	-1.69275	0.012195	0.050658	0.976	4076	tags=48%, list=28%, signal=67%
GO_POSITIVE_REGULATION_OF_LYMPHOCYTE_MEDIATED_IMMUNITY	65	-0.46897	-1.692	0	0.050853	0.977	4076	tags=46%, list=28%, signal=64%
GO_RESPIRATORY_BURST	28	-0.56433	-1.69022	0.006536	0.051296	0.978	2277	tags=50%, list=16%, signal=59%
GO_RESPONSE_TO_TYPE_I_INTERFERON	67	-0.43866	-1.68887	0	0.051558	0.979	4209	tags=49%, list=29%, signal=69%
GO_INTERLEUKIN_1_SECRETION	40	-0.51166	-1.68856	0	0.051436	0.979	2690	tags=43%, list=19%, signal=52%
GO_RESPONSE_TO_INTERLEUKIN_7	25	-0.58402	-1.68676	0	0.051907	0.981	3283	tags=68%, list=23%, signal=88%
GO_REGULATION_OF_B_CELL_DIFFERENTIATION	27	-0.55608	-1.68648	0.006623	0.051753	0.981	3691	tags=67%, list=26%, signal=89%
GO_ACTIVATION_OF_GTPASE_ACTIVITY	70	-0.4516	-1.68281	0	0.053212	0.986	3093	tags=44%, list=21%, signal=56%
GO_REGULATION_OF_DEFENSE_RESPONSE_TO_VIRUS	60	-0.45458	-1.67968	0	0.05423	0.986	4209	tags=53%, list=29%, signal=75%
GO_VIRION_ASSEMBLY	33	-0.53073	-1.67869	0.013072	0.054464	0.987	3284	tags=48%, list=23%, signal=63%
GO_TOLL_LIKE_RECEPTOR_2_SIGNALING_PATHWAY	15	-0.63189	-1.67392	0.01992	0.056105	0.99	1209	tags=33%, list=8%, signal=40%
GO_OSTECLAST_DIFFERENTIATION	75	-0.43713	-1.66824	0	0.058446	0.991	1661	tags=36%, list=11%, signal=36%
GO_PHAGOCYTOSIS_RECOGNITION	25	-0.54829	-1.66529	0.016304	0.059727	0.991	681	tags=20%, list=5%, signal=21%
GO_DEFENSE_RESPONSE_TO_VIRUS	168	-0.39858	-1.66468	0	0.059665	0.991	4245	tags=48%, list=29%, signal=67%
GO_REGULATORY_T_CELL_DIFFERENTIATION	21	-0.56922	-1.66096	0.015873	0.061299	0.992	2718	tags=52%, list=19%, signal=64%
GO_RIG_1_SIGNALING_PATHWAY	18	-0.59129	-1.65515	0.034335	0.063912	0.994	3867	tags=61%, list=27%, signal=83%
GO_MULTI_ORGANISM_CELLULAR_PROCESS	39	-0.49018	-1.65131	0	0.065619	0.996	4439	tags=59%, list=31%, signal=85%
GO_NEGATIVE_REGULATION_OF_CHROMATIN_ORGANIZATION	46	-0.47338	-1.65109	0	0.0654	0.996	3303	tags=43%, list=23%, signal=56%
GO_NEGATIVE_REGULATION_OF_ALPHA_BETA_T_CELL_ACTIVATION	31	-0.50542	-1.65084	0.020134	0.065219	0.996	3806	tags=58%, list=26%, signal=79%
GO_PLATELET_ACTIVATION	136	-0.39141	-1.64934	0	0.065684	0.998	2909	tags=46%, list=20%, signal=57%
GO_REGULATION_OF_MACROPHAGE_DIFFERENTIATION	21	-0.56475	-1.64686	0.009852	0.066664	0.998	1639	tags=52%, list=11%, signal=59%
GO_POSITIVE_REGULATION_OF_INTERLEUKIN_6_PRODUCTION	64	-0.43695	-1.64556	0	0.066946	0.998	3234	tags=48%, list=22%, signal=62%
GO_NATURAL_KILLER_CELL_DIFFERENTIATION	17	-0.59843	-1.64513	0.020305	0.06688	0.998	2816	tags=53%, list=19%, signal=66%
GO_CLEAVAGE_INVOLVED_IN_RRNA_PROCESSING	21	-0.56112	-1.64508	0.00578	0.066613	0.998	1135	tags=24%, list=8%, signal=26%
GO_CHROMATIN_ORGANIZATION_INVOLVED_IN_REGULATION_OF_TRANSCRIPTION	79	-0.44265	-1.64455	0	0.066597	0.998	3186	tags=37%, list=22%, signal=47%
GO_REGULATION_OF_T_HELPER_CELL_DIFFERENTIATION	26	-0.54367	-1.64414	0.006135	0.066464	0.998	2491	tags=42%, list=17%, signal=51%
GO_REGULATION_OF_RESPONSE_TO_INTERFERON_GAMMA	20	-0.58412	-1.63826	0.033981	0.068702	0.999	4079	tags=55%, list=28%, signal=77%
GO_METHYLATION_DEPENDENT_CHROMATIN_SILENCING	17	-0.59916	-1.6358	0.014218	0.069842	1	2786	tags=47%, list=19%, signal=58%
GO_VENTRICULAR_SYSTEM_DEVELOPMENT	21	-0.58555	-1.63213	0.027322	0.071466	1	2632	tags=48%, list=18%, signal=58%
GO_TERMINATION_OF_RNA_POLYMERASE_II_TRANSCRIPTION	33	-0.51118	-1.63077	0	0.071919	1	5148	tags=67%, list=36%, signal=103%
GO_INTERLEUKIN_6_BIOSYNTHETIC_PROCESS	16	-0.61015	-1.63021	0.025424	0.07196	1	2730	tags=56%, list=19%, signal=69%
GO_BONE_RESORPTION	45	-0.47021	-1.63008	0.009901	0.071705	1	1743	tags=47%, list=12%, signal=53%
GO_REGULATION_OF_MYELOID_CELL_DIFFERENTIATION	192	-0.3699	-1.62709	0	0.073377	1	2756	tags=40%, list=19%, signal=49%
GO_REGULATION_OF_HISTONE_H3_K9_METHYLATION	18	-0.58484	-1.62638	0.020202	0.073483	1	3303	tags=44%, list=23%, signal=58%
GO_NEGATIVE_REGULATION_OF_CD4_POSITIVE_ALPHA_BETA_T_CELL_ACTIVATION	24	-0.55595	-1.62594	0.03352	0.073418	1	3806	tags=58%, list=26%, signal=79%
GO_LYSOSOME_LOCALIZATION	56	-0.44192	-1.62551	0	0.073395	1	1739	tags=34%, list=12%, signal=38%
GO_NEGATIVE_REGULATION_OF_T_CELL_APOPTOTIC_PROCESS	17	-0.58734	-1.62279	0.023148	0.074534	1	1445	tags=35%, list=10%, signal=39%
GO_T_CELL_ACTIVATION_INVOLVED_IN_IMMUNE_RESPONSE	67	-0.45399	-1.62073	0	0.075324	1	2534	tags=46%, list=18%, signal=56%
GO_POSITIVE_REGULATION_OF_INTERLEUKIN_1_SECRETION	24	-0.53685	-1.61943	0.031746	0.075799	1	2667	tags=46%, list=18%, signal=56%
GO_RESPONSE_TO_NITRIC_OXIDE	16	-0.62589	-1.61789	0.022523	0.076356	1	499	tags=19%, list=3%, signal=19%
GO_NEGATIVE_REGULATION_OF_TUMOR_NECROSIS_FACTOR_SUPERFAMILY_CYTOKINE_PRODUCTION	43	-0.47937	-1.61592	0.009174	0.077008	1	1959	tags=33%, list=14%, signal=38%
GO_DNA_METHYLATION	48	-0.47612	-1.61267	0	0.078406	1	2992	tags=38%, list=21%, signal=47%
GO_POSITIVE_REGULATION_OF_MULTI_ORGANISM_PROCESS	146	-0.3888	-1.60624	0	0.081751	1	3748	tags=42%, list=26%, signal=56%
GO_POSITIVE_REGULATION_OF_PROTEIN_LOCALIZATION_TO_NUCLEUS	66	-0.42011	-1.60582	0	0.081656	1	2674	tags=30%, list=18%, signal=37%
GO_REGULATION_OF_PRODUCTION_OF_SMALL_RNA_INVOLVED_IN_GENE_SILENCING_BY_RNA	19	-0.56979	-1.60305	0.017937	0.083016	1	3146	tags=47%, list=22%, signal=60%
GO_MEGAKARYOCYTE_DIFFERENTIATION	63	-0.44254	-1.60105	0	0.083972	1	3522	tags=48%, list=24%, signal=63%
GO_NUCLEOBASE_BIOSYNTHETIC_PROCESS	16	-0.58568	-1.58894	0.028302	0.091201	1	4075	tags=63%, list=28%, signal=87%
GO_POSITIVE_REGULATION_OF_NITRIC_OXIDE_BIOSYNTHETIC_PROCESS	30	-0.51711	-1.58715	0.031646	0.091854	1	3510	tags=60%, list=24%, signal=79%
GO_NEUROINFLAMMATORY_RESPONSE	45	-0.44742	-1.58704	0.011364	0.091614	1	2088	tags=36%, list=14%, signal=41%
GO_HETEROZYTIPT_CELL_CELL_ADHESION	43	-0.46647	-1.5853	0	0.092325	1	2904	tags=51%, list=20%, signal=64%
GO_VIRAL_RNA_GENOME_REPLICATION	22	-0.53518	-1.58023	0.029703	0.095181	1	3162	tags=50%, list=22%, signal=64%
GO_REGULATION_OF_LEUKOCYTE_MEDIATED_IMMUNITY	137	-0.41384	-1.57283	0	0.100001	1	3087	tags=34%, list=21%, signal=43%
GO_REGULATION_OF_PHAGOCYTOSIS	73	-0.41779	-1.57254	0	0.099816	1	2876	tags=45%, list=20%, signal=56%
GO_ATP_DEPENDENT_CHROMATIN_REMODELING	61	-0.43373	-1.57131	0	0.10028	1	3565	tags=31%, list=25%, signal=41%
GO_REGULATION_OF_POSTTRANSCRIPTIONAL_GENE_SILENCING	81	-0.41585	-1.571	0	0.100056	1	3371	tags=46%, list=23%, signal=59%
GO_NEGATIVE_REGULATION_OF_INNATE_IMMUNE_RESPONSE	34	-0.47947	-1.5705	0.023256	0.100063	1	2913	tags=35%, list=20%, signal=44%
GO_MATURATION_OF_S5U_RRNA_FROM_TRICISTRONIC_RRNA_TRANSCRIPT_S5U_RRNA_5_8S_RRNA_LSU_RRNA	33	-0.49221	-1.56859	0.006623	0.100792	1	1852	tags=21%, list=13%, signal=24%
GO_NEGATIVE_REGULATION_OF_LEUKOCYTE_DIFFERENTIATION	74	-0.39875	-1.56803	0	0.100786	1	2491	tags=36%, list=17%, signal=44%
GO_LEUKOCYTE_MEDIATED_CYTOTOXICITY	68	-0.43877	-1.56671	0	0.101303	1	4108	tags=53%, list=28%, signal=74%
GO_NEGATIVE_REGULATION_OF_CELL_CELL_ADHESION	127	-0.38465	-1.56535	0	0.10186	1	3711	tags=47%, list=26%, signal=63%
GO_REGULATION_OF_MICROGLIAL_CELL_ACTIVATION	19	-0.55001	-1.56531	0.036649	0.101513	1	2088	tags=37%, list=14%, signal=43%
GO_NUCLEAR_TRANSCRIBED_MRNA_CATABOLIC_PROCESS_DEADENYLATION_DEPENDENT_DECAY	67	-0.42643	-1.56463	0	0.10153	1	3804	tags=48%, list=26%, signal=65%
GO_REGULATION_OF_IMMUNE_EFFECTOR_PROCESS	286	-0.34125	-1.56395	0	0.101718	1	2898	tags=34%, list=20%, signal=42%
GO_NEGATIVE_REGULATION_OF_CELL_ACTIVATION	148	-0.37014	-1.56276	0	0.102139	1	2401	tags=35%, list=17%, signal=42%
GO_SPLEEN_DEVELOPMENT	24	-0.55091	-1.56153	0.046512	0.102641	1	3839	tags=63%, list=27%, signal=85%
GO_PROTEIN_INSERTION_INTO_MITOCHONDRIAL_MEMBRANE_INVOLVED_IN_APOPTOTIC_SIGNALING_PATHWAY	25	-0.501	-1.55959	0.034286	0.103754	1	4322	tags=56%, list=30%, signal=80%
GO_PH_REDUCTION	37	-0.48602	-1.55674	0.008475	0.105306	1	3010	tags=49%, list=21%, signal=61%
GO_TOLL_LIKE_RECEPTOR_9_SIGNALING_PATHWAY	20	-0.53289	-1.55542	0.028846	0.10585	1	1915	tags=45%, list=13%, signal=52%
GO_POSITIVE_REGULATION_OF_REACTIVE_OXYGEN_SPECIES_BIOSYNTHETIC_PROCESS	35	-0.47996	-1.55413	0.007246	0.106269	1	3510	tags=60%, list=24%, signal=79%
GO_T_CELL_DIFFERENTIATION_INVOLVED_IN_IMMUNE_RESPONSE	54	-0.42845	-1.55322	0.012195	0.106372	1	2491	tags=44%, list=17%, signal=53%
GO_MIDBODY_ABSCISSION	15	-0.58511	-1.55093	0.033195	0.107728	1	3505	tags=53%, list=24%, signal=70%
GO_POSITIVE_REGULATION_OF_ALPHA_BETA_T_CELL_PROLIFERATION	15	-0.59165	-1.55061	0.05	0.10757	1	3991	tags=73%, list=28%, signal=101%
GO_POSITIVE_REGULATION_OF_RESPONSE_TO_CYTOKINE_STIMULUS	49	-0.45211	-1.54974	0.009615	0.107807	1	2750	tags=39%, list=19%, signal=48%



NAME	SIZE	ES	NES	NOM p-val	FDR q-val	FWER p-val	RANK AT MAX	LEADING EDGE
GO_REGULATION_OF_SYMBIOSIS_ENCOMPASSING_MUTUALISM_THROUGH_PARASITISM	175	-0.36191	-1.54116	0	0.113529		1	2947 tags=32%, list=20%, signal=40%
GO_NCRNA_CATABOLIC_PROCESS	27	-0.50377	-1.53992	0.042169	0.113892		1	4095 tags=44%, list=28%, signal=62%
GO_CELLULAR_RESPONSE_TO_LEPTIN_STIMULUS	15	-0.59658	-1.53781	0.054167	0.115253		1	875 tags=20%, list=6%, signal=21%
GO_INNATE_IMMUNE_RESPONSE_ACTIVATING_CELL_SURFACE_RECEPTOR_SIGNALING_PATHWAY	91	-0.39603	-1.53712	0	0.115436		1	2841 tags=29%, list=20%, signal=35%
GO_CYTOPLASMIC_PATTERN_RECOGNITION_RECEPTOR_SIGNALING_PATHWAY_IN_RESPONSE_TO_VIRUS	25	-0.52117	-1.53693	0.042169	0.11511		1	4439 tags=60%, list=31%, signal=86%
GO_CYTOKINE_SECRETION	154	-0.35296	-1.5365	0	0.115043		1	3536 tags=44%, list=24%, signal=58%
GO_INTERLEUKIN_1_BETA_PRODUCTION	56	-0.40594	-1.53478	0.014286	0.115964		1	1405 tags=27%, list=10%, signal=30%
GO_NEUTROPHIL_HOMEOSTASIS	15	-0.59887	-1.53336	0.059289	0.116516		1	2308 tags=60%, list=16%, signal=71%
GO_CHEMOKINE_PRODUCTION	65	-0.3975	-1.52739	0	0.1204		1	3135 tags=48%, list=22%, signal=61%
GO_NEGATIVE_REGULATION_OF_ANTIGEN_RECEPTOR_MEDIATED_SIGNALING_PATHWAY	22	-0.54165	-1.52729	0.042328	0.120056		1	1888 tags=41%, list=13%, signal=47%
GO_REGULATION_OF_EARLY_ENDOSOME_TO_LATE_ENDOSOME_TRANSPORT	17	-0.5584	-1.52526	0.044053	0.121098		1	3489 tags=47%, list=24%, signal=62%
GO_REGULATION_OF_NATURAL_KILLER_CELL_MEDIATED_IMMUNITY	27	-0.49715	-1.52283	0.04375	0.122502		1	4076 tags=48%, list=28%, signal=67%
GO_CELLULAR_RESPONSE_TO_BIOTIC_STIMULUS	177	-0.34042	-1.51767	0	0.125717		1	2353 tags=31%, list=16%, signal=36%
GO_HOMEOSTASIS_OF_NUMBER_OF_CELLS	218	-0.34835	-1.51463	0	0.127703		1	2968 tags=39%, list=21%, signal=48%
GO_RESPONSE_TO_MURAMYL_DIPEPTIDE	17	-0.56877	-1.5137	0.054299	0.127956		1	2619 tags=65%, list=18%, signal=79%
GO_POSITIVE_REGULATION_OF_T_CELL_PROLIFERATION	64	-0.40696	-1.51173	0	0.129198		1	3053 tags=38%, list=21%, signal=47%
GO_NEGATIVE_REGULATION_OF_CHROMOSOME_ORGANIZATION	120	-0.36199	-1.51106	0	0.129295		1	4207 tags=43%, list=29%, signal=61%
GO_HISTONE_MRNA_METABOLIC_PROCESS	24	-0.50469	-1.50818	0.05	0.131094		1	4985 tags=67%, list=34%, signal=102%
GO_INTERLEUKIN_8_PRODUCTION	59	-0.41279	-1.50681	0	0.131767		1	3266 tags=49%, list=23%, signal=63%
GO_REGULATION_OF_ACTIN_CYTOSKELETON_REORGANIZATION	28	-0.49664	-1.5066	0.030488	0.131525		1	1467 tags=29%, list=10%, signal=32%
GO_POSITIVE_REGULATION_OF_IMMUNE_EFFECTOR_PROCESS	148	-0.36611	-1.50585	0	0.131636		1	2407 tags=30%, list=17%, signal=35%
GO_CYTOPLASMIC_PATTERN_RECOGNITION_RECEPTOR_SIGNALING_PATHWAY	58	-0.41445	-1.50519	0.013333	0.131767		1	2619 tags=34%, list=18%, signal=42%
GO_FOAM_CELL_DIFFERENTIATION	26	-0.51351	-1.50474	0.051948	0.13175		1	1990 tags=46%, list=14%, signal=53%
GO_RETROGRADE_TRANSPORT_ENDOSOME_TO_GOLGI	71	-0.37965	-1.50416	0	0.131832		1	4477 tags=58%, list=31%, signal=83%
GO_PROTEIN_TARGETING_TO_LYSOSOME	19	-0.53539	-1.50397	0.064378	0.131555		1	3462 tags=63%, list=24%, signal=83%
GO_POSITIVE_REGULATION_OF_TISSUE_REMODELING	22	-0.50047	-1.50389	0.053191	0.131213		1	2927 tags=55%, list=20%, signal=68%
GO_REGULATION_OF_DEFENSE_RESPONSE_TO_VIRUS_BY_HOST	29	-0.4916	-1.49943	0.025806	0.134454		1	4209 tags=59%, list=29%, signal=83%
GO_INTERLEUKIN_17_PRODUCTION	20	-0.53238	-1.49809	0.046154	0.135087		1	2816 tags=60%, list=19%, signal=74%
GO_RESPONSE_TO_VIRUS	240	-0.3656	-1.4967	0	0.135738		1	4090 tags=45%, list=28%, signal=61%
GO_REGULATION_OF_ADAPTIVE_IMMUNE_RESPONSE	117	-0.36077	-1.49392	0	0.137596		1	4143 tags=47%, list=29%, signal=65%
GO_MATURATION_OF_S5U_RRNA	42	-0.43373	-1.49125	0.027273	0.139081		1	1852 tags=17%, list=13%, signal=19%
GO_REGULATION_OF_NUCLEAR_TRANSCRIBED_MRNA_CATABOLIC_PROCESS_DEADENYLATION_DEPENDENT_DECAY	18	-0.52128	-1.49111	0.04955	0.138728		1	3804 tags=67%, list=26%, signal=90%
GO_INTERLEUKIN_7_MEDIATED_SIGNALING_PATHWAY	16	-0.55471	-1.49043	0.066946	0.138721		1	2987 tags=63%, list=21%, signal=79%
GO_TOLL_LIKE_RECEPTOR_3_SIGNALING_PATHWAY	19	-0.53841	-1.48943	0.067873	0.139098		1	2730 tags=58%, list=19%, signal=71%
GO_POSITIVE_REGULATION_OF_LYMPHOCYTE_MIGRATION	29	-0.47646	-1.4894	0.033333	0.138697		1	3432 tags=55%, list=24%, signal=72%
GO_REGULATION_OF_FIBROBLAST_MIGRATION	27	-0.49929	-1.48889	0.023952	0.138684		1	1457 tags=41%, list=10%, signal=45%
GO_ENTRY_INTO_OTHER_ORGANISM_INVOLVED_IN_SYMBIOTIC_INTERACTION	110	-0.36676	-1.48746	0	0.139512		1	2244 tags=31%, list=16%, signal=36%
GO_NEGATIVE_REGULATION_OF_PHAGOCYTOSIS	19	-0.53354	-1.48637	0.059113	0.139954		1	1776 tags=42%, list=12%, signal=48%
GO_CELLULAR_RESPONSE_TO_AMMONIUM_ION	38	-0.45008	-1.48594	0.027778	0.139868		1	3864 tags=63%, list=27%, signal=86%
GO_RESPONSE_TO_DSRNA	37	-0.44069	-1.4851	0.023438	0.140167		1	2667 tags=38%, list=18%, signal=46%
GO_REGULATION_OF_LEUKOCYTE_ADHESION_TO_VASCULAR_ENDOTHELIAL_CELL	15	-0.56288	-1.48454	0.052632	0.140314		1	2904 tags=53%, list=20%, signal=67%
GO_POSITIVE_REGULATION_OF_NITRIC_OXIDE_SYNTHASE_ACTIVITY	18	-0.53705	-1.4779	0.059072	0.14558		1	4751 tags=61%, list=33%, signal=91%
GO_NEGATIVE_REGULATION_OF_LIPID_STORAGE	16	-0.55008	-1.47771	0.09375	0.145304		1	1743 tags=31%, list=12%, signal=35%
GO_RESPONSE_TO_ZINC_ION	28	-0.47161	-1.47496	0.051613	0.147455		1	1626 tags=43%, list=11%, signal=48%
GO_POSITIVE_REGULATION_OF_INFLAMMATORY_RESPONSE	100	-0.38592	-1.47283	0.041667	0.148872		1	3234 tags=46%, list=22%, signal=59%
GO_POSITIVE_REGULATION_OF_GLYCOGENESIS	53	-0.411	-1.47241	0.013158	0.148836		1	1566 tags=32%, list=11%, signal=36%
GO_POSITIVE_REGULATION_OF_NIK_NF_KAPPAB_SIGNALING	64	-0.38178	-1.47219	0	0.148579		1	3234 tags=42%, list=22%, signal=54%
GO_REGULATION_OF_LIPOPOLYSACCHARIDE_MEDIATED_SIGNALING_PATHWAY	20	-0.51608	-1.47142	0.057292	0.148902		1	2913 tags=40%, list=20%, signal=50%
GO_G_PROTEIN_COUPLED_PURINERGIC_RECEPTOR_SIGNALING_PATHWAY	18	-0.53364	-1.46974	0.055085	0.150056		1	3087 tags=56%, list=21%, signal=71%
GO_REGULATION_OF_TYPE_1_INTERFERON_MEDIATED_SIGNALING_PATHWAY	28	-0.47755	-1.46947	0.062112	0.14986		1	4209 tags=50%, list=29%, signal=70%
GO_T_CELL_DIFFERENTIATION_IN_THYMUS	62	-0.40747	-1.46698	0.015625	0.151597		1	2756 tags=34%, list=19%, signal=42%
GO_REGULATION_OF_VIRAL_INDUCED_CYTOPLASMIC_PATTERN_RECOGNITION_RECEPTOR_SIGNALING_PATHWAY	19	-0.52833	-1.46579	0.070485	0.152042		1	3867 tags=58%, list=27%, signal=79%
GO_NEGATIVE_REGULATION_OF_HISTONE_MODIFICATION	35	-0.45158	-1.46198	0.034188	0.154973		1	3911 tags=54%, list=27%, signal=74%
GO_SPINDLE_LOCALIZATION	36	-0.44292	-1.45414	0.046512	0.162015		1	1587 tags=22%, list=11%, signal=25%
GO_PHAGOSOME_ACIDIFICATION	20	-0.51378	-1.45407	0.058333	0.161636		1	1719 tags=40%, list=12%, signal=45%
GO_CERAMIDE_CATABOLIC_PROCESS	15	-0.53228	-1.45155	0.095041	0.163776		1	2602 tags=40%, list=18%, signal=49%
GO_SPERM_MOTILITY	28	-0.47609	-1.45151	0.043478	0.16332		1	580 tags=18%, list=4%, signal=19%
GO_REGULATION_OF_RESPONSE_TO_BIOTIC_STIMULUS	110	-0.36377	-1.44956	0	0.164965		1	2913 tags=32%, list=20%, signal=40%
GO_REGULATION_OF_OSTEOCLAST_DIFFERENTIATION	46	-0.41215	-1.44896	0.042105	0.165059		1	1661 tags=37%, list=11%, signal=42%
GO_RESPONSE_TO_INTERFERON_ALPHA	18	-0.51975	-1.44844	0.052863	0.165037		1	3410 tags=44%, list=24%, signal=58%
GO_RNA_POLYADENYLATION	44	-0.41918	-1.44835	0	0.16463		1	3535 tags=50%, list=24%, signal=66%
GO_POSITIVE_REGULATION_OF_CHEMOKINE_PRODUCTION	42	-0.43634	-1.44829	0.042105	0.16421		1	1311 tags=31%, list=9%, signal=34%
GO_T_CELL_CHEMOTAXIS	19	-0.51352	-1.44701	0.085973	0.164843		1	3373 tags=53%, list=23%, signal=69%
GO_CELLULAR_RESPONSE_TO_CADMIUM_ION	23	-0.46967	-1.44556	0.024096	0.165565		1	3558 tags=48%, list=25%, signal=63%
GO_POSITIVE_REGULATION_OF_PHAGOCYTOSIS	51	-0.40893	-1.44479	0.022989	0.165745		1	2876 tags=45%, list=20%, signal=56%
GO_DNA_TEMPLATED_TRANSCRIPTION_TERMINATION	71	-0.38848	-1.44331	0.016667	0.16665		1	5257 tags=59%, list=36%, signal=92%
GO_NCRNA_EXPORT_FROM_NUCLEUS	37	-0.43136	-1.43931	0.049587	0.169953		1	2343 tags=35%, list=16%, signal=42%
GO_RNA_PHOSPHODIESTER_BOND_HYDROLYSIS_EXONUCLEOLYTIC	37	-0.42573	-1.43828	0.023077	0.170383		1	4350 tags=49%, list=30%, signal=69%
GO_POSITIVE_REGULATION_OF_T_CELL_CYTOKINE_PRODUCTION	15	-0.5619	-1.43722	0.079498	0.170931		1	3373 tags=40%, list=23%, signal=52%
GO_TRNA_TRANSPORT	33	-0.4514	-1.43553	0.069444	0.172233		1	2343 tags=39%, list=16%, signal=47%
GO_PHOSPHATIDYLINOSITOL_DEPHOSPHORYLATION	22	-0.47707	-1.43516	0.059172	0.172171		1	829 tags=18%, list=6%, signal=19%
GO_INTERFERON_ALPHA_PRODUCTION	26	-0.47304	-1.43503	0.057692	0.171812		1	992 tags=23%, list=7%, signal=25%
GO_PRODUCTION_OF_MOLECULAR_MEDIATOR_OF_IMMUNE_RESPONSE	145	-0.3448	-1.43346	0	0.172737		1	2373 tags=27%, list=16%, signal=32%
GO_POSITIVE_REGULATION_OF_TRANSCRIPTION_BY_RNA_POLYMERASE_I	22	-0.49283	-1.43101	0.044586	0.174749		1	3260 tags=36%, list=23%, signal=47%
GO_PYRIMIDINE_RIBONUCLEOTIDE_BIOSYNTHETIC_PROCESS	16	-0.51973	-1.43092	0.095833	0.174333		1	3988 tags=63%, list=28%, signal=86%
GO_NEGATIVE_REGULATION_OF_T_CELL_DIFFERENTIATION	30	-0.448	-1.4271	0.05298	0.177707		1	2491 tags=33%, list=17%, signal=40%
GO_PROTEIN_MONOUBIQUITINATION	62	-0.38095	-1.42411	0.041667	0.179957		1	1886 tags=23%, list=13%, signal=26%
GO_CYTOPLASMIC_MRNA_PROCESSING_BODY_ASSEMBLY	19	-0.5016	-1.42391	0.076923	0.179651		1	2701 tags=47%, list=19%, signal=58%
GO_NUCLEAR_TRANSCRIBED_MRNA_CATABOLIC_PROCESS_NONSENSE_MEDIATED_DECAY	115	-0.36424	-1.42298	0.045455	0.180021		1	6060 tags=54%, list=42%, signal=92%
GO_POSITIVE_REGULATION_OF_ACTIN_FILAMENT_POLYMERIZATION	82	-0.35758	-1.42031	0	0.182244		1	1761 tags=39%, list=12%, signal=44%
GO_NUCLEAR_TRANSCRIBED_MRNA_CATABOLIC_PROCESS_EXONUCLEOLYTIC	34	-0.43088	-1.41987	0.053846	0.182231		1	4944 tags=56%, list=34%, signal=85%
GO_POSITIVE_REGULATION_OF_ERYTHROCYTE_DIFFERENTIATION	27	-0.46629	-1.41677	0.065476	0.184929		1	3651 tags=52%, list=25%, signal=69%
GO_REGULATION_OF_TRANSCRIPTION_ELONGATION_FROM_RNA_POLYMERASE_II_PROMOTER	24	-0.47975	-1.4152	0.04878	0.186073		1	4642 tags=58%, list=32%, signal=86%
GO_EXIT_FROM_MITOSIS	27	-0.47694	-1.4151	0.045455	0.185669		1	3734 tags=41%, list=26%, signal=55%
GO_MULTIVESICULAR_BODY_ORGANIZATION	26	-0.45969	-1.41389	0.073171	0.186238		1	3278 tags=38%, list=23%, signal=50%
GO_REGULATION_OF_CYSINE_TYPE_ENDOPEPTIDASE_ACTIVITY_INVOLVED_IN_AP_OPTIC_SIGNALING_PATHWAY	17	-0.49635	-1.41222	0.085837	0.187635		1	2007 tags=29%, list=14%, signal=34%
GO_REGULATION_OF_T_HELPER_1_TYPE_IMMUNE_RESPONSE	19	-0.50502	-1.41069	0.08134	0.188565		1	4818 tags=68%, list=33%, signal=102%
GO_LENS_FIBER_CELL_DIFFERENTIATION	22	-0.48373	-1.41053	0.074074	0.188163		1	943 tags=18%, list=7%, signal=19%
GO_NEGATIVE_REGULATION_OF_TYPE_1_INTERFERON_PRODUCTION	40	-0.42023	-1.41044	0.062016	0.187771		1	2005 tags=33%, list=14%, signal=38%
GO_POSITIVE_REGULATION_OF_CYTOKINESIS	25	-0.46669	-1.41026	0.067039	0.187457		1	3232 tags=36%, list=22%, signal=46%

NAME	SIZE	ES	NES	NOM p-val	FDR q-val	FWER p-val	RANK AT MAX	LEADING EDGE
GO_TUMOR_NECROSIS_FACTOR_SECRETION	18	-0.53822	-1.40969	0.087805	0.187559	1	612	tags=22%, list=4%, signal=23%
GO_DNA_DAMAGE_RESPONSE_DETECTION_OF_DNA_DAMAGE	36	-0.43553	-1.40825	0.059259	0.188444	1	3397	tags=31%, list=23%, signal=40%
GO_REGULATION_OF_HISTONE_METHYLATION	53	-0.39526	-1.40812	0.030303	0.188115	1	3303	tags=42%, list=23%, signal=54%
GO_POSITIVE_REGULATION_OF_NATURAL_KILLER_CELL_MEDIATED_IMMUNITY	17	-0.50199	-1.40798	0.092105	0.187773	1	4076	tags=53%, list=28%, signal=74%
GO_REGULATION_OF_RESPONSE_TO_CYTOKINE_STIMULUS	138	-0.34661	-1.4076	0	0.187607	1	2913	tags=33%, list=20%, signal=40%
GO_NCRNA_TRANSCRIPTION	99	-0.36256	-1.40441	0.032258	0.190414	1	3260	tags=31%, list=23%, signal=40%
GO_CHOLESTEROL_STORAGE	15	-0.5342	-1.40337	0.123348	0.190997	1	1416	tags=33%, list=10%, signal=37%
GO_HEPARAN_SULFATE_PROTEOGLYCAN_METABOLIC_PROCESS	27	-0.46644	-1.4025	0.046358	0.191326	1	3203	tags=37%, list=22%, signal=47%
GO_NEGATIVE_REGULATION_OF_VIRAL_TRANSCRIPTION	20	-0.50185	-1.40243	0.099526	0.190915	1	1959	tags=40%, list=14%, signal=46%
GO_POSITIVE_REGULATION_OF_LYMPHOCYTE_CHEMOTAXIS	15	-0.52227	-1.39768	0.112	0.195453	1	3373	tags=53%, list=23%, signal=69%
GO_POSITIVE_REGULATION_OF_ACTIN_NUCLEATION	16	-0.52696	-1.39479	0.116883	0.198093	1	2467	tags=56%, list=17%, signal=68%
GO_POSITIVE_REGULATION_OF_T_HELPER_1_TYPE_IMMUNE_RESPONSE	15	-0.50994	-1.39374	0.101266	0.198927	1	4818	tags=67%, list=33%, signal=100%
GO_POSITIVE_REGULATION_OF_STEROL_TRANSPORT	18	-0.51182	-1.39173	0.113636	0.200697	1	852	tags=17%, list=6%, signal=18%
GO_MONONUCLEAR_CELL_DIFFERENTIATION	31	-0.42884	-1.39089	0.068027	0.201173	1	2143	tags=39%, list=15%, signal=45%
GO_LEUKOCYTE_ACTIVATION_INVOLVED_IN_INFLAMMATORY_RESPONSE	32	-0.43317	-1.39005	0.057554	0.201429	1	2088	tags=34%, list=14%, signal=40%
GO_RESPONSE_TO_INTERLEUKIN_4	30	-0.4489	-1.38931	0.06135	0.201712	1	2756	tags=33%, list=19%, signal=41%
GO_TRANSFERRIN_TRANSPORT	28	-0.46705	-1.38829	0.090361	0.202333	1	1005	tags=29%, list=7%, signal=31%
GO_PLASMA_LIPOPROTEIN_PARTICLE_CLEARANCE	38	-0.41161	-1.38568	0.056452	0.204931	1	2241	tags=39%, list=15%, signal=47%
GO_NEGATIVE_REGULATION_OF_B_CELL_ACTIVATION	27	-0.45023	-1.38369	0.056604	0.206907	1	3636	tags=74%, list=25%, signal=99%
GO_NEGATIVE_REGULATION_OF_IMMUNE_RESPONSE	98	-0.35212	-1.38207	0.044444	0.208171	1	922	tags=17%, list=6%, signal=18%
GO_POSITIVE_REGULATION_OF_MACROPHAGE_ACTIVATION	23	-0.45122	-1.38128	0.052632	0.20856	1	2088	tags=35%, list=14%, signal=41%
GO_REGULATION_OF_ACTIN_NUCLEATION	25	-0.46345	-1.38013	0.073034	0.20955	1	2467	tags=48%, list=17%, signal=58%
GO_PROTEIN_LOCALIZATION_TO_KINETOCHORE	17	-0.49701	-1.37929	0.099526	0.210176	1	2635	tags=24%, list=18%, signal=29%
GO_POSITIVE_REGULATION_OF_ORGANELLE_ASSEMBLY	58	-0.37818	-1.37905	0.04918	0.209994	1	2920	tags=38%, list=20%, signal=47%
GO_NEGATIVE_REGULATION_OF_HEMOPOIESIS	110	-0.33043	-1.37836	0	0.210276	1	2491	tags=33%, list=17%, signal=39%
GO_PROTEIN_TARGETING_TO_VACUOLE	32	-0.44337	-1.37756	0.08125	0.210615	1	3970	tags=50%, list=27%, signal=69%
GO_CELL_KILLING	79	-0.3619	-1.37557	0.044444	0.211204	1	4108	tags=46%, list=28%, signal=63%
GO_MYD88_INDEPENDENT_TOLL_LIKE_RECEPTOR_SIGNALING_PATHWAY	29	-0.44345	-1.37268	0.07362	0.214785	1	2116	tags=24%, list=15%, signal=28%
GO_POSITIVE_REGULATION_OF_OSTEOCLAST_DIFFERENTIATION	16	-0.52282	-1.37052	0.103139	0.216604	1	1626	tags=50%, list=11%, signal=56%
GO_INFLAMMATORY_RESPONSE_TO_ANTIAGENIC_STIMULUS	34	-0.43634	-1.36976	0.0625	0.216839	1	1541	tags=26%, list=11%, signal=30%
GO_NEGATIVE_REGULATION_OF_CYTOKINE_PRODUCTION	203	-0.30603	-1.36741	0	0.219145	1	2094	tags=28%, list=14%, signal=32%
GO_HISTONE_DEUBIQUITINATION	20	-0.48066	-1.36405	0.109524	0.222403	1	2968	tags=40%, list=21%, signal=50%
GO_REGULATION_OF_MACROPHAGE_DERIVED_FOAM_CELL_DIFFERENTIATION	20	-0.47479	-1.36376	0.098361	0.222158	1	1990	tags=45%, list=14%, signal=52%
GO_SUPEROXIDE_ANION_GENERATION	25	-0.44273	-1.3625	0.066667	0.223057	1	1801	tags=40%, list=12%, signal=46%
GO_INTERLEUKIN_1_PRODUCTION	66	-0.37059	-1.36126	0	0.224092	1	1405	tags=23%, list=10%, signal=25%
GO_POSITIVE_REGULATION_OF_NEUROINFLAMMATORY_RESPONSE	15	-0.52925	-1.35937	0.150442	0.225741	1	2088	tags=40%, list=14%, signal=47%
GO_LYTIC_VACUOLE_ORGANIZATION	55	-0.37107	-1.35929	0.013158	0.225308	1	2667	tags=35%, list=18%, signal=42%
GO_CHROMATIN_REMODELING	136	-0.31746	-1.35894	0	0.225244	1	3565	tags=38%, list=25%, signal=50%
GO_REGULATION_OF_MAST_CELL_ACTIVATION_INVOLVED_IN_IMMUNE_RESPONSE	23	-0.45137	-1.3584	0.099476	0.225215	1	1739	tags=39%, list=12%, signal=44%
GO_REGULATION_OF_CHROMATIN_ORGANIZATION	152	-0.30339	-1.35732	0	0.225946	1	3531	tags=40%, list=24%, signal=53%
GO_REGULATION_OF_LYMPHOCYTE_MEDIATED_IMMUNITY	97	-0.35031	-1.35522	0.096774	0.227806	1	3058	tags=31%, list=21%, signal=39%
GO_REGULATION_OF KERATINOCYTE DIFFERENTIATION	24	-0.44534	-1.35435	0.083333	0.228412	1	1428	tags=38%, list=10%, signal=42%
GO_MYELOID_CELL_APOPTOTIC_PROCESS	26	-0.44329	-1.35348	0.067039	0.228826	1	2825	tags=50%, list=20%, signal=62%
GO_MODIFICATION_OF_MORPHOLOGY_OR_PHYSIOLOGY_OF_OTHER_ORGANISM_INVOLVED_IN_SYMBIOTIC_INTERACTION	85	-0.36271	-1.35307	0	0.228772	1	2906	tags=29%, list=20%, signal=37%
GO_REGULATION_OF_REACTIVE_OXYGEN_SPECIES_BIOSYNTHETIC_PROCESS	64	-0.37365	-1.35297	0.033898	0.228338	1	1816	tags=31%, list=13%, signal=36%
GO_CELLULAR_RESPONSE_TO_ARSENIC_CONTAINING_SUBSTANCE	17	-0.49526	-1.34913	0.099585	0.232245	1	3806	tags=47%, list=26%, signal=64%
GO_TELOMERASE_RNA_LOCALIZATION	19	-0.48672	-1.34847	0.124424	0.23257	1	4938	tags=53%, list=34%, signal=80%
GO_SENSORIAL_PERCEPTION_OF_CHEMICAL_STIMULUS	29	-0.43623	-1.34809	0.075	0.23249	1	1494	tags=28%, list=10%, signal=31%
GO_GLIAL_CELL_ACTIVATION	39	-0.40887	-1.34687	0.067164	0.23336	1	1405	tags=26%, list=10%, signal=28%
GO_IMPORT_INTO_NUCLEUS	123	-0.30166	-1.34592	0	0.233898	1	2983	tags=32%, list=21%, signal=40%
GO_INTERFERON_GAMMA_MEDIATED_SIGNALING_PATHWAY	56	-0.39205	-1.34488	0.014085	0.234709	1	2750	tags=43%, list=19%, signal=53%
GO_GLIAL_CELL_PROLIFERATION	36	-0.39169	-1.34455	0.07	0.234557	1	1812	tags=31%, list=13%, signal=35%
GO_NEGATIVE_REGULATION_OF_CYTOKINE_SECRETION	43	-0.40061	-1.34372	0.031579	0.235005	1	3629	tags=56%, list=25%, signal=74%
GO_PLATELET_AGGREGATION	53	-0.37791	-1.34324	0.050633	0.234936	1	2739	tags=45%, list=19%, signal=56%
GO_REGULATION_OF_HEMATOPOIETIC_PROGENITOR_CELL_DIFFERENTIATION	78	-0.35315	-1.34279	0	0.23448	1	3429	tags=29%, list=24%, signal=38%
GO_VACUOLAR_TRANSPORT	120	-0.32443	-1.34278	0	0.234348	1	3462	tags=42%, list=24%, signal=54%
GO_SNRNA_3_END_PROCESSING	16	-0.50758	-1.34138	0.105263	0.235649	1	2461	tags=38%, list=17%, signal=45%
GO_HISTONE_H4_K5_ACETYLATION	16	-0.48183	-1.34082	0.142857	0.235775	1	1498	tags=31%, list=10%, signal=35%
GO_OSTEOCLAST_DEVELOPMENT	16	-0.50873	-1.3393	0.122449	0.237059	1	2085	tags=50%, list=14%, signal=58%
GO_INTESTINAL_ABSORPTION	16	-0.48874	-1.33922	0.108597	0.2366	1	593	tags=19%, list=4%, signal=20%
GO_PROTEIN_DEGLYCOSYLATION	27	-0.43091	-1.33819	0.086667	0.23735	1	2782	tags=44%, list=19%, signal=55%
GO_NEGATIVE_REGULATION_OF_RESPONSE_TO_BIOTIC_STIMULUS	34	-0.40955	-1.33475	0.07438	0.240918	1	1601	tags=26%, list=11%, signal=30%
GO_T_CELL_MIGRATION	49	-0.37614	-1.33372	0.027397	0.241594	1	3432	tags=55%, list=24%, signal=72%
GO_NEGATIVE_REGULATION_OF_CYSINE_TYPE_ENDOPEPTIDASE_ACTIVITY	70	-0.36223	-1.33332	0.072727	0.241621	1	1141	tags=20%, list=8%, signal=22%
GO_POSITIVE_REGULATION_OF_I_KAPPA_B_KINASE_NF_KAPPA_B_SIGNALING	157	-0.30609	-1.33197	0	0.242587	1	2770	tags=34%, list=19%, signal=42%
GO_COLUMNAR_CUBOIDAL_EPITHELIAL_CELL_DEVELOPMENT	41	-0.38584	-1.32989	0.065041	0.244437	1	1628	tags=27%, list=11%, signal=30%
GO_NEGATIVE_REGULATION_OF_RNA_METABOLIC_PROCESS	44	-0.3909	-1.32836	0.045045	0.245791	1	2765	tags=30%, list=19%, signal=36%
GO_ESTABLISHMENT_OF_PROTEIN_LOCALIZATION_TO_VACUOLE	36	-0.40035	-1.32513	0.104839	0.249188	1	3699	tags=44%, list=26%, signal=60%
GO_NEGATIVE_REGULATION_OF_INTERLEUKIN_1_PRODUCTION	17	-0.48375	-1.32513	0.114155	0.248633	1	866	tags=18%, list=6%, signal=19%

### APPENDIX III: DETAILS OF AMENDMENTS MADE TO THE THESIS

Page amended	Amended text or correction
Page 39	<p>The <i>Osx1-GFP:Cre</i> and <i>Rptor<sup>fl/fl</sup></i> mice lines were bred separately. The <i>Osx1-GFP:Cre</i> line was maintained by mating F1 males harboring a single copy of the <i>tTA:Osx1-GFP:cre</i> transgene with wildtype C57BL/6J females. For the <i>Rptor<sup>fl/fl</sup></i> line, all F2 mice were produced from the offspring of F1 breeders. For the <i>Osx1-GFP:Cre</i> x <i>Rptor<sup>fl/fl</sup></i> crosses, all F2 mice were produced by new crosses between separate F1 male <i>Osx1-GFP:Cre</i> and female <i>Rptor<sup>fl/fl</sup></i> mice. As preliminary studies revealed that serum OCN levels (both total and undercarboxylated), fasting glucose levels and glucose metabolism (glucose tolerance and insulin sensitivity) were unaltered in <i>Osx1-GFP:Cre</i> mice relative to age/sex matched wildtype mice, wildtype <i>Osx1-GFP:Cre-negative; Rptor<sup>fl/fl</sup></i> littermates were used as the control group (Supplementary Figure 2.1, A-I). It is also important to note that no detectable off-target Cre recombinase activity in metabolic tissues including spleen, liver, brain and intestine has been observed in <i>Osx1-GFP:Cre</i> mice<sup>5</sup>. Furthermore, as <i>Osx1-GFP:Cre</i> line has been reported to develop malocclusion when maintain without doxycycline<sup>6</sup> all <i>Osx1-GFP:Cre</i>-positive animals were closely monitored and their teeth were trimmed fortnightly. Animals were weighed twice-weekly for the duration of the study and at the end of the study, body length and whole-body lean and fat mass were measured post-mortem using a dedicated mouse dual X-ray absorbitometer (DXA) (Lunar Piximus II, GE Medical Systems, Madison WI, USA).</p>
Page 42	<p>2.3.9 RNA isolation and quantitative RT-PCR. Unless otherwise stated, all RNA extractions were carried out using TRIzol reagent (Sigma) according to manufacturer's instructions. Total RNA (1.5 µg) was reverse transcribed into cDNA using Superscript IV Reverse Transcriptase (Invitrogen, Carlsbad, CA, USA). Real-time PCR reactions were performed using RT<sup>2</sup> SYBR Green ROX reagent (QIAGEN, Hilden, Germany) in a CFX Connect™ Real-Time PCR machine (Bio-Rad). Forward and reverse primer pairs, designed to amplify across intron-exon boundaries, are listed in Supplementary Table 2.2. The efficiencies of PCR were assessed with visual assessment of geometric amplification slopes and relative mRNA expression was determined using the 2<sup>-ΔΔCt</sup> method<sup>7</sup>.</p> <p>2.3.10 Statistical analysis. All data are presented as mean ± standard error of the mean (SEM). Statistical analyses were performed using a one-way or two-way ANOVA with a Tukey test or an unpaired Students t-test using GraphPad Prism (GraphPad Software Inc, CA, USA). Significance was accepted at p&lt;0.05, with asterisks denoting p-value levels: *p &lt; 0.05; **p&lt; 0.01; ***p &lt; 0.001.</p>
Page 45	Figure 2.1K was amended with correct representative images. The

	figure legend describing Figure 2.1 has been amended to replace on-way ANOVA with two-way ANOVA.
Page 48	Figure 2.2I and J were amended to present the absolute glucose levels. The figure legend describing Figure 2.2 has been amended to replace on-way ANOVA with two-way ANOVA.
Page 51	<p>Figure 2.3B and C were amended to present food intake as kcal or kcal normalised to gram of lean mass, respectively and the legend have been updated as follows:</p> <p><b>Fig. 2.3 Loss of OB-mTORC1 function shifts whole-body fuel utilisation toward fat oxidation.</b> (A) Serum leptin levels in 9-week old male and female mice (n=7-15/genotype). (B) Food intake per day, measured over 48-h, presented as absolute food intake (kcal/day), or (C) normalised to lean mass (kcal/g lean mass/day). (D) Faecal lipid content (% lipid/g faeces) (n=7-10/genotype). (E) Ambulatory X+Y axis activity per day. (F) Z-axis (rearing) locomotor activity per day. (G) Total energy expenditure, normalised to lean mass, per light and dark cycle, and (H) over a 48-h time course in male mice. (I) Average respiratory quotient (RQ) per light and dark cycle, or (J) over a 48-h time course in male mice. (K) Total energy expenditure, normalised to lean mass, per light and dark cycle, and (L) over a 48-h time course in female mice. (M) Average respiratory quotient (RQ) per light and dark cycle, or (N) over a 48-h time course in female mice. (O) Fasting serum ketone body levels (n=4-5/genotype). (P) Serum triglyceride levels measured at non-fasted condition (n=6-10/genotype). (Q) Serum free fatty acid levels measured at non-fasted condition (n=8-11/genotype). All panels: data are expressed as mean ± SEM from n=5-6/group, unless indicated otherwise. *p&lt;0.05, **p&lt;0.01, ***p&lt;0.001, two-way ANOVA with Tukey's post-hoc test. Panels H, J, L, N: shaded regions represent dark cycle.</p>
Page 84	<p>Both male and female <i>Rptor<sub>ob</sub><sup>-/-</sup></i> mice weighed significantly less the control mice (Fig.3.1A and B). As shown in Figure 3.1C and D, <i>Rptor<sub>ob</sub><sup>-/-</sup></i> mice initially gained weight on the HFD at a similar rate to control and <i>Rptor<sub>ob</sub><sup>+/+</sup></i> mice, and in the case of female mice, gained weight more rapidly. However, unlike the control and <i>Rptor<sub>ob</sub><sup>+/+</sup></i> mice, which continued to gain weight in response to the obesogenic diet, weight gain in the <i>Rptor<sub>ob</sub><sup>-/-</sup></i> mice plateaued after approximately 6 weeks and they gained only a small amount of additional weight thereafter (i.e. from 6-13 weeks on HFD, control mice gained 9.3g and 7.2g in male and female respectively, whereas <i>Rptor<sub>ob</sub><sup>-/-</sup></i> mice gained only 1.7g; Fig. 3.1C-D).</p> <p>The lower body weight of <i>Rptor<sub>ob</sub><sup>-/-</sup></i> mice was independent of difference in their body length but rather due to the changes in the body composition as suggested by a significant lower BMI in the <i>Rptor<sub>ob</sub><sup>-/-</sup></i> mice (Supplementary Fig. 3.2A-B). Further examination of body composition in these HFD-fed mice revealed that the difference in their</p>

	<p>body weight was largely attributable to a significant reduction in fat mass in <i>Rptor<sub>ob</sub><sup>-/-</sup></i> mice (Fig. 3.1E), with a modest reduction in lean mass also observed (Supplementary Fig. 3.2C-D). When expressed as a percentage of total body mass, fat mass in male or female <i>Rptor<sub>ob</sub><sup>-/-</sup></i> mice was 50% lower than that of the control mice (Fig. 3.1F). The total fat mass and % fat mass of HFD-fed <i>Rptor<sub>ob</sub><sup>+/-</sup></i> mice was also found to be significantly lower than the controls in the male, but not female cohorts (Fig. 3.1E and F). Furthermore, the difference in fat mass in HFD-fed <i>Rptor<sub>ob</sub><sup>-/-</sup></i> mice was clearly evident upon dissection and analysis of individual fat pad weights (Fig. 3.1G and H), whereas no such differences in lean organ weights (i.e. liver, heart, kidney, brain, spleen; Supplementary Fig. 3.2E and F) were observed in <i>Rptor<sub>ob</sub><sup>-/-</sup></i> mice compared to controls.</p>
Page 85	<p>This suggests that <i>Rptor<sub>ob</sub><sup>-/-</sup></i> mice maintain their constant weight and energy balance through greater substrate flexibility, with greater utilization of fat storage during the light cycle which provide a glycerol substrate for increased gluconeogenesis, thus resulting in higher carbohydrate oxidation in the dark cycle (Fig. 3.1K and L). Conversely, in <i>Rptor<sub>ob</sub><sup>+/-</sup></i> mice, higher carbohydrate oxidation and lipid synthesis in the dark cycle was not offset by greater utilization of fat storage during the light cycle. Thus, even with greater substrate flexibility, as is evident in <i>Rptor<sub>ob</sub><sup>-/-</sup></i> mice, higher energy storage during the dark cycle surpassed fat oxidation during the light cycle, resulting in overall continuous weight gain. In contrast, the average phasic RQ values of the control mice remained approximately constant, which is indicative of fewer shifts in their fat storage and oxidation and a more constant accumulation of adipose tissue mass.</p>
Page 86	<p>Figure 3.1 was amended to include total body weight over the time-course of high fat diet feeding (panel A and B) and the legend have been updated as follows:</p> <p><b>Fig. 3.1 HFD-fed <i>Rptor<sub>ob</sub><sup>-/-</sup></i> mice are protected against diet-induced obesity and exhibit greater substrate flexibility.</b> (A-B) Temporal body weight changes in male and female mice (n≥15/genotype). (C-D) Body weight gained in response to high fat diet (HFD) in male and female mice (n≥15/group). Dotted lines indicate the point at which <i>Rptor<sub>ob</sub><sup>-/-</sup></i> mice became resistant to further weight gain. (E-F) DXA analysis of total fat mass and % fat mass normalised to total body weight in 18-week old HFD-fed mice (n=4-5/genotype). (G-H) gWAT and iWAT fat pad mass, normalised to body weight, in male and female mice at 18-week of age (n=4-9/genotype). (I-J) Total energy expenditure, normalised to lean mass, over a 48-h time course (<i>left</i>) and per light/dark cycle (<i>right</i>) in male and female HFD-fed mice (n=5-7/genotype). (K-L) Average respiratory quotient (RQ) over a 48-h time course (<i>left</i>) and per light and dark cycle (<i>right</i>) in male and female mice (n=5-7/genotype). All panels: data are expressed as mean ± SEM.</p>

	*p<0.05, **p<0.01, ***p<0.001, two-way ANOVA with Tukey's post-hoc test. Panels H-K: shaded regions represent dark cycle.
Page 93	<p>Male <i>Rptor<sub>ob</sub><sup>-/-</sup></i> mice showed a trend toward decreasing fasting glucose levels over the time course of HFD. Specifically, in 16-week old male <i>Rptor<sub>ob</sub><sup>-/-</sup></i> mice, the fasting glucose levels were significantly lower than <i>Rptor<sub>ob</sub><sup>-/+</sup></i> and control mice (Fig. 3.5A) while the fasting glucose levels of female <i>Rptor<sub>ob</sub><sup>-/-</sup></i> mice were persistently lower than the control mice (Fig. 3.5B). The lower levels of fasting glucose in the <i>Rptor<sub>ob</sub><sup>-/-</sup></i> mice were accompanied by a significant lower fasting insulin levels (Fig. 3.5C). As a result, calculation of homeostatic model assessment of insulin resistance (HOMA-IR) identify them as being more insulin-sensitive than both the <i>Rptor<sub>ob</sub><sup>-/+</sup></i> and control mice (Fig. 3.3D). Studies<sup>12</sup> suggest that in cases of significant difference in the fasting glucose levels, assessing glucose levels as a percentage of basal glucose for an ITT, can lead to erroneous interpretation of the results and thus all the ITT results were presented as absolute glucose levels. At 16 weeks of age, both male and female <i>Rptor<sub>ob</sub><sup>-/-</sup></i> mice recapitulated all the key features of the metabolic profiles that were evident in the normal chow-fed studies, including the maintenance of higher glucose tolerance (Fig. 3.5E-G) as evidenced by with consistently lower glucose levels and significantly lower incremental area under the curve (iAUC) and higher responsiveness to insulin (Fig. 3.5H- J) compared to the controls. The improvements in glucose disposal in both male and female <i>Rptor<sub>ob</sub><sup>-/-</sup></i> mice were associated with a higher fold change of insulin levels at 30 minutes post glucose injection, as measured by glucose-stimulated insulin secretion tests (Fig. 3.5K-N). Moreover, smaller <math>\beta</math>-cell islet hypertrophy was observed in male <i>Rptor<sub>ob</sub><sup>-/-</sup></i> mice (Fig. 3.5N) which may have been a secondary effect of persistently low glucose levels.</p>
Page 94	<p>Figure 3.5 and the legend have been updated as follows:  <b>Fig. 3.5 HFD-fed <i>Rptor<sub>ob</sub><sup>-/-</sup></i> mice are protected against diet-induced insulin resistance.</b> (A-B) Fasting glucose levels over 8-17 weeks old male (A) and female (B) mice (n=5-15/genotype). (C) Fasting insulin levels (n=8-10/genotype). (D) HOMA-IR calculations of HFD-fed female mice (n=3-8/genotype). (E-F) Glucose tolerance tests (GTTs) in 17-week old male (E) and female (F) mice (n=6-15/genotype). (G) Incremental area under the curve analysis from (E-F). (H-I) Insulin tolerance tests (ITTs) in 16-week old male (H) and female (I) mice (n=6-15/genotype). (J) Area under the curve analysis from (H-I). (K-N) Insulin levels during a glucose-stimulated insulin secretion tests (GSIS) in male (K) and female (M) and Fold change in insulin levels at 30 minutes post glucose injection relative to basal levels (L and N) (n=8-10/genotypes). (O) Mean pancreatic islet area (n=5/genotype) and representative image of insulin immunostaining of pancreas at 18-week of age, scale bar=50<math>\mu</math>m. All panels except E, F, H and I: data are</p>

	expressed as mean $\pm$ SEM. * $p$ <0.05, ** $p$ <0.01, *** $p$ <0.001, two-way ANOVA with Tukey's post-hoc test. For panel E, F, H and I: * $p$ <0.05 between $Rptor_{ob}^{-/-}$ and Ctrl, # $p$ <0.05 between $Rptor_{ob}^{-/-}$ and $Rptor_{ob}^{-/+}$ and \$ $p$ <0.05 between $Rptor_{ob}^{-/+}$ and Ctrl, two-way ANOVA with Tukey's post-hoc test.
Page 96	Figure 3.6B was amended to include quantification of protein of interest at the basal levels.
Page 97	Figure 3.7B was amended to include quantification of protein of interest at the basal levels.
Page 107	Based on the data generated herein, the mechanisms underlying the obesity-resistance phenotype of $Rptor_{ob}^{-/-}$ mice likely include (i) their ability to switch substrate oxidation during the light and dark period, and (ii) their ability to increase browning of iWAT via upregulation of <i>Ucp1</i> expression.
Page 110	Supplementary Figure 3.1 and 3.2 were swapped.
Page 111	Supplementary Figure 3.2 was amended to include body length (panel A), body mass index (panel B) and percentage of lean mass (panel D) and the legend have been updated as follows: <b>Supplementary Fig. 3.2 Daily food intake, physical activities and % of fecal lipid are normal in HFD-fed <math>Rptor_{ob}^{-/-}</math> mice.</b> (A) Body length of 18-week old mice, as measured from nose to anus (n=4-5/genotype). (D) Body mass index (BMI) (n=4-5/genotype). (B-D) DXA analysis of total lean mass and % lean mass in male and female HFD-fed mice (n=4-5/genotype). (E-F) Lean organ weights, normalised to total body weight, in 18-week-old HFD-fed male and female mice (n=4-9/genotype). (G) %lipid content of 1g faeces collected from male and female HFD-fed mice (n=9-10/genotype). (E-F) Food intake normalised to lean mass (kcal/g lean mass), measured over a 48-h period ( <i>left</i> ) and per 12-h light/dark cycle ( <i>right</i> ) in HFD-fed male and female mice (n=5-7/genotype). (H-I) Total activity (distance of movement) measured over a 48-h period ( <i>left</i> ) and per 12-h light/dark cycle ( <i>right</i> ) in HFD-fed male and female mice (n=5-7/genotype). All panels: data are expressed as mean $\pm$ SEM. * $p$ <0.05, two-way ANOVA with Tukey's post-hoc test. Panels E-H: shaded regions represent dark cycle.